Development of a Targeted Diagnostic and Therapeutic Delivery system for Cholangiocarcinoma

Amit Nair MB BS, MS, FRCS (Gen)

Submitted in accordance with the requirements for the degree of
Doctor of Medicine

The University of Leeds
School of Medicine
August 2016

The candidate confirms that the work submitted is his/her own and that appropriate credit has been given where reference has been made to the work of others.

This copy has been supplied on the understanding that it is copyright material and that no quotation from the thesis may be published without proper acknowledgement

The right of Amit Nair to be identified as Author of this work has been asserted by him in accordance with the Copyright, Designs and Patents Act 1988.

Acknowledgements

I wish to express my sincere gratitude and appreciation to:

Dr Louise Coletta, for her steadfast guidance and support throughout my research tenure.

Mr K Raj Prasad, for the opportunity to work in Leeds, clinical exposure, unwavering encouragement and constant push to think off the beaten track.

Dr Judy Wyatt, Professor Stephen D Evans and Dr Kevin Critchley, for their help and support.

Professor Sir Alex Markham, for his mentorship and advice, not to mention the opportunity to play in some of Yorkshire's finest cricket grounds.

Dr Nicola Ingram and Ms Sarah Perry, whose hands-on help, time and advice without I would not have got this work done.

My write-up room colleagues Eldo Verghese, Baek Kim, Jim Tiernan, Samir Pathak and John Hutchinson for the lively debates, discussions, and coffee breaks.

The faculty, post-docs and staff of Level 9, Wellcome Trust Brenner building, University of Leeds.

The Ray of Hope charity, St James' University Hospital, Leeds, whose funding allowed this project to see the light of day.

The faculty, staff and my colleagues in the Department of Transplant and Hepatobiliary Surgery at St James' University Hospital, Leeds.

And finally, to my long suffering wife and our lovely children, who are now breathing a sigh of relief that I have completed this work.

Abstract

The current outcomes of peri-hilar cholangiocarcinoma (PH-CCA) are in general poor with no proven roles for any treatment modalities in improving survival apart from complete surgical extirpation. The dismal prognosis observed is contributed to by both delays in diagnosis and aggressive tumour biology. The advent of molecular targeting of solid cancers allows harnessing this property on microbubble and nanotechnology based platforms. Such a system provides for concurrent diagnosis and therapeutic effect (theragnosis), the feasibility of which is explored in this work.

The expression of two candidate biomarkers with established roles in cancer progression, namely Neutrophil Gelatinase-Associated Lipocalin (NGAL) and Matrix Metalloproteinase-9 (MMP9) were examined by Immunohistochemistry in 54 human samples of resected PH-CCA. These markers were then evaluated for their potential as molecular targets in theragnostic platforms in cholangiocarcinoma.

Both NGAL and MMP9 were found to be abundantly expressed in both tumour tissue and control liver. Although higher NGAL expression was associated with nodal metastases, no prognostic impact was seen for either marker. NGAL expression was further interrogated in six cholangiocarcinoma cell lines by Western blotting, Immunofluorescence and ELISA techniques, which revealed localisation of NGAL to the cell membrane and its secretion, both indicating its suitability to a targeting platform. Nonetheless, its expression in normal liver tissue could lead to off-target effects.

Concurrently, the expression of vascular ligands CD31, CD105 and Vascular Endothelial Growth Factor Receptor-2 were each assessed in the same cohort of

tissue samples. CD105 expression was found to be independently predictive of poorer overall survival. Subsequent *in vitro* flow assay experiments using CD105 antibody conjugated microbubbles showed it bound murine SVR endothelial cells significantly more in comparison to isotype control microbubbles. Furthermore, evaluation of *in vivo* targeting with the aid of high frequency ultrasound demonstrated CD105-microbubbles bound to tumour endothelium significantly more than control microbubbles in a subcutaneous murine xenograft model of cholangiocarcinoma.

This work therefore indicates NGAL is suited to a theragnostic approach in cholangiocarcinoma although larger data sets are required to explore its prognostic impact. CD105-microbubbles could be utilised in the delivery of such theragnostic particles to cholangiocarcinoma tissue, whilst in themselves providing a non-invasive index of tumour vascularity when imaged with ultrasound.

Table of Contents

List of Tables

List of Figures

Abbreviations

CCA	Cholangiocarcinoma
7AAD	7-Amino-actinomycin D
ABC	Avidin biotin complex
AJCC	American Joint Cancer Committee
AN	Amit Nair
AUC	Area under curve
CA 19-9	Carbohydrate Antigen 19-9
CEA	Carcino-Embryonic Antigen
CI	Confidence interval
CT	Computerized Tomography
DAB	3,3'-diaminobenzidine tetrahydrochloride
DAPI	4',6-diamidino-2-phenylindole
DFS	Disease-free survival
DPPC	Dipalmitoylphosphatidylcholine
DSPE	1,2-Distearoyl-sn-glycero-3-phosphoethanolamine
EDTA	Ethylenediaminetetraacetic acid
EGFR	Epidermal Growth Factor Receptor
EH-CCA	Extrahepatic Cholangiocarcinoma
ELISA	Enzyme Linked Immunosorbent Assay
EPR	Enhanced Permeability and Retention
EV	Eldo Verghese
FC	Flow Cytometry

FFPE	Formalin-fixed paraffin embedded
GEMOX	Gemcitabine- Oxaliplatin
H&E	Haematoxylin and Eosin
HCC	Hepatocellular Carcinoma
HPF	High power field
HR	Hazard Ratio
HRP	Horse Radish Peroxidase
IF	Immunofluorescence
IG	Intra-ductal Growth
IGF-1	Insulin-like Growth Factor-1
IHC	Immunohistochemistry
IH-CCA	Intrahepatic Cholangiocarcinoma
IQR	Inter-quartile range
MAb	Monoclonal antibody
MB	Microbubble
MF	Mass Forming
MMP9	Matrix Metalloproteinase-9
MRCP	Magnetic Resonance Cholangiopancreatography
MVD	Microvessel density
NGAL	Neutrophil Gelatinase-Associated Lipocalin
NGALR	Neutrophil Gelatinase-Associated Lipocalin Receptor
NIR	Near-infrared
NP	Nanoparticle

NS	Not significant
OLT	Orthotopic Liver Transplantation
OS	Overall survival
PBS	Phosphate buffered saline
PDGFR	Platelet Derived Growth Factor Receptor
PECAM	Platelet Endothelial Cell Adhesion Molecule
PEG	Polyethylene Glycol
PFA	Paraformaldehyde
PFC	Perfluorocarbon
PH-CCA	Peri-hilar Cholangiocarcinoma
PI	Peri-ductal Infiltrating
PSC	Primary Sclerosing Cholangitis
PVDF	Polyvinylidene difluoride
R0	Negative resection margin
R1	Positive resection margin
RIPA	Radioimmunoprecipitation assay
ROC	Receiver operating characteristic
RT	Room temperature
RTK	Receptor Tyrosine Kinase
SVR	Sven-1 ras
TBS(-T)	Tris-Buffered Saline(-Tween-20)
TGF	Transforming Growth Factor
TIMP	Tissue Inhibitors of Metalloproteinase
TNF	Tumour necrosis factor alpha
TNM	Tumour Node Metastasis

UICC	Union for International Cancer Control
US	Ultrasound
VEGF	Vascular Endothelial Growth Factor
VEGFR	Vascular Endothelial Growth Factor Receptor
w/v	Weight/Volume

List of Presentations and Abstracts

Presentations

- Matrix metalloproteinase-9, Neutrophil Gelatinase-Associated Lipocalin and tumour endothelial markers in Perihilar Cholangiocarcinoma: Developing biomarkers for targeted therapies. Oral presentation at the International Surgical Congress of the Association of Surgeons of Great Britain and Ireland (ASGBI); SECC, Glasgow (3rd May, 2013)

- Neutrophil Gelatinase Associated Lipocalin (NGAL) as a theragnostic biomarker for perihilar cholangiocarcinoma. Poster presentation at the 11th International Congress of the European-African Hepato-Pancreato-Biliary Association. Manchester, UK (21st – 24th April, 2015)

Abstracts

- Nair A, Verghese ET, Perry S, Coletta PL, Prasad KR. Matrix Metalloproteinase-9, Neutrophil Gelatinase-Associated Lipocalin and Tumour Endothelial Markers in Perihilar Cholangiocarcinoma: Developing Biomarkers for Targeted Therapies. Br J Surg 2013; 100 (S7): 8

- Nair A, Ingram N, Verghese E, Wijetunga I, Markham A, Prasad KR, Coletta PL. Evaluation of the endothelial marker CD105 as a prognostic biomarker and target for molecular theragnostics in perihilar cholangiocarcinoma. Eur J Cancer 2015; 51 (S3): S467

- Nair A, Verghese E, Ingram N, Wijetunga I, Markham A, Wyatt J, Prasad KR, Coletta PL. Neutrophil Gelatinase Associated Lipocalin (NGAL) as a theragnostic biomarker for perihilar cholangiocarcinoma. HPB 2016; 18 (S2): e682

Manuscripts in preparation

- Nair A, Verghese E, Ingram N, Wijetunga I, Markham A, Wyatt J, Prasad KR, Coletta PL. Evaluation of the theragnostic utility of targeting Neutrophil Gelatinase Associated Lipocalin in Perihilar Cholangiocarcinoma

- Nair A, Ingram N, Verghese E, Wijetunga I, Markham A, Wyatt J, Prasad KR, Coletta PL. Targeting Vascular Endothelium in Perihilar Cholangiocarcinoma- evaluating the theragnostic potential of an anti-CD105 strategy

1 Introduction

1.1 Cholangiocarcinoma

Cholangiocarcinoma (CCA) is an aggressive cancer of the biliary tract arising from malignant transformation of bile duct epithelium (Esposito and Schirmacher, 2008). Categorized broadly into intra-hepatic (IH-CCA) and extra-hepatic (EH-CCA) forms, it is endemic in Far East Asia but assuming an increasing global relevance. With a median survival of 3.9 months from diagnosis in the absence of treatment (Park et al., 2009), the adverse outcomes for CCA are disconcerting given the increasing incidence of CCA, particularly in Western nations (Blechacz and Gores, 2008a). Hallmarks of the disease include late detection and poor prognosis, which have not been seen any significant improvements in recent decades. Resectional surgery and, on occasion, liver transplantation (Darwish Murad et al., 2012) provide the only means for cure, albeit only for a minority of cases.

1.1.1 Epidemiology

CCA accounts for 10- 15% of primary liver cancers worldwide and ranks second in incidence to Hepatocellular Carcinoma (HCC) (Blechacz and Gores, 2008a). Extra-hepatic CCA is the commoner type of this tumour and accounts for up to 90% of all CCA cases (Blechacz and Gores, 2008b).

The prevalence of CCA varies globally (Figure 1). Nations in South East Asia encounter the bulk of the disease (Shaib and El-Serag, 2004; Khan et al., 2008), reflecting regional differences in aetiological factors and pathogenesis. In the West, the incidence and mortality of IH-CCA has been shown to be on the rise whilst that
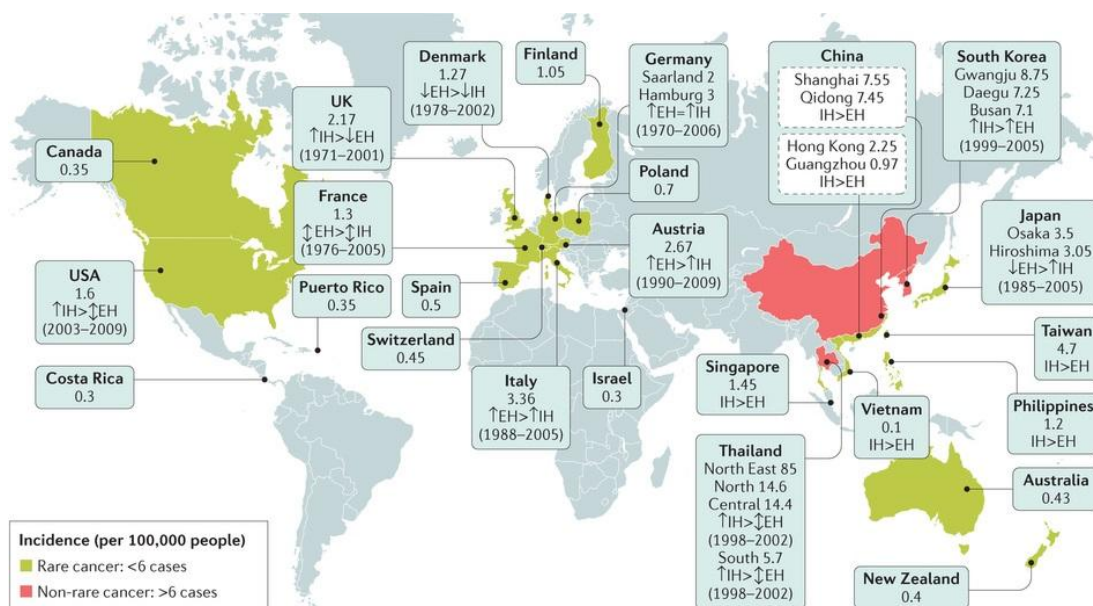
Figure 1: Worldwide incidence (per 100,000) of CCA

(From Banales et al. Expert consensus document: Cholangiocarcinoma: current knowledge and future perspectives consensus statement from the European Network for the Study of Cholangiocarcinoma (ENS-CCA). *Nat Rev Gastroenterol Hepatol* 2016;13:261–280. DOI:10.1038/nrgastro.2016.51. Used under a Creative Commons Attribution 4.0 International License (http://creativecommons.org/licenses/by/4.0/)

of EH-CCA has remained static or declined (Patel, 2002; Welzel et al., 2006; West et al., 2006; Blechacz and Gores, 2008a), for reasons that are not entirely clear (Figure 2). However, it must be noted that this phenomenon is at least in part attributable to the misclassification of peri-hilar cholangiocarcinoma (PH-CCA) as IH-CCA in the 2nd edition of the International Classification of Diseases for Oncology (ICD-O-2), issued in 1990 (Welzel et al., 2006). This error has only been partially addressed in the 3rd edition of this classification (ICD-O-3) published in 2000, which allows PH-CCA to be categorized into either IH-CCA or EH-CCA groups.

Keeping this fact in mind, data from the United States has revealed the age-adjusted incidence of IH-CCA to be increasing, with rates of 0.85/100,000 over the period 1995-99 (Patel, 2001). In the United Kingdom (England & Wales), IH-CCA incidence from 1999- 2001 was 1.33 and 1.06 per 100,000 in men and women respectively (West et al., 2006). Statistics from the Far East from 1998- 2002 show considerable heterogeneity in CCA occurrence between nations of the region. The highest rates of IH-CCA are seen in Thailand (averaging between 0.5- 8.2/100,000 across both sexes), whilst Korea has the highest incidence of EH-CCA, of 3.6 and 2.6/100,000 in men and women respectively. Nations such as China, Vietnam and Philippines have similar rates of CCA to Western countries (Shin et al., 2010a).

The mean age at presentation is 50 years worldwide, although Western data suggests a peak in the seventh decade of life (Blechacz and Gores, 2008a; Khan et al., 2008; Gatto and Alvaro, 2010). There is a male preponderance globally with between 50-60% of cases diagnosed in men (Blechacz and Gores, 2008a).

Incidence (cases/100,000) IH-CCA vs EH-CCA

		IH-CCA	EH-CCA	
China	Qidong	7.45‡	0	
	Guangzhou	0.2&	0.95&	
	Hong Kong	2&+	0.25&+	
	Shanghai	6.15&° +	1.4&° +	
Korea	Gwangiu	4.55^$	4.2^$	
	Busan	3.95^$	3.15^$	
	Daegu	4.1^$	3.15^$	Eastern countries IH > EH
Singapore		1.1&	0.35&	
Taiwan		4.1‡	0.6‡	
Thailand	Khon Kaen	51.45&	0.25&	
	Chiang Mai	6.1&	0.3&	
	Bangkok	1.95&	0.2&	
	Songkhla	1.05& ‡	0.15& ‡	
VietNam		0.1& ‡	0	
Philippines		1.1‡	0.1‡	
UK-Scotland †		1.05&	0.4&	
USA		0.58 ‡	0.88 ‡	
Italy		0.88 ‡	1.55 ‡	
Denmark		0.62#	0.65#	Western countries EH > IH
France		0.2^	1.1^	
Japan ††	Hiroshima	1.25&	1.8&	
	Osaka	1.3&	2.1&	

legend

(# = ICD-O-1)
(& = ICD-O-2)
(‡ = ICD-O-3)
(^ = ICD-10)
(° = ICD-V9)
(+ = ICD-V10)
(% = ICD-O)
† = Western Europe
†† = Eastern Asia

Abbreviations
IH=intrahepatic
EH=extrahepatic
CCA=cholangio-carcinoma
ICD=internatiomal classification of diseases
O=oncology

Figure 2: Differences in incidence of IH-CCA and EH-CCA worldwide.
(From Bragazzi et al. Cholangiocarcinoma: Epidemiology and risk factors. *Transl Gastrointest Cancer* 2012; 1:21-32. DOI: 10.3978/j.issn.2224-4778.2011.11.04). Reproduced with permission from the publisher.

1.1.2 Relevant hepatic anatomy

The liver is the largest solid organ in the body, and occupies the right upper quadrant region of the abdomen. Topographically it is demarcated into a larger right lobe and a smaller left lobe based on the attachment of the Falciform ligament to its anterior surface, and in adults the organ weighs approximately 2% of total body weight (Urata et al., 1995). The vasculature of the liver consists broadly of the portal vein and hepatic artery (comprising the hepatic inflow vessels) and three hepatic veins which provide venous drainage into the vena cava. The liver hilum is the area at which the inflow vessels branch and enter the parenchyma, and also has the bile duct with its first-order branches viz. left and right hepatic ducts running through it. This particular intimate spatial configuration of all these structures is relevant to the poor resectability rates seen in PH-CCA, as this cancer can easily involve these important inflow vessels (Figure 3).

The most popular anatomical classification of the liver is that of Couinaud, who proposed subdivision of the hepatic parenchyma into eight segments, as shown in Figure 4 (Couinaud, 1957). This particular system has the most relevance from a surgical standpoint, as each segment is supplied with its own branch of the portal vein, hepatic artery and hepatic vein.

At a microscopic level, the liver parenchyma is organised into polygonal hepatic lobules (Figure 5). These consist of sheets of hepatocytes (cords) centred on a terminal branch of the hepatic vein, called the central vein. Portal tracts, which comprise a branch of the portal vein, hepatic artery and bile duct along with lymphatics, are found at the periphery of lobules (Figure 6). In contrast, the hepatic acinus (the functional unit of the liver) consists of a portal tract at its centre and is bordered by central veins. The acinus is divided into three zones (numbered 1 to 3)
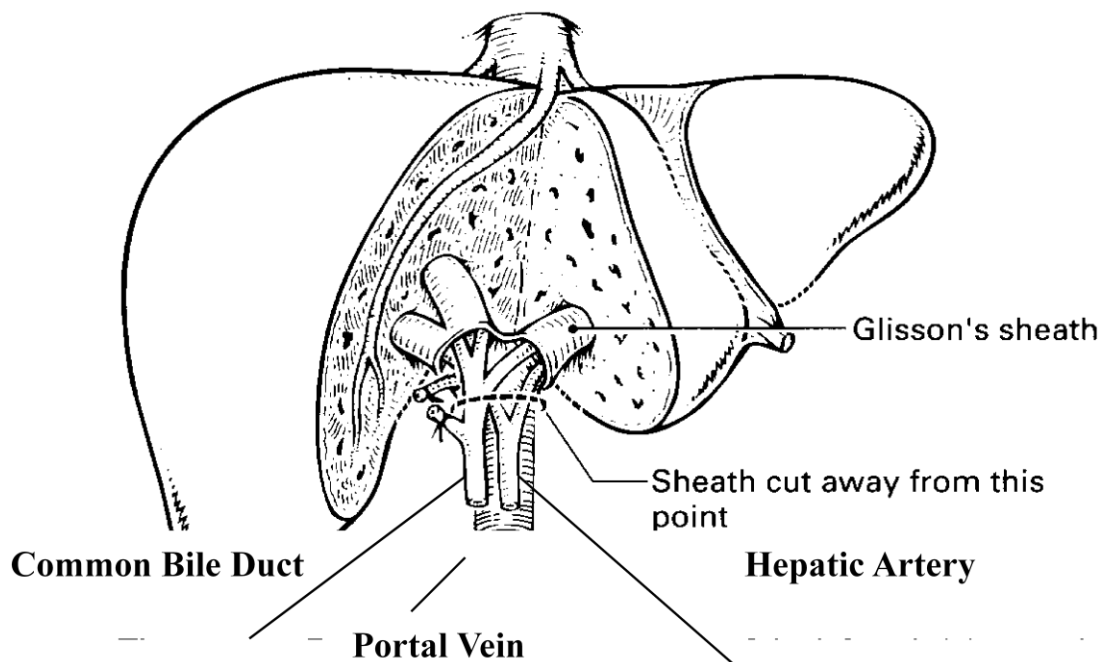
Figure 3: Cut-away section of the central portion of the liver showing the compact arrangement of structures at the liver hilum
From Chamberlain RS. *Essential Functional Hepatic and Biliary Anatomy for the Surgeon.* In Hepatic Surgery 2013, Abdeldayem H (Ed), InTech, DOI: 10.5772/53849. Used under the Creative Commons Attribution 3.0 Unported License (https://creativecommons.org/licenses/by/3.0/)
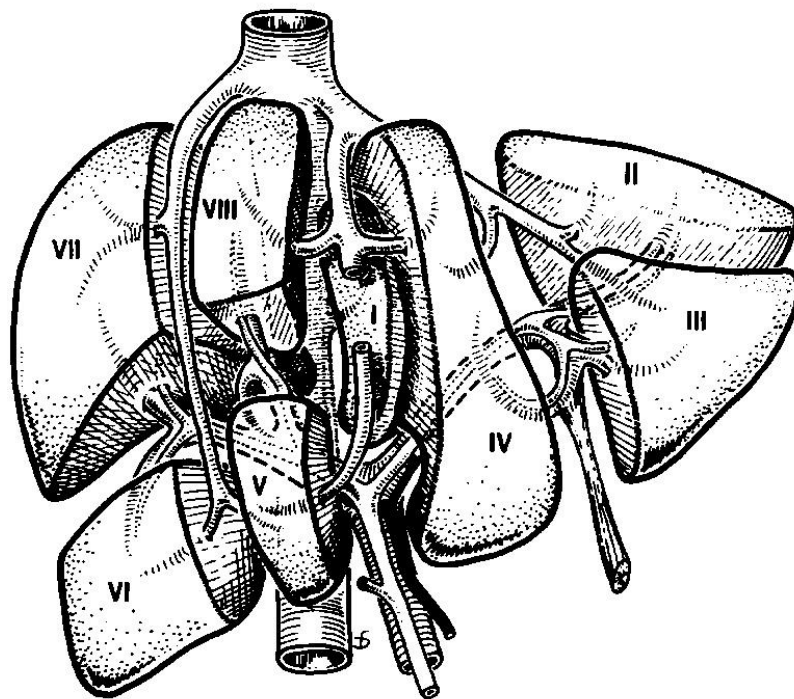
Figure 4: Couinaud's segmental anatomy of the liver
A total of eight segments are seen, each having its own branch of inflow and outflow
vessels, and biliary drainage.
From Chamberlain RS. *Essential Functional Hepatic and Biliary Anatomy for the
Surgeon.* In Hepatic Surgery 2013, Abdeldayem H (Ed), InTech, DOI: 10.5772/53849. Used
under the Creative Commons Attribution 3.0 Unported License
(https://creativecommons.org/licenses/by/3.0/)
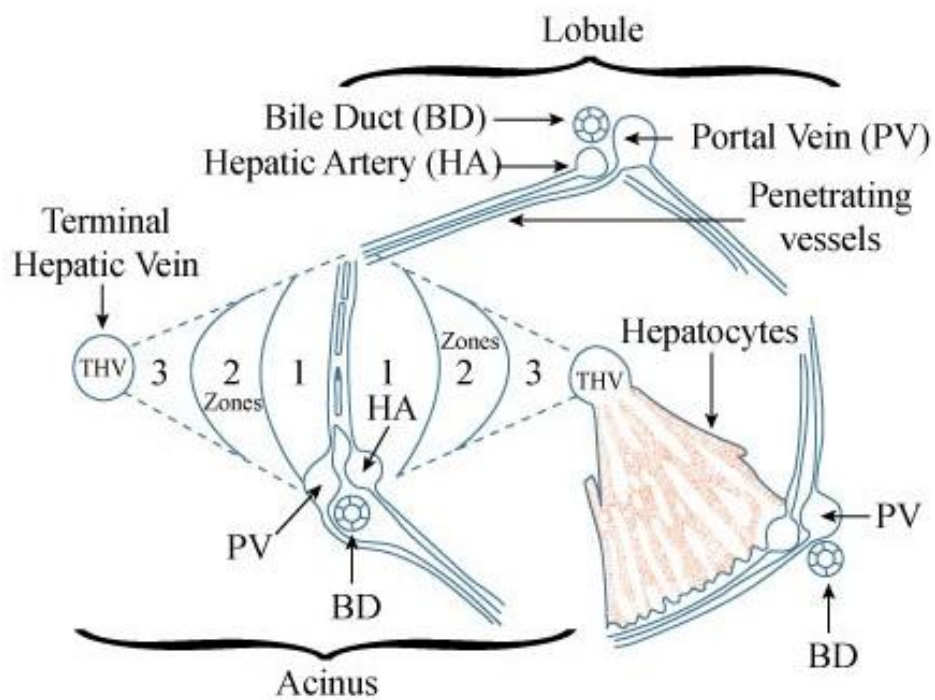
Figure 5: The functional unit of the liver
Schematic diagram showing the microscopic arrangement of liver parenchyma into a classical lobule and the functional unit termed the hepatic acinus. Hepatic parenchymal zones corresponding to periportal, mid and pericentral areas are numbered 1 to 3. Blood entering the portal tract flows along these zones in succession via endothelial cell lined channels (hepatic sinusoids) becoming progressively deoxygenated and nutrient depleted as it drains towards the central vein (Krishna, 2013)
From https://www.flickr.com/photos/mitopencourseware/3694426132 and used under the Creative Commons Attribution-Non Commercial-ShareAlike 4.0 International Public License (https://creativecommons.org/licenses/by-nc-sa/4.0/)
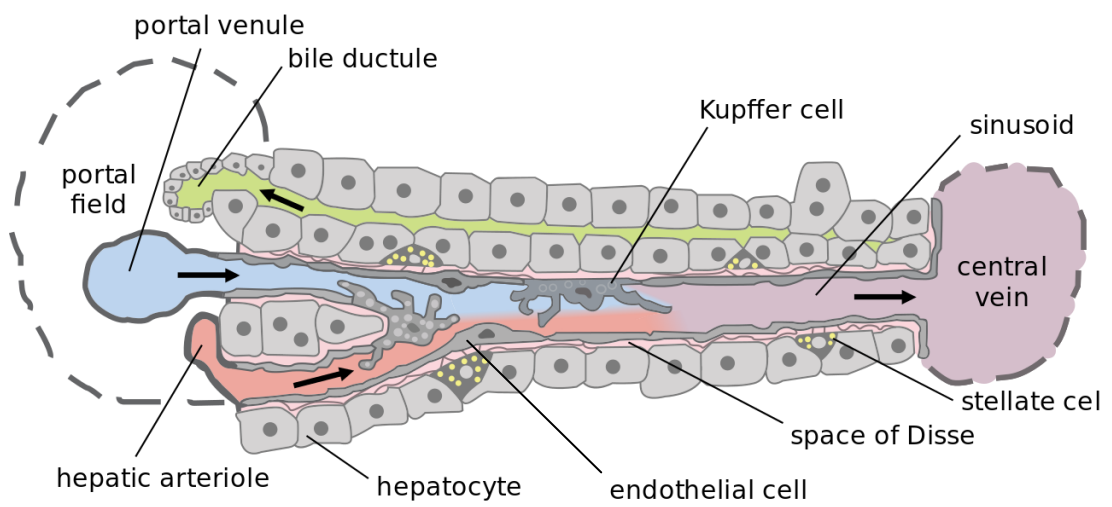
Figure 6: Microscopic arrangement of blood flow within the liver parenchyma
Diagram showing mixing of portal venous and hepatic arterial blood along the hepatic sinusoids before collecting into the central vein. A liver-specific systemically administered theragnostic agent would gain access to liver parenchyma via these sinusoids.
From https://commons.wikimedia.org/wiki/File:Hepatic_structure2.svg and used under the Creative Commons Attribution 2.5 Generic License
(https://creativecommons.org/licenses/by/2.5/)

.

1.1.3 Classification

Although CCA is classified broadly as being intra-hepatic or extra-hepatic in type, 3 topographical forms are recognised in an effort to improve clinical applicability: intra-hepatic, peri-hilar (Klatskin) and distal (Nakeeb et al., 1996; Esposito and Schirmacher, 2008; Ebata et al., 2009) as represented in Figure 7. PH-CCA has been variably defined, viz. extra-hepatic bile duct cancers within 2 cms of the common hepatic duct bifurcation (Aljiffry et al., 2009; Cardinale et al., 2010), and alternatively those actually involving the hepatic duct bifurcation (Nakeeb et al., 1996). A more contemporary definition of PH-CCA encompasses tumours proximal to the origin of the cystic duct up to second-generation tributaries of the left and right hepatic ducts (Deoliveira et al., 2011). Regardless, peri-hilar tumours are the most frequent type of CCA, accounting for 50-70% of all cases (Nakeeb et al., 1996; Khan et al., 2002; DeOliveira et al., 2007a). Approximately 20-30% of CCAs are of the distal extra-hepatic variety whereas 5-10% are within the liver (IH-CCA) (Aljiffry et al., 2009).

A popular classification for PH-CCA is that proposed by Bismuth and Corlette (Bismuth and Corlette, 1975) though this system is simplistic and does not factor in the radial spread of this tumour (Figure 8).

Figure 7:Topographical representation of all three forms of CCA
Schematic diagram showing the liver (brown borders) superimposed on
the biliary tree and gall bladder (green borders). The 3 types of CCA (IH-
CCA, brown shading; PH-CCA, blue shading; and EH-CCA, red shading)
are shown
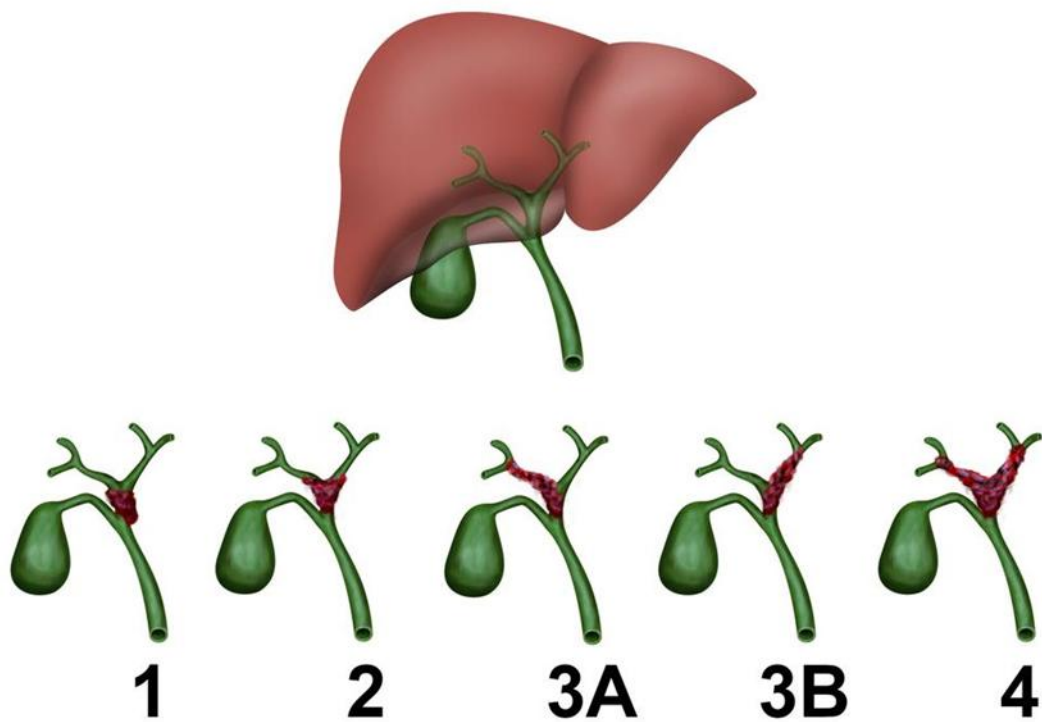
Figure 8: Bismuth-Corlette classification of PH-CCA
Type 1 tumours are confined to the common hepatic duct whereas Type 2 lesions involve the biliary confluence. Type 3 tumours are subdivided based on whether they additionally involve the right (3A) or left hepatic duct (3B). Lastly, Type 4 cancers affect the confluence and extend up both ducts. From http://radiopaedia.org/cases/diagram-bismuth-corlette-classification-of-perihilar-cholangiocarcinoma (Matt Skalski). Used under the Creative Commons Attribution-Non-commercial-Share Alike 3.0 Unported License (https://creativecommons.org/licenses/by-nc-sa/3.0/)

1.1.4 Risk factors

Common risk factors for CCA are shown in Table 1. Regional variations in aetiology exist, with the prevalent cause in South East Asia being parasitic infestations of the liver (Shin et al., 2010b). In the West, CCA shares a close association with primary sclerosing cholangitis (PSC), although around 90% of patients do not have any attributable risk factor at the time of diagnosis (Ben-Menachem, 2007). However, all risks converge to a scenario of chronic inflammation of bile ducts and biliary stasis, which appear to be the final common denominators leading to CCA development (Cardinale et al., 2010; Gatto and Alvaro, 2010).

1.1.5 Pathology

1.1.5.1 Gross Pathology

Macroscopic growth patterns of IH-CCA have been categorized into mass forming (MF), peri-ductal infiltrating (PI) and intra-ductal growth (IG) types by the Liver Cancer Study Group of Japan (Yamasaki, 2003). MF CCA tends to originate from smaller bile ducts and is hence found peripherally within the liver. In contrast, CCA arising from larger ducts (and therefore more central in location, towards the hilar region) can be of the PI, MF or IG type (Nakanuma et al., 2010). Mass forming tumours are the most common phenotypic variant of IH-CCA and have the worst prognosis too (Sirica et al., 2009). IG type CCA is the rarest of the three and carries the best prognosis following surgery.

Risk factors for development of Cholangiocarcinoma

Primary Sclerosing Cholangitis

Liver fluke infestation (Opisthorchis viverrini, Clonorchis sinensis)

Hepatolithiasis

Choledochal cysts, Carolis' disease

Hepatitis B, C

Cirrhosis

Obesity, Non-insulin dependent Diabetes

Toxins (Thorotrast)

Alcohol

Genetic polymorphisms

Surgical biliary-enteric drainage

Table 1: Risk factors for CCA
(Charbel and Al-Kawas, 2011; Tyson and El-Serag, 2011; Bragazzi et al., 2012)

MF CCA appears to the naked eye appear as firm to hard whitish masses, usually in the background of non-cirrhotic liver tissue. Satellite nodules are occasionally seen and extensive tumour necrosis is not a predominant feature (Esposito and Schirmacher, 2008). The PI variant grows axially along affected bile ducts often causing associated stricturing, whereas the IG type tends to show polypoid or papillary tumour projections into the bile duct lumen (Nakanuma et al., 2010).

EH-CCA grossly takes on a whitish, fibrotic and scarred appearance, and in the peri-hilar region invasion of adjacent liver parenchyma may be a feature. On the background of PSC, dense fibrosis may make appreciation of tumour tissue difficult outwith, although neoplastic ingrowth into the biliary lumen may be apparent on sectioning the duct.

1.1.5.2 Histopathology

Histologically CCAs are usually adenocarcinomas of varying grade, though rare variants such as squamous, mucinous and clear cell types have also been described. Background desmoplasia is often seen, as is perineural and lymphovascular invasion by tumour cells.

1.1.5.3 Spread

Local spread of CCA can occur by several routes viz. longitudinally along the bile duct, via nerve sheaths (perineural spread) and radially into adjacent structures (Esposito and Schirmacher, 2008). In IH-CCA, invasion of adjoining liver vasculature can lead to intra-hepatic metastases, whereas peritoneal dissemination may be a result of serosal involvement, especially in EH-CCA. Regional lymph

nodal metastases are encountered in excess of 30% cases (Kitagawa et al., 2001; de Jong et al., 2011b), more so with advancing tumour stage, periductal infiltrating type and poorer cell differentiation (Choi et al., 2009). Nodes in the pericholedochal region and hepatoduodenal ligament are most often the first to be involved, followed by those in the para-aortic area. Distant metastases are a late feature with reported sites including lungs, brain and bone (Choi et al., 2009).

1.1.5.4 Staging

Accurate staging of a cancer at diagnosis serves to provide individual prognostic information and guides therapy, whilst helping standardise and inform existing and future treatment protocols worldwide. Cholangiocarcinoma has varying clinical behaviour based on its location and this is reflected in the different staging systems that are in place for each subtype of this cancer.

The most widely used staging system in CCA is that proposed by the American Joint Cancer Committee (AJCC) and adopted by the Union for International Cancer Control (UICC) and is based on the characteristics of the primary tumour (T), state of regional lymph nodes (N) and the presence of metastatic disease (M), together known as the TNM stage. The latest (7th) edition of the AJCC cancer manual issued in 2009 incorporates important changes to its predecessor from 2002 with respect to CCA staging (Edge and American Joint Committee on Cancer., 2010):

- In IH-CCA, tumour size no longer contributes to T stage. Tumours breaching visceral peritoneum or invading adjacent structures are now included under T3 stage rather than T4. In the 7th edition, T4 tumours are those which exhibit features of periductal invasion.

- PH-CCA (Table 2) and EH-CCA have both been given dedicated staging systems, which is in contrast to the previous edition where they were both

Primary tumour (T)

Tx	Primary Tumour cannot be assessed
T0	No evidence of primary tumour
Tis	Carcinoma in situ
T1	Tumour confined to the bile duct, with extension up to the muscle layer or fibrous tissue
T2a	Tumour invades beyond the wall of the bile duct to surrounding adipose tissue
T2b	Tumour invades adjacent hepatic parenchyma
T3	Tumour invades unilateral branches of the portal vein or hepatic artery
T4	Tumour invades main portal vein or its branches bilaterally; the common hepatic artery; the second-order biliary radicals bilaterally; or the second-order biliary radicals unilaterally, with contralateral portal vein or hepatic artery involvement

Regional lymph nodes (N)

Nx	Regional lymph nodes cannot be assessed
N0	No regional lymph node metastasis
N1	Regional lymph node metastasis (including nodes along the cystic duct, common bile duct, hepatic artery, and portal vein)
N2	Metastasis to peri-aortic, peri-caval, superior mesenteric artery, and/or celiac artery lymph nodes

Distant metastasis (M)

M0	No distant metastasis
M1	Distant metastasis

Stage grouping

Stage 0	Tis	N0	M0
Stage 1	T1	N0	M0
Stage II	T2a/b	N0	M0
Stage IIIA	T3	N0	M0
Stage IIIB	T1-3	N1	M0
Stage IVA	T4	N0-1	M0
Stage IVB	Any T	N2	M0
	Any T	Any N	M1

Table 2: TNM staging for PH-CCA
(adapted from 7th edition of the AJCC manual)

clubbed under the label of Extrahepatic bile duct cancer. Stage IV disease in PH-CCA now denotes non-resectability, as opposed to Stage III disease in the previous version.

1.1.6 Diagnosis

1.1.6.1 Biomarkers

The lack of effective modalities to enable timely diagnosis of CCA or permit screening for the condition has led to extensive research on this front. A number of potential biomarkers (Table 3) have been identified over recent years by analysis of serum, bile and tumour tissue (Alvaro, 2009). Though many have shown potential in terms of applicability, only a minority of these markers have as yet found widespread use in clinical practice at present, with none specific for CCA.

Serum Carbohydrate Antigen 19-9 (CA 19-9) remains the most popular biomarker currently in use for CCA diagnosis (Alvaro, 2009; Gatto and Alvaro, 2010; Gatto et al., 2010). The sensitivity and specificity of CA 19-9 measurements in diagnosing CCA is however subject to wide variation, dependent on the population under scrutiny and the cut-off values assigned as significant.

In biliary obstruction, biliary levels of insulin-like growth factor-1 (IGF-1) have been shown to be 15-20 times higher in EH-CCA patients than in those with pancreatic cancer or benign biliary disorders (Alvaro et al., 2007). Encouragingly, both the sensitivity and specificity for biliary IGF-1 in diagnosing EH-CCA was 100% and in contrast, serum IGF-1 levels were comparable between these 3 groups. As yet, there have been no further studies to lend support to these findings.

Marker	Sensitivity %	Specificity %
Serum		
Carbohydrate Antigen 19-9 (CA 19-9)	53-92	50-98
Carcino-embryonic Antigen (CEA)	33-68	79-100
Interleukin-6	73	92
Bile		
CA 19-9	46-61	60-70
Carcino-embryonic Antigen (CEA)	67-84	33-80
Insulin-like Growth Factor (IGF-1)	100	100
Tissue		
Cytokeratin-7	78-100	-
Cytokeratin-19	44-80	-

Table 3: Notable biomarkers in CCA
(Alvaro, 2009; Chan and Yeh, 2010). Aggregate sensitivities and specificities for each marker are shown where available.

1.1.6.2 Imaging

A variety of imaging options are used in CCA (Table 4), reflective of the differing utilities of these modalities in diagnosing this cancer. In routine practice, Computerized Tomography (CT) and Magnetic Resonance Cholangio-pancreatography (MRCP) are mostly able to complete staging once a diagnosis has been made.

1.1.7 Treatment

1.1.7.1 Surgery

Surgical removal of the tumour offers the only means for cure of CCA and though resectability rates generally remain low, they vary from 18-70% (Morise et al., 2010). The more proximal the location of the tumour up the biliary tree, the higher the incidence of non-resectability at diagnosis (Nakeeb et al., 1996). CCA is prone to local recurrence, a phenomenon most likely explained by metastatic regional nodal disease or microscopic tumour burden at resection margins at the time of surgery. Despite surgery, clear resection margin (R_0) rates are often less than 50% (Meza-Junco et al., 2010). Therefore although much attention is currently focused on earlier diagnosis, it is paramount that negative surgical margins be achieved for optimal patient outcome.

Imaging modality	Main utility	Reference
Transabdominal Ultrasonography	Screening for cholestasis, intrahepatic lesions	(Choi et al., 2004)
Endoscopic& Intraductal Ultrasonography	Assessment of tumour size	(Garrow et al., 2007; Tamada et al., 2011)
Endoscopic Retrograde Cholangiography	Tissue biopsy, therapeutic duct decompression	(Aljiffry et al., 2009)
Cholangioscopy	Direct visualization and biopsy	(Tamada et al., 2011)
Computerized Tomography	Loco-regional & distant spread	(Vilgrain, 2008)
Magnetic Resonance Cholangiography	Tumour size	(Kaltenthaler et al., 2006)
Positron Emission Tomography	Indeterminate lesions, distant spread	(Moon et al., 2011)

Table 4: Imaging modalities in CCA and their uses

.

1.1.7.1.1 IH-CCA

The rates of resectability in IH-CCA are disappointing, ranging from 18-70% (Morise et al., 2010). As for other types of CCA, the intra-hepatic variety mandates complete excision in order to improve survival. Given the propensity for IH-CCA to have associated satellite nodules, anatomical (segmental) resections are frequently required, which also remains the need in larger tumours. The recommended width of tumour-free margin has been a matter of debate, and presently no agreement exists (Agrawal and Belghiti, 2011). However, there is consensus that microscopically negative margins be achieved (Nathan and Pawlik, 2010) and with smaller tumour size, a non-anatomical/wedge resection should therefore suffice provided this requirement is satisfied. Five-year survival rates after hepatectomy for IH-CCA are 20-40% with adverse prognostic markers including positive resection margins, nodal involvement and presence of satellite nodules. Patients with nodal metastases are at increased risk of recurrence following surgery, the remnant liver and lung being common sites for this. "Re-do" surgery may help prolong survival in these patients (Morise et al., 2010). Dissection in the region of the hepatoduodenal ligament provides a representative yield of lymph nodes and in addition to providing prognostic information, can offer survival benefit in selected patients (Agrawal and Belghiti, 2011).

1.1.7.1.2 EH-CCA

The capacity for these tumours to spread longitudinally beyond evident macroscopic margins has implications on surgical planning for resection. To enhance the prospects of a R_0 resection, current recommendations favour a 10mm gross free

margin at the time of surgery in tumours with infiltrating morphology whereas 20mm is advocated for those with mass forming or intraductal phenotype (Akamatsu et al., 2011). There is however conflict in the literature regarding the value of intra-operative frozen section analysis to assess resection margins with extra-hepatic CCA due to both poor sensitivity (Endo et al., 2008) and the questionable effect of positive margins on overall survival in this scenario (Hernandez et al., 2008; Shingu et al., 2010). Lymphadenectomy in the region of the hepatoduodenal ligament is advisable (as for IH-CCA) as it provides prognostic information and possibly some survival advantage. Extended nodal retrieval beyond this basin is not recommended, as it does not add to survival (Aljiffry et al., 2009; Akamatsu et al., 2011).

1.1.7.1.3 Perihilar CCA

Radial extension of perihilar tumours leads to invasion of liver parenchyma and structures within the hepatoduodenal ligament (portal vein & hepatic artery). Hepatic involvement necessitates liver resection, which in most circumstances implies an en-bloc caudate (segment 1) lobectomy (Agrawal and Belghiti, 2011). Extended right or left hemihepatectomy with removal of the affected extra-hepatic bile ducts is currently a standard for these tumours (Akamatsu et al., 2011). The laterality of resection is determined primarily by tumour location but also by technical ease. Right-sided resections are well suited for even central tumours and enable easier reconstructions of the remnant portal vein and biliary system (Agrawal and Belghiti, 2011; Akamatsu et al., 2011). Central (meso) hepatectomy (removal of segments 4a, 4b, 5 and 8) provides an alternative to extended resections, and lessens the risk of postoperative liver failure although technically is more demanding. Variations exist in this theme such as the 'Taj Mahal' resection, which utilises a dome shaped

incision to remove segments 1, 4a and 5 whilst allowing for relatively easier biliary reconstruction (Kawarada et al., 1999). Vessel involvement within the hepatoduodenal ligament can be managed with resection and reconstruction, though the impact of this on overall survival is currently unclear (Agrawal and Belghiti, 2011). Survival statistics indicate that hepatectomy and bile duct excision for hilar CCA provides 20-42% survival at 5 years (Akamatsu et al., 2011). Detrimental prognostic factors include increasing depth of tumour invasion into bile duct wall, poorer tumour differentiation (de Jong et al., 2011a) and nodal involvement.

1.1.7.1.4 Distal EH-CCA

Obtaining negative surgical margins usually implies resorting to Whipple's resection/ pancreaticoduodenectomy for distal CCA, as opposed to segmental bile duct excision alone. Five-year survival following pancreatoduodenectomy in this situation ranges from 16-52% (Akamatsu et al., 2011).

1.1.7.2 Transplantation

The results of orthotopic liver transplantation (OLT) in CCA has improved with the institution of dedicated protocols in well-selected patients (De Vreede et al., 2000). Historically associated with discouraging results due to early tumour recurrence in up to 80% of patients (Petrowsky and Hong, 2009) and poor long-term survival of 10-20% at 5 years (Aljiffry et al., 2009), OLT in CCA is currently the remit of specialised centres that can offer both appropriate neoadjuvant treatment and surgical expertise. Stage I/II intrahepatic and hilar CCA that are not resectable would normally be considered candidates for OLT in this setting. Patients with early

stage CCA on a background of PSC with risk of multi-focal tumours lend further support to transplantation (Grossman and Millis, 2010). Local criteria precluding resectability are bilobar disease, bilateral hepatic artery/portal venous involvement, suboptimal future liver remnant (with poor response to pre-operative portal vein embolization) and additionally in the case of hilar tumours, unilobar disease with involvement of contralateral vasculature (Petrowsky and Hong, 2009). Factors such as peritoneal disease, regional nodal involvement and distant metastases rule out OLT. Appropriate neoadjuvant options include external beam radiation, chemotherapy and intraluminal brachytherapy (Grossman and Millis, 2010). With the institution of such regimes in carefully selected patients, survival rates of 80% at 5 years are achievable (Aljiffry et al., 2009; Grossman and Millis, 2010). The prognosis for incidentally detected CCA on explants following OLT for other indications is variable, with a focus on reducing the intensity of immunosuppression vital to reduce the risk of recurrence (Petrowsky and Hong, 2009).

1.1.7.3 Adjuvant treatment

There is currently no convincing evidence to suggest adjuvant therapy (using chemotherapeutic agents, radiation or both) has an effect on improving survival following successful resection (Ramirez-Merino et al., 2013).

1.1.7.3.1 Radiation

External beam radiation has variable results after resection of CCA, though at present it is thought to be more beneficial in those who have microscopic remnant disease after surgery. A contemporary meta-analysis of relevant observational studies has revealed an overall survival pooled hazard ratio of 0.62 (95% CI 0.48–

0.78) in favour of adjuvant radiation versus observation alone in EH-CCA, suggesting that these patients would benefit from the former (Bonet Beltran et al., 2011). Most subjects in this group however had positive resection margins and/or lymph node metastases. In IH-CCA, data from a large retrospective series has suggested that overall survival is significantly improved with the institution of post-operative radiation, although information regarding resection margins was not available to the investigators (Shinohara et al., 2008).

1.1.7.3.2 Chemotherapy

Improved survival outcomes at 5 years have been reported from retrospective data following administration of intravenous gemcitabine and S-1 (an oral fluoropyrimidine) chemotherapy when compared to observation alone following resection of extra-hepatic biliary carcinomas (Murakami et al., 2009). In contrast, a prospective randomized trial examining a regime consisting of mitomycin C and 5-fluorouracil showed no significant survival benefit for these agents following surgery for patients with bile duct cancer, although it did prove useful to those with gall bladder carcinoma (Takada et al., 2002). Both these studies did not segregate patients for chemotherapy based on surgical margins or nodal status. The impact of capecitabine after attempted curative resection of biliary tract cancer is being analysed in a randomized, prospective fashion in the United Kingdom currently (BILCAP study), which completed patient recruitment in 2014 (Vazquez and Bridgewater, 2011).

1.1.7.3.3 Chemoradiation

Not surprisingly, there is lack of rigorous evidence to support the use of adjuvant chemoradiation following resection of CCA. Retrospective data on small numbers (n=34) supported the use of concurrent 5-fluorouracil therapy and radiation in the adjuvant setting following pancreatoduodenectomy for distal bile duct cancers (Hughes et al., 2007). The improved survival in this study was seen in comparison to historical controls and was present irrespective of nodal status. Older statistics have also indicated better survival following adjuvant chemoradiation compared to observation alone in patients with CCA (n=92), achieving statistical significance in those with distal tumours (Serafini et al., 2001).

1.1.7.4 Palliation

Surgery remains the only means for cure in CCA and in the absence of the former, treatment is essentially palliative. Though options for palliation are many, the choice of optimal therapy remains frequently centre specific due to the sparse level-1 evidence and recommendations in this domain.

1.1.7.4.1 Radiation

The effect of brachytherapy (using ^{192}Ir) in the palliation of CCA has been addressed in studies albeit mostly with smaller sample sets and in conjunction with external beam radiation. The value of brachytherapy alone in extending survival is questionable with data to show both benefit and lack thereof (Chen et al., 2004; Shinohara et al., 2010). It is however thought to extend the patency of biliary metal stents by preventing tumour ingrowth. Newer modalities such as radioembolization

utilising Yttrium-90 microspheres are currently gaining credence in the palliative treatment of IH-CCA, with possible improvement in life expectancy (Ibrahim et al., 2008; Hoffmann et al., 2011). Taking into account all modalities of radiation treatment, there appears to be some survival benefit to its use in advanced or unresectable CCA, with studies noting an improvement in median survival from 4 months in the absence of any treatment to 9-11 months with radiation alone (Shinohara et al., 2009; Shinohara et al., 2010). The risk for potential local toxicity including cholangitis, duodenal stenosis, bowel obstruction and gastrointestinal bleeding must however be considered in these situations.

1.1.7.4.2 Chemotherapy

Palliative chemotherapy now has an established role in advanced CCA, combination treatment with Cisplatin and Gemcitabine offering good response rates and tumour control (Eckel and Schmid, 2007). Multi-centre phase-3 prospective randomized data from the contemporary Advanced Biliary Cancer (ABC)-02 trial has revealed improved progress free survival and an overall survival advantage (8 months vs. 5 months) to patients receiving combination therapy with these same agents in comparison to monotherapy with Gemcitabine (Valle et al., 2010). More recently there has been phase-2 trial data to highlight the potential for targeted treatments in advanced CCA. The incorporation of Bevacizumab (a monoclonal antibody against Vascular Endothelial Growth Factor [VEGF]-A) into a regime containing Gemcitabine and Oxaliplatin (GEMOX) showed the combination to have an acceptable side effect profile whilst showing stable or improved tumour burden (as evidenced on combined Positron Emission Tomography-CT imaging) in 69% of the tested patient cohort (Zhu et al., 2010). In another phase-2 study, the epidermal growth factor receptor inhibitor Cetuximab was similarly combined with GEMOX to

give good response in 63% of the tested group. Notably 30% of this cohort subsequently had potentially curative surgery in light of their response to treatment (Gruenberger et al., 2010).

1.2 Targeted Diagnostics and Drug Delivery in Solid Cancers

Since the advent of Nitrogen mustards following the 2nd World War as a primary systemic treatment for lymphomas, much progress has been made into the therapy and control of various cancers (DeVita and Chu, 2008). Adjuvant chemotherapeutic regimens came in to the fore with breast cancers in the 1970s before this concept was expanded to the treatment of other solid malignancies. The realization that systemic chemotherapeutic agents exert their effects on non-cancerous normal tissue with consequent side effects has been a significant factor driving research into identifying targeted strategies. Such an approach also offers the possibility of specific and enhanced treatment delivery to target tissue thus improving therapeutic efficacy.

The discovery of signalling pathways involved in both carcinogenesis and normal cellular activity were made through the efforts of the Special Virus Cancer Program in the 1970s and its subsequent incarnation as the Program of Molecular Biology. This laid the foundations for targeted molecular therapies (Morrison, 2010). Monoclonal antibodies were produced in the 1990s with the anti-CD20 antibody Rituximab proving to be the first such therapeutic antibody approved for the treatment of cancer, specifically lymphoma (Vacchelli et al., 2014). Another early example of the efforts into targeted cancer treatment was the drug Imatinib mesylate, a tyrosine kinase inhibitor used in the treatment of Chronic myelogenous leukemia (DeVita and Chu, 2008).

There has been recent focus on increasing the specificity of management approaches to solid cancers including CCA in order to increase diagnostic accuracy and treatment efficacy whilst minimizing side effects. The two main avenues of research in this respect are related to targeted drug delivery and development of targeted signalling pathway inhibitors.

The premise that tumour blood vessels are unique to and differ from their normal counterparts has stimulated much research into this field with a view towards preferentially targeting the former. Tumour tissue is additionally the seat of accelerated angiogenesis with the formation of new vessels that aid tumour growth and invasion. A variety of molecules have accordingly been devised (Klotz et al., 2012), some of which have reached human trials/clinical application as summarized in

Table 5 and Figure 9.

Molecule	Type	Angiogenic targets	Applications
Bevacizumab *(Avastin)*	Humanized IgG$_1$ Monoclonal antibody	VEGF	Colorectal, Renal & Hepatocellular cancers
TRC105	IgG$_1$ monoclonal antibody	CD105	Phase I/II trials in advanced solid cancers
AMG 386 (Trebananib)	Peptide-Fc fusion protein	Tie-2 receptor	Phase II/III trials in recurrent ovarian cancer
Sorafenib			Hepatocellular Cancer
Sunitinib	Small molecule; Tyrosine kinase inhibitor	VEGFR 1,2,3 PDGFR-β	Renal & Hepatocellular Cancer, Gastrointestinal stromal tumours
Pazopanib			Renal Cell Carcinoma

Table 5: Angiogenic inhibitors in clinical use
VEGFR- Vascular Endothelial Growth Factor Receptor, PDGFR- Platelet Derived Growth Factor Receptor.
(Weis and Cheresh, 2011; Eroglu et al., 2013; Paauwe et al., 2013)
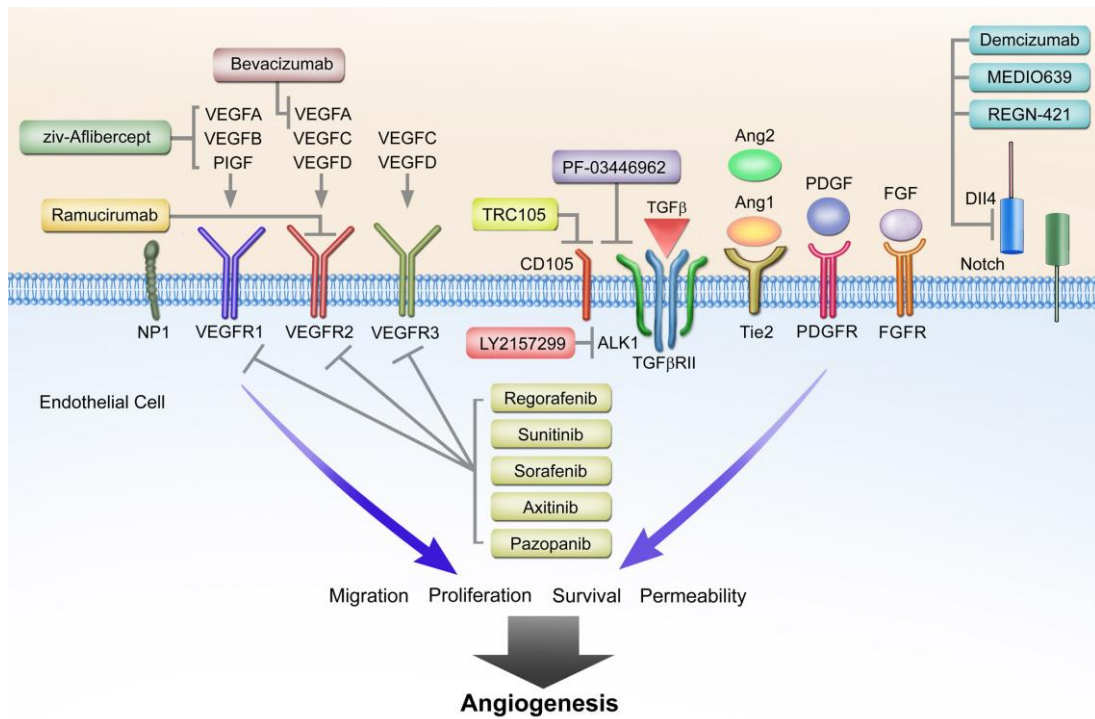
Figure 9: An overview of membrane receptors mediating angiogenesis and their inhibitors

Depiction of VEGF and non-VEGF mediated angiogenic membrane receptors, their ligands (circles) with drugs that can block their actions (rectangles). VEGF(R)- Vascular Endothelial Growth Factor (Receptor), PDGF(R)- Platelet Derived Growth Factor(Receptor), FGF(R)- Fibroblast Growth Factor(Receptor), Ang- Angiopoietin, TGF(R)- Transforming Growth Factor (Receptor),NP- Neuropillin, ALK- Activin Receptor-like Kinase.
(From Clarke JM and Hurwitz HI. Understanding and targeting resistance to anti-angiogenic therapies. *J Gastrointest Oncol*. 2013; 4: 253–263. DOI: 10.3978/j.issn.2078-6891.2013.036). Reproduced with permission from the publisher.

1.2.1 CD31

CD31 is a 130kDa transmembrane glycoprotein receptor, also termed Platelet Endothelial Cell Adhesion Molecule (PECAM)-1 is ubiquitous to vascular endothelium where it is a component of endothelial intercellular junctions. The molecule is therefore considered more of a vascular marker and provides an index of angiogenesis, rather than a target. It is also present on the surface of non-erythroid haemopoietic cells such as macrophages, monocytes, platelets and neutrophils. CD31 is believed to play a vital part in the maintenance of normal vascular integrity, whereas during the inflammatory cascade it promotes leucocyte migration from the circulation into tissues. Separate to these functions, CD31 has also been shown to serve a crucial role in angiogenesis by hastening endothelial cell migration, intercellular junctional development and capillary formation. Its abilities to prevent platelet activation and stimulate vessel prostacyclin production further aid in its regulatory role in vascular homeostasis (Privratsky and Newman, 2014).

In immunohistochemistry (IHC) studies, CD31 has earned its reputation as a pan-endothelial marker and is frequently used as the reference standard or denominator (along with markers such as CD34) against which other angiogenic markers are assessed in tumour tissue. It is not without its drawbacks nonetheless (Nico et al., 2008). As indicated above, it is not specific for vascular endothelium, and shows affinity for peri-vascular stromal tissue. The distribution pattern of CD31 within normal liver tissue shows it to be in abundance, with hepatic sinusoids, centrilobular veins, portal venules and arterioles all showing strong positivity to the marker (Pusztaszeri et al., 2006). Additionally, the marker is not able to distinguish between proliferating and mature endothelium (Nico et al., 2008).

The prognostic impact of CD31 expression in cholangiocarcinoma has been examined in some detail in prior publications. Thelen and associates assessed CD31 microvessel density (MVD) in 60 cases of resected PH-CCA and divided patients into 2 groups based on a seemingly arbitrary MVD cut-off value of 20. They found a higher incidence of nodal metastases and local recurrence in those tumours with a higher MVD, which also translated into a significantly poorer overall survival (OS) and disease-free survival (DFS) in this cohort (Thelen et al., 2008). The same authors in a subsequent paper examined CD31 expression in 114 cases of intra-hepatic CCA and following stratification of patients based on a mean MVD value of 12.6, found higher T stage tumours, R1 (positive margin) resection rates and recurrence in those with higher MVD. Interestingly, in this scenario high MVD had no bearing on nodal metastases, though it retained an independent adverse prognostic effect on OS (Thelen et al., 2010).

1.2.2 Vascular Endothelial Growth Factor Receptor-2

VEGF is integral to vessel development in both normal and tumour tissue. The VEGF family consists of A, B, C and D subtypes of which VEGF-A is considered to be the rate-limiting factor in angiogenesis whereas VEGF-C & D are involved in lymphangiogenesis (Ferrara et al., 2004). VEGF-A is expressed by endothelial cells and tumour tissue but is also secreted and bound to the extracellular matrix in significant amounts. The actions of this molecule are exerted through 3 of its tyrosine kinase receptors (VEGFR1, 2 and 3). Vascular Endothelial Growth Factor Receptor-2 (VEGFR2) is thought to be more relevant to the angiogenic and mitogenic actions of VEGF-A though not exclusive to it. VEGFR3 mediates the actions of VEGF-C and D on lymphatic endothelium.

Current evidence supports the fact that VEGFR2 & 3 are overexpressed on tumour endothelium of various solid cancers, compared to corresponding normal tissue (Smith et al., 2010). In EH- and IH-CCA, studies have shown VEGF-A expression to be increased though not to any prognostic level (Tang et al., 2006; Mobius et al., 2007). Nonetheless, as discussed earlier, when combined with standard chemotherapeutic agents in the treatment of advanced biliary cancer in a phase-II trial, the monoclonal antibody to VEGF Bevacizumab has shown some degree of anti-tumour activity (Zhu et al., 2010).

1.2.3 CD105

CD105 (Endoglin) is a 180kDa transmembrane glycoprotein receptor present mostly in vascular endothelium, and to a lesser degree in vascular smooth muscle/stroma, tissue macrophages and erythroid precursors (Fonsatti and Maio, 2004). The molecule forms part of the cell surface receptor complex to Transforming Growth Factor (TGF) - β1 and β3, where it modulates signalling of the latter. CD105 is induced in hypoxic conditions, and counteracts the anti-angiogenic actions of TGF-β1. Thus in the relatively ischaemic confines of tumour tissue, CD105 is understood to play a vital role in promoting angiogenesis (Duff et al., 2003). The mechanisms accounting for its actions on vasculature are in part due to the positive modulatory effects of CD105 on endothelial Nitric Oxide synthase and Cyclooxygenase-2 expression (Dallas et al., 2008; Fonsatti et al., 2010). CD105 is also believed to possess cellular functions independent of its actions via the TGF-β1 pathway, including protection of endothelial cells against apoptosis under hypoxic stress conditions (Fonsatti and Maio, 2004).

In contrast to pan-endothelial markers such as CD31 and CD34, CD105 is thought to be specific for immature or proliferating ("activated") endothelium (Dallas et al., 2008; Fonsatti et al., 2010). Accordingly, the marker has been purported to be the most specific for tumour vasculature, though this view is not entirely accurate as indicated above.

Discrepant staining patterns of various CD105 monoclonal antibodies on both normal and tumour tissue have been noted in the literature, and have been attributed to the several distinctive epitopes of the receptor that react to different monoclonal antibodies (Duff et al., 2003; Fonsatti et al., 2010). This finding bears relevance when designing a relevant theragnostic model as all relevant epitopes must be tested to strike an optimal balance between adequate tumour targeting and minimal off-target effects on normal tissues (Fonsatti and Maio, 2004).

There is an abundance of literature looking into the expression of CD105 in various solid cancers including adenocarcinomas of the upper digestive tract, colon, breast and prostate, and most show an association between higher tumoral CD105 MVD and metastasis and poorer OS (Dallas et al., 2008). In terms of hepatic malignancy a few reports have delved into CD105 expression in hepatocellular carcinoma but none into CCA. Yang et al from China examined the impact of CD105 expression in 113 HCC specimens utilising the SN6h clone of mAb. It was found that there was absent expression of the marker in all non-tumourous tissue and CD105 carried a prognostic impact on OS (Yang et al., 2006). Predating this was a report by Ho and colleagues who scrutinised the expression pattern of CD105 in 86 cases of resected HCCs and found disparate results. A lower CD105 MVD score correlated with larger tumour size (>5cms), higher tumour stage and tumours with venous invasion. No prognostic effect was noted with tumoural CD105 expression on this occasion and the authors also noted a diffuse CD105 staining pattern in peri-tumoural liver tissue (in 23% of cases) that was associated with increased risk of recurrence. Though the

reasons for this phenomenon were not clear, it was noted that HCCs develop on the background of chronic liver disease and cirrhosis, where angiogenesis is expected to be active (Ho et al., 2005). This latter observation was confirmed in a separate study that analysed CD105 expression in 3 distinct areas of 64 resected HCC specimens (tumour tissue, peri-tumoural and distant liver >5cms away) as well as normal non-diseased liver controls. These authors showed diffuse CD105 positivity in hepatic sinusoidal cells of the peri-tumoural and distant liver groups but not so in normal controls, where expression was seen only in hepatic sinusoidal cells adjacent to portal tracts. CD105 protein was in fact found to be significantly increased in peri-tumoural and distant liver compared to tumour tissue, and it was therefore opined that in the presence of background liver disease such as cirrhosis, anti-angiogenic therapy using CD105-based approaches may not be beneficial due to off-target effects. The observation of increased CD105 expression in peri-tumoural tissue has also been noted elsewhere, in this instance both in the case of HCCs and liver metastases (Nakamura, 2009), and the injury and regeneration of hepatocytes in this region is believed to be the cause. These findings were mirrored in more recent papers that have shown CD105 expression to progressively decrease from regenerative nodules through dysplastic nodules to small HCCs (Paschoal et al., 2014; Segatelli et al., 2014).

The feasibility of a tumour imaging platform utilising CD105 has been long established in various pre-clinical studies. In one of the first such reports dating back to 2000, one group showed that intravenously administered radiolabelled CD105 antibody highlighted spontaneous mammary cancers in 2 canine subjects, with no adverse effects related to the agent during 3 months of follow up (Fonsatti et al., 2000). In a similar study, Bredow and associates utilized a radiolabelled monoclonal antibody to CD105 to demonstrate tumour localization in a mouse model of melanoma (Bredow et al., 2000). More recently, the use of a CD105-based

MB tumour imaging system to monitor response to treatment was described by Korpanty and colleagues (Korpanty et al., 2007). They used MBs coated with antibody to CD105 to demonstrate diminished tumour vascularity (as evidenced by lower video intensity on US) as a result of Gemcitabine treatment in a pancreatic murine xenograft model. These findings were confirmed by lower MVD scores in harvested xenograft tissue.

In terms of clinical translation, the results of human Phase 1 trials using the monoclonal CD105 antibody TRC105 have been reported recently (Rosen et al., 2012). Fifty patients with various types of advanced solid malignancy not amenable to any curative therapy were recruited into the study, and further to treatment improved or stable disease was observed in 47% of subjects. Notable side effects of therapy included hypo-proliferative anaemia and cutaneous telangiectasia. Overall, grade 3 adverse reactions were seen in 3 patients.

1.3 Applications of Tumour Targeted Treatments and the Development of Novel Drug Delivery and Diagnostic Particles

The development of nanoscale particles and the physical and biological attributes of these molecules *in vivo* have allowed the investigation of new approaches to the management of various pathophysiological processes including cancer.

1.3.1 Microbubbles

Microbubbles (MBs) are micron-sized (2-5μm) encapsulated gas bubbles comprising an outer stabilizing shell and an inner gaseous core (Deshpande et al., 2010). The inherent ability of MBs to remain confined to the circulation after systemic injection (due to their size) coupled with their acoustic reflectivity render them useful as intra-vascular ultrasound contrast agents. Additionally, the physicochemical properties of MBs allow them to maintain their physical integrity within the circulation yet they exhibit structural instability and leakage when exposed to a suitable trigger. This property of MBs is harnessed in targeted applications where they are coated with various payloads (such as drugs) on their surface. These payloads can then be released into tumour specific circulation upon the topical application of a MB-destructive regional ultrasonic pulse to the area of tumour. Thus MBs have the potential to simultaneously aid in diagnosis and therapeutics (theragnosis) and this is a field that has generated much interest in recent years.

Methods of MB production involve processes such as mechanical agitation, agitation utilising ultrasound frequencies (sonication) or the use of microfluidic devices (Kiessling et al., 2012; Peyman et al., 2012). MB shells are made of varying materials including albumin, polymers or phospholipids, whereas the gaseous centre consists typically of a mixture of high molecular weight inert gases (such as perfluorocarbon [PFC] or sulphur hexafluoride) and air (Deshpande et al., 2010). This gas mixture at the core of MBs confers them with their unique ultrasound characteristics and provides them with physical stability *in vivo*. The use of too high a concentration of air leads to MB collapse due to diffusion of nitrogen away from its core, whereas an excess of inert gas promotes core liquefaction leading to shrinkage (Ibsen et al., 2013). However, nanoscale dimension MBs (less than 1.5 µm size, termed micro/nanobubbles) are also being developed and can carry molecules such as oxygen beyond most capillary beds directly into tissue (Matsuki et al., 2014).

The circulatory half-life of conventional unbound MBs is to the order of 3-15 minutes. This period can be prolonged by instituting measures such as coating the MB shell with polyethylene glycol (PEG), which prevents the bubbles from coalescing within the circulation (steric protection). Enhancing circulatory time in this fashion allows more passes of MBs through tumour vasculature and augments the potential for these agents to exert more therapeutic effect. MB clearance is effected by the reticulo-endothelial system viz. the liver and spleen (Ibsen et al., 2013). A relevant concern in this regard is the potential for off-target effects once unused MBs are degraded and metabolised in these organs.

Cellular targeting using MBs can involve 2 distinct processes. Passive targeting makes use of MB shell properties to help localize them to cells or tissues of interest eg. albumin shells attract the binding of leucocytes (Kiessling et al., 2012) and can

help them localize to areas of inflammation. Alternatively, active targeting refers to the use of specific targeting ligands (to vascular endothelium) attached to the MB shell through covalent or non-covalent means. The diagnostic capabilities of MBs arise from their acoustic reflectivity under ultrasound (US) insonation once they are bound to specific antigens in the area of interest through the use of targeting ligands. On the other hand, the therapeutic potential afforded by MBs stems from the physiological effects of ultrasonic waves on MBs. At the high acoustic pressures (mechanical index >0.4) created by ultrasound, circulating MBs in the field begin to oscillate and ultimately burst or implode, causing cavitation and micro-jet formation (Figure 10). These processes release any attached payload from MBs into the immediate vicinity. In addition, these processes and the resulting fluid microstreaming in the surrounding blood leads to transient changes in vascular endothelium and cell membranes, a phenomenon termed sonoporation. Vascular and cell permeability is increased through sonoporation driving MB payloads intracellularly, where they can exert their effects (Smith et al., 2011; Ibsen et al., 2013) as shown in Figure 11.

Enabling MBs with targeting capability involves attaching specific vascular ligands to their shells. This process traditionally involves utilising linker molecules such (Strept)Avidin (on the MB shell) and Biotin (on the antibody). Avidin is a protein ubiquitous in egg white whilst its bacterial equivalent Streptavidin is found in *Streptomyces avidinii*. Both these proteins carry 4 binding sites per molecule for Biotin (Vitamin B7) and this non-covalent interaction is characterised by its high degree of stability and strength (Diamandis and Christopoulos, 1991), rendering them useful in MB targeting applications (Figure 12). This interaction is not without
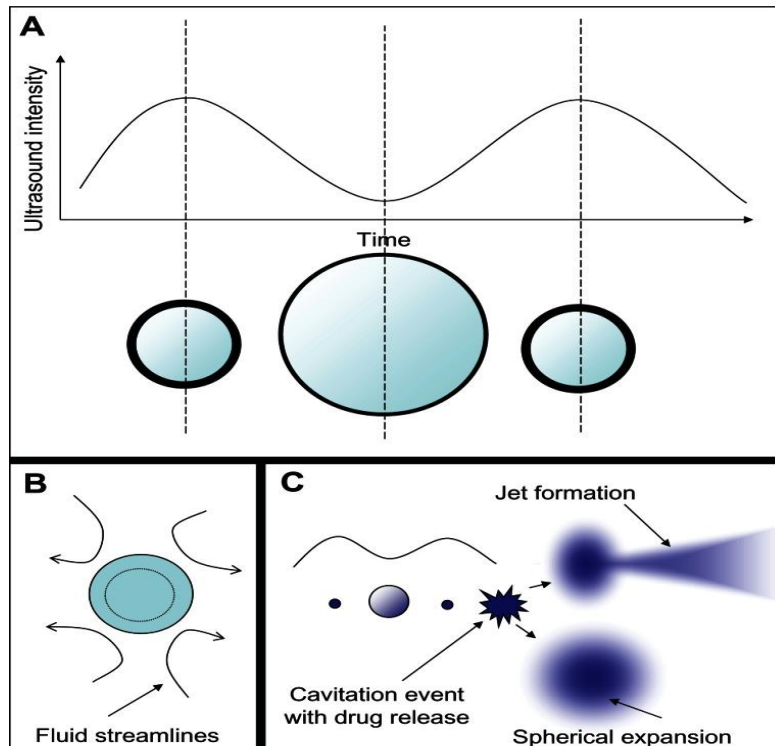
Figure 10: Effects of therapeutic ultrasound (US) application to intravascular microbubbles (MBs)

Panel A showing the shrinkage and expansion of MBs during the compression an rarefaction phases respectively of an incoming US wave. Panel B- Fluid streamlines are produced around MBs due to changes in MB diameter when exposed to US, which aid in sonoporation. Panel C displays the direct consequences of MB lysis under the effects of US.

Taken from Ibsen et al. Microbubble-mediated ultrasound therapy: a review of its potential in cancer treatment. *Drug Des Devel Ther*. 2013; 7: 375–388. doi: 10.2147/DDDT.S31564. Used under the Creative Commons Attribution - Non Commercial (unported, v3.0) License (https://creativecommons.org/licenses/by-nc/3.0/)
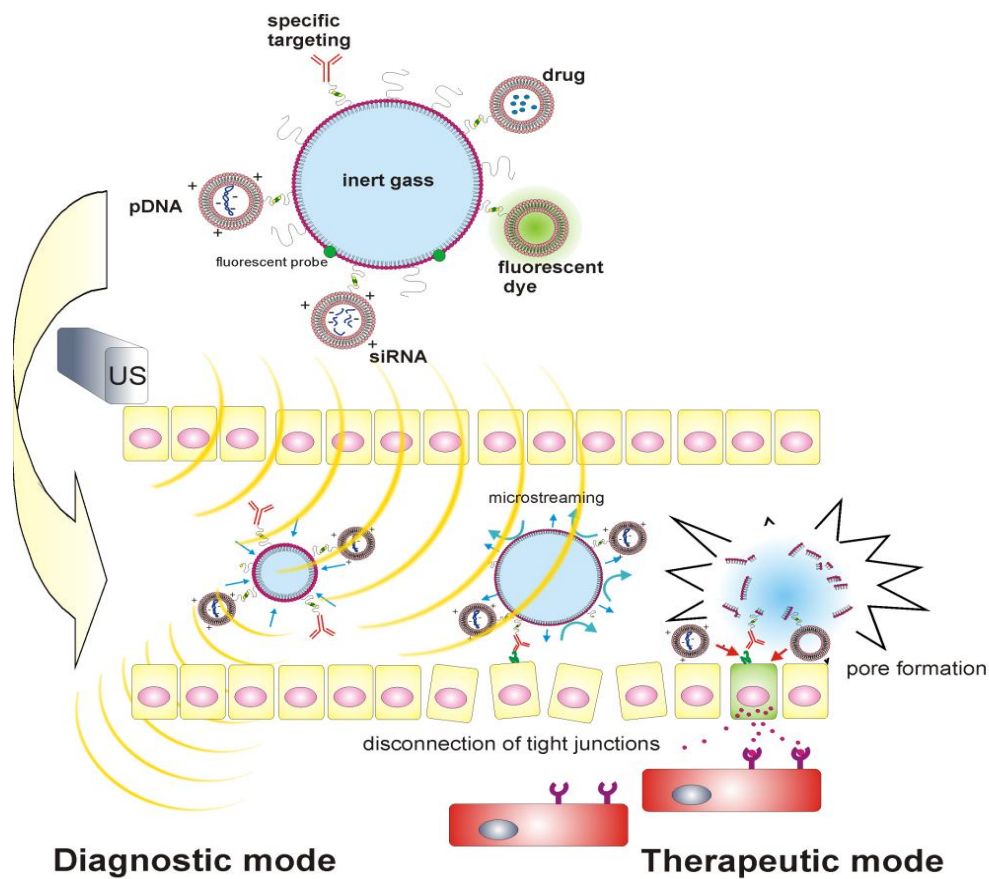
Figure 11: Payload delivery using microbubbles
Upper panel showing various possible payloads for MBs. Lower panel illustrating how payloads can be driven into target tissue under the influence of therapeutic mode US. Modified from Turánek et al. *Lipid-Based Nanoparticles and Microbubbles – Multifunctional Lipid-Based Biocompatible Particles for in vivo Imaging and Theranostics.* In Advances in Bioengineering 2015, Serra P (Ed), InTech, DOI: 10.5772/59870. Used under the Creative Commons Attribution 3.0 Unported License (https://creativecommons.org/licenses/by/3.0/)
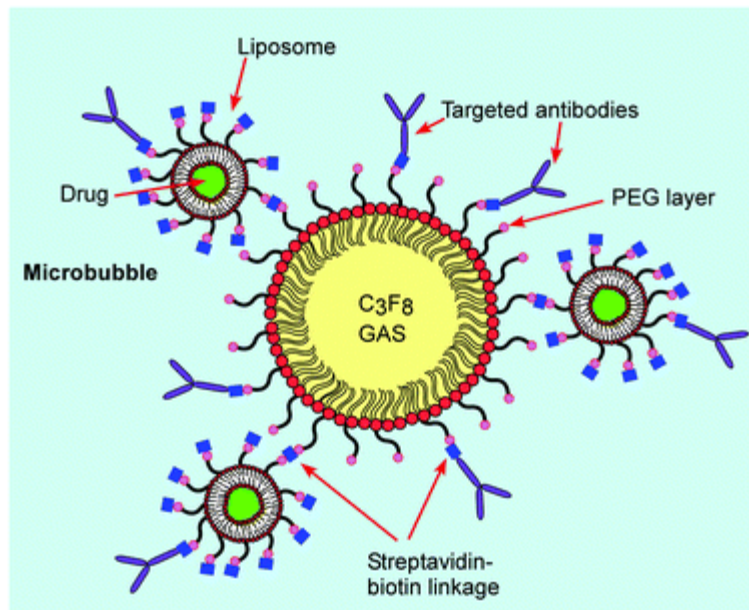
Figure 12: Microbubble structure with targeting ligands and payloads
Diagram of a targeted lipid shell MB showing the utility of avidin-biotin linkages in aiding the attachment of theragnostic payloads such as drug containing liposomes or antibodies. Taken from Peyman et al. Expanding 3D geometry for enhanced on-chip microbubble production and single step formation of liposome modified microbubbles. *Lab Chip*, 2012;12: 4544-4552 DOI: 10.1039/C2LC40634A. Reproduced with permission from the publisher.

its disadvantages though, and the main drawback of this system is the inherent immunogenicity of (Strept)avidin in humans, which limits its *in vivo* use. Alternative bio-conjugation strategies have been explored as a result and show promise, including maleimide-thiol conjugation (Yeh et al., 2015).

Conventional MBs are largely well tolerated in their current clinical applications though reported side effects include hypersensitivity, allergic reactions, embolic events and microvascular damage (Kiessling et al., 2012). In terms of targeted applications, progress has been made into the clinical setting with a recently completed trial of VEGFR2 directed MBs (BR55) in patients with prostate cancer prior to surgery, although the results of this study are still pending. Histopathological and Immunohistochemical examination of resected specimens will reveal if pre-operative imaging with BR55 bears correlation with areas of VEGFR2 expression in tumours (Willmann).

1.3.2 Nanoparticles and Nanomedicine

Nanotechnology in the field of medicine refers to the use of biological materials in the nanoscale dimension i.e. typically <100nm size. Within the scope of cancer therapeutics, nanotechnology is an attractive proposition on account of the Enhanced Permeability and Retention (EPR) effect exhibited by tumour endothelium. This endothelium is often aberrant and leaky with gaps between cells ranging several hundred nanometers (Wang et al., 2012). In addition, tumour lymphatics are frequently defective leading to impaired clearance of substances from the interstitium. These 2 phenomena allow nanoparticles (NPs) to selectively accumulate within tumour tissue (passive targeting) when compared to other macromolecules. However, only around 5% of a total administered dose localises to

tumour in this fashion (Bae and Park, 2011). In contrast, active targeting of NPs refers to ligand-mediated selectivity and enables an added level of homing in of payloads to target tissue. NPs can be coated with a target specific ligand that imparts additional targeting capacity to these molecules. Ligands used in this fashion include transferrin, folate and tumour necrosis factor-α (Galvin et al., 2012). Various forms of NPs exist including liposomes, polymerosomes, metal nanoparticles, dendrimers and quantum dots (Galvin et al., 2012) as shown in Table 6. Liposomes were one of the first NPs to reach clinical application and consist of an aqueous core encapsulated by a shell. The latter is typically composed of lipid and is arranged into a bi-layered membrane. This configuration allows liposomes to carry hydrophilic molecules within its core, or hydrophobic materials within its shell. The fact that liposomes are easily biodegraded make them particularly useful, which is in contrast to metal NPs that can accumulate *in vivo*, leading to concerns regarding toxicity (Wang et al., 2012).

Nanoparticles are metabolised in a similar fashion to MBs via the Reticulo-endothelial system, and Kupffer cells within the liver and splenic macrophages play a significant role in effecting this. As for MBs, modifying NPs with processes such as PEGylation serve to enhance their circulatory half-life by masking their surface charge and helping decrease the rate of opsonisation and phagocytosis of these materials by Immune cells. Nonetheless, by virtue of their size, NPs can pass not only through endothelium that is deficient/leaky (as is observed in the tumour milieu) but also through fenestrated endothelium which is native to liver, spleen and bone marrow. Thus some accumulation in these organs is unavoidable (Duskey and Rice, 2014). In fact, up to 95% of a systemically administered, standard NP dose is cleared by the Immune system within minutes, preventing adequate tumour localisation. (Lazarovits et al., 2015).

Name	Size (nm)	Characteristics
Liposomes	50-100	Bilayered , phospholipid vesicles with hydrophilic core & hydrophobic lamellae
Dendrimers	<10	Branching, radially symmetric macromolecules composed of amino acids, sugars or nucleotides
Metal nanoparticles	10-20	Composed of biocompatible, inert (eg. Gold) or magnetic (Iron) metals but prone to accumulation *in vivo*
Quantum Dots	10-15	Fluorescent semiconductor materials able to link biological molecules
Polymeric nanoparticles	<100	Self assembling, bio-degradable polymers with hydrophobic core and hydrophilic shell

Table 6: Nanoparticles commonly used in biomedical research applications
(Gao et al., 2004; Johnson et al., 2010; Wang et al., 2012)

The ground realities with the efficacy and kinetics of NP usage in humans are somewhat different to those expected with active and passive targeting mechanisms alone (Figure 13). There is evidence that systemic NPs interact with plasma proteins soon after intravenous injection and this leads to the formation of a 'corona' that masks targeting ligands on the NP surface. This aids off-target cellular binding and increases net NP molecular weight which impedes EPR (Lazarovits et al., 2015).

1.4 The search for theragnostic biomarkers in Cholangiocarcinoma

With the lack of consistent, specific biomarkers in CCA, the ability to target these tumours at a molecular level to facilitate diagnosis or therapeutic delivery is currently inadequate. Bile may contain more valid CCA biomarkers than serum (though the latter is more easily collected) since bile is a 'proximal' fluid to such tumours and literally bathes the surfaces of these malignant cells. Farid and colleagues undertook proteomic analysis of bile in 4 patients with peri-hilar CCA with a view towards identifying potential biomarker candidates (Farid et al., 2011). Through this work, the group was able to identify various proteins that were over-expressed in the bile secretome. Of these, Matrix metalloproteinase- 9 (MMP9) and Neutrophil Gelatinase- Associated Lipocalin (NGAL) were found to be preferentially expressed (Farid, 2014). Given the potential of these 2 proteins as CCA biomarkers, they were subsequently taken forward to explore their applicability as diagnostic and therapeutic targets in CCA.

Expected Outcome

Active Targeting

Passive Targeting

True Outcome

Active Targeting

Passive Targeting
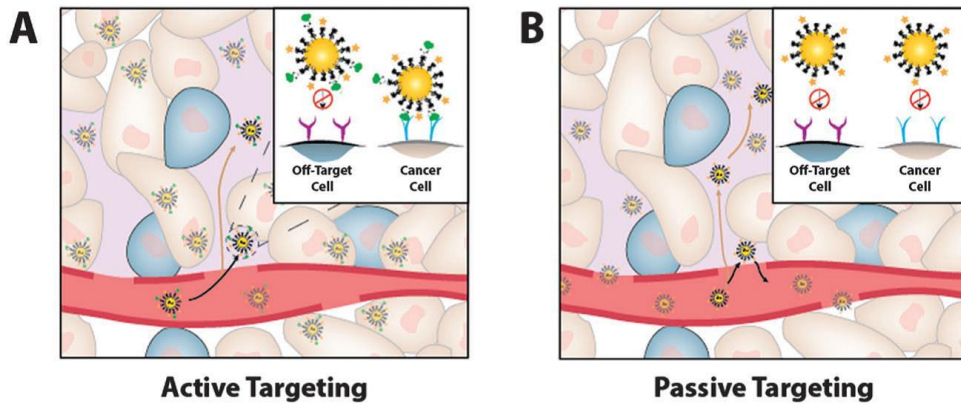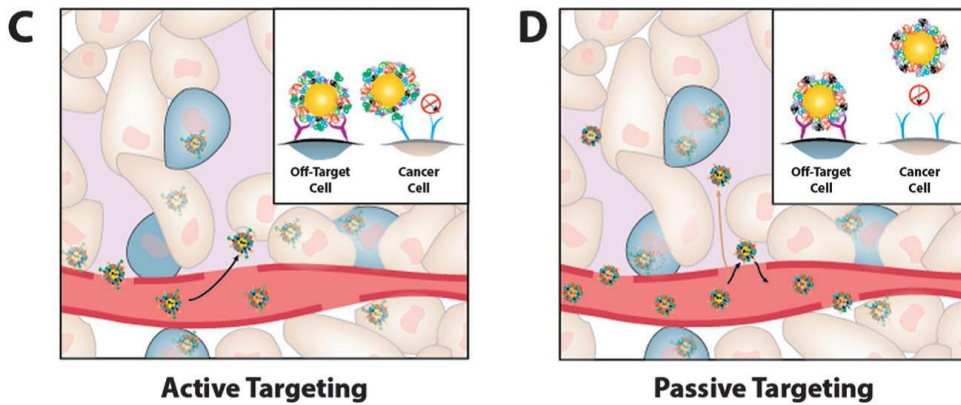
Figure 13: Expected versus actual nanoparticle interactions with target tissues

Illustration of the expected *in vivo* effects of nanoparticles on target tissues (Panels A and B) versus the observed effects (Panels C and D). The interaction of NPs with plasma proteins leads to diminished active and passive targeting, with the promotion of off-target side effects. Taken from Lazarovits et al. Nanoparticle–blood interactions: the implications on solid tumour targeting. *Chem. Commun* 2015; 51: 2756-2767; DOI: 10.1039/C4CC07644C. Reproduced with permission from the publisher

The exact roles played by NGAL and MMP9 in the progression of solid cancers are yet to be fully elucidated. It is understood that NGAL exerts antimicrobial effects *in vivo* which are closely linked to its function as an iron chelator and these are mediated through the NGAL cell surface receptor 24p3R. Intracellular iron depletion is also known to induce apoptosis and may be one of the mechanisms by which NGAL induces cancer cell death (Devireddy et al., 2005). Other pathways by which NGAL may exert anti-cancer effects is through the inhibition of VEGF synthesis via the down-regulation of Hypoxia inducible factor-1alpha and by the inhibition of Focal Adhesion Kinase phosphorylation (Candido et al., 2015). Somewhat paradoxically, NGAL also functions as a MMP9 stabilizer in the extra-cellular matrix which helps promote tumour invasiveness and metastatic capability in certain cancers by virtue of MMP9's gelatinase activity (Chakraborty et al., 2012).

1.4.1 Neutrophil Gelatinase-Associated Lipocalin

Neutrophil Gelatinase-Associated Lipocalin (NGAL/Uterocalin/Siderocalin/oncogene 24p3/Lipocalin-2) is a 198 amino acid long glycoprotein that is a member of a group of secreted transport proteins termed lipocalins. These proteins are afforded specific ligand binding properties by virtue of a common tertiary protein structure termed the 'lipocalin fold' which renders them capable of transporting lipophilic substances (Chakraborty et al., 2012). NGAL has in recent years attracted increasing interest as a marker of homeostatic dysregulation since serum and tissue concentrations of this protein are frequently deranged in acute inflammation and neoplasia. Initially discovered as a complex with the 92kDa Type-IV gelatinase (i.e. MMP9) within human neutrophils (thus lending it its name), this covalently linked 135 kDa complex was found not to be the main form of the NGAL protein, but rather as a freestanding 25kDa peptide. (Kjeldsen et al., 1993). The NGAL gene is

located on chromosome 9q and the NGAL protein is exocytosed mostly in a free form from late granules of neutrophils. Subsequent work has shown that various tissues normally express NGAL including the bronchus, sections of the gastrointestinal tract, kidneys, breast, colon and prostate (Friedl et al., 1999; Chakraborty et al., 2012). A prime function of NGAL is believed to be the transport of iron intracellularly, which is achieved through a specific 24p3R (megalin) receptor (Bolignano et al., 2010), a phenomenon that helps prevent apoptosis in these cells (Devireddy et al., 2005). The molecule is understood to aid in innate immunity by both depleting bacteria of iron thus causing their death and promoting neutrophil chemotaxis. This ties-in with its behaviour as an acute phase protein with increased serum levels of NGAL seen following a stress event.

Within the spectrum of benign pathology, NGAL expression is understood to be up-regulated in several inflammatory disorders such as psoriasis, chronic eczema, myocarditis, and inflammatory bowel disease. Ischaemic conditions such as cerebral and myocardial infarction and acute kidney injury also lead to a rise in local NGAL whereas metabolic diseases leading to raised levels of the protein include Diabetes Mellitus and obesity (Chakraborty et al., 2012).

NGAL also plays an important role in promoting cancer growth that is believed to be mainly via the positive modulatory and stabilizing effects it has on MMP9 extracellularly, though other mechanisms independent of MMP9 may exist such as anti-apoptotic effects. There is data to support increased NGAL expression in malignancies of the breast, upper digestive tract and thyroid amongst others with positive correlation noted between it and tumour parameters such as differentiation and stage (Chakraborty et al., 2012) but paradoxically other studies have shown it may exert anti-neoplastic effects, viz. in pancreatic, ovarian and colonic cancers (Bolignano et al., 2010). These contradictions are perhaps not fully attributable to

technical aspects between studies such as differences in antibodies used, and may actually indicate a varying role for this marker amongst different cancers. Nonetheless, current evidence supports NGAL to be pro-neoplastic in CCA.

The feasibility of utilising serum and biliary NGAL levels to differentiate CCA from benign conditions of the biliary tract has been explored in several reports, with conflicting results. Leelawat et al (Leelawat et al., 2011) analysed serum levels of NGAL and CA 19-9 in a group of 50 patients with CCA (of which 72% cases were PH-CCA) and observed that levels of both these biomarkers were significantly elevated in comparison to levels within a group of 50 patients with benign biliary tract disorders (stone disease and strictures). The area under curve (AUC)-receiver operating characteristic (ROC) was noted to be 0.79 for NGAL and 0.81 for CA 19-9. It must be added that the degree of biliary obstruction (as evidenced by bilirubin levels) was significantly higher in the CCA group as well in this study. Significantly higher NGAL titres were also noted in those patients with advanced stage CCA when compared to early stage tumours. In a similar fashion, Budzynska and colleagues determined serum NGAL and CA 19-9 levels in a group of 40 patients with biliary obstruction (16 CCA, 6 pancreatic cancer and 18 benign strictures) but found no difference in NGAL levels between malignant and benign groups (Budzynska et al., 2013). However, they did also concurrently analyse biliary NGAL levels and found this to be significantly raised in the malignant cohort (AUC-ROC 0.73), as were serum CA 19-9 levels (AUC-ROC 0.86). These findings mirror the results obtained through the earlier work of Zabron and co-workers (Zabron et al., 2011) who further to upfront biliary proteomics work, determined biliary NGAL levels in an initial "discovery" cohort of 38 patients, 16 of which had malignant biliary obstruction (2 CCA cases). They noted statistically higher levels of biliary NGAL in malignant obstruction (AUC-ROC 0.76) and replicated these findings within a further "validation" cohort of 21 patients (7 malignant cases, no CCA). Peak bilirubin levels

in the malignant group were significantly higher than in their benign counterparts, in both discovery and validation cohorts.

The tissue expression of NGAL in CCA and normal liver tissue has not been analysed in detail to date. Nuntagowat and co-workers whilst noting decreased *in vitro* invasiveness of the CCA cell line RMCCA-1 with siRNA-induced NGAL knockdown were unable to show any correlation between NGAL IHC expression and tumour differentiation, lymph nodal status or metastases in their cohort of 24 CCA cases (Nuntagowat et al., 2010). Although it is unclear whether their tissue samples were taken from a homogenous group of one particular CCA subtype, they did observe NGAL expression in all their tumours with strong staining in 75% of cases, and no staining was seen in non-tumorous tissue. Friedl and associates in an older study assessed NGAL staining patterns in several normal tissues and found normal hepatocytes to be negative, whereas smaller intra-hepatic bile ducts showed focal positivity (Friedl et al., 1999). Nonetheless, under conditions of experimental liver injury or cholestasis, NGAL tissue expression and serum levels have been observed to be markedly increased, with injured hepatocytes being the source (Borkham-Kamphorst et al., 2011). Despite the relative lack of data with NGAL in CCA, the former has been studied in better detail in other hepatopancreatobiliary malignancies. One report looked into the impact of NGAL in HCC, and through the use of HCC cell lines in *in vitro* and *in vivo* studies, this group was able to show that the proliferation, local invasiveness, and metastatic capability of HCC was dampened by NGAL (Wang et al., 2013). This was attributable to NGAL mediated suppression of Epithelial to Mesenchymal Transition via downregulation of Epidermal Growth Factor and Transforming Growth Factor -beta1 (TGF-β1). Conversely, an earlier IHC study using 138 cases of HCC from curative resection samples showed significant up-regulation of NGAL and its receptor (NGALR) in those patients with features of vascular invasion and higher TNM stage.

Furthermore, Cox regression analysis identified NGAL and NGALR expression as independent predictors of poorer overall survival in HCC (Zhang et al., 2012). The expression profile of NGAL in pancreatic adenocarcinoma has been explored as well, with one IHC report noting 100% positivity in a sample cohort of 27 cases. An increasing stain intensity was seen with better tumour differentiation, along with a significantly lower degree of staining in normal pancreatic tissue (Moniaux et al., 2008). Similar results were arrived at in another report where significantly higher proportion (45%) of 73 pancreatic cancer tissue samples stained positive for NGAL when compared to 26% of 77 normal/chronic pancreatitis controls (Tong et al., 2008). The data regarding NGAL expression in other solid cancers is disparate at best, with both pro- invasive and anti-cancer effects noted in cancers of the breast, oesophagus, stomach, and colon (Chakraborty et al., 2012; Candido et al., 2015).

1.4.2 Matrix metalloproteinase-9

Matrix metalloproteinases (MMPs) are a group of zinc dependent endopeptidases that play a pivotal role in normal tissue homeostasis, inflammation and tumour progression, of which there are currently 23 known members (Kessenbrock et al., 2010). MMPs share a structure having three common domains in their amino acid sequence. The pro-peptide domain contains a cysteine residue that interacts with a zinc ion in the catalytic domain maintaining enzyme latency. MMPs are activated upon disruption of the cysteine-zinc interaction by means of a "cysteine switch", which involves proteolysis of the pro-peptide domain. Various cells express these enzymes including neutrophils, lymphocytes and endothelial cells in addition to stromal elements such as macrophages and fibroblasts. Physiological inhibition of MMPs is achieved through tissue inhibitors of metalloproteinase (TIMP) of which there are currently 4 subtypes (Kessenbrock et al., 2010).

Matrix metalloproteinase-9 (MMP9/92 kDa Gelatinase/92 kDa Type IV Collagenase) is secreted into the extra-cellular space as a latent 92kDa protein. It is subsequently cleaved to active 82 and 65kDa isoforms, which aid in digesting the extra-cellular matrix (Vempati et al., 2007). It is unique in its role in tumour progression and acts at various levels. In the setting of malignancy MMP9 can activate TGF-β signalling via the CD44 receptor in a deregulated manner leading to increased tumour invasiveness (Yu and Stamenkovic, 2000). Additionally in conjunction with MMP2 and MMP14, MMP9 plays an important role in promoting tumour angiogenesis by increasing the local bioavailability of VEGF (Kessenbrock et al., 2010).

There is data to suggest a role for MMP9 in the progression of CCA. Whilst serum levels of MMP9 have not reliably helped to differentiate benign from malignant biliary pathology (Leelawat et al., 2009), immunohistochemistry studies have shown divergent results. A preliminary report looked at the expression of various MMPs and TIMPs in normal liver tissue, IH-CCA and HCC (Terada et al., 1996). It noted a lack of MMPs and TIMPs in normal hepatocytes though marginal staining was observed in bile ducts. The degree of epithelial positivity of both sets of markers correlated with local invasiveness but not tumour differentiation, and a small degree of stromal expression was also seen. MMP9 expression in IH-CCA was detected in only 27% (3 out of 11) cases. A similar report from Japan analysed MMP9 expression in 37 resected cases of intrahepatic CCA, and noted positivity in 43% of cases (Shirabe et al., 1999). Higher expression of MMP9 was significantly associated with the risk of nodal metastases and poorer overall survival, as well as nodal recurrence. Another group analysed tissue expression of MMP9 in 42 cases of PH-CCA using reverse-transcriptase Polymerase Chain Reaction techniques and found it to be increased relative to normal liver tissue. No clinical data was however available in this study (Li et al., 2005). Kirimlioglu and colleagues subsequently ascertained the expression of MMP9 amongst other MMPs in a heterogenous group

of 44 biliary cancers, 8 of which were PH-CCA cases (Kirimlioglu et al., 2009). MMP9 was observed to be expressed in both normal hepatocytes and tumour epithelia in PH-CCA, and more so in cases with neural invasion. No particular correlation between staining intensity and any other clinicopathological variable was seen in this series. More recent work involving 58 patients who had curative resection of PH-CCA has also highlighted the lack of correlation of degree of MMP9 expression with clinicopathological data although it was also shown that high expression of MMP9 and the presence of nodal metastases were independently associated with poorer overall survival (Sun et al., 2014). There is anecdotal evidence into the use of MMP9 inhibitors as palliative therapy in unresectable CCA, and a reduction in CA 19-9 levels was noted in 2 of the four patients offered this treatment with oral Marimastat (French et al., 2005). The median survival noted was 22 months. Whilst MMP inhibitors such as Marimastat have thus far failed to reach effective clinical translation in solid cancers, this is in part attributed to their non-specific nature leading to musculoskeletal toxicity and intolerance (Bramhall et al., 2002; Fingleton, 2008).There is therefore scope to improve MMP therapeutics by tumour specific targeting and delivery.

1.5 Aims and Objectives

1.5.1 Aims

The aims of this project were to:

1. Assess the prognostic relevance of NGAL and MMP9 expression in PH-CCA and evaluate the validity and potential of these biomarkers in the future development of a targeted theragnostic system in CCA.

2. Examine the expression of the vascular endothelial markers CD105 and VEGFR2 in PH-CCA and assess the efficacy of vascular endothelial targeting using *in vitro* and *in vivo* models.

1.5.2 Objectives

The objectives of this study were as follows:

a) To investigate NGAL and MMP9 as biomarkers in PH-CCA using IHC on archival formalin-fixed paraffin embedded (FFPE) tissue, and to relate their tissue expression to clinicopathological outcomes.

b) To assess a panel of CCA cell lines for expression and cellular localization of NGAL and MMP9 by Western blotting, Immunofluorescence (IF) and flow cytometry (FC) studies, towards investigating their utility as theragnostic agents *in vitro* and *in vivo*. Evidence of extracellular secretion of biomarkers would be assessed by Enzyme-linked Immunosorbent Assay (ELISA) studies to highlight the value of targeting these markers in tumour stroma.

c) To evaluate the utility of CD105 and VEGFR2 as endothelial targets by IHC on FFPE PH-CCA tissue and correlate MVD to clinicopathological parameters.

d) To examine the efficacy of a targeting strategy using MBs through *in vitro* studies.

e) To set up a murine subcutaneous xenograft model of EH-CCA using suitable cell lines. This would enable the assessment of a MB-based targeted delivery system using vascular ligands in a pre-clinical model of CCA.

2   Materials & Methods

2.1   Tissue Blocks & Ethics

A notice of Substantial Amendment to the concurrent local study on usage of biliary proteomics in the development of diagnostic markers of biliary malignancy was submitted to the Leeds East NRES Committee, to include the additional study of archival paraffin embedded tissue samples. Following approval (REC 06/Q1206/136; 18th July 2011; Section 7.1), peri-hilar CCA tissue blocks from 54 patients who underwent surgical resection of these tumours at this institution from January 2000 to September 2010 were acquired with the kind assistance of Dr Judy Wyatt, consultant histopathologist at St James's University Hospital, Leeds. Blocks of matched normal liver tissue where possible were also obtained and subjected to IHC. All runs were performed with relevant positive and negative controls.

2.1.1   Immunohistochemistry

Immunohistochemistry protocols for antibodies to NGAL and MMP9 were optimized for antibody concentration and retrieval method. Protocols for optimal staining of CD31, CD105 and VEGFR2 antibodies were already established in our laboratory.

2.1.1.1   Selection of Target biomarkers (NGAL and MMP9) and antibodies

My decision to focus on the proteins NGAL and MMP9 was determined by the results obtained by prior work at our institution into biliary proteomics in CCA

patients (Farid, 2014), which identified these two proteins as being secreted in relatively high amounts in bile. This group in the course of their work optimized the following antibodies for Western blot applications on bile:

- Mouse monoclonal Anti-NGAL (Abcam, Cambridge; ab23477)
- Mouse monoclonal Anti-MMP9 (Abcam, Cambridge; ab58803)

As these antibodies are specified as being additionally suitable for Immunohistochemistry applications, they were selected upfront for these experiments. As elaborated in detail later, the final choice of antibodies changed based on the experiments conducted, as the original choices were not without their drawbacks.

2.1.1.2 Immunohistochemistry for expression of selected biomarkers

Five micron-thick tissue sections were cut from FFPE tissue blocks using a tissue microtome (Leica RM2235) and fixed onto glass slides (Superfrost Plus®, Thermo Scientific) overnight at 37°C. Sections were dewaxed and hydrated using a series of xylene, ethanol and water steps. Antigen retrieval was performed if necessary (see specific details for each antibody in the following sections) before endogenous peroxidase quenching with 0.3% v/v hydrogen peroxide for 10 minutes. Primary antibodies were diluted in Antibody diluent reagent solution (Invitrogen, Camarilo, CA) before application to sections. Sections were washed in Tris-buffered saline with 10% Tween-20 (TBS-T) for 5 minutes (x2) followed by 5 minutes in TBS alone, after primary incubation. Following incubation with a Horseradish peroxidase (HRP)-conjugated secondary antibody, washes were repeated as detailed above. Incubation with 3,3'-diaminobenzidine tetrahydrochloride (DAB)+ Substrate

Chromogen System (Dako, Carpinteria, CA) revealed the expression pattern of the antibody. Sections were counterstained with Haematoxylin, 'blued' in Scott's tap water then dehydrated through ethanol and xylene. Sections were permanently mounted using DPX (Sigma, UK) under a glass coverslip. Serial tissue sections were used for endothelial cell staining protocols (CD31, CD105 & VEGFR2) in order to study similar regions across sections. No-primary (Secondary antibody only) slides were included in all runs to establish that staining was specific for the primary antibodies used and appropriate in-house positive controls were used.

2.1.1.2.1 NGAL and MMP9

These antibodies required optimization to identify ideal dilutions, as elaborated in the next chapter.

2.1.1.2.2 CD31

The primary antibody used was an anti-human CD31 mouse monoclonal antibody (Dako, Glostrup, Denmark, Clone JC70A) at 1/40 dilution with overnight incubation at 4°C. The Dako EnVision™ System-HRP as detailed above for MMP9 was employed for secondary incubation in the protocol.

2.1.1.2.3 CD105

Antigen retrieval was performed by immersing sections in 100μl Proteinase-K enzyme (20μg/ml) in 50ml phosphate buffered saline [PBS]) for 25 minutes at 37°C in a water bath. A mouse monoclonal anti-human CD105 antibody (Dako, Glostrup, Denmark; Clone SN6H) was applied at 1/20 dilution for 1 hour whilst the Dako

EnVision™ System-HRP kit for mouse antibodies was again utilized for secondary incubation.

2.1.1.2.4 VEGFR2

A section of mouse subcutaneous tissue was used to stain hair follicles as a positive control. Antigen retrieval was performed by heating sections in 0.05 M Tris-EDTA pH 9.0 buffer at 800W in a microwave for 5 minutes. A Casein block was utilized before addition of a rabbit monoclonal anti-human/mouse VEGR Receptor-2 antibody (Cell Signaling Technology, MA) at 1/100 dilution for one hour at room temperature. Secondary incubation was carried out using the Dako EnVision™ System-HRP for use with rabbit primary antibodies (Dako, Carpinteria, CA).

2.1.1.3 Visual scoring of staining intensity

For quantitation of MMP9 and NGAL IHC staining, the Histoscore method (Jonat et al., 1986) was adopted . Briefly, using an Olympus CHA microscope, CCA tumour tissue was identified in each section, at x40 magnification. Subsequently, at x400 magnification (=1 High Power Field [HPF]), a maximum of 100 tumour epithelial cells were assessed for intensity of staining, from 0 (none) to 3 (highest) per cell. This step was repeated across 10 HPFs and the total numbers of cells for each intensity recorded. The Histoscore was calculated using the formula: $H = P (i+1)$

- Where H= Histoscore for a given intensity
- P= percentage of cells positive for a given intensity score
- i= Intensity score

The net sum of histoscores for all intensities per section yielded the final Histoscore, which was recorded.

Estimation of vascular staining was performed by calculation of MVD as previously described (Weidner, 1995). At x40 magnification, 3 areas of highest vascular density ("hot spot") were identified on the CD31 tissue section, preferably at tumour margins. Subsequently, at x200 magnification, the number of discrete endothelial staining patterns per field (x3) was counted. These steps were repeated for adjacent CD105 and VEGFR2 sections in the same fields as were used for CD31 MVD assessment. The final MVD score per antibody was the average of counts from all 3 fields per section. All scores for the initial third of cases were recorded by two independent observers (AN and EV) blinded to clinical parameters related to the assessed tissue sections. If the degree of disagreement between scorers was substantial, scores were re-done by combined assessment. The latter two thirds of cases were scored solely by AN.

2.2 Patient database

Details of all 54 patients whose tissue blocks were sourced for IHC studies were retrieved from a prospectively maintained database held within the Department of Hepatobiliary and Transplant Surgery at St James's University Hospital, Leeds. Anonymised clinical parameters including age at surgery, gender, details of surgical procedure were collected, in addition to follow up data such as times to recurrence/metastasis, demise or last follow up, as the case may be. Pathological parameters looked into included details of TNM staging (as per the 7th edition of the AJCC system for peri-hilar CCA), tumour size and grade, nodal positivity, microscopic vascular invasion and resection margin status.

2.3 Cell lines

Cholangiocarcinoma cell lines were sourced from various repositories and as gifts from allied institutions, as detailed in Table 7.

Cell lines were grown in 10% (v/v) foetal calf serum (Invitrogen, UK) with RPMI medium (Life Technologies), with the exception of 2 cell lines: EGI-1, which required DMEM medium (Life Technologies) with 10% FCS, and H69, which required a specially formulated medium (7.2). All lines were maintained in an incubator at 37°C with 5% carbon dioxide in $75cm^2$ flasks with a canted neck and vent cap (Corning, Acton, MA). Cells were passaged before confluence using trypsin and were then seeded into fresh flasks at 1/5 to 1/10 dilutions.

Once obtained, all cell lines were authenticated in-house using Short Tandem Repeat analysis with the kind assistance of Dr Claire Taylor, Genomics Facility, Cancer Research UK Cancer Centre, Leeds.

2.3.1 Immunofluorescence

Approximately 5×10^5 cells in 2 ml of medium were seeded onto a glass coverslip in a 6 well plate and incubated for 2 days. At confluence, adherent cells were fixed with 4% v/v paraformaldehyde (PFA) to enable membrane-bound proteins to be studied. During optimization of primary antibodies for immunofluorescence and Western blotting, the anti-MMP9 and anti-NGAL mouse monoclonal antibodies from Abcam used for IHC were found not to be suitable for IF applications and hence alternatives were optimized. As the IHC run on all CCA sections with the Abcam anti-MMP9 antibody had been completed by this stage, equivalent staining by IHC was demonstrated between Abcam and my final choice of antibody for IF (Chemicon) on similar tissue sections.

Cell line	Derivation	Source	Reference
EGI-1	EH-CCA	DSMZ, Germany	N/A
TFK-1	EH-CCA	DSMZ, Germany	(Saijyo et al., 1995)
HuCCT-1	IH-CCA	JCRB, Japan	(Miyagiwa et al., 1989)
Huh-28	IH-CCA	JCRB, Japan	(Kusaka et al., 1988)
OZ	EH-CCA	JCRB, Japan	(Homma et al., 1987)
SkChA-1	EH-CCA	Gifted by Mr Rob Hutchins,	(Knuth et al., 1985)
H69	Normal cholangiocytes	Imperial College, London	(Grubman et al., 1994)
SVR	Murine pancreatic islet endothelium	ATCC, USA	(Arbiser et al., 1997)

Table 7: Cell lines used in this study

Primary antibodies were applied as follows:

NGAL
- Goat polyclonal NGAL (R&D Systems, Minneapolis, MN; AF1757); 1-hour incubation at 1/50 dilution

MMP-9
- Rabbit polyclonal MMP9 (Chemicon, Temecula, CA; ab13458); 1 hour incubation at 1/100 dilution (the Abcam MMP9 antibody did not yield positive results for Immunofluorescence applications in my cohort of cell lines)

CD105
- Monoclonal Rat anti-mouse CD105 (Clone MJ7/18 , BD Pharmingen; 550546); 1 hour incubation at 1/50 dilution

'No-primary' (secondary antibody only) slides were included to define any non-specific staining. Following washing with TBS, a secondary fluorophore-conjugated antibody was added as follows for 30 minutes in the dark, as follows:

- For NGAL primary antibody: 1/300 dilution (in TBS) Donkey anti-goat Alexafluor 488 (Invitrogen; Cat A11055), or
- For MMP9 primary antibody: 1/300 dilution (in TBS) Donkey anti-rabbit Alexafluor 594 (Invitrogen; Cat A21207), *or*
- For CD105 primary antibody: 1/300 dilution (in TBS) Donkey anti-rat Alexafluor 594 (Invitrogen; Cat A-21209)

Further TBS washes were performed in the dark. Coverslips were mounted onto glass slides (Superfrost Plus®, Thermo Scientific) using Prolong® Gold antifade

reagent with 4', 6-diamidino-2-phenylindole (DAPI) (Invitrogen, Eugene, OR; P36931). This mountant was allowed to dry in the dark overnight and the edges of the coverslips were sealed with nail polish. A Zeiss Axioimager.Z1 apotome fluorescent microscope (Carl Zeiss, Thornwood, NY) was used to image the cells. Exposure times on the microscope were obtained using the Zeiss AxioVision software and were standardized to the brightest cell line in each antibody run, so as to assess relative staining intensities between different cell lines.

2.3.2 Western blotting

2.3.2.1 Cell lysates and protein quantification

Whole-cell lysates were made from confluent cultures of all seven cell-lines (Table 7). Briefly, cells were washed with serum-free media before addition of ice-cold lysis buffer solution (consisting of a 1:1 mix of 2X radio-immunoprecipitation assay (RIPA) buffer (10mM Tris HCl pH 7.4, 300 mM NaCl and 2% NP40) and 'cOmplete' Protease Inhibitor Cocktail (Roche, Mannheim, Germany) 2X solution). Following incubation at 4°C for 10 minutes, cells were scraped off and the resultant solution centrifuged at 16000x g for 10 minutes. The supernatant was stored in aliquots at -80°C.

Lysates enriched for cell membrane proteins were similarly collected using the ProteoExtract® Transmembrane protein extraction kit (Novagen®; 71772-3) as per manufacturer's instructions. Cytoplasmic extracts were also obtained as a result of this process. All samples were stored at -20°C.

Protein standardization was performed with the Bio-Rad DC™ protein assay reagents package (Bio-Rad; 500-0116) using the manufacturer's instructions and

analysed at 630nm using a Dynex OpSys MR™ microplate photometric reader (Dynex, Chantilly, VA). A standard curve incorporating linear regression points of increasing dilutions of bovine serum albumin standards (2, 1, 0.5 and 0.1 mg/ml) was constructed and corresponding concentrations of test samples (lysates) were extrapolated from this.

2.3.2.2 Protein extraction and gel electrophoresis

A standard amount of protein (ranging from 10-30µg) was mixed with a 5:1 mixture of 2-mercaptoethanol (Sigma-Aldrich). NuPage® LDS 4X Sample buffer (Invitrogen, Carlsbad, CA) was added with de-ionized water to equalize volumes of all test samples and achieve a final 1X concentration of sample buffer. These were then denatured at 100°C for 5 minutes, and then stored on ice until gel loading.

NuPage® 12% Bis-Tris 1.0mm x 10 well Gels (Novex, Carlsbad, CA) were used for gel electrophoresis. Gels were placed in a XCell SureLock™ Mini-cell electrophoresis system (Invitrogen, Carlsbad, CA). The system was filled with a 1X NuPage® MOPS SDS Running buffer (Invitrogen, Carlsbad, CA). Samples were then loaded into the wells, alongside 5µl of MagicMark™ XP Western Protein Standard (Invitrogen, Carlsbad, CA) and 15µl Color Plus Prestained Protein Marker (New England BioLabs, Ipswich, MA). The gel was run at at 180V for 60-120 minutes (Bio-Rad Power Pac 300), allowing larger molecular weight proteins more time to migrate down the gel.

2.3.2.3 Protein transfer

A polyvinylidene fluoride (PVDF) membrane (Thermo Scientific, Rockford, IL; 88518) was cut to the size of the gel and activated by immersed in methanol for 30 seconds. The gel was placed on to the activated membrane, and flanked on either side with filter paper. This was sandwiched between several layers of sponge that had been soaked in the transfer buffer and loaded into a XCell II Blot Module (Invitrogen, Carlsbad, CA). The module was placed into the mini-electrophoresis system and 1X NuPage® Transfer buffer (Invitrogen, Carlsbad, CA; NP0006-1) containing 10% methanol was poured into module until the sandwich was submerged. De-ionized water was then poured into the outer chamber of the system. Protein transfer was performed at either 12V overnight or 30V over 90 minutes.

2.3.2.4 Protein blocking

The PVDF membrane once removed from the assembly was immersed in Ponceau-S to ensure equal protein transfer by visualization of proteins. This was washed off in deionized water, and the membrane was placed in a 5% (w/v) milk powder solution (Marvel in TBS) on a Denley Spiramix roller mixer machine for one hour.

2.3.2.5 Antibody incubation

Antibodies were diluted in a 1% (w/v) skimmed milk solution containing the membrane using the following dilutions:

- NGAL (R&D Systems, Minneapolis, MN; AF1757): 0.1 µl/ml for 1 hour at room temperature

- MMP9 (Chemicon, Temecula, CA; ab13458; 1 mg/mL): 1/250 for 2 hours at room temperature (the Abcam MMP9 antibody did not yield positive results for Western blot applications in my cohort of cell lines)

For assessment of equal protein loading, the following antibodies were used:

- Mouse monoclonal β-actin (Clone AC-15, Sigma-Aldrich, St Louis, MO; A5441): 1/20000; or

- Mouse monoclonal α-tubulin (Clone B-5-1-2, Sigma-Aldrich, St Louis, MO; T5168): 1/5000

The membrane was then washed in 3 x 10 minute washes of TBS-T before the appropriate HRP conjugated secondary antibody was added as follows:

- Polyclonal swine anti-rabbit Immunoglobulin-HRP (Dakocytomation, Glostrup, Denmark; P0217): 1/2000

- Polyclonal rabbit anti-mouse Immunoglobulin-HRP (Dakocytomation, Glostrup, Denmark; P0260): 1/2000

- Polyclonal rabbit anti-goat Immunoglobulin-HRP (Dakocytomation, Glostrup, Denmark; P0449): 1/2000

Finally 3x10 minute washes in TBS-T were performed before chemiluminescent detection.

2.3.2.6 Protein detection

The SuperSignal® West Pico Trial kit (Thermo Scientific, Rockford, IL; 34079) was reconstituted as per manufacturer's instructions and the resultant solution poured on to the membrane. Images were acquired after 5 minutes using a Bio-Rad Gel Doc Imaging system and Image Lab™ software (Version 4.0.1). If protein bands were not detected using the Pico kit, the membrane was washed in TBS-T before application of the SuperSignal® West Femto Trial kit (Thermo Scientific, Rockford, IL; 34094). Densitometric assessment of Western blot images was done using ImageJ software v1.49 for Windows (http://rsb.info.nih.gov/ij/download.html).

Once images were obtained, membranes were washed again and then immersed in TBS for storage in an airtight container at 4°C (short-term) or -20°C (long-term).

2.3.3 Flow cytometry

2.3.3.1 Flow cytometry protocol

To clarify the cell surface expression of MMP9 and NGAL on CCA cell lines, FC was utilized. As no fluorophore-conjugated Anti-MMP9 and anti-NGAL antibodies suitable for FC applications were readily at my disposal, I sought to titrate fluorophore conjugated secondary antibodies against my primary antibodies from Abcam suited for FC. Briefly, confluent 75cmm cultures of CCA cells were treated with 5mM EDTA for 10 minutes at room temperature, before trypsinization and centrifugation at 400g for 5 minutes. The cell pellet was resuspended in 5% Fetal calf serum/PBS mixture and cells counted in a Neubauer chamber. Cells were re-

suspended to a count of 10^7 cells/ml. A volume of 50µL of cells was added to a Flow cytometer tube and the following antibodies were added:

Primary

- Mouse monoclonal anti-NGAL (Abcam, Cambridge; ab23477), or

- Rabbit monoclonal anti-MMP9 (Abcam, Cambridge; ab76003)

Secondary (at 1:50 dilution)

- Pacific blue™ Goat anti-mouse (F(ab')2 fragment) IgG (Invitrogen, Carlsbad, CA; P31581), or

- Alexafluor 488 Goat Anti-Rabbit IgG (Invitrogen, Carlsbad, CA; A11008)

The primary antibodies were added as per Table 13 and tubes incubated on ice for 30 minutes in the dark. 2mls of 5%FCS in PBS was added per tube and centrifuged for 5 mins at 400g at 4°C. The supernatant was flicked off before adding secondary antibodies as detailed in the table. Incubation in the dark for 30 minutes on ice was again undertaken, followed by adding 5%FCS/PBS and centrifugation as before. Finally 50µL of diluted 7-Amino-actinomycin D (7AAD) (BD Biosciences, San Jose, CA; 51-68981E) was added as per the table before incubation on ice in the dark for 10 minutes, to highlight non-viable cell populations. Samples were then taken to the Flow cytometer for analysis.

2.3.4 NGAL Enzyme linked immunosorbent assay (ELISA) using CCA cell line supernatants

The Quantikine NGAL ELISA kit (R&D Systems, MN, USA) was employed as per the manufacturer's directions for the purpose of quantifying NGAL secretion into CCA cell culture supernatants. Briefly, supernatants were separated by centrifugation of confluent cultures to separate out particulate matter and the former immediately frozen in aliquots at -20°C until the time of assay. After preparation of the NGAL Standard solutions, 1/20 dilutions of samples were mixed with an Assay diluent solution in each well of a 96-well plate coated with NGAL antibody and incubated for 2 hours at 2-8°C. The wells were then emptied and washed (x4) with Wash buffer, following which NGAL conjugate was added to each well. Further cold incubation for 2 hours ensued. Another set of wash cycles was then performed, after which Substrate solution was placed in each well for 30 minutes away from light. Finally a Stop solution was added, followed by reading of the plate in a microplate reader at 570nm. Optical density results from the reader were extrapolated to actual concentrations using the standard curve constructed with the NGAL Standard solutions.

2.3.5 *In vitro* flow assays using CD105 labelled Micromarker and Microfluidics Microbubbles on the SVR cell line

In vitro assays to ascertain the degree of binding of CD105 target antibody-labelled microbubbles to murine Sven-1 Ras (SVR) cell lines were conducted as follows:

2.3.5.1 Targeted (CD105) Microbubble preparation

Two types of MBs were utilised separately in the flow assay experiments:. Microfluidics MBs produced in-house and those commercially obtained viz. Micromarker™ (Vevo Visualsonics).

2.3.5.1.1 Microfluidics Microbubbles

These MBs were synthesized in-house using methods described in detail previously (Peyman et al., 2012), enabling the production of a largely monodispersible (homogenous) population of MBs of average diameter 2-5µm, in concentrations $>10^8$ ml^{-1} in line with what clinical applications mandate to prevent the risk of end organ embolism and ischaemia. Briefly, 2mg of a 6:1 mixture of dried lipids (DPPC; Dipalmitoylphosphatidylcholine) and biotinylated Pegylated 1,2-Distearoyl-sn-glycero-3-phosphoethanolamine (DSPE-PEG(2000) Biotin) (Avanti Polar Lipids, Alabaster, Al, USA) was dissolved in 1 cc of bubble buffer (consisting of a solution of 4% Sodium chloride and 1% glycerol) before being subjected to sonication in a bubble bath, typically over 45 minutes until a homogenous cloudy solution was obtained. NeutrAvidin® Biotin-binding Protein (Molecular Probes, Life Technologies, UK) was then added to this mixture (at 16.67µM) to enable cross linking of biotinylated MBs with biotinylated target antibody in the final step of synthesis. After vortexing, the solution was stored at 4°C for 20 minutes before use.

The next step in manufacture involved set up of the microfluidics chip assembly as schematically illustrated in Figure 14. These tailor made polycarbonate-epoxy chip devices (Epigem, Redcar, UK) provide an interface for gas and lipid interaction to form MBs. They incorporate separate microchannels for gas and liquid flow in either single module or multiplex configurations, the latter allowing for better rates of MB
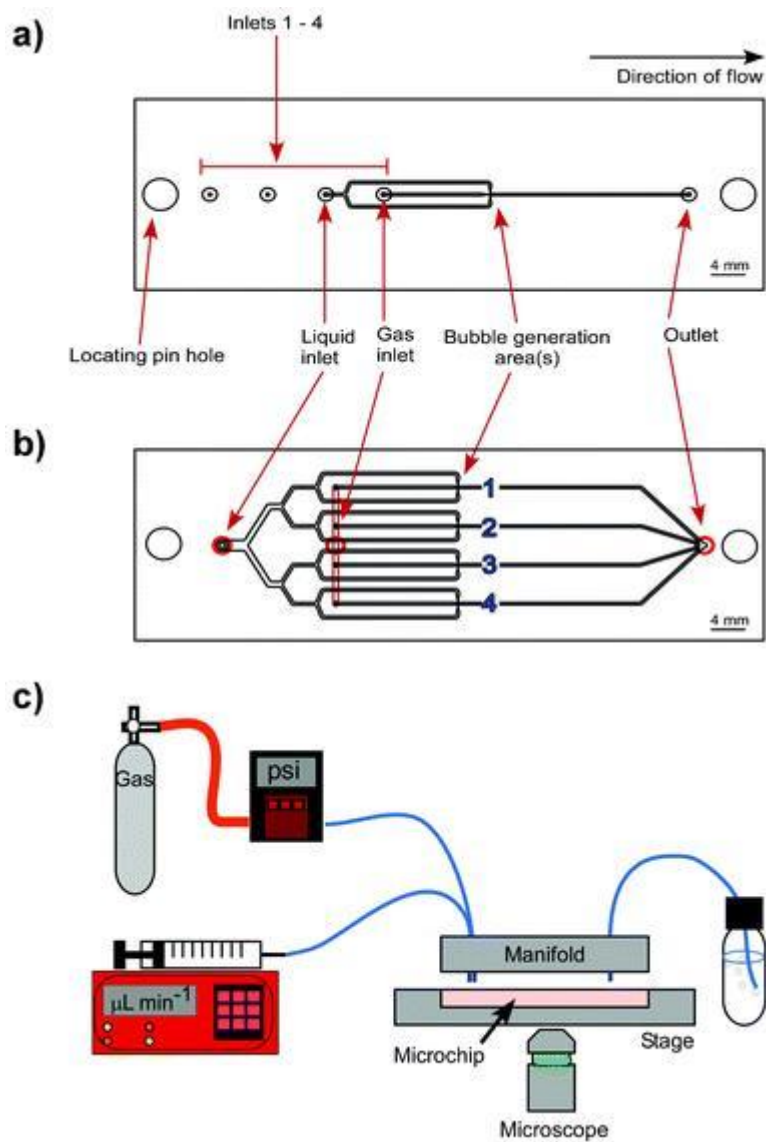
Figure 14: Epigem microfluidics chips used for MB manufacture

a- single module; b- multiplex module; c: Assembly incorporating microchip and gas/liquid lipid inlet channels with outlet channel to reservoir collecting new MBs. Taken from Peyman et al. *Expanding 3D geometry for enhanced on-chip microbubble production and single step formation of liposome modified microbubbles. Lab Chip*, 2012; 12: 4544-4552 DOI: 10.1039/C2LC40634A. Reproduced with permission from the publisher.

production. An abrupt increase in diameter of the combined output channel at the meeting point of the narrower gas and liquid inflow channels causes an acute pressure drop at this point leading to MB generation. A manifold apparatus clamps down the chip on to a stage sealing the whole system and rendering it gas-tight.

Perfluoropropane gas (C_3F_8) was delivered at 13.5psi through the gas inlet channel of the chip, whilst the cooled lipid solution was administered through the liquid inlet channel via a 0.4µm filter using a motorised syringe driver (World Precision Instruments, FL, USA) at 20 µL min^{-1}. The adequacy of MB production was qualitatively assessed in real time by means of an inverted light microscope (Eclipse, Nikon, Japan) whose objective lens (x10) was placed under the bubble generation area.

Once collected, MB concentration was calculated by means of a bespoke counting chamber and the ImageJ software (http://imagej.nih.gov/ij/index.html).

The rat anti-mouse biotinylated CD105 antibody (eBiosciences, CA, USA; Cat 13-1051) and its IgG2a isotype control (Stock solution 0.5 mg/ml) were added to separate MB solutions in concentrations of 0.1 µg/10^7 MBs, 0.05 and 0.01 µg/10^7 MBs respectively as part of serial optimization flow assays for the antibody.

2.3.5.1.2 Micromarker microbubbles

Micromarker™ (Vevo Visualsonics Target-ready contrast agent) MBs were reconstituted as per the manufacturer's instructions. Briefly, target-ready contrast agent was rehydrated with 700ul of PBS by direct injection into the containing vial. The administering 21G needle was momentarily left in place through the cap to equilibrate pressures across it, after which the needle was withdrawn and the vial gently agitated for 10 seconds before being left at room temperature for 5 minutes. The resultant final MB concentration in the vial was 2×10^9 MBs ml^{-1}.

Biotinylated CD105 antibody (eBiosciences, CA, USA; Cat 13-1051) was then added to the solution at 10μg per 10^9MB, and following subsequent agitation for a minute, left for 15 minutes at room temperature prior to use. Again, 10^7 MBs were utilised per flow assay experiment.

2.3.5.2 Ibidi slide plating and Flow assay experiments

To simulate the shear stress conditions of capillary blood flow in an *in vitro* model and thus determine the targeting capabilities of ligand coated microbubbles in such an environment, flow assays were set up as described by McLauglan and co-workers (McLaughlan et al., 2013). Briefly, 30μL of 5×10^5 SVR cells/ml were each plated into 6 channels of a μ–Slide VI $^{0.4}$ (Ibidi, Martinsried, Germany) and the latter incubated at 37°C in 5% carbon dioxide for 48 hours until cells reached approximately 80-90% confluence. To allow the cells to grow on the upper surface of the channels, slides were initially stored in an inverted position. The flow assay assembly consisted of a motorised syringe driver pump (World Precision Instruments, FL, USA) with adjustable flow rate, net volume and syringe diameter functions. Following 3 initial PBS flush cycles to clear away culture media and loose cells, the driver delivered 10^7 MBs (suspended in PBS) at a rate of 0.2mls min^{-1} for

5 mins via a flexible connector tubing connected into the reservoir at one end of the Ibidi chip channel. Fluid once traversed the channel collected into a reservoir at the opposite end and continued on into a waste pot via a second segment of connector tubing. A further cycle of PBS wash was delivered before analysis of the flow channels under inverted light microscopy (x40 magnification) for MB binding. Using a digital camera in-line with the optics of the microscope, 5 images were taken of different fields within each flow channel. MBs were identified in these images as double layered refractile rounded objects. The number of MBs bound to (i.e. in contact with) SVR cells was counted in each image, along with the total number of SVR cells in that field. This process was repeated for all 5 images and the degree of binding expressed as a ratio of bound MBs to total cells.

2.4 Xenograft models

2.4.1 Animals

CD1 nude (nu/nu) and Balb/c congenitally athymic female mice (originally sourced from Charles River Laboratories, Margate, Kent and subsequently maintained in-house) were utilized for xenograft work. All mice were specific pathogen free (SPF) and maintained in a dedicated facility ensuring high standard health conditions. They were housed in individually vented cages (IVC) with food and water provided *ad libitum*. All interventions were approved by the UK Home Office and carried out as per the *Animals* (*Scientific Procedures*) *Act* 1986 regulations.

To develop and in vivo model in which to test targeted therapies, all 7 CCA cell lines were assessed for their potential to grow as heterotopic (subcutaneous) xenografts in these immunodeficient mice. Briefly, CCA cell lines were grown to confluence in

several 150cm^2 flasks (Corning, Acton, MA) before trypsinization and centrifugation down to a pellet of cells. Cell counts were carried out using a Neubauer chamber and the total number of cells in solution was calculated to the volume, adjusted to achieve the intended cell number (5-10 million cells) in 100µl injection volume in serum-free medium. Injections were made into the subcutaneous region of either flank of the nude mouse after application of topical anaesthesia. Tumour growth was measured weekly using calipers. Xenograft volume was calculated using the modified ellipsoid formula:

- $v = 0.5\ (l \times b^2)\ \text{mm}^3$

where v= volume, l= length (mm) & b= breadth (mm) of the xenograft (Tomayko and Reynolds, 1989). Growth curves for each cell line were generated as shown in Figure 15. Appreciable tumour growth was seen only in 3 cell lines, and on occasion, spontaneous tumour regression as also observed.

After 6 weeks from inoculation, or following experiments, mice were sacrificed and xenografts harvested as appropriate. Tumours were fixed in 4% (v/v) PFA and embedded in paraffin, prior to obtaining tissue sections for Haematoxylin/Eosin (H&E) staining or immunohistochemistry.

2.4.2 *In vivo* binding assays with CD105 labelled Microbubbles on CCA xenografts using High Frequency Ultrasound assessment

Experiments were conducted approximately 4-6 weeks following subcutaneous injection as described previously. Firstly, Target-Ready MBs/Targeted Vevo MicroMarker™ Contrast Agent (VisualSonics, Toronto, ON, Canada; Bracco Research, Geneva, Switzerland) for injection were prepared as per the manufacturer's instructions. Briefly, to one vial of Target-Ready MBs (containing $2x10^9$ MBs), 20µg in PBS of anti-mouse CD105 antibody (R&D Systems/ AF1320) or IgG isotype control was added and the net volume made up to 1000 µL PBS.

Under inhaled Isoflurane anaesthesia administered by face mask at 2L/min, mice were fastened to an electroconductive board that allowed real time monitoring of heart rate and temperature. This assembly was placed under a warming light. A 40-MHz linear transducer high-frequency US probe (RMV-704; VisualSonics) was placed over the xenograft and real time imaging performed using the Vevo 770 system (Fujifilm VisualSonics).

Two-dimensional US mode was used to identify the centre (largest diameter) of the xenograft and then the probe was fixed into position on the assembly. The tail vein of the mouse was identified for intravenous injection.

Using a tail vein catheter, initially 50 µL (equivalent to 10^8 MBs) isotype control MBs was injected at a rate of 0.6ml/min using a motorised syringe driver. Four minutes were given to allow injected MBs to bind to xenograft vasculature and readings were saved. Subsequently, a destructive US pulse (10 MHz) was administered

through the fixed probe and readings obtained again. This process was repeated for CD105 MBs after a lapse of 10-20 minutes, to allow isotype control MBs to be eliminated from the circulation.

In the post-processing phase, the VisualSonics software was utilised to generate a 3-dimensional image and volume of the tumour. This was performed by outlining the xenograft border using the software every 10-20 frames. Next, the final 100 frames in sequence from the experiment (for each antibody run) was taken as a baseline to calculate signal amount from bound and flowing MBs (pre-destruction pulse) and that from flowing MBs alone (post-destruction pulse). Subtraction of the latter from the former gave the subtracted molecular signal (i.e. signal due to bound MBs alone), indicative of the amount of CD105 receptors in the scanned vasculature. If the subtracted molecular signal was higher with CD105 MBs in comparison to that of isotype control MBs, specific binding was deemed as having occurred.

2.4.3 CD105 Immunohistochemistry of Xenograft sections

Following *in vivo* experiments with CD105 tagged microbubbles, CCA xenografts and mouse tissue (liver, spleen and kidneys) were harvested and paraffin embedded prior to microtome sectioning as described previously. Five micron sections were dewaxed and hydrated as detailed previously. No antigen retrieval was required. Endogenous peroxidase activity was quenched and Avidin-Biotin block done using a blocking kit (Vector, Burlingame, CA). A Casein block (Vector, Burlingame, CA, diluted in Antibody diluent reagent solution) was incubated with the sections for 20 minutes to reduce background staining further. A goat polyclonal anti-mouse CD105 antibody (AF 1320, R&D Systems, Minneapolis, MN) was used at 1/500 dilution for 1 hour at room temperature. A polyclonal rabbit anti-goat

biotinylated immunoglobulin (Dako, Carpinteria, CA) was utilized at 1/200 dilution for 30 minutes, for secondary incubation. The Vectastain® Elite® ABC kit (Vector, Burlingame, CA) was then added to sections before addition of DAB. Sections were finally dehydrated through ethanol and xylene before coverslips were mounted using DePex mounting fluid (Sigma, UK) and slides dried overnight in a fume cupboard.

Additionally, Haematoxylin and Eosin staining of harvested xenograft sections was performed separately. Five-micron sections were deparaffinised in xylene followed by hydration in ethanol. Slides were immersed in Haematoxylin (Sigma, UK) for 1 minute followed by one minute rinse in tap water. Slides were then incubated in 1% (v/v) Eosin (Sigma, UK) for one minute and rinsed under tap water for one minute. These were then dehydrated and mounted as described above.

2.5 Statistical analysis

The statistical software package SPSS version 22 (IBM, Armonk, NY, USA) was used for data analysis, with a p value <0.05 used to denote statistical significance. Categorical variables were analysed using the Fisher's exact test whereas the Mann-Whitney U test was used for comparisons between continuous data. Correlations between continuous variables were assessed with the Spearman test, and the Wilcoxon signed rank test was utilised for matched tissue comparisons. Using an online tool (http://molpath.charite.de/cutoff) (Budczies et al., 2012), analysis of the AUC-ROC of NGAL and MMP9 Histoscores was performed to determine optimal cut-off points predictive of nodal metastasis and mortality. This tool was also utilised for dichotomising continuous variables at the best cut-off for survival analysis. Survival curves were generated using the Kaplan-Meier method

and differences between proposed predictive factors assessed using the log rank test. Censoring of data towards calculation of survival statistics was done for all cases of peri-operative death, patients who died later due to non-CCA related causes/lost to follow up and in those alive at the end of 5 years. Factors found to be significantly associated with mortality on univariate analysis were entered into Cox regression models to ascertain independent determinants of survival. Graphs were generated with the use of GraphPad Prism v7 software for Macintosh (GraphPad Software Inc, La Jolla, CA, USA).

3 Characterisation of NGAL and MMP9 expression in CCA

3.1 Introduction

The purpose of the experiments in this Chapter was firstly to ascertain the validity of NGAL and MMP9 as theragnostic biomarkers in CCA, in light of prior biliary proteomics work in our institution on PH-CCA patients that had shown these 2 biomarkers to be overexpressed in comparison to control bile. This was evaluated by means of WB, IF, FC and ELISA techniques on various CCA cell lines. I also sought to clarify whether any prognostic effect was evident with the tissue expression of either marker in the cohort of 54 patients with resected PH-CCA. IHC was conducted on all tissue samples and expression quantified by Histoscore assessment. The latter was compared to clinicopathological patient variables including survival.

3.2 Results

3.2.1 Antibodies and their optimization

Anti-MMP9 and anti-NGAL antibodies were tested on CCA sections (as summarized in

Table 8 until optimal staining (i.e. balancing adequate tumour staining against minimum background staining) was achieved. Notable points regarding this process are mentioned below:

Antibody	Manufacturer/ Code	Antigen retrieval methods	Antibody dilutions tested	Antibody incubation periods	Final retrieval/dilution/ incubation used
MMP9	Abcam/ ab58803	None	1/50,1/100, 1/200	1 hour RT	None, 1/100, 1 hr RT
		Citrate buffer	1/50,1/100, 1/200		
	Chemicon/ ab13458	None	1/100	1 hour RT	Done to establish equivalence with ab58803
NGAL	Abcam/ ab23477	None	1/25	1 hour RT Overnight 4°C	Aborted (No staining)
		Citrate buffer	1/25,1/50		
	R&D Systems/ AF1757	None (ABC method)	1/25,1/50, 1/100	1 hour RT	None, 1/100 (in Casein), 1 hr RT
			Casein vs. No casein diluent		

Table 8: Optimization strategies for MMP9 and NGAL antibodies used for IHC in the study
RT- room temperature, ABC- avidin-biotin complex

3.2.1.1 MMP9

The anti-MMP9 antibody ab58803 (Abcam, Cambridge, UK) was optimized for IHC, and used with the EnVision™ detection system. Human ovarian tissue sections (from our gift tissue bank) were used as a positive control, and optimal tumour staining was obtained with a 1/100 dilution of antibody (Figure 15). Background staining in normal liver was seen at all dilutions, which can be attributed to a combination of factors viz. true expression of this marker in hepatocytes, along with elements of non-specific binding that is often seen in normal liver tissue despite the use of EnVision™ kits. Of note, this antibody was found not to work for Western blotting applications in spite of its datasheet advice to the contrary. In light of this, another MMP9 antibody (Chemicon, ab13458) present in-house was then tested and found to be reliable for Western blotting purposes. To ensure the Chemicon antibody was detecting the same protein in tissues as the Abcam antibody, IHC staining patterns and intensities between the two antibodies was evaluated (Figure 16) and found to be comparable.

3.2.1.2 NGAL

My experience with the anti-NGAL antibody ab23477 (Abcam, Cambdrige, UK) on PH-CCA proved non-optimal as the staining observed, if any, was very weak in many of the tested sections. As a result, following a literature search for anti-NGAL antibodies used for IHC of CCA tissue, the R&D antibody AF1757 was chosen for use. Comparison of staining between these 2 antibodies is shown in Figure 17, and clearly shows the R&D antibody provided better staining to that seen with Abcam.
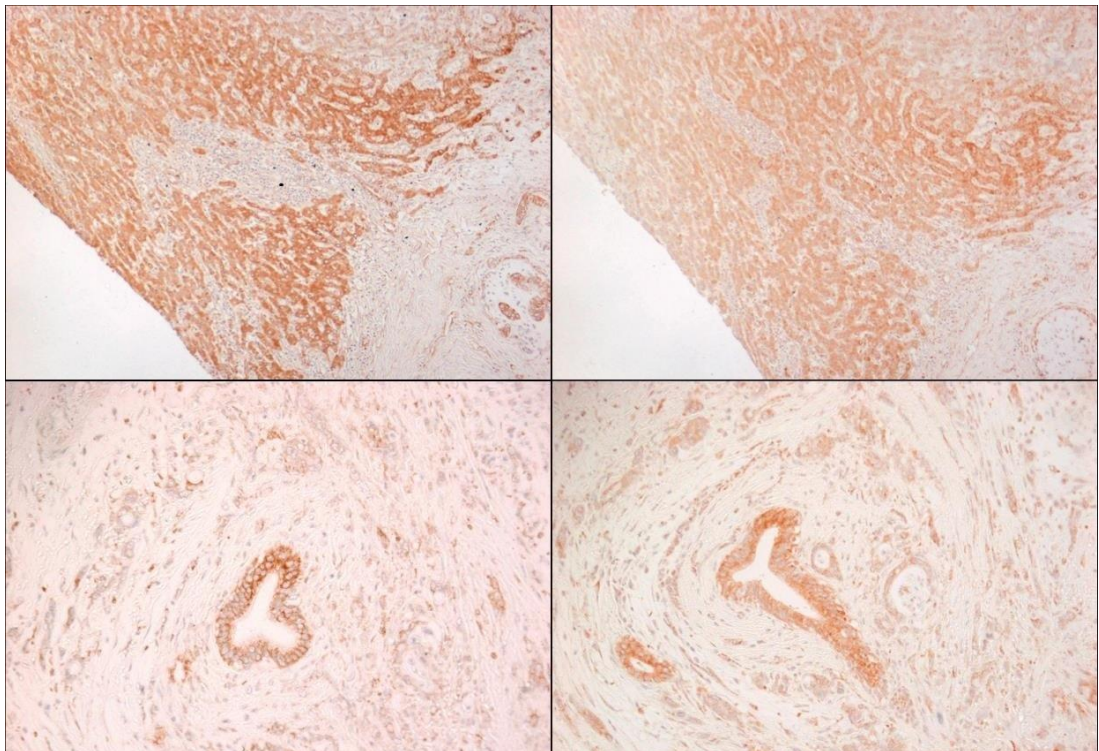
Figure 15: Optimization of MMP9 staining in normal liver and CCA tumour tissue
Top panels showing sections of normal liver (x4 magnification) and bottom panels CCA
sections (x10 magnification). Comparison of staining using ab58803 (Abcam) at 1/50 (left
half images) and 1/100 (right half images) antibody dilutions demonstrates less intense
staining of normal liver tissue whilst retaining relatively strong, specific tumour staining at
1/100 dilution.
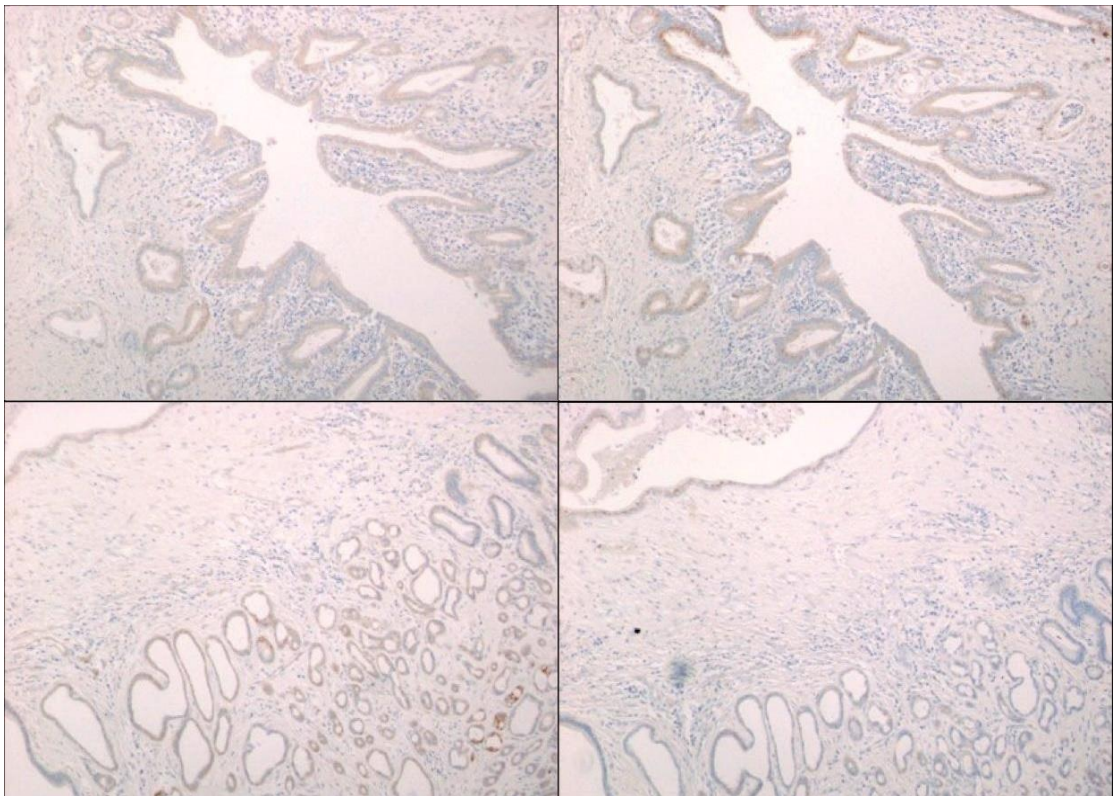
Figure 16: Comparative staining of Abcam and Chemicon anti-MMP9 antibodies.
Staining from Abcam shown on the left half whereas that of Chemicon shown on the right half. Equivalence of staining by both antibodies at 1/100 dilution demonstrated in two different CCA specimens (upper and lower panels respectively).
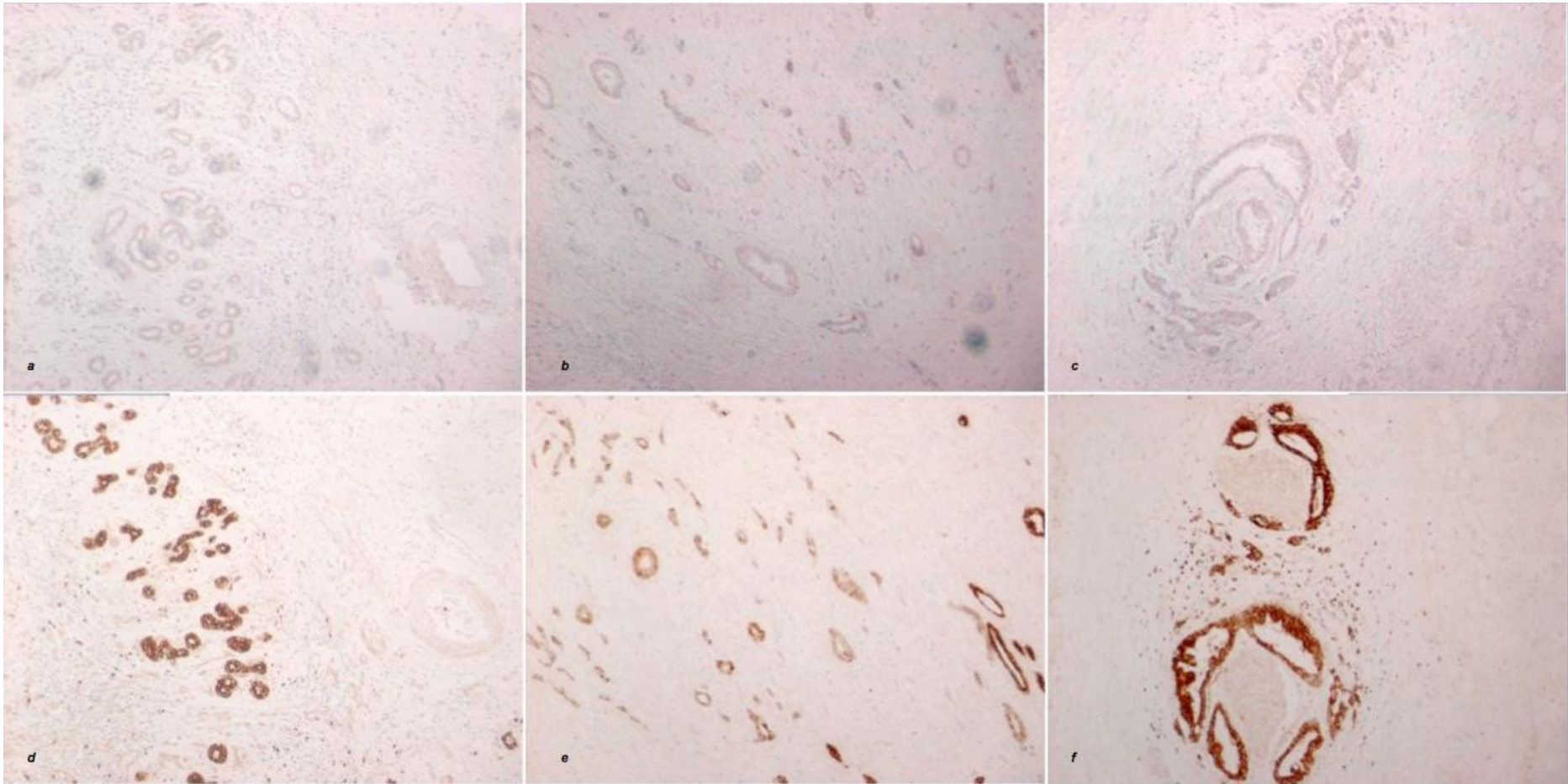
Figure 17: Comparison of NGAL staining using 2 different antibodies.
Top row (panels a, b, c) showing paucity of staining with Abcam anti-NGAL antibody at 1/25 dilution. Bottom row (panels d, e, f) demonstrating significantly improved staining across similar sections with R&D anti-NGAL antibody at 1/100 dilution (Images x10 magnification).

3.2.2 Final dilutions/lists of antibodies used for IHC applications

3.2.2.1 NGAL

Following blocking of endogenous peroxidase, Avidin-Biotin block was carried out using a blocking kit (Vector, Burlingame, CA). To reduce background staining further, casein block (Vector, Burlingame, CA, diluted in Antibody diluent reagent solution) was incubated with the sections for 20 minutes. A goat polyclonal anti-human NGAL antibody (R&D Systems, Minneapolis, MN) was used at 1/100 dilution for 1 hour at room temperature. A polyclonal rabbit anti-goat biotinylated immunoglobulin (Dako, Carpinteria, CA) was utilized at 1/200 dilution for 30 minutes, for secondary incubation. The Vectastain® Elite® ABC kit (Vector, Burlingame, CA) was then added to sections before addition of DAB.

3.2.2.2 MMP9

A mouse monoclonal anti-human MMP9 (Abcam, Cambridge; 56-2A4, 1 mg/ml) at 1/100 dilution for 1 hour at room temperature was used. The Dako EnVision™ System-HRP for use with Mouse primary antibodies (Dako, Carpinteria, CA) was utilized for secondary incubation for 30 minutes.

3.2.3 NGAL and MMP9 are expressed in both CCA tissue samples and control normal liver tissue by Immunohistochemistry

IHC for NGAL and MMP9 was performed on PH-CCA sections from 54 patient samples along with available matched normal liver tissue. In terms of localization,

expression of both markers was seen in tumour cell cytoplasm and membrane, along with variable degrees of stromal staining (Figure 18 and Figure 19). Staining of matched normal liver tissue revealed varying degrees of expression in hepatocytes and cholangiocytes. All tumour and matched liver sections expressed both markers to some extent.

Both NGAL and MMP9 showed evidence of expression in tumour stroma in varying, albeit lesser intensities in comparison to corresponding tumour parenchymal cells..

Quantitative assessment of expression of NGAL and MMP9 was performed by 2 blinded scorers independent of each other (as detailed in the Methods section) for the first 20 cases. The correlation between their scores is shown in Figure 20. As demonstrated in this data, there was good agreement between both scorers in their assessment of both biomarkers, and these observations were statistically significant.
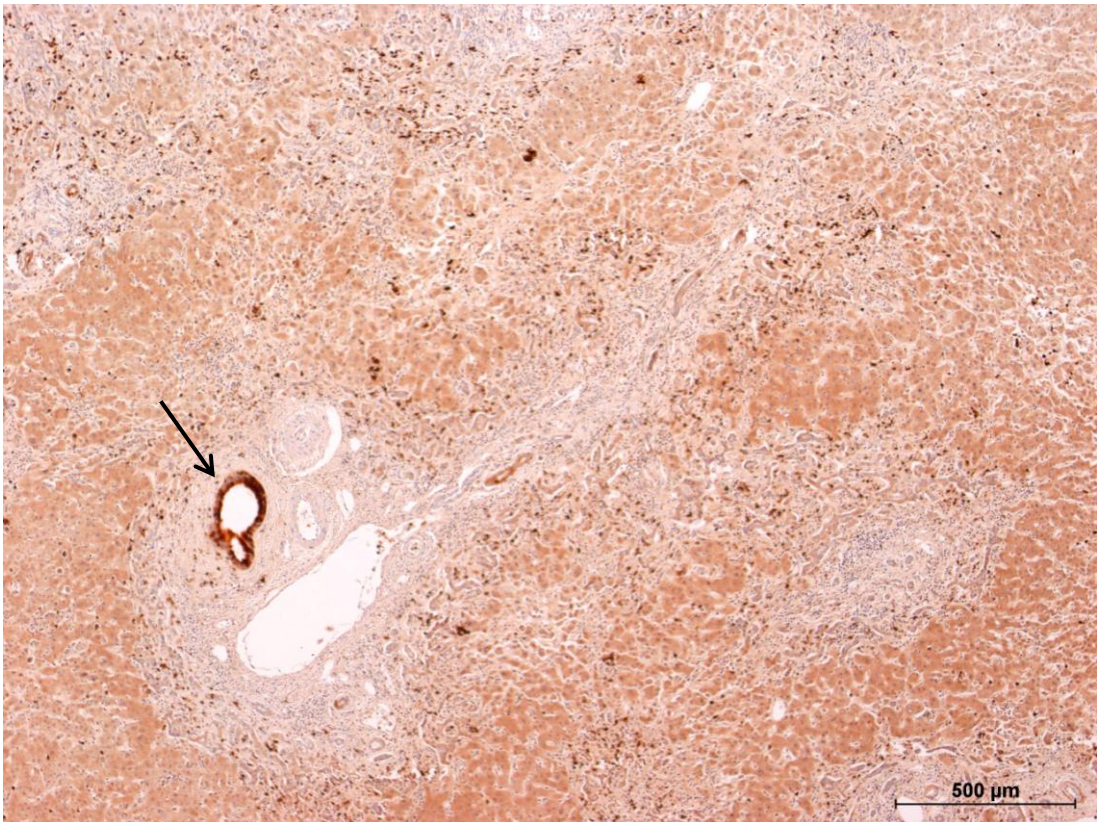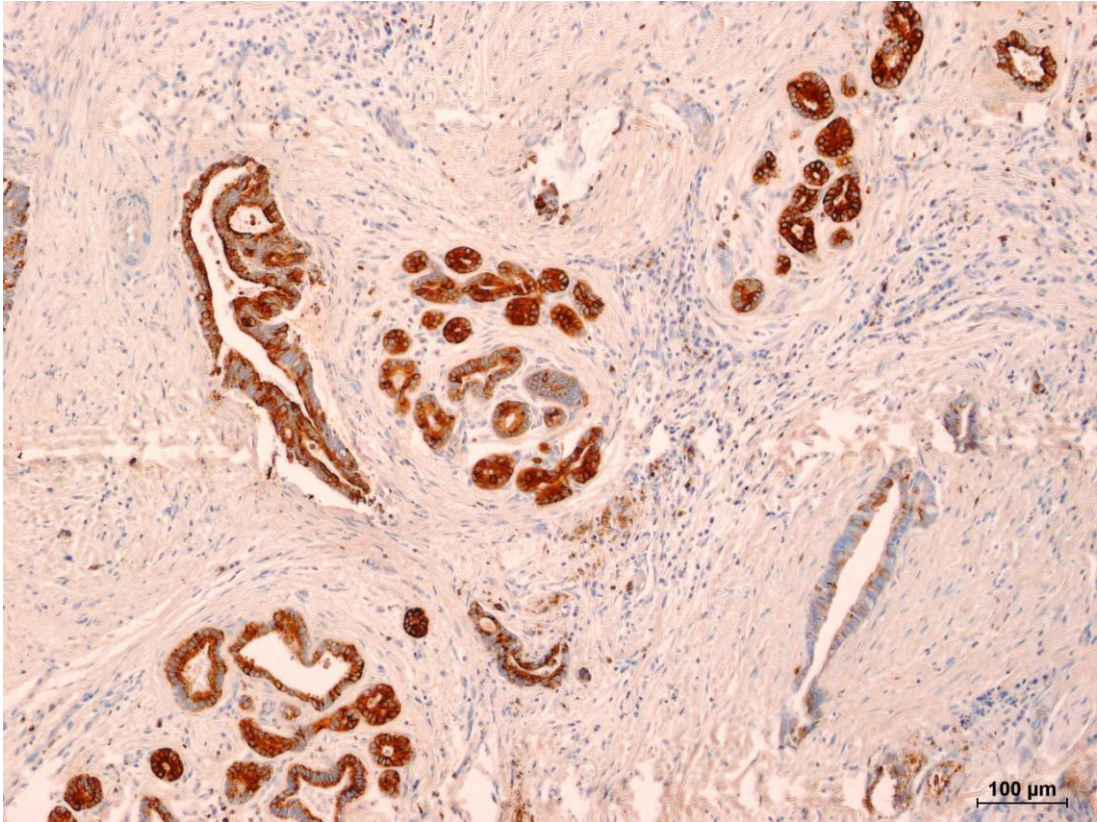
Figure 18: NGAL expression in PH-CCA tissue and matched control liver.
IHC showing strong expression in PH-CCA glandular tissue with mild stromal positivity (top panel). Also seen in the lower panel is diffuse staining of matched normal liver parenchyma, along with positivity of normal cholangiocytes in biliary radicles (arrow) within a portal triad. These findings were typical and representative of the whole cohort.
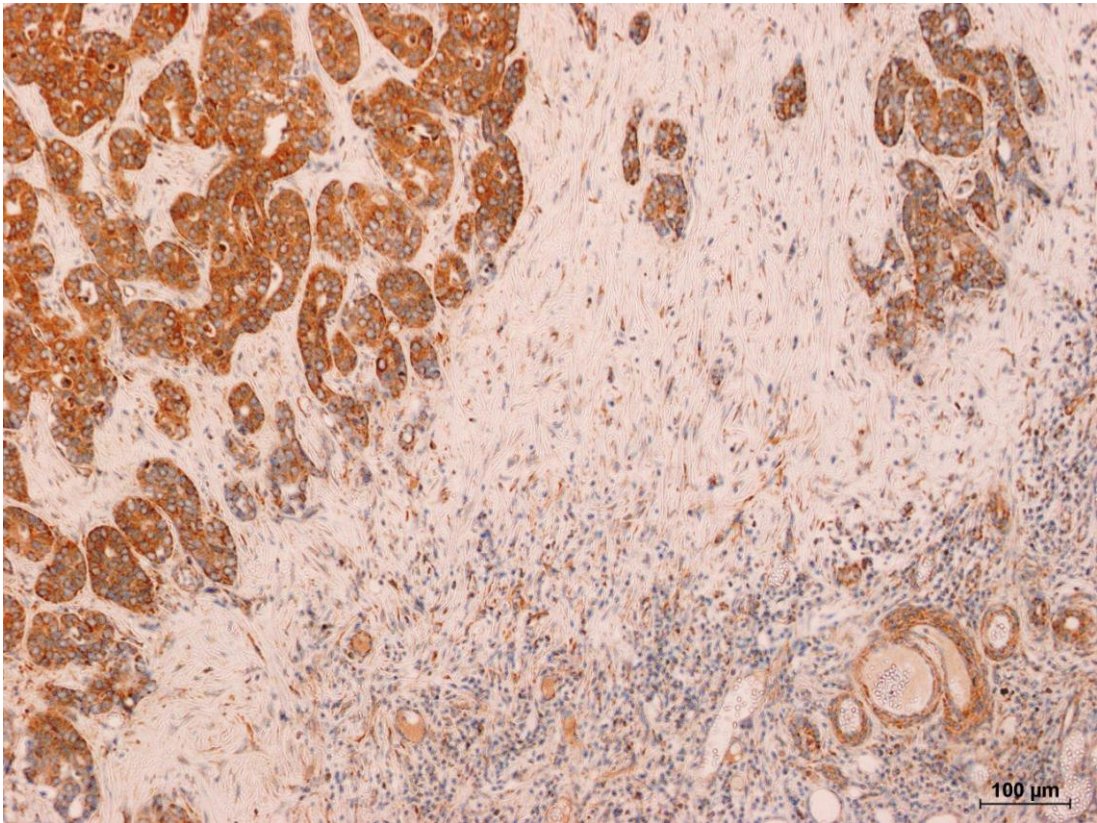
Figure 19: MMP9 expression in PH-CCA tissue and matched liver control.
IHC demonstrating strong expression in PH-CCA glandular tissue and mild stromal staining (top panel). Once again, as seen in the lower panel, a substantial degree of parenchymal expression in seen in matched normal liver tissue, and within normal cholangiocytes (arrow). These findings were representative of the whole cohort.
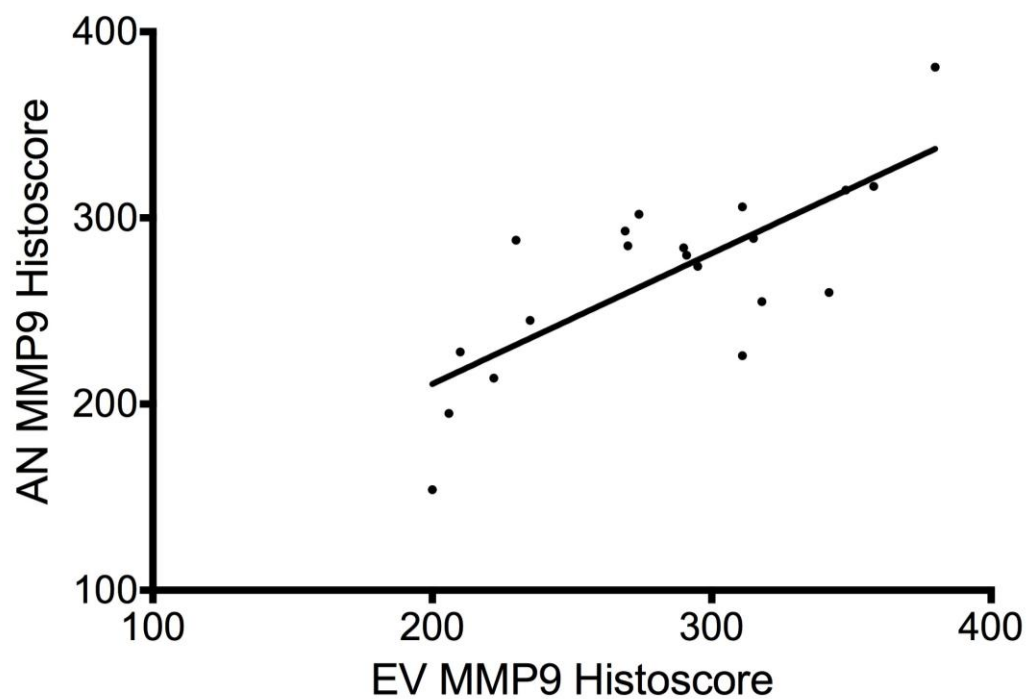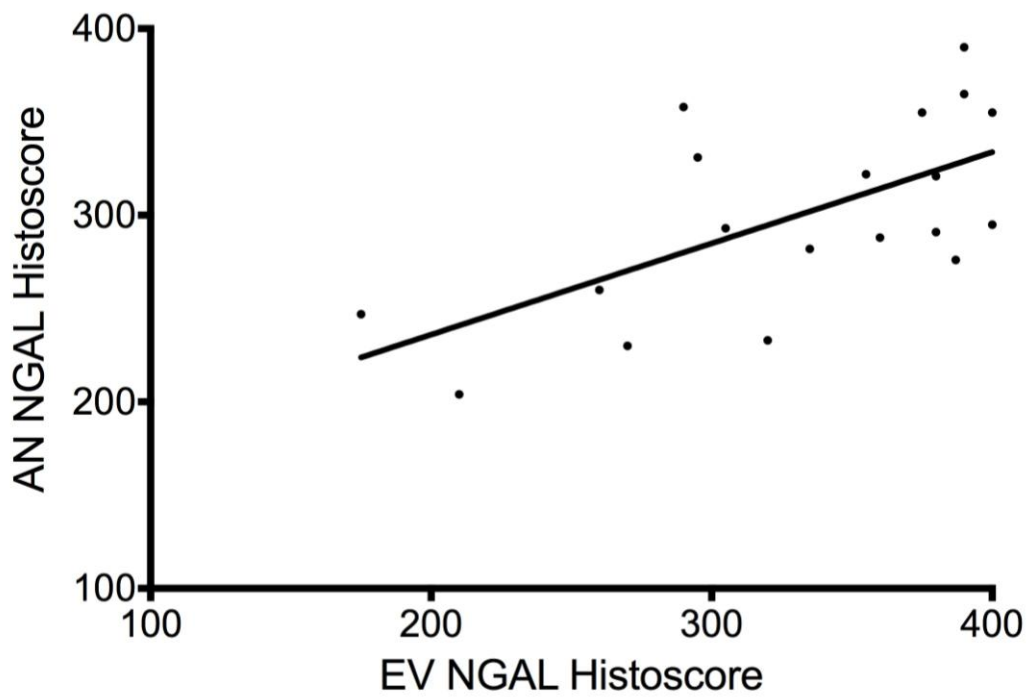
Figure 20: Inter-observer correlations for NGAL and MMP9 Histoscores.
Plotted data and line of best fit shown for both graphs. Top panel (n=19) showing data for NGAL (Spearman r=0.58, p=0.008) and bottom panel (n=20) showing data for MMP9 (Spearman r=0.64, p=0.002). AN and EV denote the initials of the scorers.

3.2.4 Tumoural expression of NGAL is significantly higher than that of matched normal liver parenchyma

The median (inter-quartile range) tumoural NGAL Histoscore was 327 (282-366), whereas the related figure for control NGAL expression was 200 (160-220). Figure 21 demonstrates the Histoscores for PH-CCA tissue matched with control liver tissue. As can be seen in this illustration, Histoscore values in PH-CCA for NGAL were significantly higher in comparison to matched liver parenchyma ($p<0.001$), and that for MMP9 just achieving statistical significance ($p=0.049$).

The paired NGAL and MMP9 Histoscores for all 54 patients are plotted as shown in Figure 22. This shows there was no statistically significant correlation between NGAL and MMP9 Histoscores.
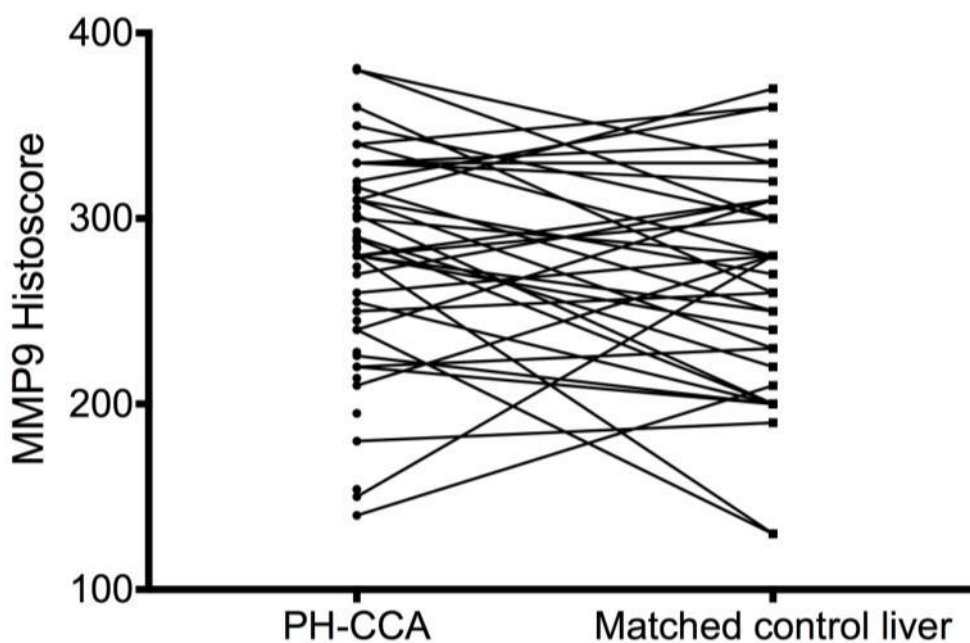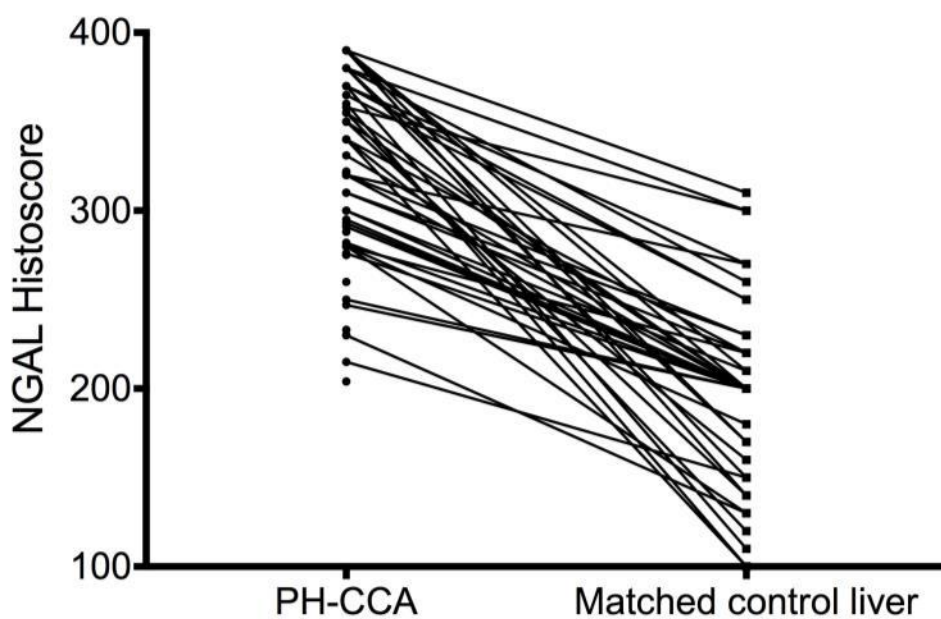
Figure 21: Plotted data of NGAL and MMP9 Histoscores in tumour versus matched control liver tissue.
A significantly higher Histoscore was seen in tumour tissue compared to control liver with NGAL (p<0.001) (top panel; n=44) but for MMP9 was borderline significant (p=0.049) (bottom panel; n=39); Wilcoxon Signed Rank test. Notably no tumour tissue sample stained negative for either marker.
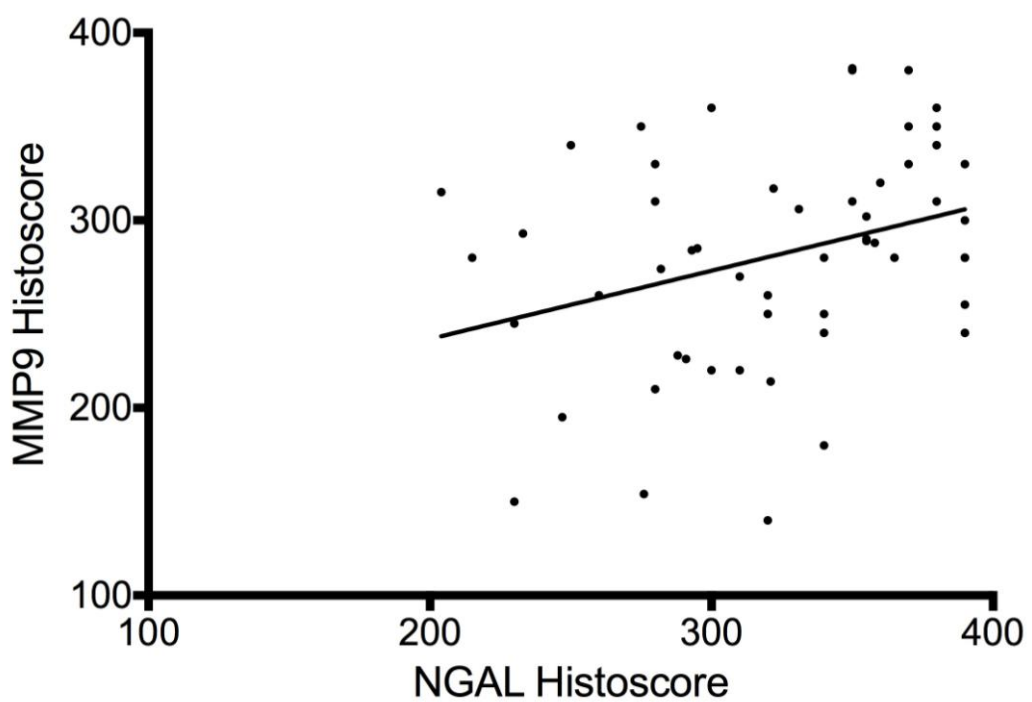
Figure 22: Scatter plot of NGAL versus MMP9 Histoscores in PH-CCA tissue, with the line of best fit shown.
The correlation of Histoscores between these 2 markers was low (Spearman r=0.32) and this finding was statistically significant (p=0.017); n=54

3.2.5 Correlation of clinicopathological variables with NGAL and MMP expression.

Clinicopathological variables for all 54 patients forming the study group were collated and analysed. The baseline patient parameters are summarised in Table 9, and were derived from analysis of the patient database as detailed in the Methods section. The median patient age was 57 years and the majority of the cohort was comprised of males (57%). The surgical procedure most commonly performed to resect the tumour was a right extended hepatectomy (35%). Notably, T1 disease was seen only in a minority of patients (4%) and most had evidence of lymph nodal involvement at surgery (54%).

The associations if any between NGAL and MMP9 Histoscores and patient variables were next interrogated as demonstrated in Table 10. Interestingly, lymph nodal metastasis was found to be significantly associated with NGAL expression (p=0.021). The only other clinicopathological factor found to have a statistically significant association with NGAL and MMP9 expression was local recurrence.

Experimental models of cholestasis have shown an association with hepatic NGAL expression (Borkham-Kamphorst et al., 2011) and therefore, a potential correlation between control liver NGAL expression and degree of pre-operative biliary obstruction was investigated as shown in Figure 23. However, no such association was found.

Variable	n (total = 54)	%
Median age (range) in years	57.6 (33-81)	
Gender		
Male	31	57.4
Female	23	42.6
Surgical procedure		
Left trisectionectomy (Segments 2,3,4,5,8,±1) & bile duct excision	18	33
Left hemihepatectomy (Segments 2,3,4,±1) & bile duct excision	7	13
Right trisectionectomy (Segments 4,5,6,7,8,±1) & bile duct excision	19	35
Right hemihepatectomy (Segments 5,6,7,8,±1) & bile duct excision	7	13
Orthotopic Liver Transplant	2	4
Bile duct excision alone	1	2
Median Tumour size (range) in mm	30 (10-75)	
Tumour differentiation (grade)		
Well (G1)	27	50
Moderate (G2)	19	35.2
Poor (G3)	8	14.8
Microscopic vascular invasion	33	61.1
Perineural infiltration	48	88.9
Tumour stage		
T1	2	3.7
T2	29	53.7
T3	19	35.2
T4	4	7.4
Nodal stage		
N0	25	46.3
N1	21	38.9
N2	8	14.8
AJCC Stage (7th edition)		
I	0	0
II	15	27.8
IIIA	8	14.8
IIIB	21	38.9
IVA	2	3.7
IVB	8	14.8
Resection margin		
R0 (clear)	21	38.9
R1 (involved)	33	61.1
Local recurrence	5	9.3

Table 9: Baseline PH-CCA patient characteristics

Variable	n	%	NGAL Histoscore [median (IQR)]	*p* value	MMP9 Histoscore [median (IQR)]	*p* value
Age (years)						
<58	27	50	321 (280-370)	0.78	285 (250-330)	0.67
>58	27	50	340 (288- 365)		280 (240-320)	
Gender						
Male	31	57	310 (280-360)	0.21	280 (228-317)	0.23
Female	23	43	340 (295-370)		293 (250-340)	
Tumour size (mm)						
<30	24	46	321 (284-357)	0.97	280 (220-317)	0.35
>30	28	54	340 (276-369)		282 (253-328)	
Histological grade						
Grade 1	27	50	322 (280-370)	0.75	300 (226-330)	0.74
Grade 2/3	27	50	331 (282-358)		284 (255-306)	
Microscopic vascular invasion						
Yes	33	65	322 (280-375)	0.79	289 (242-335)	0.34
No	18	35	336 (289-366)		280 (224-311)	
Nodal metastases						
Yes	29	54	355 (296-380)	***0.02***	290 (252-330)	0.35
No	25	46	310 (278-340)		280 (240-316)	
T Stage (AJCC 7th ed)						
T1/T2	31	57	322 (276-355)	0.21	285 (240-317)	0.77
T3/T4	23	43	340 (250-380)		284 (245-330)	
Resection margins						
R0 (positive)	21	39	340 (286-380)	0.53	280 (233-324)	0.58
R1 (negative)	33	61	321 (281-362)		289 (247-325)	
Local recurrence						
Yes	5	9	280 (253-304)	***0.03***	228 (182-248)	***0.005***
No	49	91	340 (292-370)		289 (258-330)	
Metastasis						
Yes	26	48	340 (292-378)	0.21	292 (256-323)	0.32
No	28	52	321 (272-359)		280 (230-325)	

Table 10: Comparison of NGAL and MMP9 Histoscores against clinicopathological patient variables.
p-values of statistical significance in bold and italics (Mann-Whitney U tests). Local recurrence defined as recurrent disease within the surgical bed.
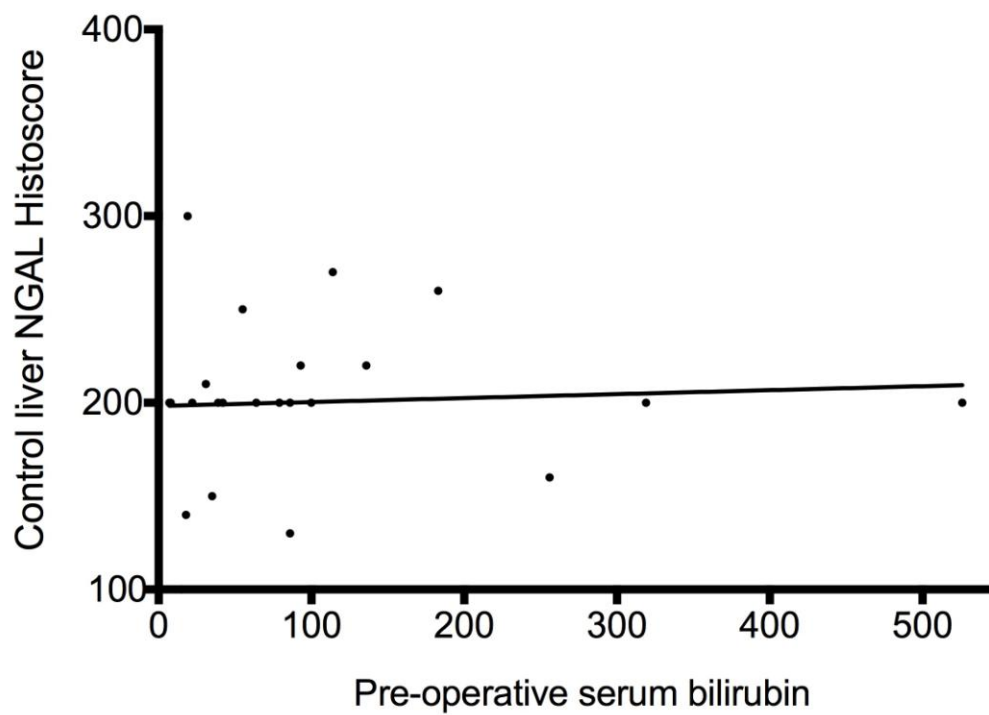
Figure 23: Scatter plot of control liver NGAL Histoscores against pre-operative serum bilirubin (μmol/L), with the line of best fit shown.
Poor agreement between these variables was observed (Spearman r=0.22) though this finding is more likely due to chance than a true effect (p=0.31); n=23

3.2.6 No prognostic impact of NGAL or MMP9 expression is evident on patient survival in this cohort

For the purposes of survival analysis, it was necessary to dichotomize the Histoscores of both NGAL and MMP9, thus rendering them categorical variables and enabling their analysis through log-rank statistical tests. Cognizant of the fact lymph nodal metastases are a prognostic determinant in PH-CCA and with the knowledge that NGAL Histoscores were predictive of nodal status in the cohort, I first identified a cut-off Histoscore of NGAL that best predicted this, and used this value to categorize this variable for survival analysis. As detailed in the Methods section, an online tool (Budczies et al., 2012) was utilised for this purpose. In the case of MMP9 Histoscores, the same tool was able to generate a cut-off that provided maximal separation of survival curves, whether statistically significant or not.

Figure 24 displays a receiver operating characteristic (ROC) curve for NGAL which shows an optimal cut-off Histoscore of 345, giving a sensitivity of 59% and specificity of 80% for predicting lymph nodal metastasis. Using this cut-off value however did not yield any significant associations on survival analysis as shown in Figure 25 and Figure 26. Log-rank tests for MMP9 also did not reveal any cut-offs that were significantly associated with poorer survival.
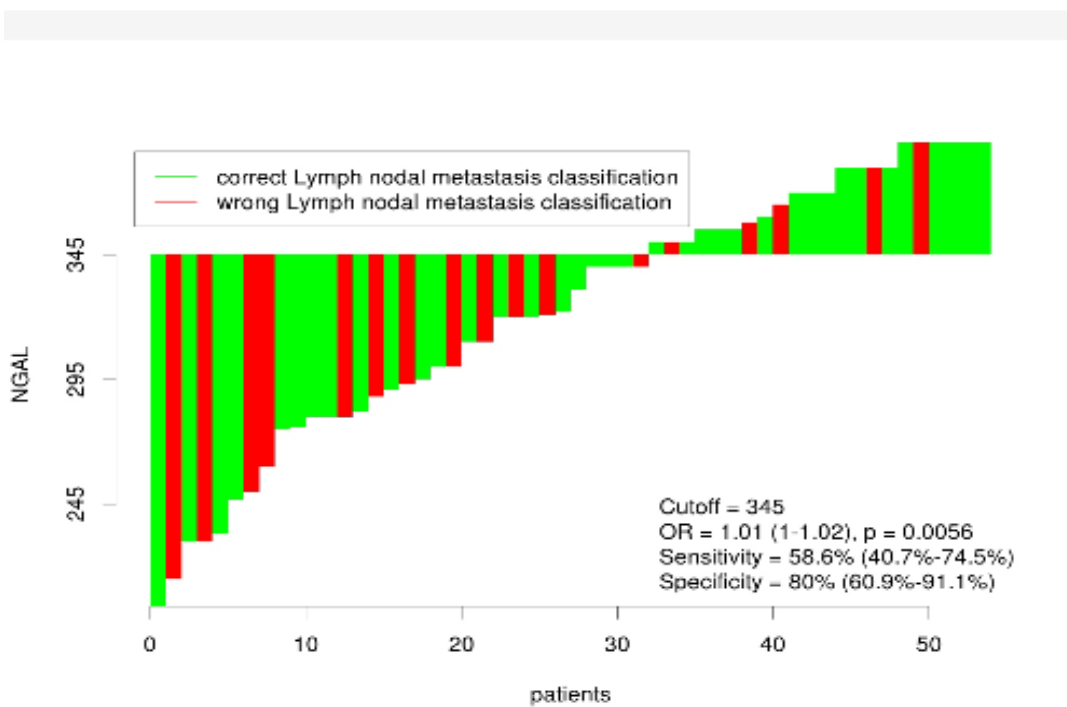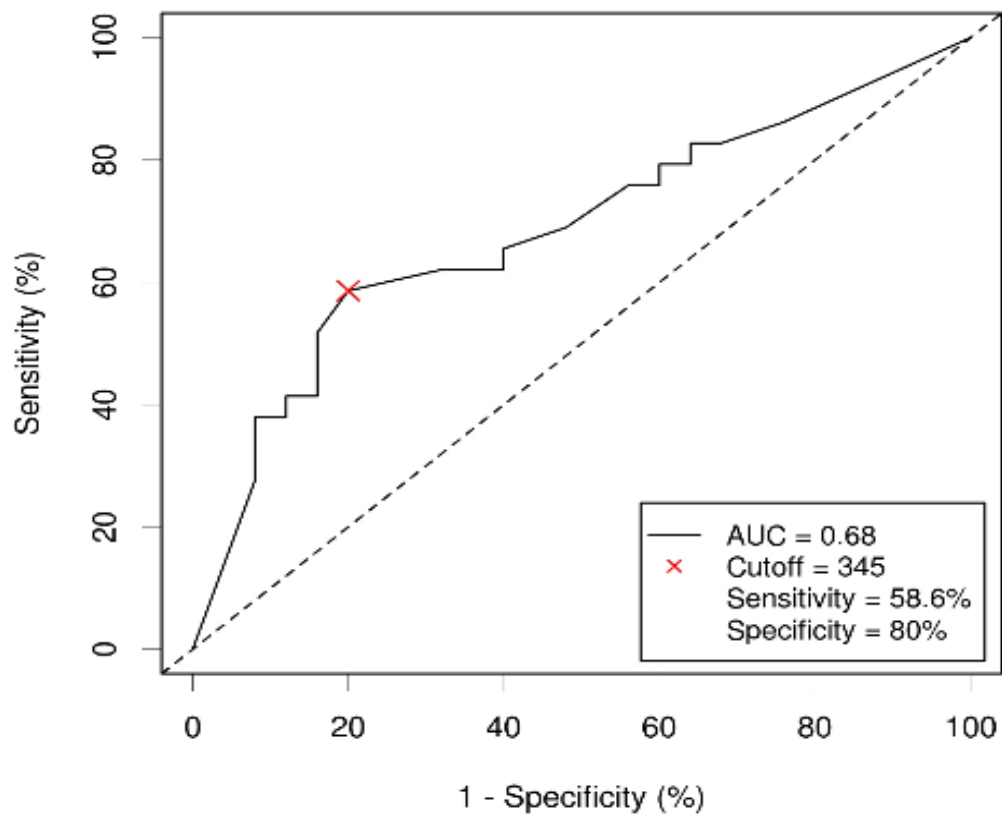
Figure 24: Receiver operating characteristic (ROC) analysis and Waterfall plot of NGAL Histoscore in predicting lymph nodal metastasis
Top panel showing the ROC curve with an optimal cut-off of 345 (marked by the red cross). The lower panel displays a Waterfall plot of the accuracy of this cut-off for nodal metastasis in all 54 patients. Here, individual Histoscores are shown as correctly or incorrectly indicating nodal involvement, on either side of the reference score of 345.
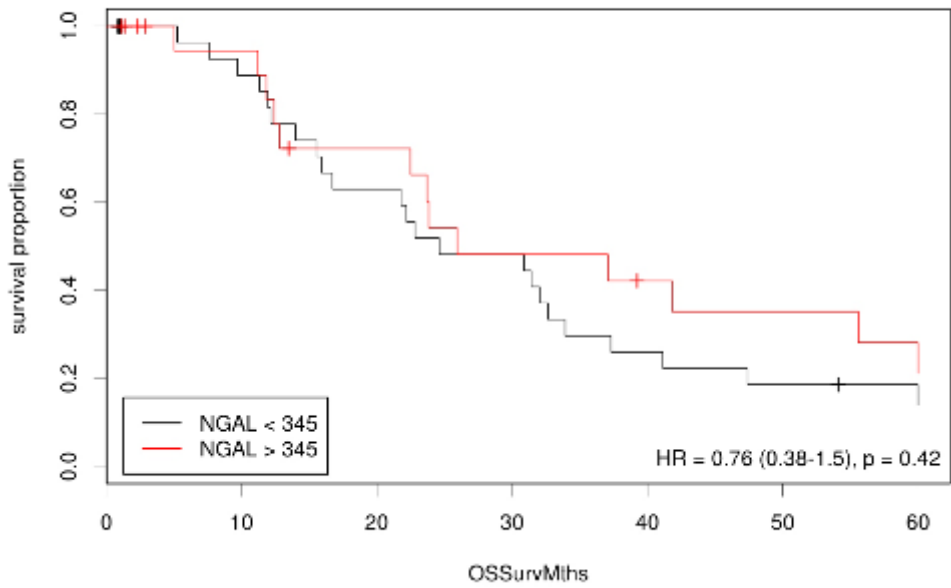
Figure 25: Kaplan Meier curves for overall survival with NGAL Histoscore cut-off 345
No significant difference in overall survival in seen in this instance (p=0.42)
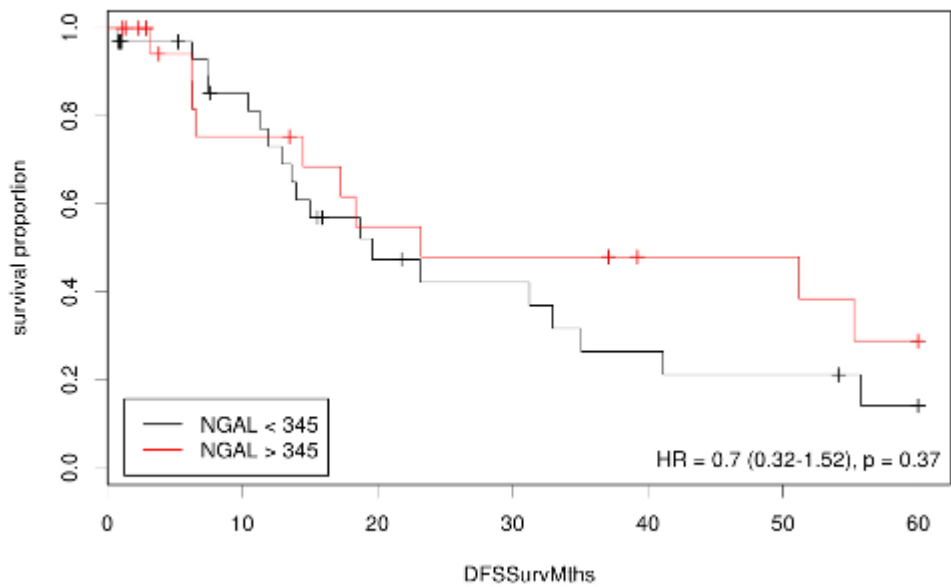
Figure 26: Kaplan Meier curves for disease-free survival with NGAL Histoscore cut-off 345.
No significant difference in disease-free survival is seen (*p*=0.37)

3.2.7 Characterising cellular expression of NGAL and MMP9 in CCA cell lines

As NGAL was found to have a significant association with the occurrence of nodal metastases, this biomarker was the primary focus of my investigative efforts in this stage for its applicability to a targeting approach. A panel of EH-CCA and IH-CCA cell lines (Table 7) were selected based their frequent use in CCA research (Zach, 2015) to ascertain any differences in biomarker expression between them. There is a relative dearth of established PH-CCA cell lines, and amongst my selection, only OZ was stipulated as being derived from PH-CCA (Homma et al., 1987). Accordingly, for the purposes of my experiments, all tested EH-CCA cell lines were taken to be representative of both extra-hepatic and peri-hilar variants. In order to assess control expression, the normal cholangiocyte cell line H69 was included in my experiments.

All experiments in this section were conducted primarily with a view towards establishing whether there was any membrane or stromal expression of NGAL, as this is a pre-requisite for a successful targeting strategy (van Oosten et al., 2011).

3.2.7.1 Immunofluorescence of CCA and normal cholangiocyte cell lines

CCA cell lines were assessed for localisation of NGAL and MMP9 by immunofluorescence (IF) staining. To minimize cellular permeabilization during fixation, the latter was performed with 4% paraformaldehyde as discussed in the Methods section.

For NGAL, the EGI-1 cell line gave the brightest staining intensity by preliminary visual assessment and hence was used for exposure standardization for image capture with all other cell lines (Figure 27). Using this as the reference image, expression in all remaining cell lines was scant (Figures 28-33). Only the IH-CCA cell line, HuCCT-1 and the normal cholangiocyte cell line, H69 showed a marginal degree of NGAL expression.

With respect to MMP9, the cell line TFK-1 gave the brightest fluorescent signal on direct visualization under the fluorescent microscope and hence all captured images were standardized to its exposure settings (Figures 34-40). However, subsequent analysis of images showed Huh-28 as the highest expressor of MMP9. This disparity may be due to difficulties in assessing differences in fluorescent intensities over background fluorescence accurately by eye. Comparison of staining intensities for both markers is shown below in Table 11.

For both antibody runs, 4% PFA appeared to permeabilize the cell membrane (despite being free of methanol in its composition) and staining therefore was visualized mostly in the cytoplasmic component of all cells. The cell line OZ however did show specific membrane staining using this modality.

In conclusion, the results of my IF experiments showed variable levels of NGAL and MMP9 expression within CCA cell lines and H69. Positivity was mostly noted in the cytoplasmic compartment, although membrane localization was noted in some instances eg. OZ cell line.
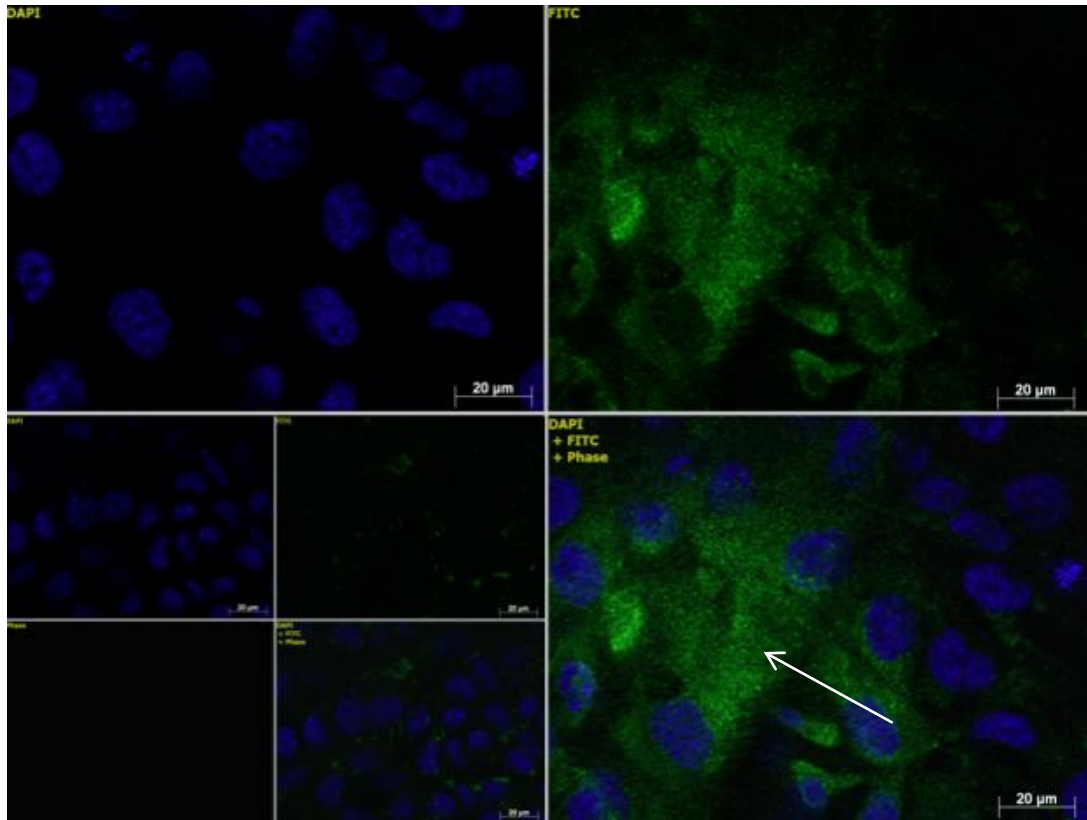
Figure 27: IF for NGAL on EGI-1
Top left panel- DAPI nuclear staining, top right panel- NGAL visualized with FITC filter,
bottom right panel- Merged image. A diffuse pattern of staining is seen intracellularly (arrow).
Bottom left insert of 3 smaller squares show same image layout with omitted primary antibody
(control). Bottom left smaller square left blank (x63 magnification)
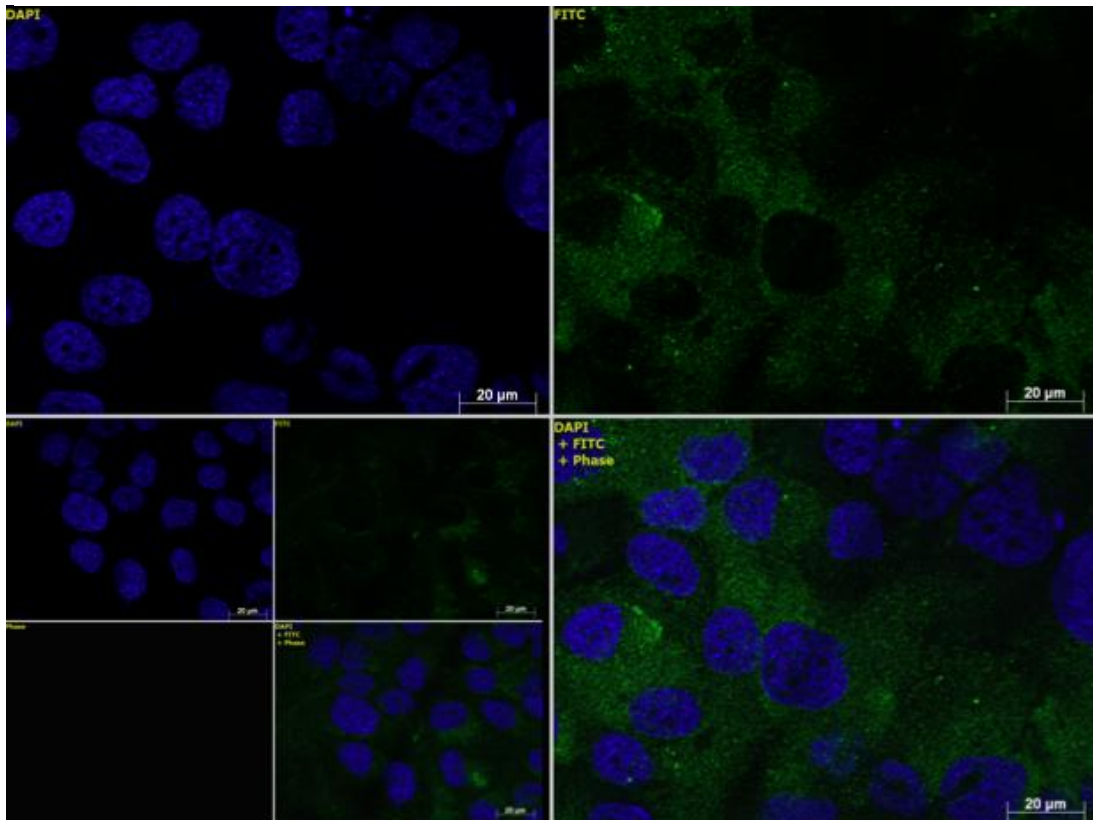
Figure 28: IF for NGAL on HuCCT-1
Relatively milder amounts of expression of NGAL is seen within cytoplasm in this instance
See Figure 27 legend for layout of panels (x63 magnification)
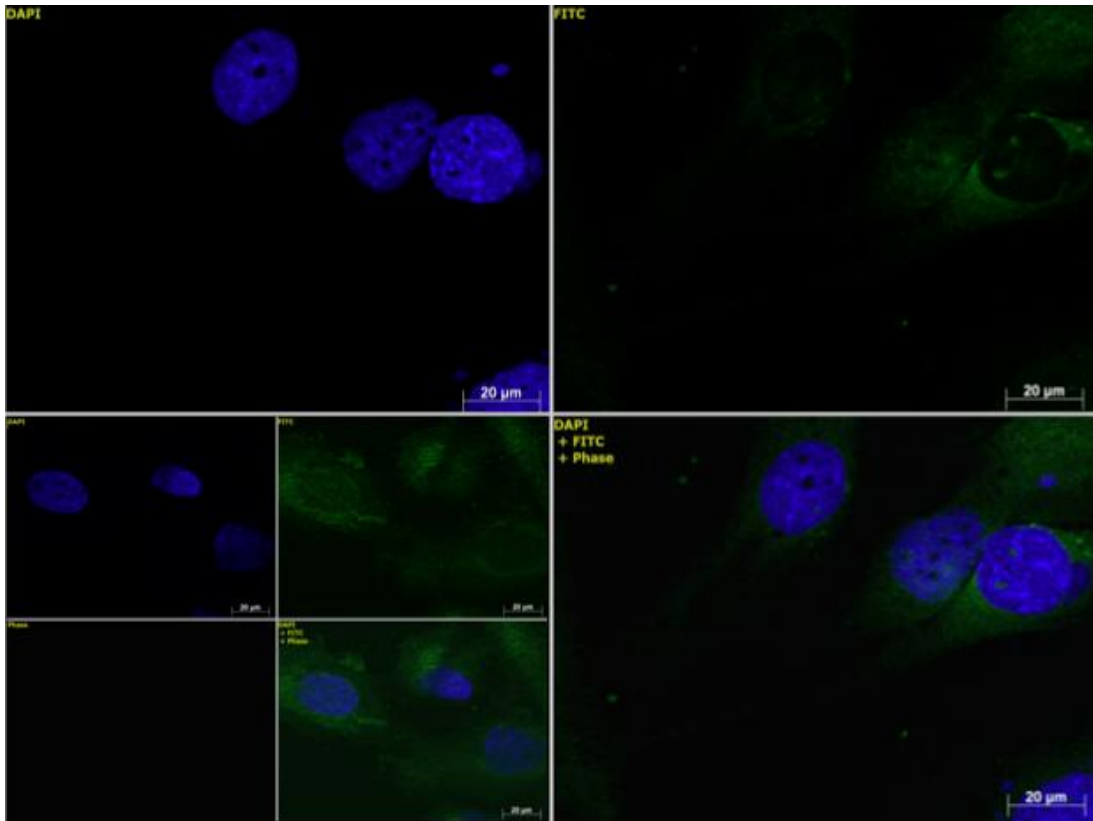
Figure 29: IF for NGAL on Huh-28
No substantial expression is seen in comparison to the background staining seen with the no-primary run. See Figure 27 legend for layout of panels (x63 magnification)
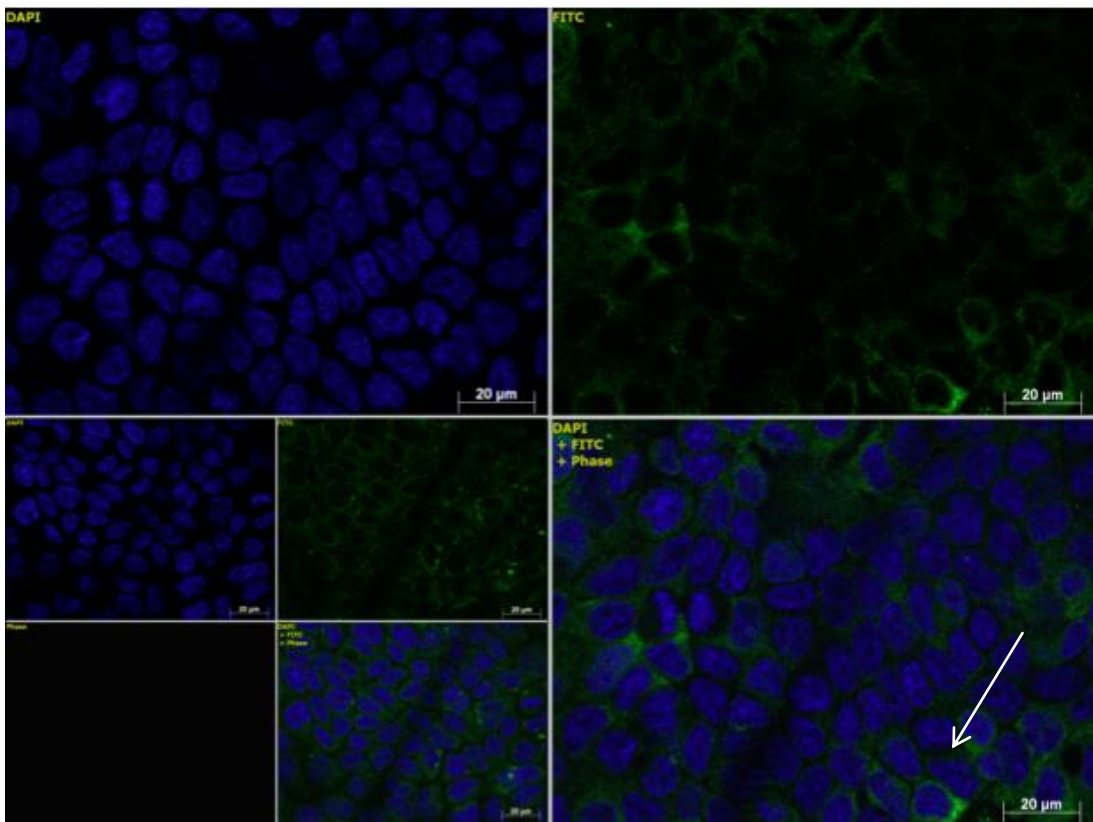
Figure 30: IF for NGAL on OZ
In this instance, membranous expression of NGAL is evident (arrow), although overall levels of positivity remain poor. See Figure 27 legend for layout of panels (x63 magnification)
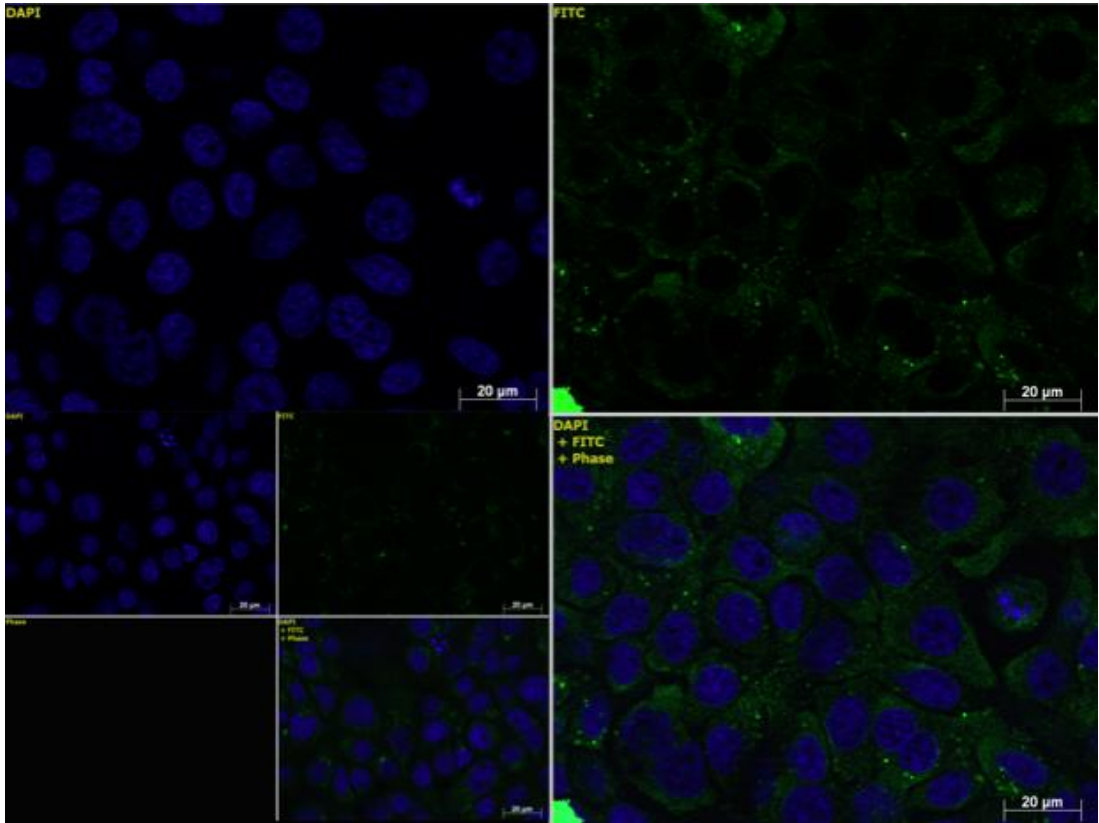
Figure 31: IF for NGAL on TFK-1
Marginal levels of NGAL expression is observed. See Figure 27 legend for layout of panels
(x63 magnification)
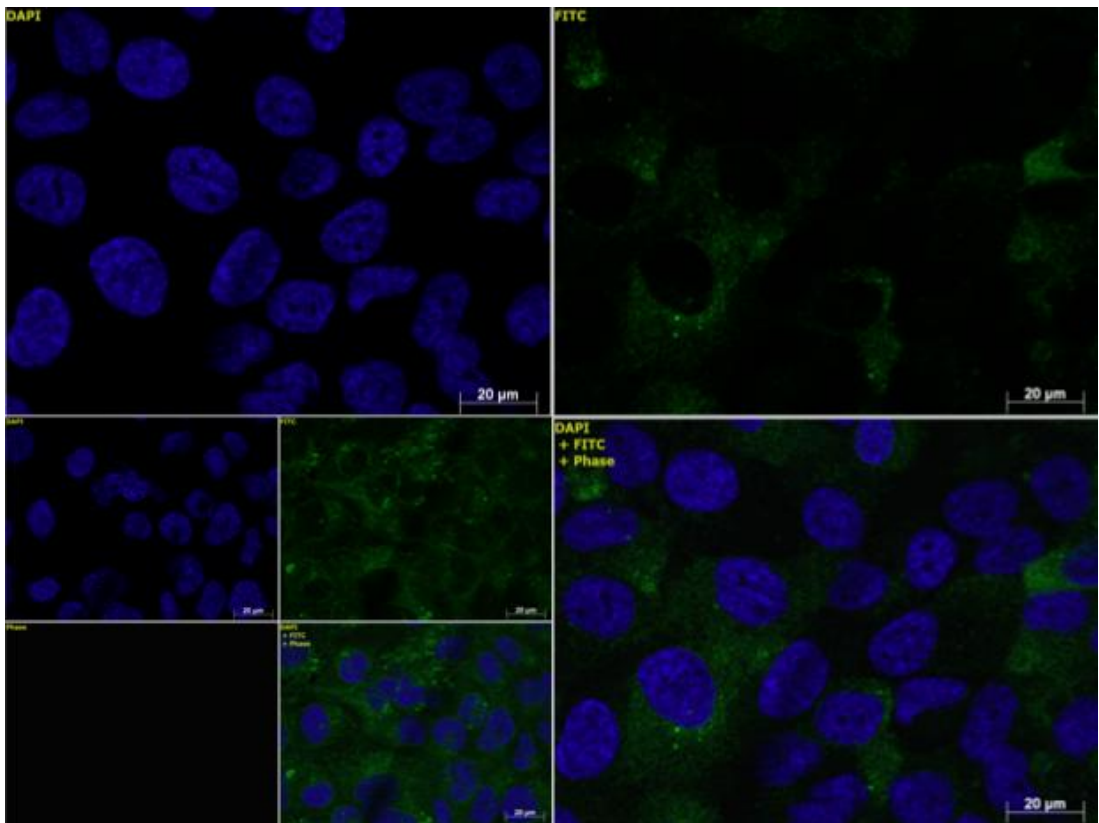
Figure 32: IF for NGAL on SkChA-1
No-primary run with an equivalent amount of background staining, indicating near absent
expression of the marker in this cell line. See Figure 27 legend for layout of panels (x63
magnification)
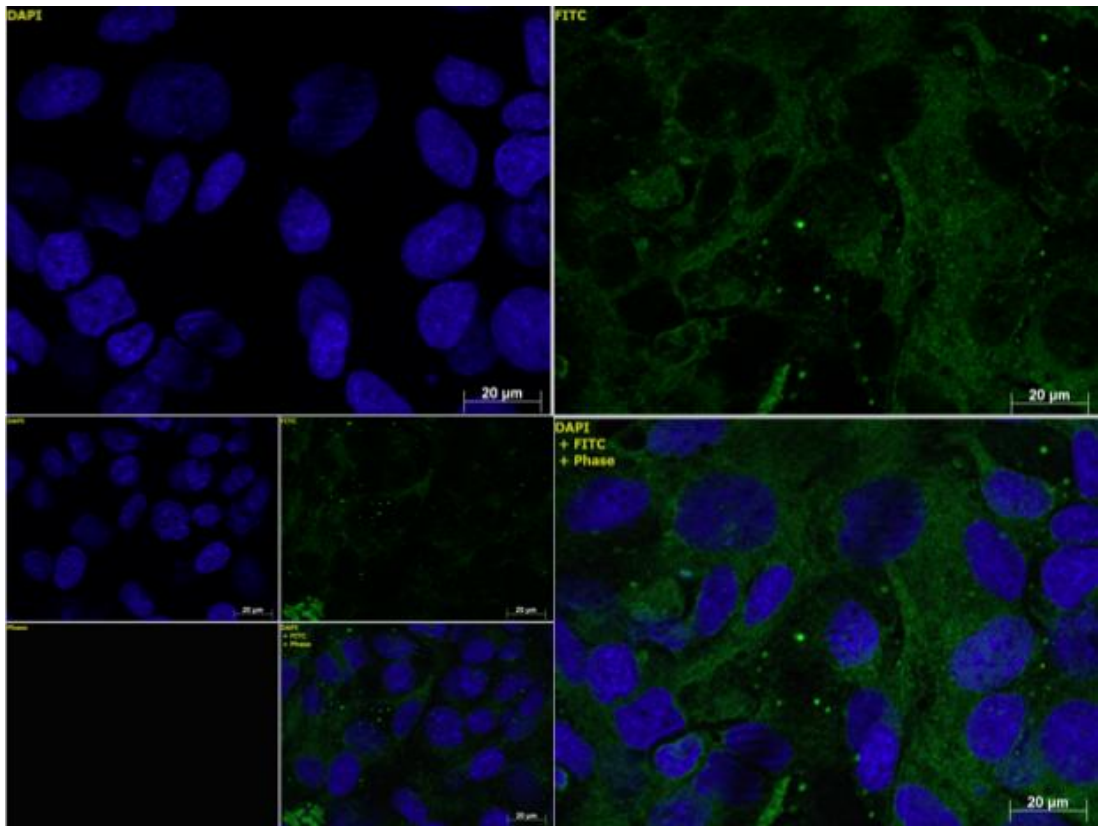
Figure 33: IF for NGAL on H69

The normal cholangiocyte cell line showed appreciable levels of NGAL expression within cytoplasm, albeit at lesser intensities than the reference image of EGI-1. See Figure 27 legend for layout of panels (x63 magnification)
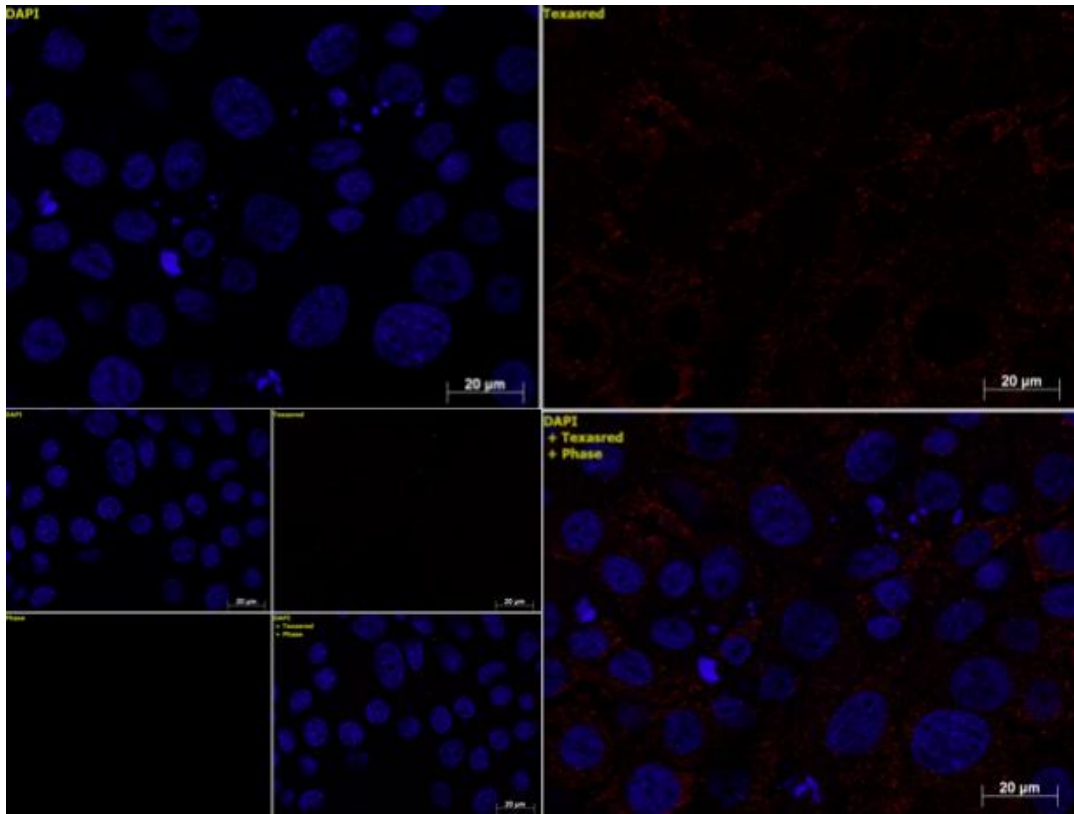
Figure 34: IF for MMP9 on TFK-1
Top left panel- DAPI nuclear staining alone, top right panel- MMP9 visualized with Texas Red filter, bottom right panel- Merged image, Bottom left insert of 3 smaller squares showing the same image layout where primary antibody was omitted (control). Although used as the reference slide for best expression by microscopic assessment, hardly any staining is seen following image capture. Bottom left smaller square left blank (x63 magnification)
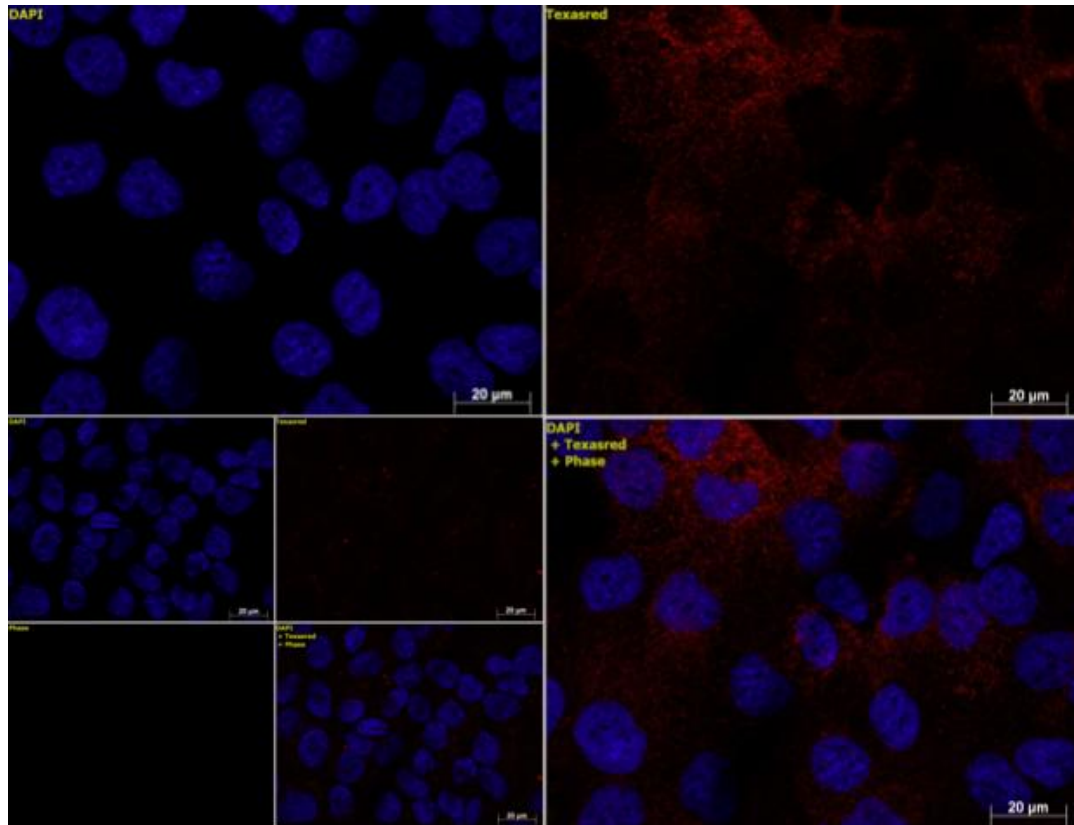
Figure 35: IF for MMP9 on HuCCT-1
Predominantly cytosolic staining is observed. See Figure 34 legend for layout of panels (x63 magnification)
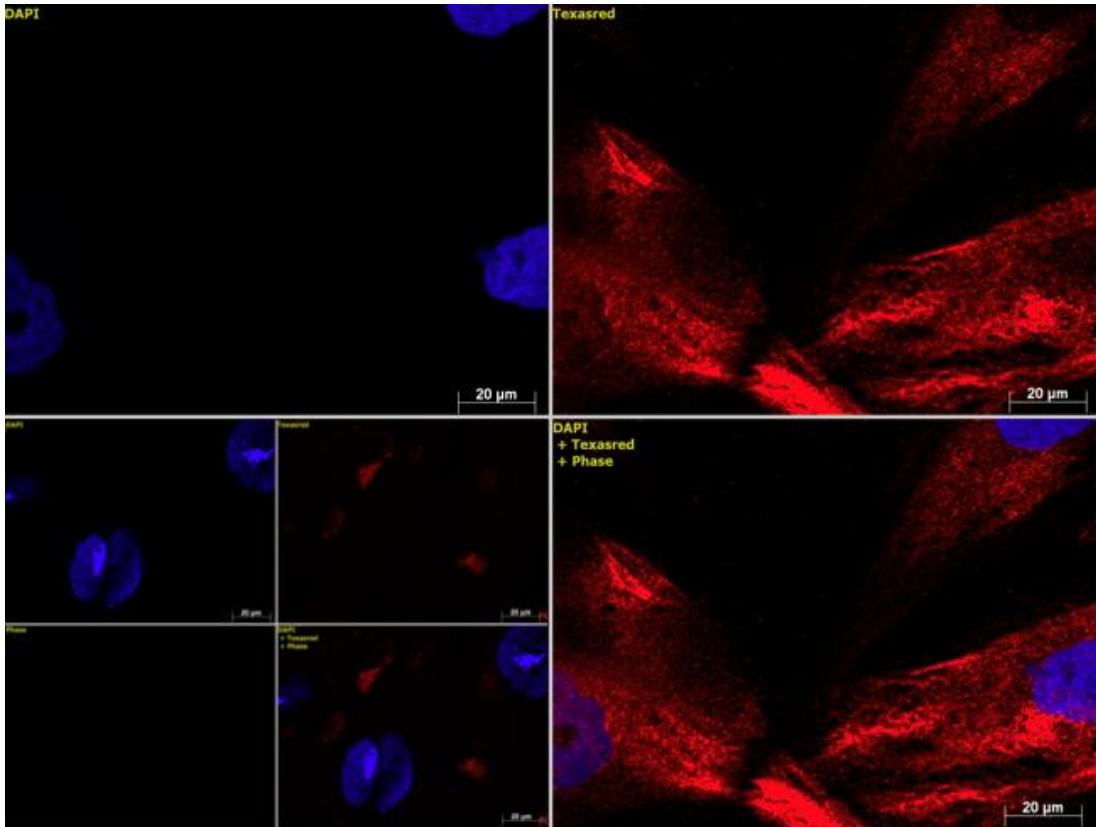
Figure 36: IF for MMP9 on Huh-28
Strong cytosolic expression of MMP9 is seen in this instance. See Figure 34 legend for layout of panels (x63 magnification)
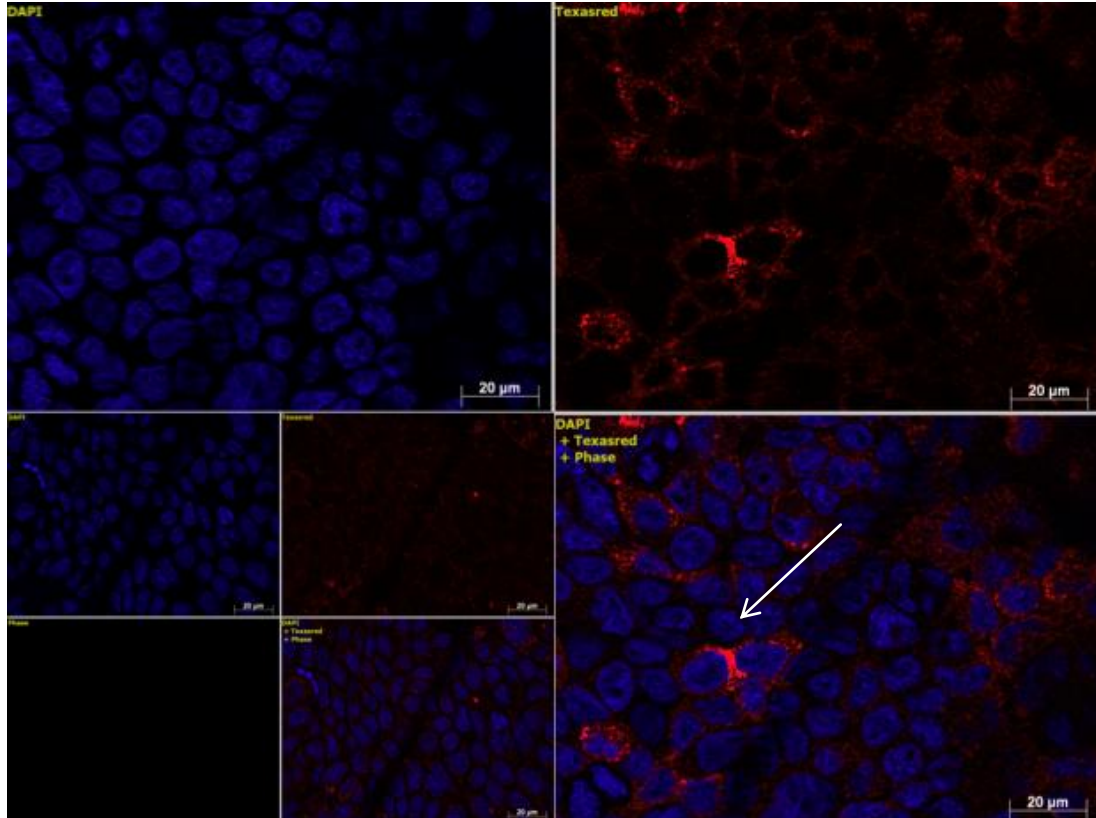
Figure 37: IF for MMP9 on OZ
Membranous staining (arrow) is noted on this occasion. See Figure 34 legend for layout of panels (x63 magnification)
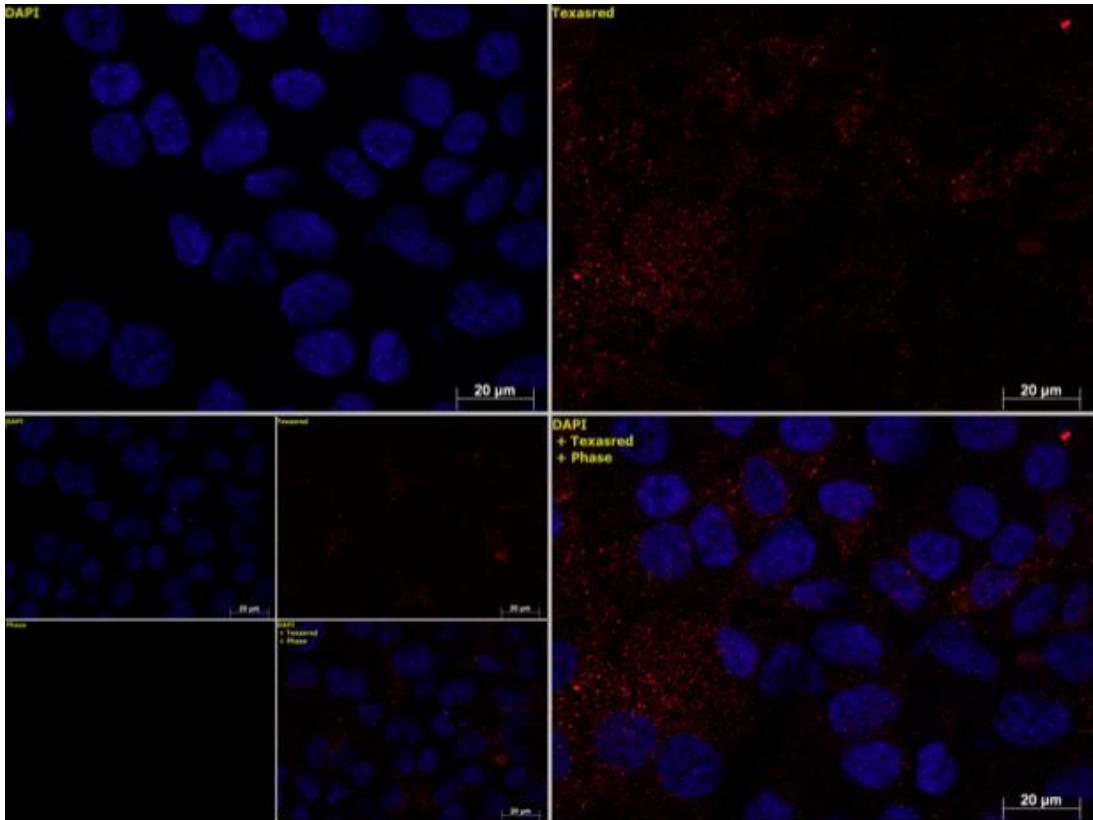
Figure 38: IF for MMP9 on EGI-1
A punctate pattern of expression is observed within cytoplasm of tumour cells. See Figure 34 legend for layout of panels (x63 magnification)
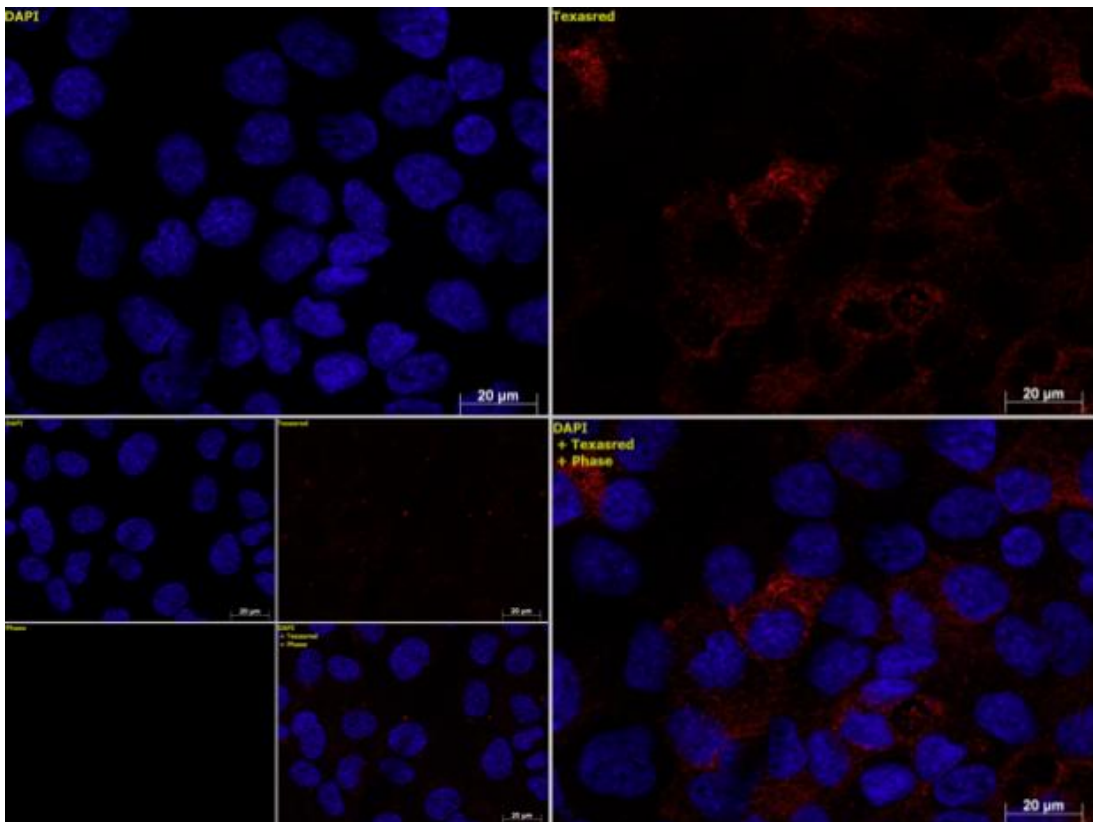
Figure 39: IF for MMP9 on SkChA-1
Small degrees of expression within tumour cytoplasm is seen. See Figure 34 legend for layout of panels (x63 magnification)
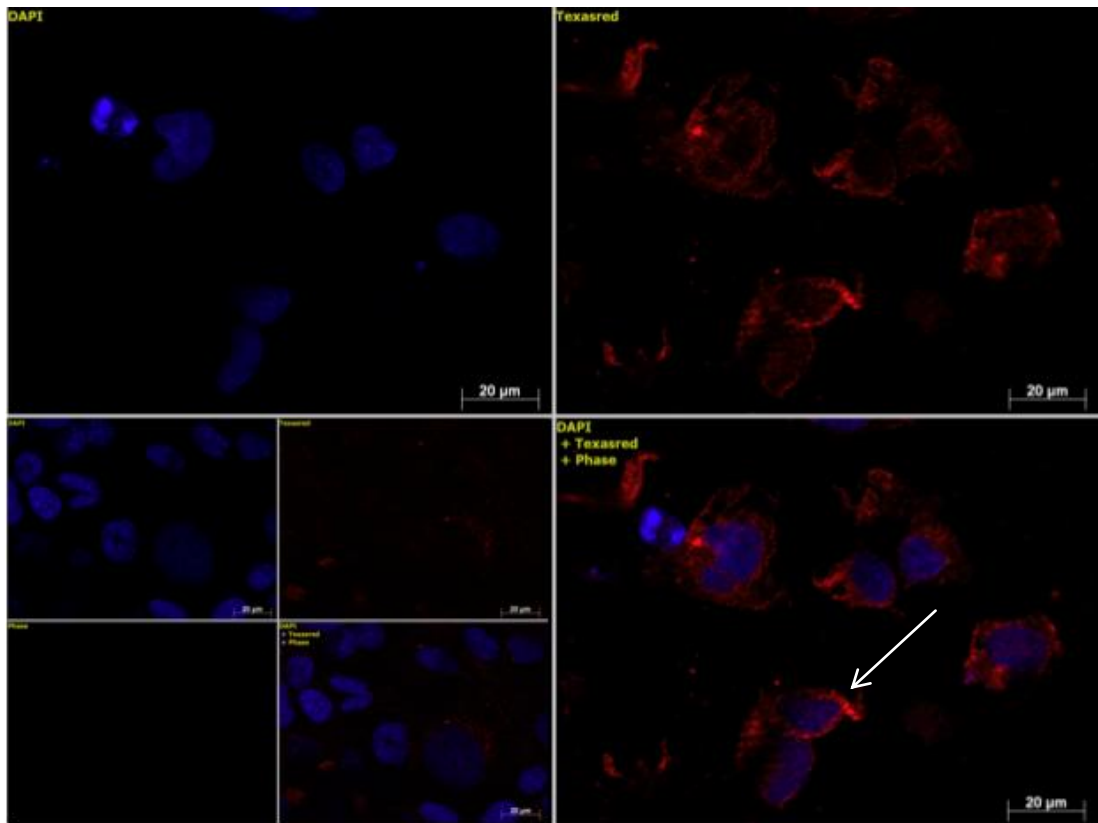
Figure 40: IF for MMP9 on H69
Membranous staining (arrow) is observed in this instance. See Figure 34 legend for layout of panels (x63 magnification)

Cell line	NGAL	MMP9
EGI-1	+++	+
HuCCT-1	++	+
Huh-28	-	+++
OZ	+	++
TFK-1	+	+
SkChA-1	-	+
H69 (normal)	++	++

Table 11: Summary of expression of NGAL and MMP9 proteins detected on CCA cell lines by IF
+++ denotes relatively strong expression, ++ moderate expression, + weak expression, - none detected.

3.2.7.2 Expression of NGAL and MMP9 in whole cell and membrane-enriched lysates of CCA and normal cholangiocyte cell lines

The objective of my Western blotting experiments was to identify if NGAL and MMP9 were present in whole cell lysates of CCA and H69 cell lines. Subsequently, these cell lines were assessed for membrane localization of NGAL using fractionated lysates.

WB analysis utilising whole cell lysates revealed the presence of NGAL in all tested extra-hepatic CCA cell lines at its expected molecular weight (25kDa), and its near absence in the intra-hepatic cell line Huh-28 (Figure 41). EGI-I, TFK-1 and OZ showed relatively strong expression of NGAL on densitometric analysis of protein bands using ImageJ software. Densitometric data for H69 was obtained from separately run blots, and shows near absence of NGAL in this cell line (Figure 42).

To determine the intracellular localisation of NGAL within the cells, membrane fractions were separated from cytoplasm as detailed in the Methods (section 2.3.2.1). Western blotting of these fractions revealed a similar pattern of expression to that obtained with total cell lysates. A predominant expression of NGAL in the membrane fraction of the CCA cell lines EGI-1, TFK-1, OZ and HuCCT-1 was detected (Figure 43 and Figure 44). Once again, the intra-hepatic CCA cell line Huh-28 and the normal cholangiocyte cell line H69 did not express any NGAL. The loading control α-tubulin (50kDa) was found to be specific for cytoplasmic fractions.
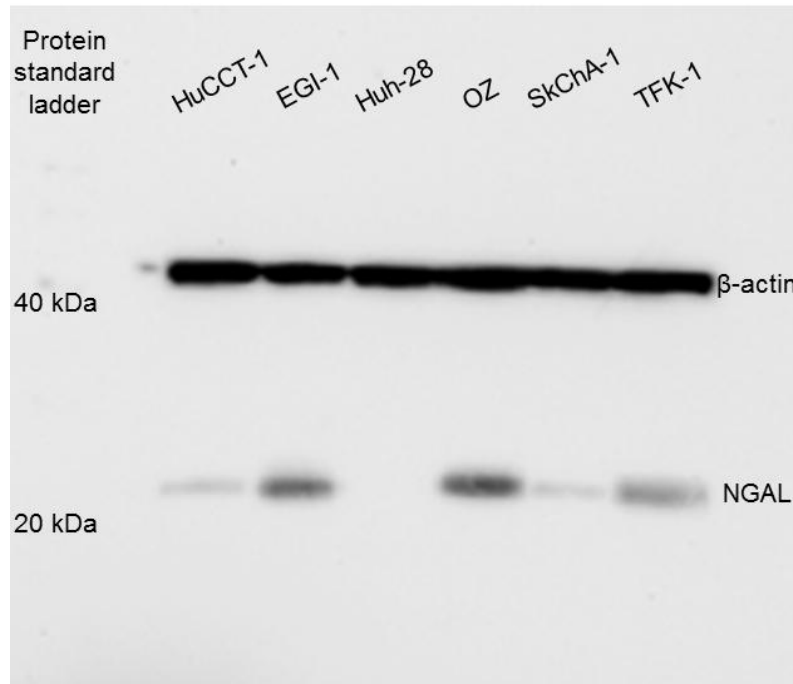
Figure 41: Western blot image showing NGAL protein (25kDa) expression in whole cell lysates of tested CCA cell lines.
The absence of expression by the cell line Huh-28 is evident, whereas OZ shows the strongest expression (β-actin [42kDa] used as loading control and shows equal protein loading across lanes).
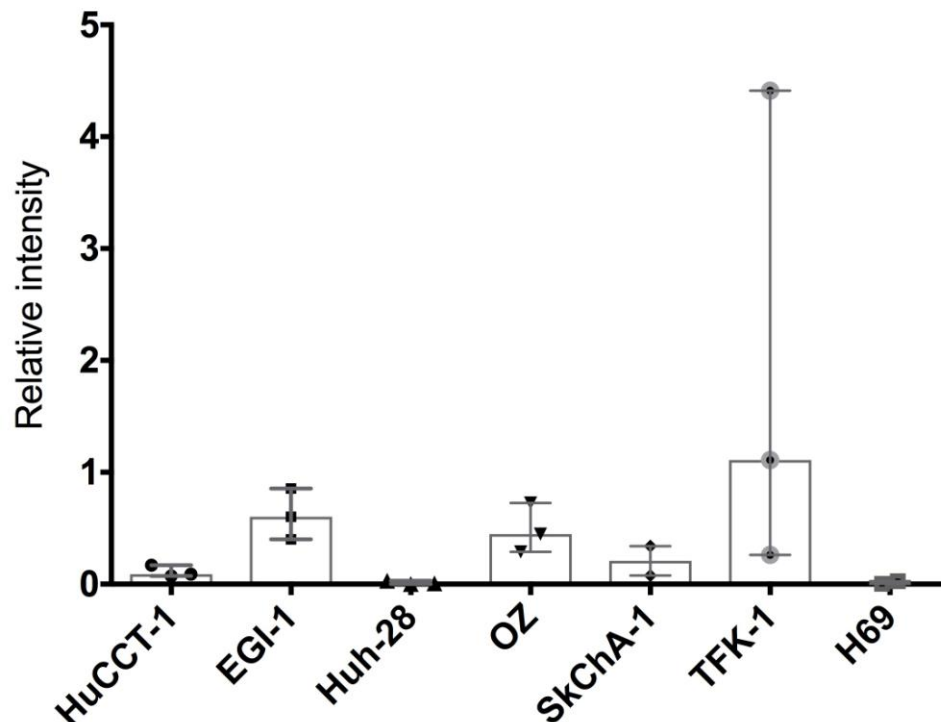
Figure 42: Bar chart of relative NGAL expression by Western blotting in whole cell lysates of CCA and normal cholangiocyte H69 cell lines
Intensities shown relative to loading control protein β-actin (given an intensity of 1). Near absent expression is observed for Huh-28 and H69 cell lines, whereas other CCA cell lines show varying degrees of NGAL expression (pooled data from 3 blots except for SkChA-1 and H69, shown as median with upper/lower values).
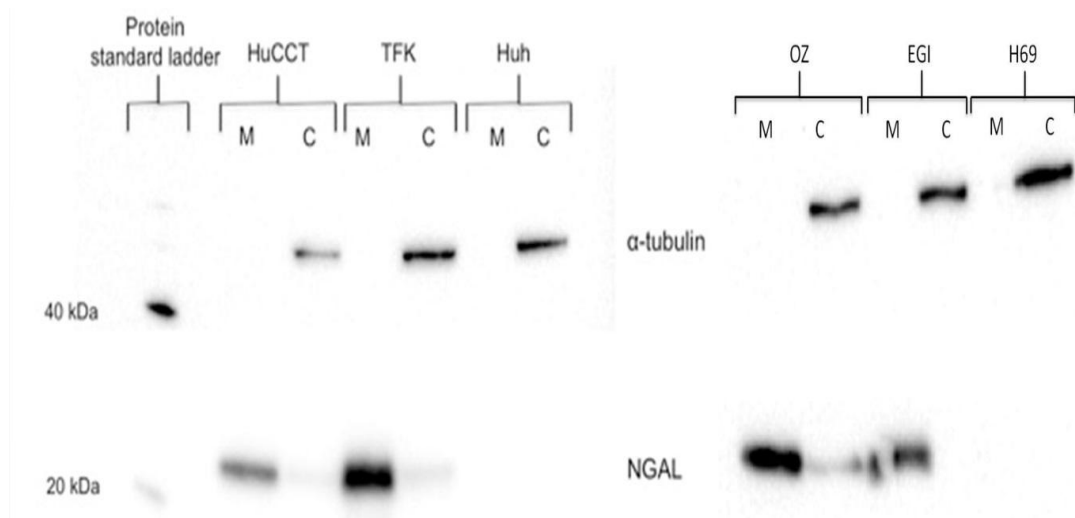
Figure 43: Western blot image demonstrating NGAL protein in membrane enriched lysates of CCA and H69 cell lines
Preferential expression of NGAL (25kDa) in the membrane portion ('M') of fractionated cell lysates when compared to their corresponding cytoplasmic portion ('C'). Expression is notably absent in Huh-28 and the normal cholangiocyte cell line H69 (α-tubulin [50kDa] used as loading control).
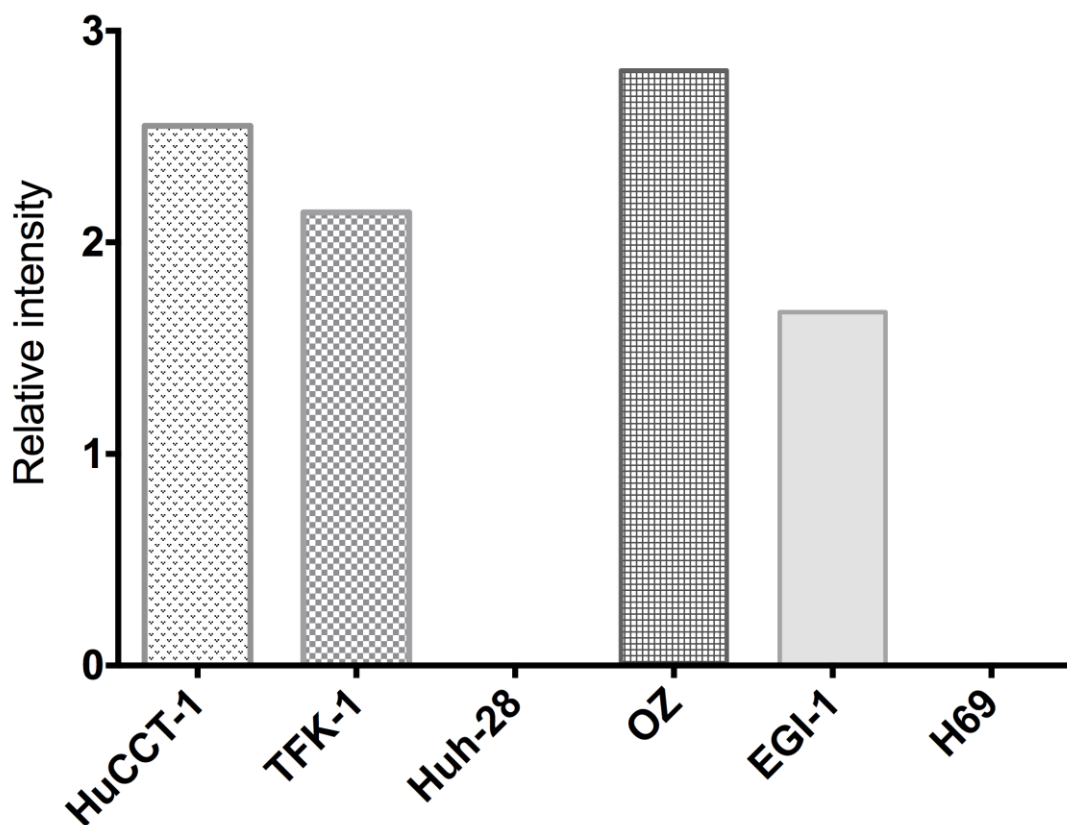
Figure 44: Bar chart of relative NGAL expression by Western blotting in membrane enriched lysates of CCA and normal cholangiocyte H69 cell lines
Intensities shown relative to loading control protein α-tubulin (given an intensity of 1), as derived from image in Figure 48. Near absent expression is once again seen in Huh-28 and H69 cell lines, whereas other CCA cell lines show varying degrees of NGAL expression.

When whole cell CCA lysates were interrogated for MMP9, the 65kDa active isoform was identified in HuCCT-1, EGI-1, OZ and TFK-1, but not so in the case of Huh-28 and SkChA-1 (Figure 45). I found that by visual assessment the expression of NGAL and MMP9 were proportional to each other across all lines (comparing Figures 41 and 45) except in the instance of HuCCT-1, which had weak NGAL expression but strong positivity for MMP9.

A summary table of expression of NGAL and MMP9 is given below in Table 12. This compares the expression seen in both whole cell lysates (and membrane fractions for NGAL). Large differences are also highlighted with regards to the expression imaged by IF of cells grown *in vitro*.
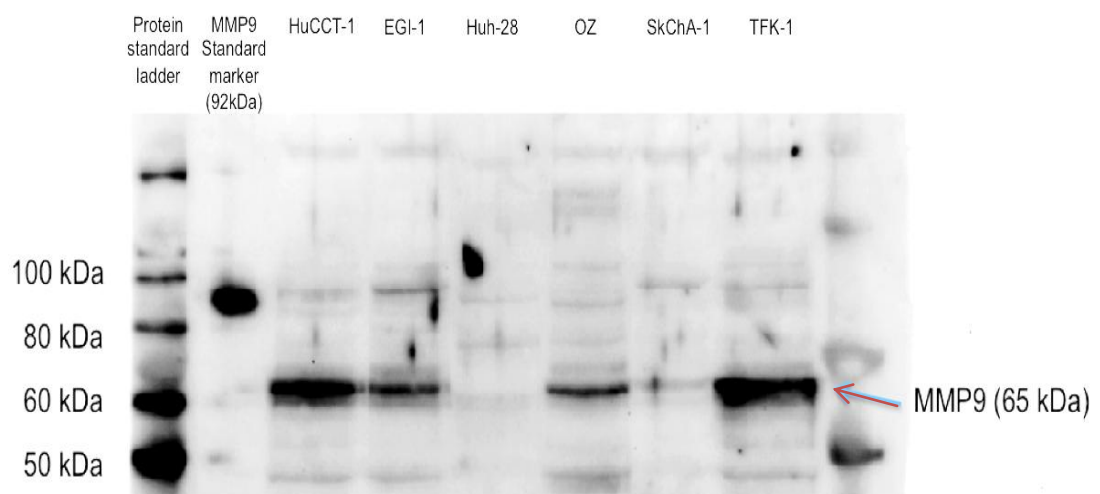
Figure 45: Western blot image showing MMP9 expression in whole lysates of CCA cell lines

Blot performed on the upper sectioned half of the membrane used in Figure 41. Purified MMP9 positive control (92kDa) seen in the second vertical lane. The most prominent protein bands are seen at the 65kDa level (arrow) rather than 92kDa, corresponding to the active and latent forms of MMP9 respectively. TFK-1 and HuCCT-1 show the strongest positivity for the 65kDa isoform, with paucity of expression seen in Huh-28. Loading controls as shown in Figure 41.

Cell line	NGAL			MMP9	
	Whole cell lysate	Membrane fraction	Comparison to IF data	Whole cell lysate	Comparison to IF data
EGI-1	++	++	Similar	++	Similar
HuCCT-1	+	+++	Similar	++	Similar
Huh-28	-	-	Much lower	-	Much lower
OZ	++	+++	Higher	++	Similar
TFK-1	+++	++	Higher	+++	Higher
SkChA-1	+	N.D.	Higher	+	Similar
H69	-	-	Much lower	N.D.	

Table 12: Comparison of relative expression of NGAL and MMP9 in each cell line between WB and IF detection of proteins

+++ denotes relatively high protein levels detected, ++ moderate levels, + low levels and –
no protein detected by Western blotting. N.D. denotes not determined.

3.2.7.3 Flow cytometry antibody optimization

The purpose of FC analysis of CCA cell lines was as in the case of Western blotting, to determine the cell surface expression of NGAL and MMP9 towards ascertaining the suitability of these biomarkers for a targeting approach. Experiments were set up as detailed in the Methods chapter (section 2.3.3).

Once samples were run, cell populations were segregated based on viability (7AAD positivity being the basis for exclusion) as shown in Figure 46, and histograms constructed for each dilution of antibody (Table 13), using the Diva software package v6 (Becton Dickinson, CA, USA). For the purposes of this optimization, SkChA-1 was used as its cells separated most easily of all CCA cell lines for sorting. The best deemed dilutions for both antibodies were taken forward for evaluation of other cell lines.

As can be seen from the median fluorescence values in Figure 47, a primary antibody dilution of 1:25 offered the best distinction of the anti-NGAL antibody from the secondary fluorophore alone (Pacific Blue) and was therefore chosen as the optimal dilution for this antibody. In the case of MMP9 as shown in Figure 48, an optimal dilution of 1:25 again provided the best discrimination between the primary antibody and the Alexa Fluor 488 secondary. Experiments using these optimized antibody dilutions were then repeated on other cell lines as illustrated in Figure 49 and Figure 50. As is evident from the displayed data, I was not able to show a significant increase in median fluorescence intensity (which would reflect increased membrane expression) of anti-NGAL or anti-MMP9 on these cell lines when compared to the cells without addition of primary antibody
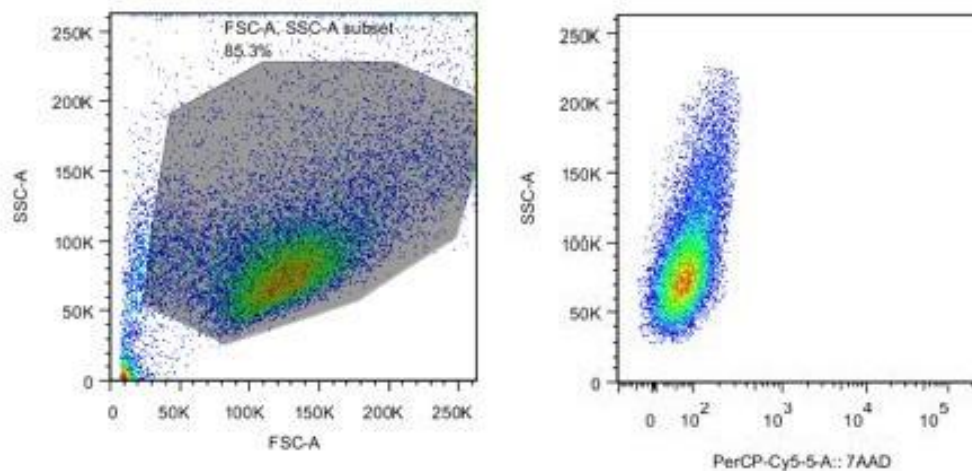
Figure 46: Cell gating strategy for flow cytometry
Left panel showing how the majority of the cell population is selected (shaded area). Right panel
illustrating the result of selection of a predominantly 7AAD negative cell population. FSC and SSC
indicating Forward and Side Scatter populations respectively.

Tube No.	Primary antibody amount in 50µl (final dilution in 100µl volume)	Secondary antibody amount in 50ul (final dilution)	Addition of 7AAD
1	None	None	No
2	None	None	Yes
3	None	Donkey anti-rabbit AlexaFluor 488 2ul (1:50)	Yes
4	None	Goat anti-mouse Pacific Blue 2ul (1:50)	Yes
5	MMP9 4µl (1:25)	Donkey anti-rabbit AlexaFluor 488 2ul (1:50)	Yes
6	MMP9 2µl (1:50)	Donkey anti-rabbit AlexaFluor 488 2ul (1:50)	Yes
7	MMP9 1µl (1:100)	Donkey anti-rabbit AlexaFluor 488 2ul (1:50)	Yes
8	MMP9 0.5µl (1:200)	Donkey anti-rabbit AlexaFluor 488 2ul (1:50)	Yes
9	NGAL 4µl (1:25)	Goat anti-mouse Pacific Blue 2ul (1:50)	Yes
10	NGAL 2µl (1:50)	Goat anti-mouse Pacific Blue 2ul (1:50)	Yes
11	NGAL1µl (1:100)	Goat anti-mouse Pacific Blue 2ul (1:50)	Yes
12	NGAL 0.5µl (1:200)	Goat anti-mouse Pacific Blue 2ul (1:50)	Yes

**Table 13: MMP9 and NGAL antibody optimization strategies for Flow Cytometry
application**
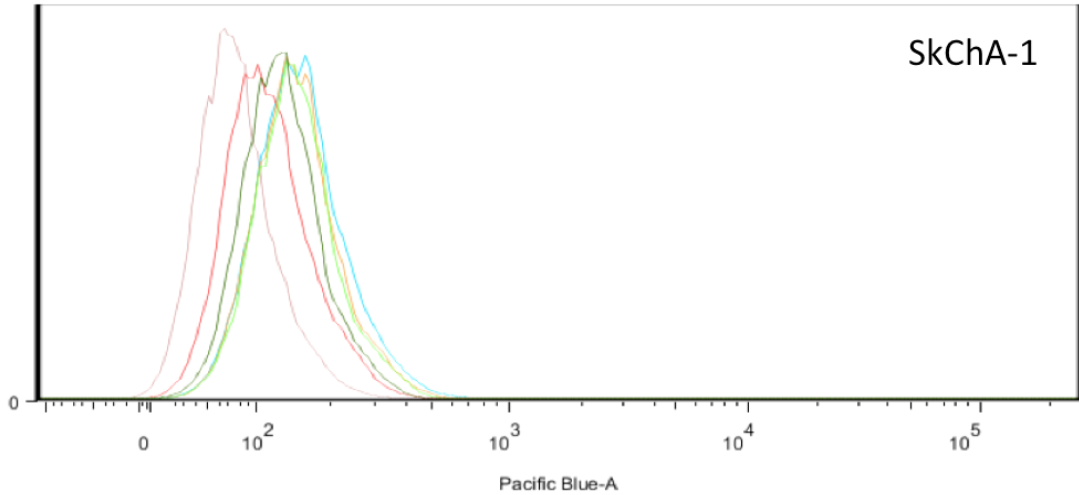
	Sample Name	Median , Pacific Blue-A	StdDev , Pacific Blue-A	Count , Pacific Blue-A
	NGAL; 1 in 200	123	77.5	23189
	NGAL; 1 in 100	142	948	22584
	NGAL; 1 in 50	143	75.4	22635
	NGAL; 1 in 25	148	946	22430
	Pacific Blue alone	105	61.5	10753
	7AAD negative cells	71.2	43.5	22676

Figure 47: Optimization of Abcam anti-NGAL antibody ab23477 on SkChA-1 cell line
The optimal difference in median fluorescence values between the primary antibody and secondary fluorophore was seen at a primary antibody dilution of 1 in 25
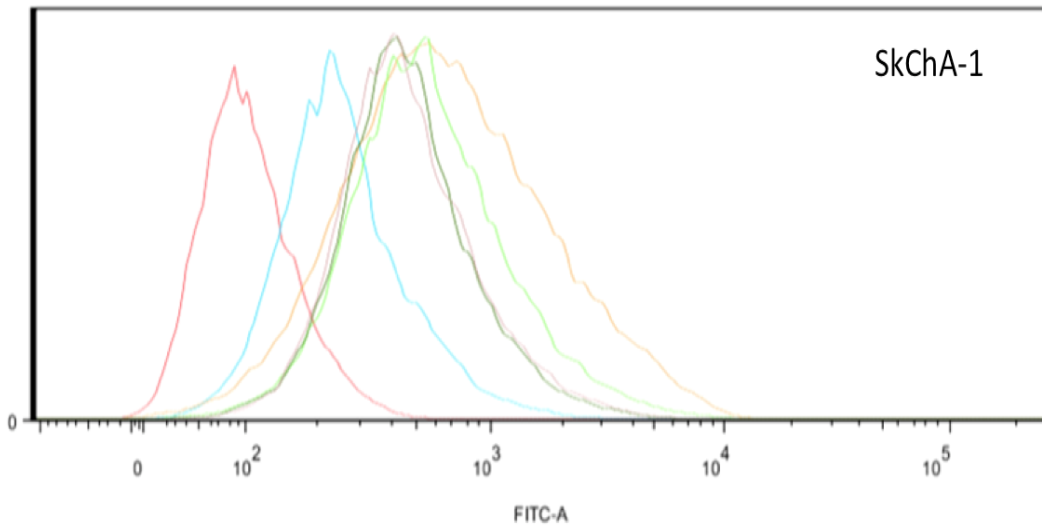
	Sample Name	Median , FITC-A	StdDev , FITC-A	Count , FITC-A
	MMP9; 1 in 200	424	546	22158
	MMP9; 1 in 100	431	514	22146
	MMP9; 1 in 50	519	813	22513
	MMP9; 1 in 25	612	1251	23277
	Alexa Fluor 488 alone	237	268	23504
	7AAD negative cells	93.4	68.0	22676

Figure 48: Optimization of Abcam anti-MMP9 antibody ab76003 on SkChA-1 cell line
Once again the optimal difference in median fluorescence values between the primary antibody and secondary fluorophore was seen at a primary antibody dilution of 1 in 25
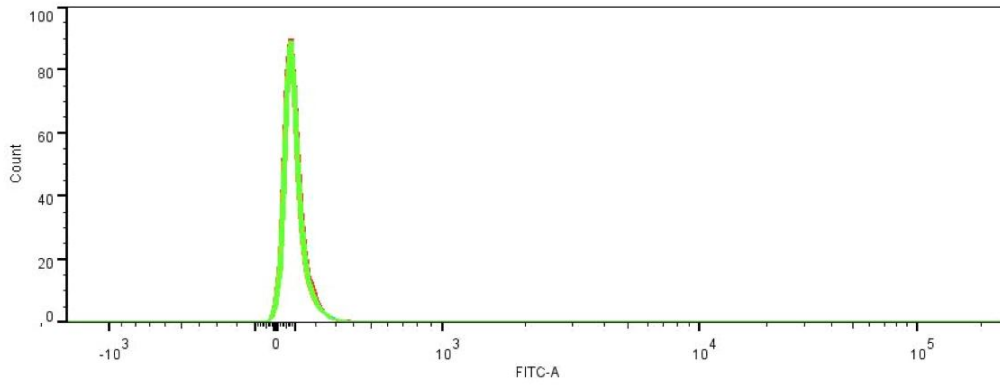
	Sample Name	Name	Median : Pacific Blue-A	CV : Pacific Blue-A	SD : Pacific Blue-A	Count
(green)	HuCCT 7AAD with NGAL.fcs	Gated population	135	54.0	83.9	10610
(orange)	HuCCT 7AAD with Pacific blue.fcs	Gated population	134	56.3	88.1	10890
(red)	HuCCT 7AAD.fcs	7AAD Neg, SSC-A subset	87.5	61.1	61.2	10883
(cyan)	HuCCTalone.fcs	Gated population	89.2	62.3	63.2	10391
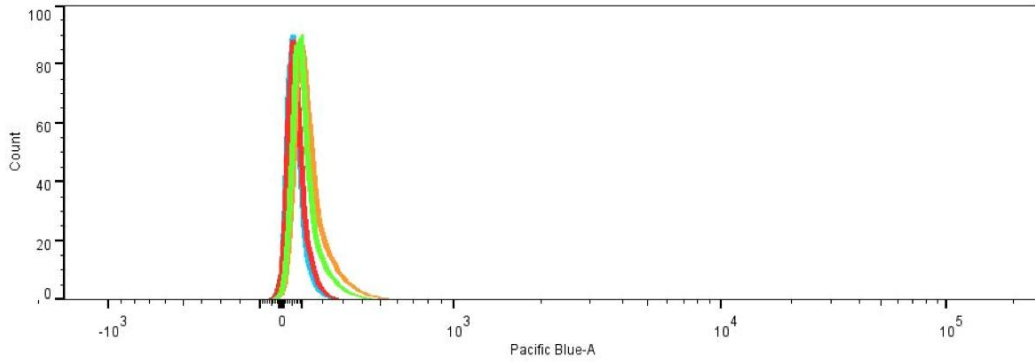
	Sample Name	Name	Median : Pacific Blue-A	CV : Pacific Blue-A	SD : Pacific Blue-A	Count
(green)	EGI 7AAD with NGAL.fcs	7AAD Neg, SSC-A subset	100	61.5	73.2	10417
(orange)	EGI 7AAD with Pacific blue.fcs	7AAD Neg, SSC-A subset	122	62.2	91.3	10565
(red)	EGI 7AAD.fcs	7AAD Neg, SSC-A subset	63.8	62.9	45.6	10714
(cyan)	EGI alone.fcs	Gated population	57.6	371	277	10403
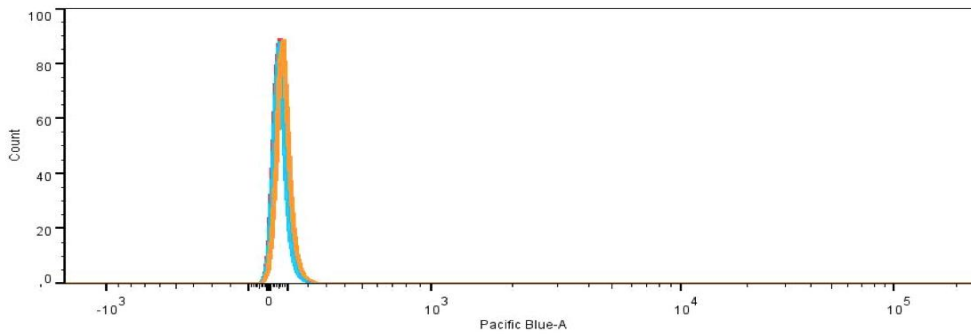
	Sample Name	Name	Median : Pacific Blue-A	CV : Pacific Blue-A	SD : Pacific Blue-A	Count
(orange)	H69 7AAD with NGAL.fcs	7AAD Neg, SSC-A subset	71.9	50.6	38.7	10637
(cyan)	H69 7AAD.fcs	7AAD Neg, SSC-A subset	52.8	57.9	33.2	10698
(red)	H69 alone.fcs	Gated population	52.3	149	87.1	10433

Figure 49: FC analysis of NGAL surface expression on the CCA cell lines
HuCCT-1 (top panel), EGI-1 (middle panel) and the normal cholangiocyte cell line H69 (bottom panel) are shown. In all 3 cell lines, no significant increase in median fluorescence counts is seen in the case of this Abcam NGAL antibody in comparison to the no-primary run.

.

144
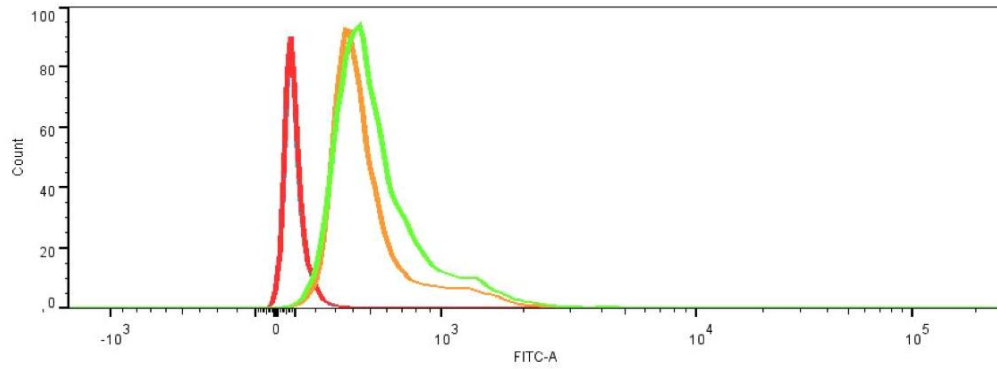
Sample Name	Name	Median : FITC-A	CV : FITC-A	SD : FITC-A	Count
HuCCT 7AAD with MMP9.fcs	Gated population	522	136	946	10813
HuCCT 7AAD with AF488.fcs	Gated population	458	67.5	388	10945
HuCCT 7AAD.fcs	7AAD Neg, SSC-A subset	81.7	71.5	67.7	10883
HuCCTalone.fcs	Gated population	81.8	74.1	70.5	10391
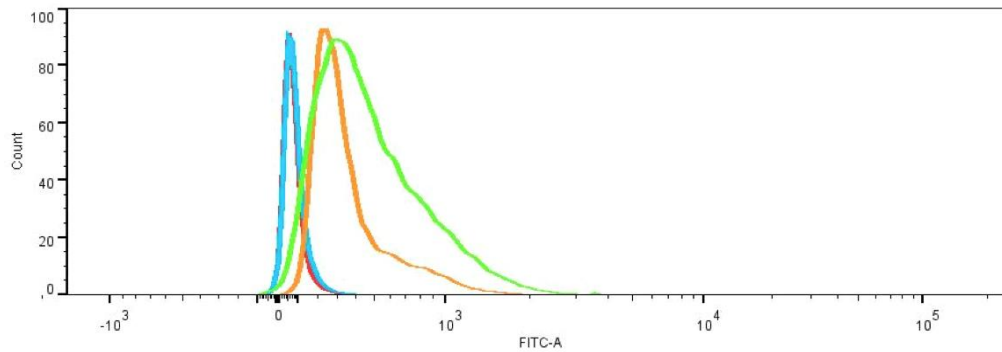
Sample Name	Name	Median : FITC-A	CV : FITC-A	SD : FITC-A	Count
EGI 7AAD with MMP9.fcs	7AAD Neg, SSC-A subset	457	93.7	544	10536
EGI 7AAD with AF488.fcs	7AAD Neg, SSC-A subset	324	71.8	299	10502
EGI 7AAD.fcs	7AAD Neg, SSC-A subset	72.1	99.8	87.7	10714
EGI alone.fcs	Gated population	65.1	183	156	10403
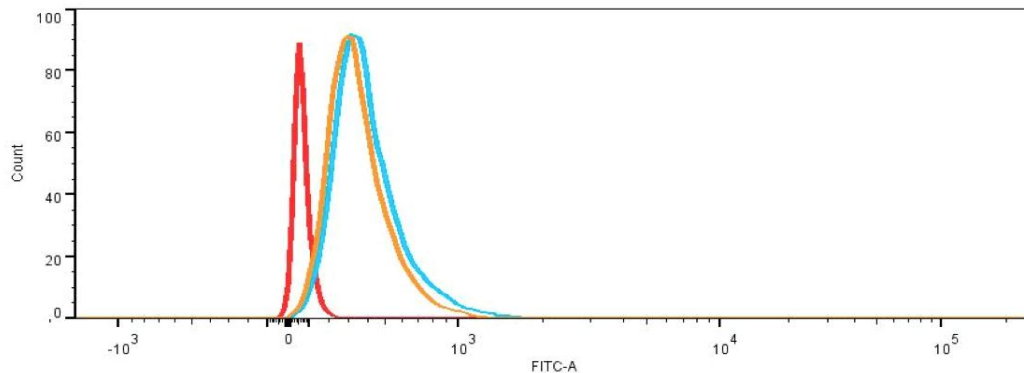
Sample Name	Name	Median : FITC-A	CV : FITC-A	SD : FITC-A	Count
H69 7AAD with MMP9.fcs	7AAD Neg, SSC-A subset	355	54.5	215	10645
H69 7AAD with AF488.fcs	7AAD Neg, SSC-A subset	400	54.5	246	10639
H69 7AAD.fcs	7AAD Neg, SSC-A subset	59.0	64.1	41.7	10698

Figure 50: FC analysis of MMP9 surface expression on the CCA cell lines
HuCCT-1 (top panel), EGI-1 (middle panel) and the normal cholangiocyte cell line H69 (bottom panel) are shown. Once again, no significant increase in median fluorescent counts is seen with the use of the Abcam MMP9 antibody in comparison to the no-primary run.

(i.e. those with secondary fluorophore alone). Similarly, no appreciable difference in intensity was seen between CCA cell lines and control cholangiocytes (H69) either. This would perhaps be indicative of poor antibody performance, or inadequate optimization. At this stage, it was agreed that the alternative means of ascertaining cell surface expression of NGAL and MMP9 (WB and IF methods) would suffice, rather than devote more time to optimizing the FC protocol.

3.2.8 ELISA of cell line supernatants shows evidence of extracellular secretion of NGAL by most CCA cell lines

With studies investigating an association between serum NGAL and a diagnosis of CCA (Leelawat et al., 2011; Budzynska et al., 2013), I investigated whether NGAL is actively secreted by CCA cell lines. Clarifying this point would also have an impact on the success of a targeted delivery system, as this would indicate additional targeting could occur in the extra-cellular tumour milieu i.e. stroma.

As illustrated in Figure 51, ELISA of 6 CCA cell line supernatants revealed the highest levels of NGAL secretion by OZ, with all other EH-CCA cell lines showing only half as much secretion of the marker. Of the IH-CCA cell lines, HuCCT-1 showed positivity, whereas Huh-28 did not show any secretion. Notably, the normal cholangiocyte line H69 demonstrated poor secretion of NGAL.
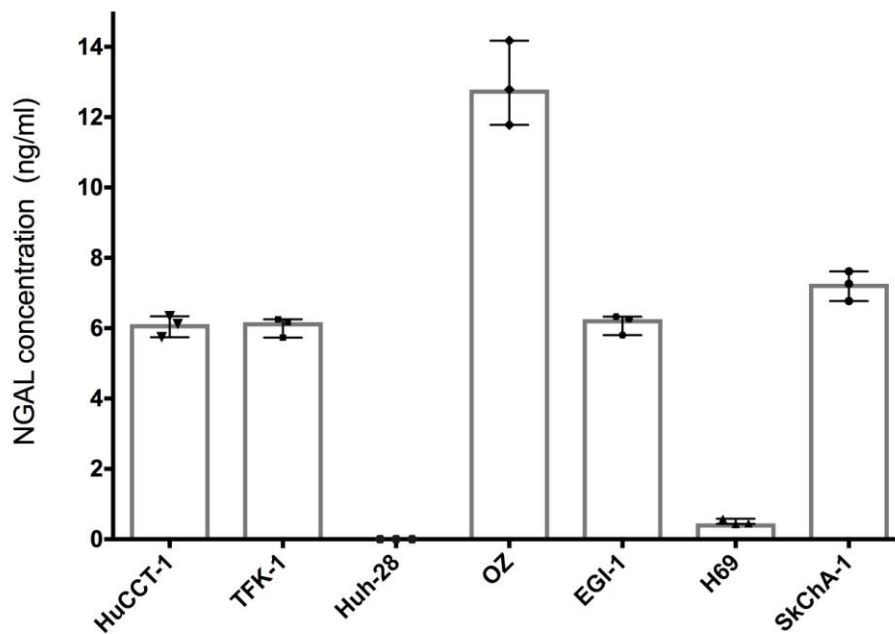
Figure 51: ELISA results showing NGAL concentrations in CCA and H69 cell culture supernatants
Assay utilising 1/20 dilutions of CCA cell line supernatants, with the exception of Huh-28 and H69 (undiluted), and final NGAL concentrations determined by extrapolation to NGAL standard curve data. Near absent NGAL secretion into the extracellular compartment is seen with Huh-28 and H69 (pooled data from 3 runs shown; points indicating median and upper/lower values)

3.3 Discussion

The major thrust for investigating the 2 particular biomarkers highlighted in this study viz. NGAL and MMP9 as theragnostic biomarkers in CCA was the backdrop provided by recent proteomics work at our institution which identified these two molecules as being overexpressed in the bile of CCA patients (Farid, 2014). The next logical step to advance this work was to assess the expression of these markers in PH-CCA tissue. Accordingly, the experiments in this chapter were aimed to fulfil this objective and concurrently ascertain any prognostic effect of NGAL and MMP9 in PH-CCA. In addition, to explore the feasibility of adopting these molecules as theragnostic targets, I conducted experiments to determine if their expression was present on cell membranes and/or stroma, a pre-requisite for cellular targeting. (van Oosten et al., 2011).

3.3.1 Tissue expression of NGAL and MMP9

In comparison to MMP9, there is a marked paucity of literature on NGAL tissue expression in CCA, a point that is not entirely surprising given that the latter molecule was identified more than 2 decades after the discovery of MMP9 in 1967 (Triebel et al., 1992; Brinckerhoff and Matrisian, 2002). There is only one other IHC study found pertaining to NGAL in CCA. This work from Thailand on a cohort of 24 CCA specimens noted NGAL expression in all samples, and mostly cytosolic in cellular location. High levels of expression were observed in 75% of cases but no significant association with tumour differentiation, nodal status or metastasis was seen. Notably, non-tumorous tissue stained negative for the marker (Nuntagowat et al., 2010). Interestingly, the NGAL antibody used in this study (R&D Systems, MN)

was identical to that utilised in ours, albeit at dilutions much lower than what I optimised for use in the sections (1/1000 vs 1/100 respectively). Furthermore, they incubated sections overnight at 4°C and did not require addition of agents that block non-specific antibody binding such as Casein. Despite the differences observed in methodology and control tissue, some similarities were noted in this cohort of PH-CCA patients. All of the specimens stained positive for NGAL and the median tumoural Histoscore was at the 82nd centile of the maximum. Important distinctions were clear too though - higher NGAL Histoscores were significantly associated with the occurrence of lymph nodal metastasis in my analysis and curiously, lower NGAL Histoscores were statistically linked with local recurrence (i.e. recurrent disease in the surgical resection bed). These two clinical parameters are both surrogates of aggressive disease and it is unclear why they are at odds with each other in terms of their association with NGAL Histoscore. A salient point observed in this series was the lack of an impact of nodal metastasis on survival, as elaborated in the next chapter. Nodal metastasis is a well established prognostic determinant in large series of PH-CCA (DeOliveira et al., 2007b; Nagino et al., 2013) and the modest numbers in this cohort most likely explains the lack of this finding in this series. One can only speculate that if NGAL has a prognostic effect in PH-CCA through an association with nodal metastasis, this may have been borne out with a larger series of patients.

There is a larger body of data published on MMP9 tissue expression by IHC in CCA although initial reports deal solely with IH-CCA. A group from Japan noted in their series of 11 IH-CCA tissue specimens that MMP9 expression was present in 27% of cases, with stronger positivity seen in association with increased invasiveness. Localisation of the biomarker was in the cytosol and tumour stroma. No association with tumour differentiation was observed (Terada et al., 1996). Another Japanese group subsequently examined 37 cases of IH-CCA and found a MMP9 expression

rate of 43%. They found an increasing incidence of nodal metastasis with higher degrees of MMP9 expression, and this translated into a worse survival for these groups too (Shirabe et al., 1999). Understandably, a cause-effect relationship between MMP9 and survival cannot be drawn here and the prognostic observations are best explained by nodal status. In another report, Jo Chae and co-workers scrutinized 76 cases of IH-CCA from Korea for MMP9 tissue expression to find 67% of cases positive for the marker. These authors also assessed expression of TIMP-1 and correlated all these findings to gross morphology of the tumour. In this fashion, it was observed that an imbalanced ratio of MMP9 to TIMP-1 expression was significantly more associated with MF and PI tumour morphology rather than IG subtype, and thus linked to more aggressive tumour behaviour (Jo Chae et al., 2004).

The profile of MMP9 expression in PH-CCA is less well studied in comparison to IH-CCA. Turkish investigators assessed the expression of a group of MMPs in a cohort of various resected biliary cancers including PH-CCA. Of the latter subset of 8 cases, MMP9 positivity was seen in all, and was significantly associated with peri-neural invasion. No relation to tumour grade, vascular invasion or metastasis was noted (Kirimlioglu et al., 2009). A Chinese group led by Sang scrutinized the tissue expression of MMP9 in 49 cases of resected PH-CCA using software-assisted optical density measurements of positivity, and found it to be significant positive correlation with occurrence of nodal metastasis, and negative correlation with poor tumour differentiation. MMP9 expression was also found to be significantly higher in tumour tissue when compared to controls with benign biliary disease. No prognostic information was available in this report (Sang et al., 2013). A more recent study also from China also delved into the expression of this marker in resected PH-CCA specimens. Of the 58 cases examined, MMP9 positivity was found in 67% with a cytoplasmic predominance. Stromal expression of MMP9 was noted in all cases as

well, albeit at less intensity in comparison to tumour parenchyma. Importantly, although no significant statistical association was found between biomarker expression and any clinicopathological variable, overexpression of MMP9 was found to be an independent prognostic factor in poorer survival. The other independent prognosticator in their sample was nodal metastasis (Sun et al., 2014). There are some similarities in these two papers with my findings. I encountered 100% positivity for MMP9 in this sample cohort. There was a predominant cytosolic staining although cell membrane and stromal positivity were seen uniformly across specimens too. A comparison of the primary antibodies used across these 3 PH-CCA studies (including ours) shows that they were mutually different, with the streptavidin-biotin complex method being utilised for staining in those reports. In my group, no significant associations were seen between MMP9 tumour expression and any clinicopathological variable with the exception of local recurrence. As in the case of NGAL, I was surprised to learn that median lower MMP9 Histoscores were associated with this phenomenon, for reasons that are again unclear. I noted peri-neural invasion in 89% of all cases, and this had no significant association with any biomarker Histoscore.

The expression of NGAL and MMP9 in control liver tissue was an interesting observation, although seen at levels significantly less than corresponding tumour parenchyma. In the case of MMP9, existing literature is conflicting in this point, with studies noting both positivity (Kirimlioglu et al., 2009) and the absence of expression (Terada et al., 1996; Jo Chae et al., 2004) in normal liver tissue. PH-CCA is typically associated with jaundice at presentation and I wondered if this phenomenon could explain the NGAL positivity of matched control liver tissue in this series. Borkham-Kamphorst and colleagues found that hepatocytes and bile ducts were induced into expressing NGAL in an experimental rodent model of liver injury caused by bile duct ligation (Borkham-Kamphorst et al., 2011). I was however unable to find a

significant correlation between pre-operative serum bilirubin and matched liver tissue NGAL Histoscore in this series. The use of avidin-biotin systems is well known to produce appreciable background signal in tissues rich in endogenous biotin such as liver, a phenomenon that is lessened with the substitution of avidin with streptavidin (Ramos-Vara, 2005). Though I used the ABC system in my NGAL staining protocol, it is difficult to say what degree of normal liver NGAL positivity is contributed to by true expression and/or methodology related factors.

3.3.2 NGAL as a theragnostic target

Considering the results of my IHC experiments and realising that the existing literature on NGAL in PH-CCA was scant, I focused primarily on this biomarker in the next phase of experiments. Accordingly, the focus of my Western blotting and Immunofluorescence experiments was to determine if NGAL could be utilised as a theragnostic target. Central to this premise was establishing if the molecule is expressed on tumour cell membranes and extracellular space. My results, in particular the Western blotting analysis, conclusively showed that NGAL was expressed in the membrane fraction of most CCA cell lines, whilst being near absent in the normal cholangiocyte cell line H69. The findings of my ELISA analysis showed evidence of NGAL secretion into the cell culture supernatants of most CCA cell lines, but not H69. Based on this, I can surmise that NGAL is also secreted into the extracellular matrix by CCA tumour parenchyma, and this ties-in with my finding of stromal NGAL expression on IHC analysis. The results of my IF analysis showed some concordance with that obtained by WB, although two factors potentially confounded my interpretation. Firstly, cellular permeabilization was encountered during fixation, leading to cytoplasmic staining, which limited accurate assessment of membranous expression. Secondly, captured images did not necessarily reflect staining intensity as seen on direct visualization under the microscope, and this phenomenon was possibly related to image standardization by the related software. Accordingly, WB data was considered the more definitive of the two methods.

The overall findings lead to the question whether NGAL is a valid theragnostic target in CCA. van Oosten and associates developed a unique weighted scoring system that aimed to help determine the validity of candidate biomarkers as targets for cancer imaging and/or therapy, as shown in Table 14(van Oosten et al., 2011):

TASC Scoring System

	Characteristics		Score
I	Extracellular protein localization	Bound to cell surface (receptor)	5
		In close proximity of tumor cell	3
II	Diffuse up-regulation through tumor tissue		4
III	T/N ratio > 10		3
IV	Percentage up-regulation in patients	>90%	6
		70%-90%	5
		50%-69%	3
		10%-49%	0
V	Previously imaged with success *in vivo*		2
VI	Enzymatic activity		1
VII	Internalization		1

Total: maximum 22
Potential target ≥ 18

Table 14: The *TA*rget *S*election *C*riteria (TASC) Scoring system for assessment of candidate biomarkers as theragnostic targets.
T- expression in tumour, N- expression in normal tissue (From van Oosten et al. Selecting Potential Targetable Biomarkers for Imaging Purposes in Colorectal Cancer Using TArget Selection Criteria (TASC): A Novel Target Identification Tool.
Transl Oncol. 2011; 4(2): 71–82; DOI:10.1593/tlo.10220
Reproduced with permission from the publisher.

Whilst devised primarily as an aid to help select molecular markers for tumour imaging, the factors enumerated in the score are applicable to therapeutic targeting as well. As can be seen from this system, the highest weights are assigned to targets that are present on cell membranes and its vicinity viz. extracellular matrix. Using this score, the authors found that biomarkers with a score >18 had the potential for targeting use. In the context of colorectal cancers, biomarkers with the highest scores included EGFR and Epithelial Cell Adhesion Molecule (20 points each), Carcino-embyronic antigen (19 points) and interestingly MMPs (18 points), all of which incidentally have been used successfully for colorectal cancer imaging in experimental *in vivo* models. Applying the results of NGAL expression from this series to this scoring system viz. where I observed membranous and extracellular NGAL expression with diffuse up-regulation in tumour tissue to the order of 70-90% of samples, one can see that the provisional score generated by this biomarker is a

minimum of 17 (if I exclude points from T/N ratio >10 and success from prior *in vivo* imaging). As elaborated below, NGAL has already been used successfully for imaging *in vivo*, and therefore the net score would rise to a total of 19, making it a valid target biomarker. Understandably, this scoring system is nonetheless the first of its kind and needs further validation.

Considering the important role that NGAL assumes in cancer regulation, it is not surprising that investigative efforts have already been made into targeting this molecule for theragnostic effects. One such report looked into the utility of a near-infrared (NIR) dye labelled monoclonal antibody to NGAL as an imaging agent for pancreatic cancer using *in vitro* experiments and *in vivo* murine xenograft models (Wang et al., 2011). Internalisation of antibody into cancer cells was noted *in vitro*. Although high tumour to background signal ratios were seen *in vivo*, specificity was poor with signal also being observed in other organs such as liver, kidneys and bladder. A more recent study incorporated the use of anti-NGAL conjugated silica-coated gold nanoshells in a murine pancreatic cancer xenograft model. These nanoparticles were doped with iron oxide and indocyanine green enabling their visualization with Magnetic Resonance Imaging and near-infrared (NIR) Fluorescence imaging respectively. The group thus demonstrated specific targeting of xenografts in this fashion, whilst showing a lack of cellular toxicity of these particles both *in vitro* and *in vivo*. Furthermore, NIR labelling facilitated successful photothermal therapy *in vitro* by the application of NIR laser at an appropriate wavelength (Chen et al., 2014).

Despite these encouraging preliminary results, the varying and contrasting roles exhibited by NGAL in tissue homeostasis and cancer progression may be a cause for off-target effects and lack of therapeutic effectiveness when attempting to validate future inhibitors of this molecule. Clinical trials of MMP inhibitors have been fraught with similar shortcomings and the negative results of these trials have been

attributed in part to the high incidence of toxicity (mostly musculoskeletal) of MMP inhibitors which precluded the effective use of therapeutic dosages of these agents (Fingleton, 2008). My results indicate that in PH-CCA, hepatic parenchymal expression of NGAL can lead to unintended normal liver targeting with an anti-NGAL strategy, although the extent to which this may occur is difficult to speculate, as tumour tissue harbours significantly more NGAL than matched normal liver parenchyma. One possible way to minimize the incidence of such effects is to confer an anti-NGAL targeting strategy further specificity using an additional homing target unique to tumour vascular endothelium, such as Vascular Endothelial Growth Factor (VEGF) and CD105 (Paauwe et al., 2013), which is the focus of my experiments in the next chapter. Nonetheless, the myriad roles played by NGAL in both normal physiology and cancer progression may well muddy the waters in the quest to use it as a specific theragnostic agent in this cancer.

4 Evaluation of vascular endothelial marker expression in PH-CCA and its applicability to a microbubble-based targeted delivery system

4.1 Introduction

The aims of the work in this chapter were firstly to investigate the tissue expression of CD31, CD105 and VEGFR2 in PH-CCA and ascertain whether any of these endothelial markers had a prognostic impact in this cancer. This would indicate whether targeting any of these vascular receptors would potentially provide therapeutic benefit. Secondly, the potential of these markers as tumour vascular targeting ligands for microbubble-based imaging and therapeutic delivery was explored. If any of these markers were found to be overexpressed in CCA, they could be targeted to deliver theragnostic payloads, independent of any prognostic impact these markers might possess

4.2 Results

The expression of 3 vascular endothelial markers viz. CD31, CD105 and VEGFR2 was assessed in tissue samples of 54 patients who underwent resection of PH-CCA from 2000 to 2010. As described in the Methodology section, measurement of micro-vessel density (MVD) using the 'Hot-spot' technique was employed for this purpose. Since CD31 is known to be a pan-endothelial marker (Pusztaszeri et al., 2006) its expression was used as the denominator against which the other 2 biomarkers were compared.

4.2.1 CD31 and CD105 are consistently expressed in PH-CCA tissue and control liver parenchyma but VEGFR2 less so

IHC was performed following optimization of antibodies as shown in Table 15. The staining patterns of CD31, CD105 and VEGFR2 in PH-CCA are demonstrated in Figure 52 and Figure 53. CD31 highlighted microvessels in all tested tumour sections with minimal background staining. The expression of CD105 in contrast showed more variability. As shown in Figure 52, CD105 showed a staining profile similar to that seen with CD31, but in other instances, a substantial amount of background stromal expression was visualized as well, as shown in Figure 53. As was the case for CD31, all sections showed positivity to CD105. When evaluating stromal CD105 staining, this was found to be absent to mild in 39%, and moderate to strong in 61% of cases.

The evaluation of VEGFR2 MVD however revealed that this marker was largely absent in the assessed 'hot-spots'. Interestingly, many sections deemed negative for VEGFR2 using the hot-spot criteria showed evidence of expression in other regions of the same sections, as demonstrated in Figure 54. In light of this finding, VEGFR2 expression was also categorised as present or absent, based on assessment of the whole section rather than just hotspots,. Using this approach, VEGFR2 was found to be absent from 26 (48%) cases.

In the instance of control liver parenchyma, CD31 was found to uniformly stain hepatic sinusoids, and vascular endothelium within portal triads, as shown in Figure 55 and Figure 56. CD105 also showed evidence of expression in both sinusoids and portal tracts in varying intensities, across all cases, albeit in general less than that seen with CD31.

Antibody	Manufacturer/ Code	Antigen retrieval methods	Antibody dilutions tested	Antibody incubation periods	Final retrieval/dilution/ incubation used
CD31	Dako/ M0823	None	1/40,1/60, 1/100	Overnight 4°C	None, 1/40, Overnight 4°C
CD105 (for human tissue)	Dako/ M3527	Proteinase K	1/20	1 hour RT Overnight 4°C	Proteinase K, 1/20, 1hr RT
VEGFR2	Cell Signaling Technology/ 55B11	Tris-EDTA buffer	1/50,1/100, 1/200	1 hour RT	Tris-EDTA, 1/100, 1hr RT
CD105 (for Mouse tissue)	R&D Systems/ AF1320	None Citrate buffer Proteinase K	1/20,1/50, 1/100,1/200, 1/500	1 hour RT Overnight 4°C	None, 1/200, 1hr RT

Table 15: IHC antibody optimization strategies for vascular endothelial markers used in the study
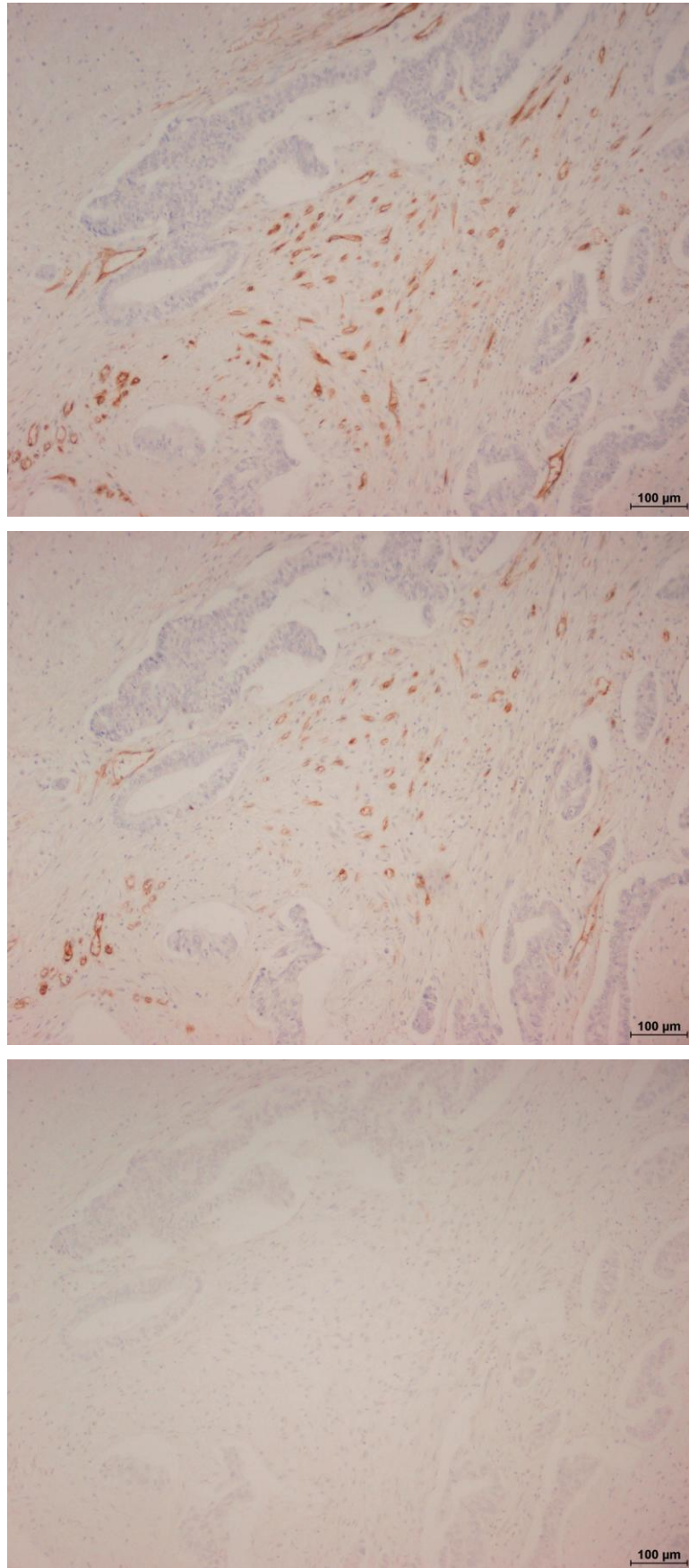
Figure 52: Consecutive sections of PH-CCA stained for CD31, CD105 and VEGFR2
CD31(top panel) is seen to have the highest MVD, whereas VEGFR2 (bottom panel) is notable by its lack of expression. CD105 (middle panel) shows a similar pattern of expression to CD31 but with less vessel density
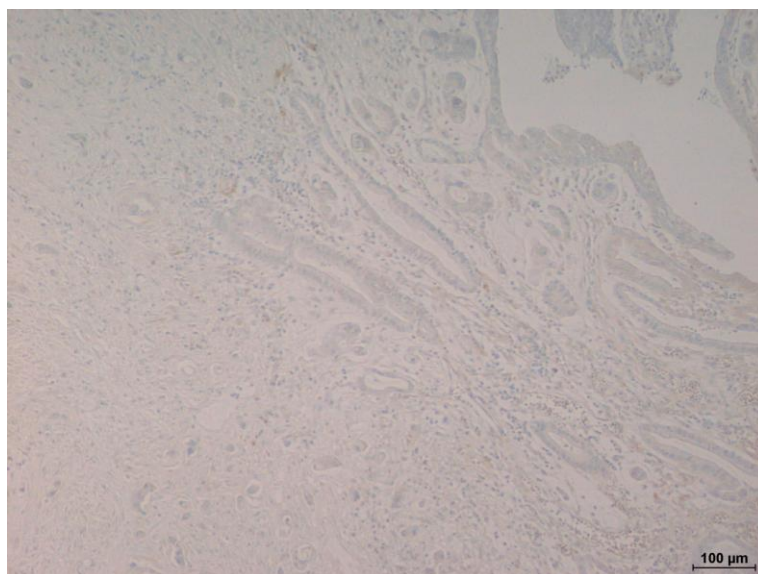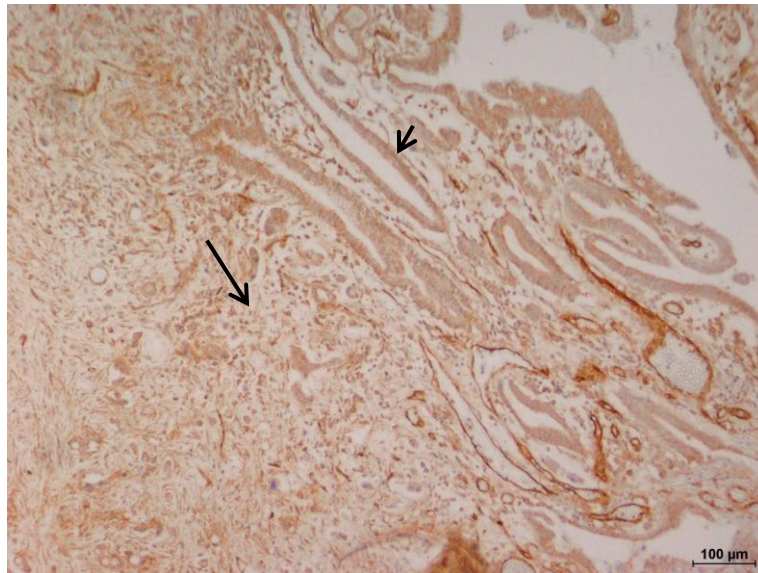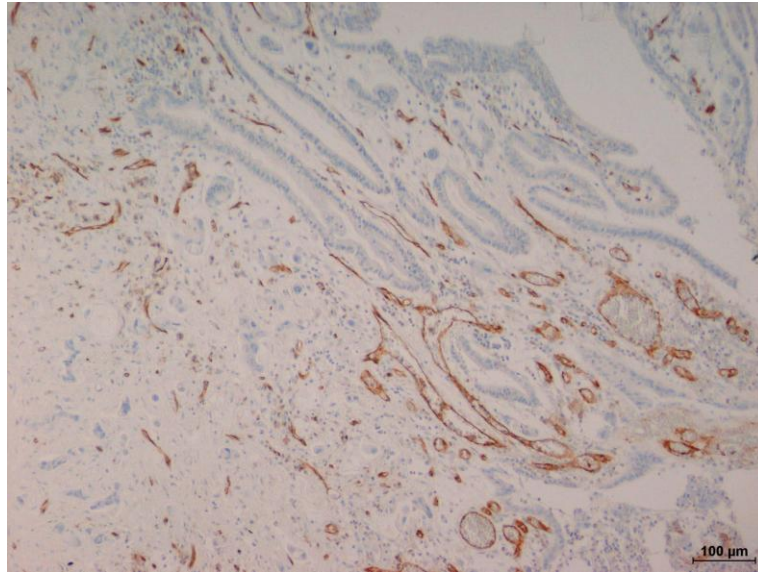
Figure 53: Consecutive sections of PH-CCA stained for CD31, CD105 and VEGFR2
In this instance, a significant degree of stromal (long arrow) and parenchyma (short arrow) staining is observed for CD105 (middle panel), whilst absent expression is noted with VEGFR2 (bottom panel)
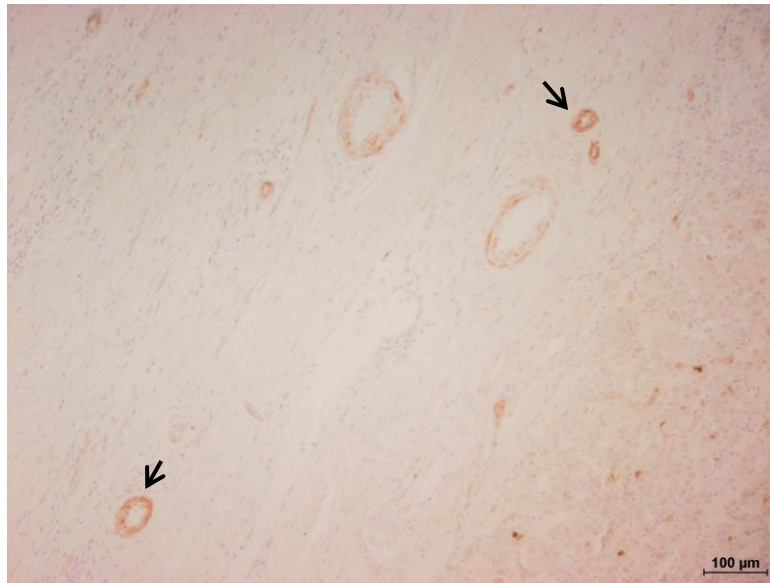
Figure 54: Evidence of VEGFR2 expression in an area outside a designated hotspot
This image was taken from the same section shown in Figure 52 and demonstrates VEGFR2 positivity (short arrows) in a case that would otherwise be deemed negative if based on MVD assessment alone.
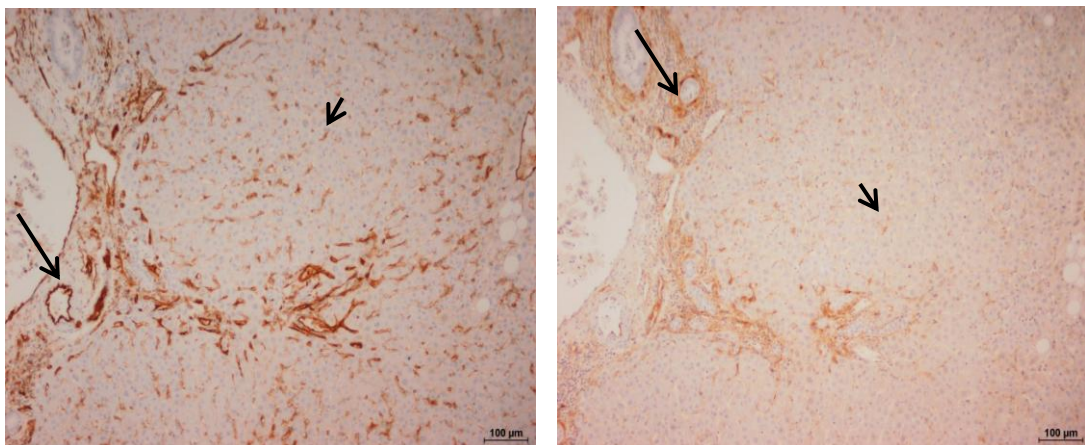
Figure 55: The expression of vascular endothelial markers CD31 and CD105 in normal liver parenchyma
CD31 staining (left panel) and CD105 (right panel) staining seen in consecutive sections of normal liver parenchyma and demonstrates the affinity of both these markers for hepatic sinusoids (short arrows) and vessels in the portal triad (long arrows).
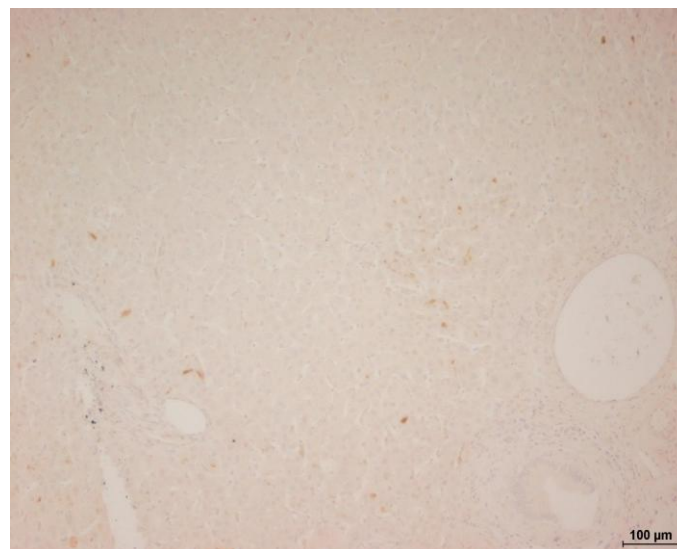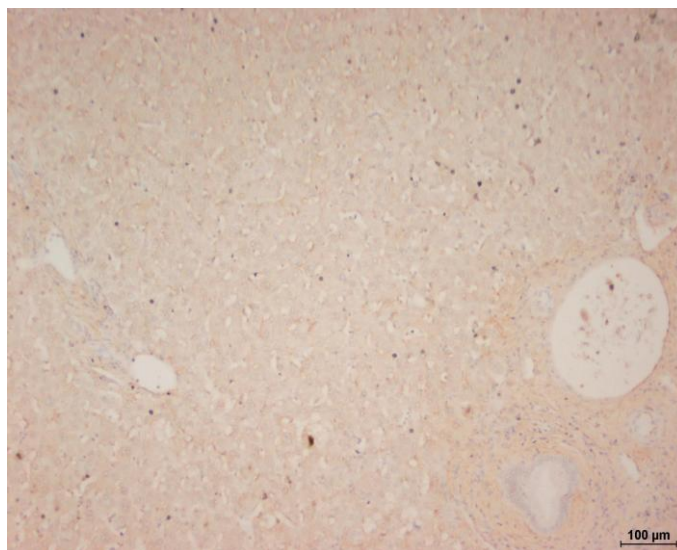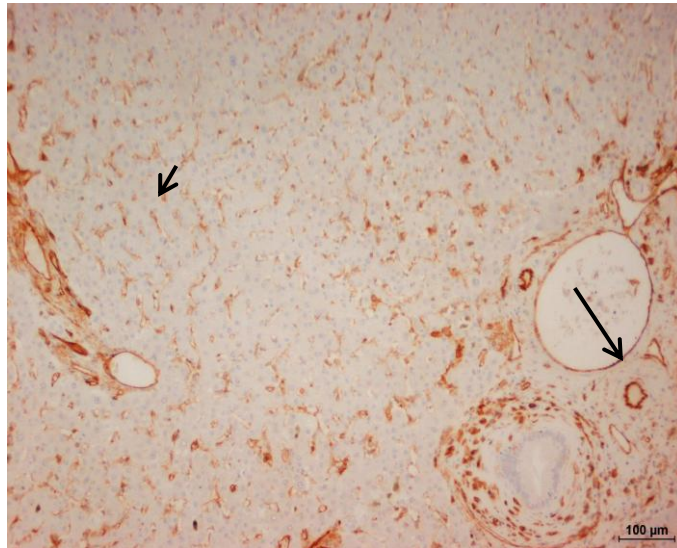
Figure 56: The expression of vascular endothelial markers CD31, CD105 and VEGFR2 in consecutive sections of control liver parenchyma
Evidence of CD31 staining (top panel) in hepatic sinusoids (short arrow) and vascular structures in the portal triad (long arrow) is demonstrated. The degree of such staining for CD105 (middle panel) in this instance is seen to be less, whereas no expression is seen with VEGFR2 (bottom panel).

4.2.2 Comparison of Micro-vessel density scores of all three endothelial markers in PH-CCA shows CD31 to have the highest expression and VEGFR2 the least

Figure 57 displays the MVD scores of all 3 endothelial markers in comparison. As can be seen, CD31 showed the highest levels of expression, whereas median CD105 MVD scores were just under half that (45 and 21.3 respectively). VEGFR2 showed negligible levels of positivity (median MVD score of 0.67), although when assessing whole sections (and not only hot spots), VEGFR2 positivity was seen in 52% of the group. A moderate degree of correlation between MVD scores of CD31 and CD105 was seen as demonstrated in Figure 58.

In the case of matched control liver parenchyma, assessment was purely qualitative as MVD scoring was not feasible in light of extensive sinusoidal staining.

As described in the Methods section, inter-observer correlations were assessed for MVD scores between 2 scorers (AN and EV) for the first third of cases. These results are displayed in Figure 59. The degree of agreement between scorers for CD31 and VEGFR2 was good (Spearman r= 0.53 and 0.60 respectively). In the case of CD105, inter-observer correlation was poor initially (r<0.4; data not shown) and the scorers re-convened to assess MVD scores again. It is interesting to note that in this instance, the correlation was excellent (r=0.93) and was due to the scorers discussing and agreeing upfront which areas of the section were to be labelled 'hot-spots'. Once this was decided, MVD scores were calculated independently as displayed.
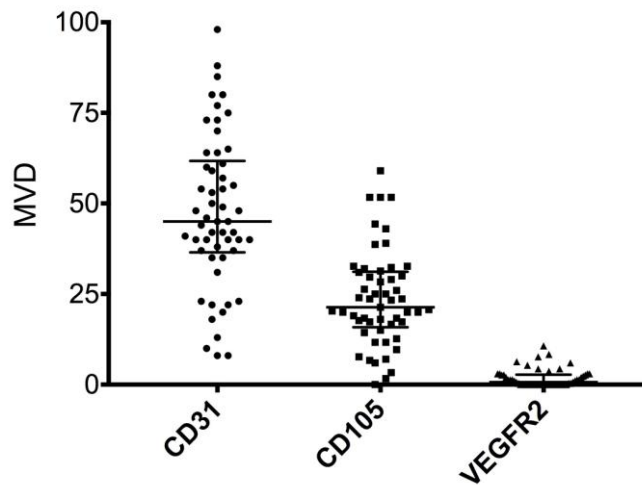
Figure 57: Scatter plot representation of MVD scores of all 3 endothelial markers in PH-CCA
CD31 showed the highest MVD scores, whereas the majority of sections expressed very poor levels of VEGFR2 (horizontal longer bars indicating median and shorter bars inter-quartile range)
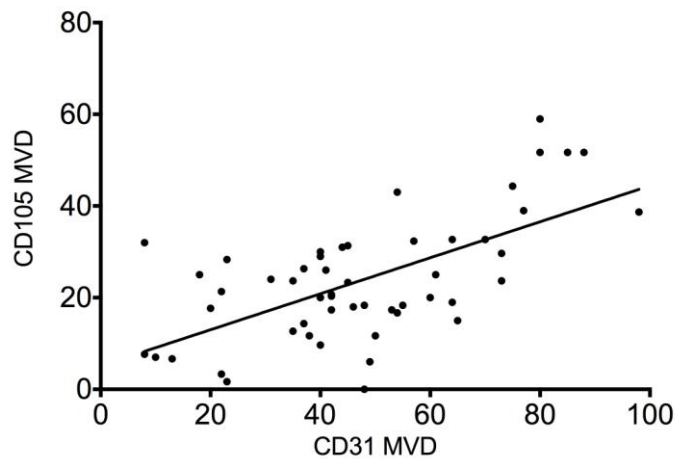
Figure 58: Scatter plot showing correlation between CD31 and CD105 MVD scores in PH-CCA
Good correlation between these 2 markers is observed in our cohort. Line of best fit drawn through (Spearman r=0.51, $p<0.0001$); n=53
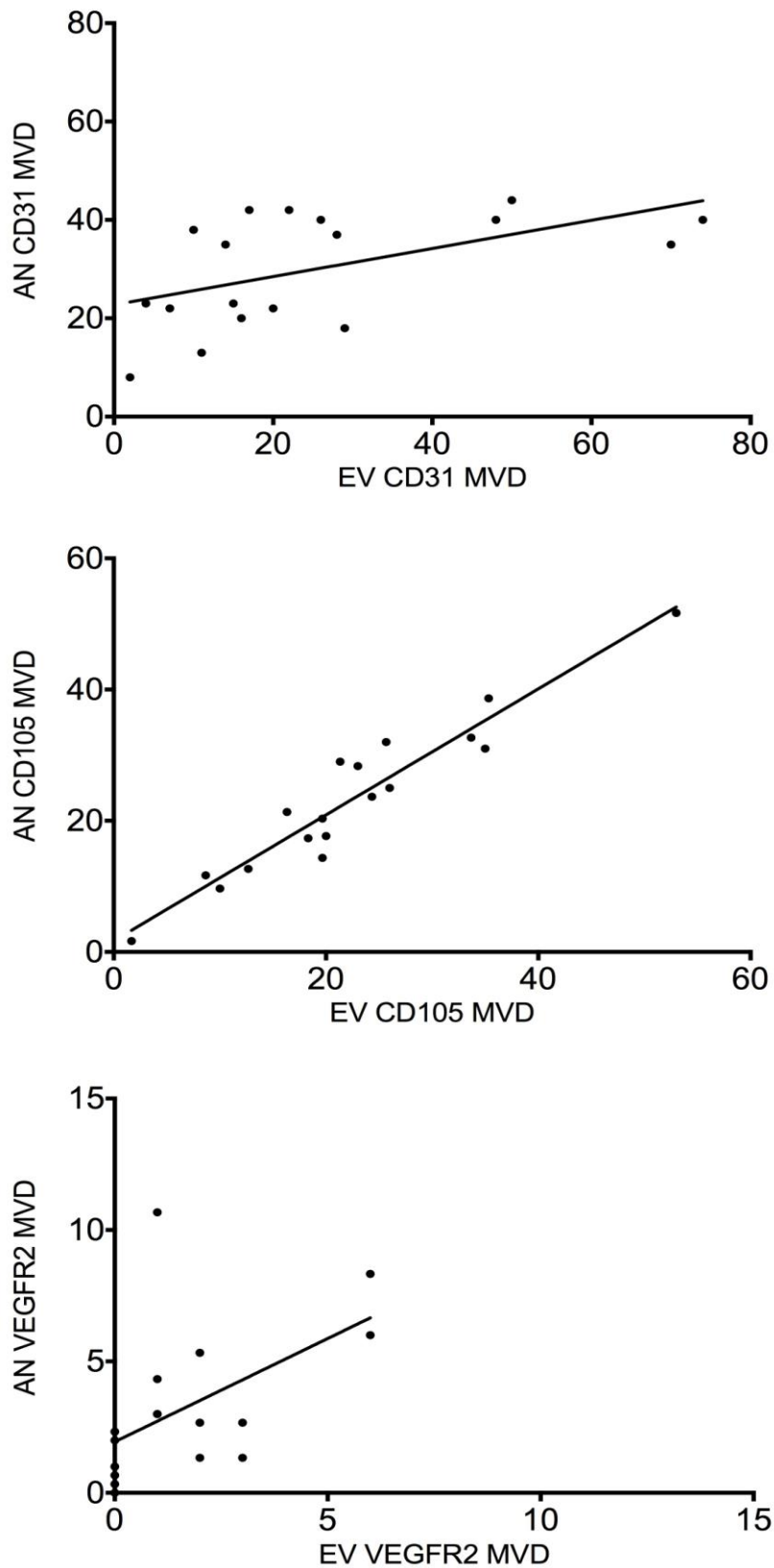
Figure 59: Inter-observer correlations for MVD assessment between 2 scorers (AN and EV) for all 3 endothelial markers
Plotted data and line of best fit shown in all graphs. Top panel (n=18) showing data for CD31 (Spearman r=0.53, p=0.022), middle panel (n=18) exhibiting data for CD105 (Spearman r=0.93, p<0.0001) and bottom panel (n=17) showing data for VEGFR2 (Spearman r=0.60, p=0.011).

4.2.3 Tissue expression of CD105 assumes prognostic significance in PH-CCA

The characteristics of the study population are summarised in the previous chapter (Table 9). The results of univariate analysis of endothelial marker expression against clinicopathological patient variables are shown in Table 16. The salient points here are that lower median CD31 MVD scores were associated with increased rates of local recurrence of tumour (i.e. within the surgical bed), whereas in the case of VEGFR2, presence of its expression was associated with the development of metastases. It is noteworthy that CD105 MVD scores bore no significant statistical association with any of the analysed variables

The median OS of the entire cohort of patients was 22.3 (IQR 10.8 - 39.7) months, whilst the group had a median DFS of 13.8 (4.8 – 33.4) months.

As elaborated in the Methods section, MVD scores for CD31 and CD105 were dichotomised at an optimal value for the purposes of survival analysis. This cut-off value was determined separately for each marker so as to generate the maximal statistical significance on log-rank (univariate) analysis.

Figure 60 and Figure 61 display the Kaplan-Meier survival curves for CD31 and CD105 at the optimal MVD cut-offs (68 and 31 respectively). As can be seen from this data, higher degrees of expression of both these endothelial markers showed significant association with poorer OS. The full results of survival analysis for analysed variables are shown in Table 17. Median OS in those patients with CD105 MVD>31 was 12 months versus 31 months in the group with CD105 MVD<31. Neither CD31 nor CD105 MVD was significantly associated with DFS, and VEGFR2 positivity did not bear any significant association with either OS or DFS.

Variable		n	%	CD31 MVD [median (IQR)]	p value	CD105 MVD [median (IQR)]	p value	VEGFR2 MVD [median (IQR)]	p value	VEGFR2 Yes	VEGFR2 No	p value
Age (years) at diagnosis	<58	27	50	44(31-59)	0.482	20(14-30)	0.203	0.3(0-2.7)	0.457	13	14	0.786
	>58	27	50	46(40-64)		24(17-33)		1.3(0-3.0)		15	12	
Gender	Male	31	57	42(23-55)	0.062	21(17-31)	0.871	1.0(0-2.7)	0.956	18	13	0.409
	Female	23	43	54(40-64)		22(14-31)		0.3(0-3.0)		10	13	
Tumour size (mm)	<30	24	46	43(35-59)	0.912	21(17-31)	0.955	0.6(0-2.7)	0.985	13	11	0.788
	>30	28	54	45(37-64)		24(14-32)		0.6(0-3.0)		14	14	
Histological grade	Grade 1	27	50	53(40-65)	0.050	21(17-30)	0.676	0.6(0-2.7)	0.493	14	13	1.000
	Grade 2/3	27	50	41(23-54)		22(9-32)		0.6(0-4.3)		14	13	
Microscopic vascular invasion	Yes	33	65	44(34-67)	0.454	24(16-32)	0.664	1.0(0-3.3)	0.654	18	15	1.000
	No	18	35	43(35-54)		21(18-28)		1.0(0-2.4)		10	8	
Nodal metastases	Yes	29	54	48(38-69)	0.138	19(16-32)	0.391	0.3(0-2.3)	0.278	15	10	0.290
	No	25	46	41(29-58)		24(18-31)		1.0(0.3.0)		13	16	
T Stage (AJCC 7th ed)	T1/T2	31	57	45(23-64)	0.687	21(17-32)	0.857	0.6(0-3.0)	0.709	17	14	0.784
	T3/T4	23	43	45(40-61)		23(14-30)		0.3(0-2.4)		11	12	
Resection Margins	R0(negative)	21	39	50(41-62)	0.245	22(17-32)	0.797	0(0)	0.063	8	13	0.163
	R1(positive)	33	61	41(35-63)		21(14-31)		1.3(0-3.3)		20	13	
Local recurrence	Yes	5	9	35(14-39)	*0.008*	25(15-28)	0.825	1.0(0-1.3)	0.602	3	2	1.000
	No	49	91	48(39-64)		20(15-32)		0.6(0-3.0)		25	24	
Metastasis	Yes	25	46	42(22-63)	0.212	24(18-29)	0.762	1.3(0-3.7)	0.063	17	8	*0.033*
	No	29	54	48(40-62)		20(12-33)		0(0-2.0)		11	18	
Progressive disease	Yes	27	50	42(23-61)	0.100	24(18-30)	0.510	1.3(0-3.0)	0.194	17	10	0.173
	No	27	50	49(40-64)		20(11-34)		0.3(0-2.7)		11	16	

Table 16: Comparison of MVD scores of all three endothelial markers and VEGFR2 positivity against clinicopathological patient variables Significant *p* values highlighted in bold and italics. Mann-Whitney U tests used for continuous variables and Fisher's exact test for dichotomous data. Local recurrence defined as recurrent disease in surgical bed. Progressive disease indicating local recurrence and/or metastasis (MVD: Micro-vessel density, IQR: Inter-quartile range)
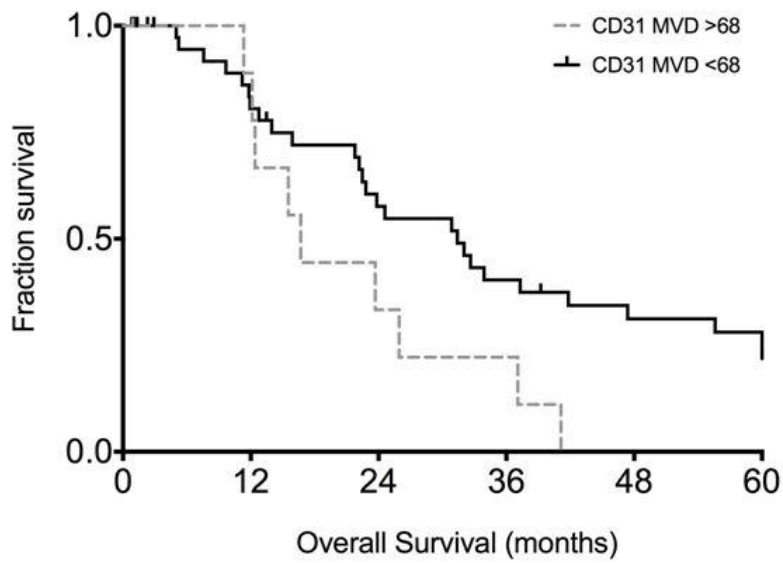
| CD31 MVD>68 | 44 | 29 | 20 | 14 | 10 | 9 |
| CD31 MVD<68 | 10 | 8 | 3 | 2 | 0 | 0 |

Figure 60: Kaplan Meier survival curves for CD31 MVD cut-off at 68
Curves demonstrating a significant difference in survival between patient groups at this MVD cut-off ($p= 0.042$, log-rank test). Table below graph indicating numbers at risk at corresponding time points.
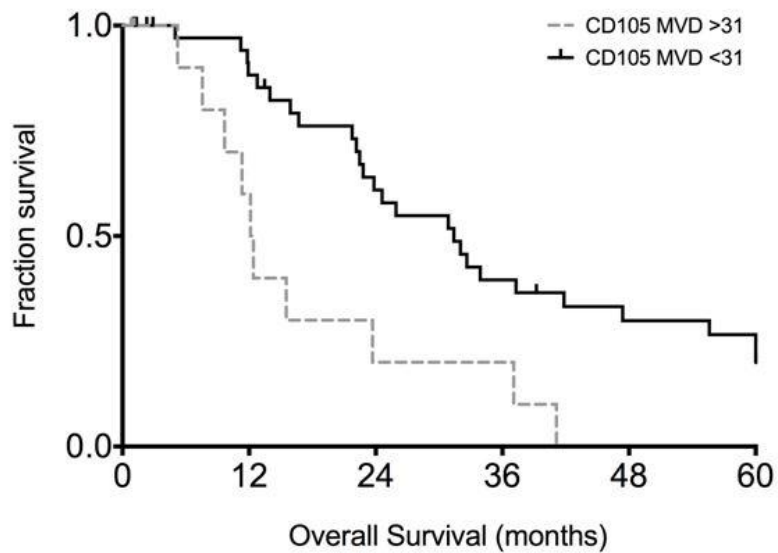
| CD105 MVD>31 | 40 | 30 | 20 | 13 | 9 | 8 |
| CD105 MVD<31 | 13 | 6 | 2 | 2 | 0 | 0 |

Figure 61: Kaplan Meier survival curves for CD105 MVD cut-off at 31
Curves demonstrating a significant difference in survival between patient groups at this MVD cut-off ($p= 0.002$, log-rank test). Table below graph indicating numbers at risk at corresponding time points.

Variable		n	Univariate analysis						Multivariate analysis			
			OS			DFS			OS		DFS	
			Median survival in months	HR (95% CI)	*p* value	Median survival in months	HR (95% CI)	*p* value	HR (95% CI)	*p* value	HR (95% CI)	*p* value
CD31 MVD	<68	44	31.4	2.2(1.0-4.9)	***0.042***	31.2	1.8(0.7-4.5)	0.212	0.2 (0.03-1.5)	0.132		
	>68	10	16.7			18.3						
CD105 MVD	<31	13	31.4	3.2(1.5-6.8)	***0.002***	23.1	1.7(0.6-4.6)	0.292	12.5(1.9-79.9)	***0.007***		
	>31	40	12.2			13.6						
VEGFR2 positivity	Yes	28	30.8		0.646	18.3		0.236				
	No	26	24.6			23.2						
Nodal metastasis	Yes	29	21.7		0.085	17.3		0.634				
	No	25	32.6			31.2						
Tumour size	<48mm	40	32.0	4.1(1.6-10.6)	***0.002***	23.2	3.3(1.2-9.5)	***0.019***	5.0 (1.9-13.4)	***0.001***	2.6 (0.9-7.7)	0.071
	>48mm	12	12.7			11.2						
Tumour stage	T1/T2	31	31.4		0.277	31.2		0.530				
	T3/T4	23	23.8			18.7						
Tumour grade	Grade 1	27	25.9		0.220	23.2		0.556				
	Grade 2/3	27	24.6			18.7						
Vascular invasion	Yes	33	24.6		0.177	18.3		0.650				
	No	18	32.0			32.9						
Resection margin	Positive	33	23.7		0.203	18.3		***0.032***			2.1 (0.9-5.2)	0.080
	Negative	21	37.0			51.2						
AJCC stage	II	15	37.3		0.116	32.9		0.504				
	III/IV	39	22.8			18.3						
Local Recurrence	Yes	5	33.9		0.568			N/A				
	No	49	23.8									
Metastasis	Yes	25	24.6		0.154			N/A				
	No	29	33.9									

Table 17: Univariate (Log -rank tests) and multivariate (Cox Regression) analysis of factors predictive of survival in this cohort of PH-CCA
Factors significant on univariate analysis were entered into the Cox Regression model. Significant *p* values highlighted in bold and italicized (OS: overall survival, DFS: disease-free survival, HR: Hazard ratio, CI: Confidence interval, MVD: micro-vessel density

Other factors that showed statistical significance included primary tumour size >48mm (for both poorer OS and DFS) and resection margin positivity (for worse DFS, but not OS). Factors significant by univariate survival analysis were entered into a multivariate (Cox proportional hazards) regression model. This revealed that CD105 MVD >31 and primary tumour size >48mm were independently associated with poorer OS in this cohort of PH-CCA patients. CD31 expression lost the statistical significance it had with OS on univariate analysis when put through this model.

4.2.4 The murine endothelial cell line SVR shows surface expression of CD105 on Immunofluorescence studies

In order to establish a targeted delivery system in CCA, it is necessary to ensure a systemically administered payload (such as that delivered by microbubbles) can home in to tumour regions. Subsequent to this would be the successful crossing of tumour capillary vascular endothelium by these payloads into the stromal/interstitial compartment, although this aspect was not investigated in this study. With a view towards translation of this concept into a murine model, I initially assessed whether CD105 could be used as an 'anchoring' target on murine vascular endothelium. The first step in this process was to establish that the murine endothelial cell line SVR expressed CD105, and this was done using IF studies as shown in Figure 62. These images clearly indicate that CD105 is expressed on the surface of SVR cells.
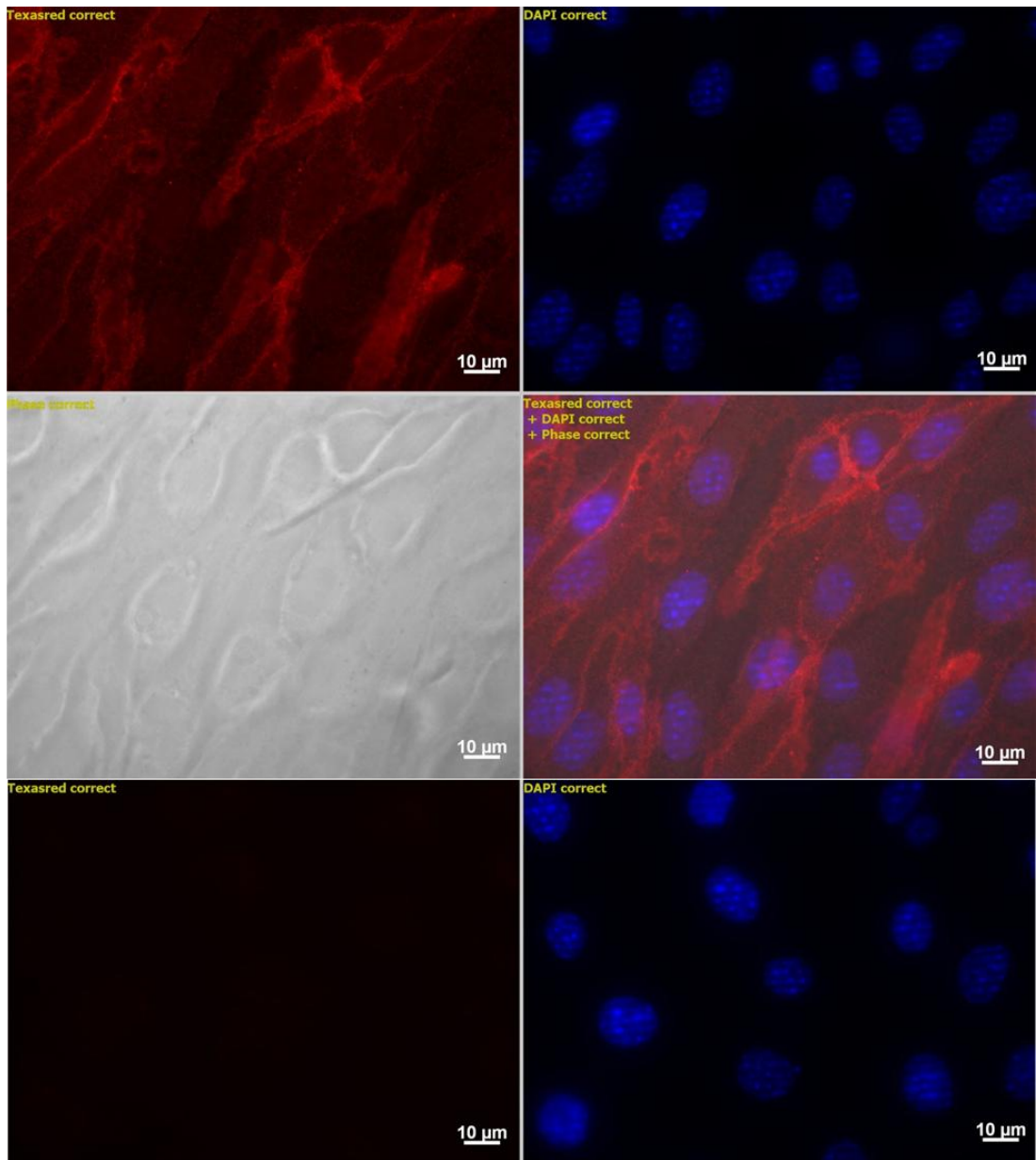
Figure 62: Immunofluorescence images of CD105 staining on the SVR cell line
The middle-right image showing a composite of the top-left (CD105 antibody alone
visualized with the Texas Red filter), top-right (showing nuclear staining alone), and middle-
left (phase contrast) images. A clear pattern of membranous expression of CD105 is seen.
The bottom-left image illustrates the lack of expression when the primary antibody is
omitted, and the bottom right image showing nuclear staining alone in this no-primary
section.

4.2.5 *In vitro* flow assays using CD105 coated microbubbles show significant binding to SVR cells

Flow assays were set up as detailed in the Methods chapter (section 2.3.5). Experiments were performed using two preparations of MBs viz. those that are commercially available (Bracco) and those generated in-house. Each preparation was used in separate experiments. MB binding was expressed in ratios between MBs in contact with cells and total number of SVR cells per assessed field.

CD105 and its isotype control facilitated binding of MBs to SVR cell line is demonstrated in Figure 63. MBs are identified in these images through their refractile, bi-layered, rounded appearance. Figure 64 shows the scatterplot data for MB binding to SVR cells. Both Microfluidics and Micromarker MBs showed significantly higher levels of binding to SVR cells when bound to CD105 than its isotype control, at optimal concentration.
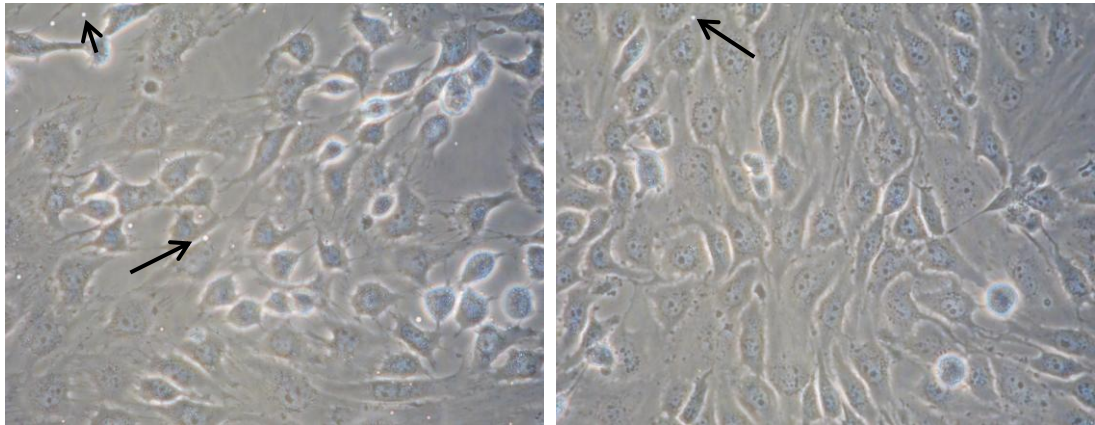
Figure 63: Inverted light microscopy examination of SVR cell lines as part of flow assay experiments

Left image taken following flow of CD105 antibody bound MB and the right image following flow of isotype control antibody. Bound MBs (long arrows) and unbound MBs (short arrow) are demonstrated. As can be observed, the number of bound MBs is relatively less in the isotype control image (x40 magnification).
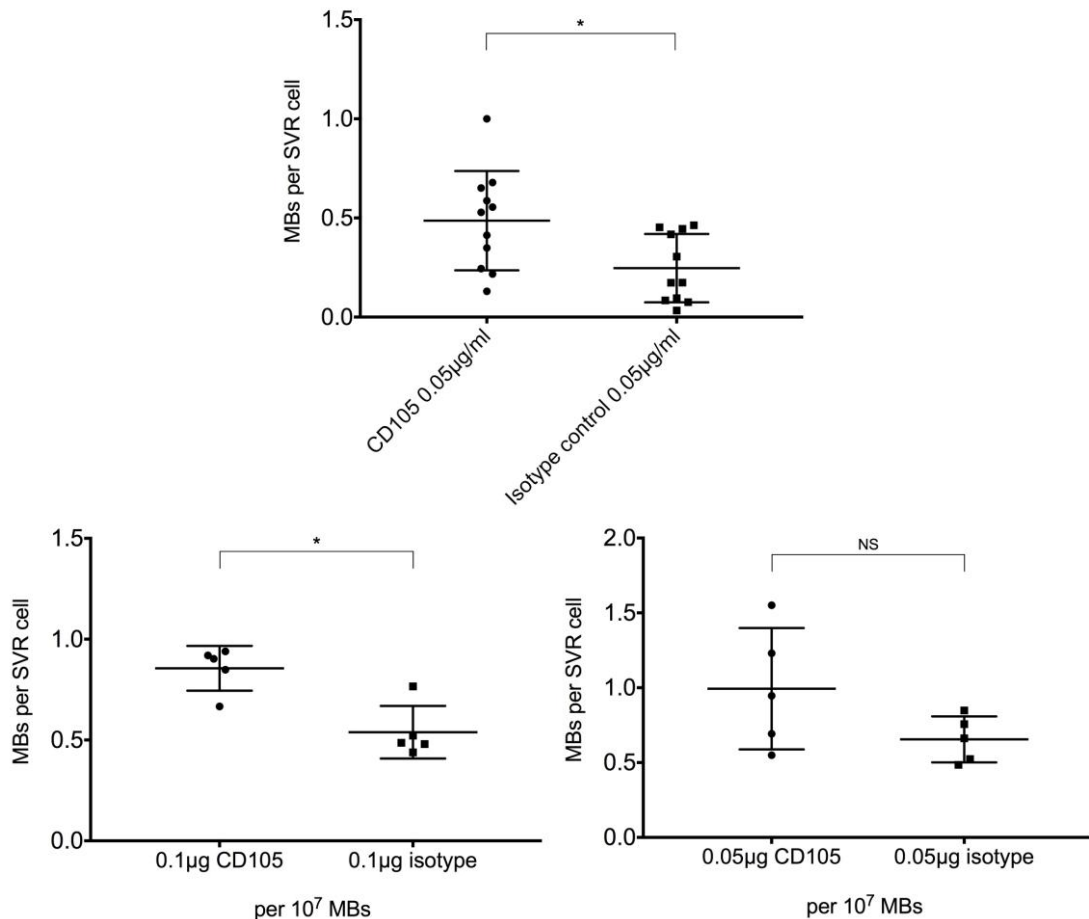
Figure 64: Scatterplot data summarising the results of flow assay experiments using CD105 and isotype control antibody-bound MBs.

Top image (n=11) showing the results of use of Microfluidics MBs and bottom two images (both n=5) that from Micromarker MBs. The use of CD105-bound Microfluidics MBs revealed significantly higher binding of SVR cells to that of isotype-control bound MBs, at an antibody concentration of 0.05µg/ml (p=0.020). CD105-bound Micromarker MBs also showed the same behaviour at an antibody concentration of 0.1µg per 10^7 MBs (p=0.016) as displayed in the bottom left image. At a lower antibody concentration of 0.05µg per 10^7 MBs, this difference was not significant (NS), as shown in the bottom right image (p=0.117). Data expressed as median with interquartile ranges. Mann-Whitney U tests used for comparisons.

4.2.6 CD105-bound Micromarker Microbubbles target EGI-1 and TFK-1 xenograft endothelium in significantly higher amounts compared to isotype control in a murine model

Of the 6 available CCA cell lines, none except TFK-1, EGI-1 and OZ generated any visible subcutaneous tumour growth following inoculation in CD1or Balb/c mice. As shown in Figure 65, EGI-1 and TFK-1 grew better tumour volume xenografts (Figure 66) although all showed an occasional tendency for spontaneous xenograft regression. For my experiments, EGI-1 and TFK-1 were finally selected for in-vivo MB testing. These cell lines were then re-established as subcutaneous xenografts in CD1 nude mice, and in-vivo testing of MB binding assessed as detailed in section 2.4.2 of the Methods chapter. The degree of binding of MBs to tumour endothelium was quantified by means of the subtracted molecular signal, which denotes the difference in signal observed between bound and flowing MBs together and flowing MBs alone (Figure 67). These results are summarised in Figure 68 and show that in 5 out of the 6 TFK-1 xenografts as well as all 4 EGI-1 xenografts, the subtracted molecular signal was significantly higher in the CD105 MB group in comparison to the isotype control MB group. This therefore indicates that TFK-1 and EGI-1 xenograft vasculature can be targeted using CD105 directed MBs, and mirrors the findings I obtained from *in vitro* tests using CD105 labelled MBs.

4.2.7 CCA xenografts show peri-tumoural vasculature that expresses CD105

Following completion of the *in vivo* CD105-MB experiments, animals were sacrificed and xenografts harvested, formalin fixed and paraffin embedded for CD105 IHC

examination. As shown in Figure 69, peri-tumoural vessels showed positivity for

CD105, thus giving credence to my *in vivo* findings.

EGI -1

TFK-1

OZ
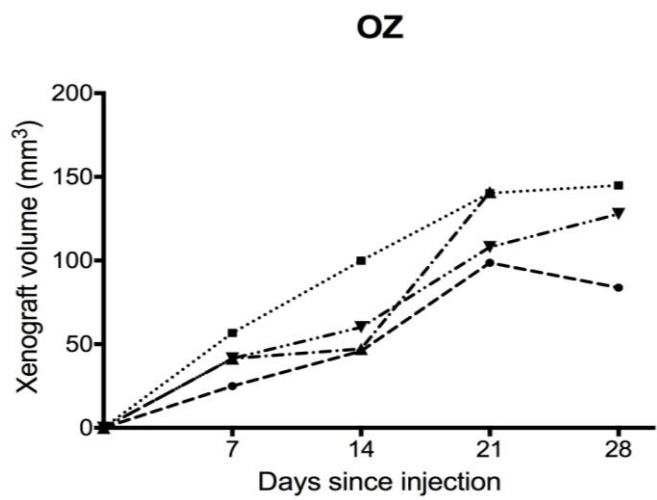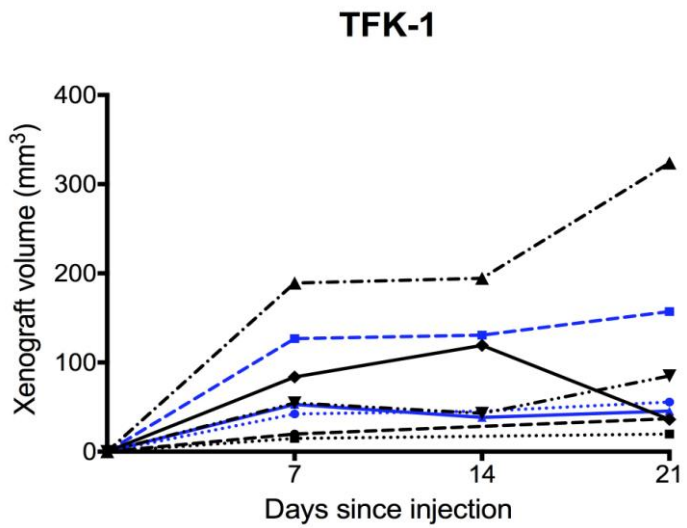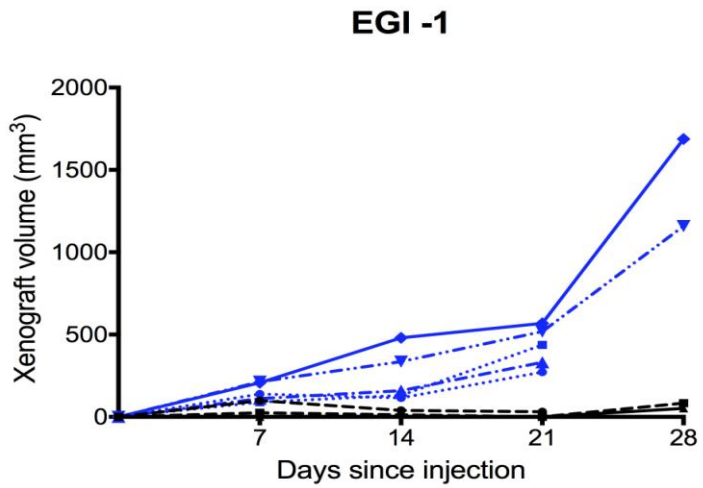
Figure 65: Xenograft growth curves for indicated CCA cell lines
Each line represents one mouse. Black lines showing data for CD1 nude mice and blue lines indicating those for balb-c mice.
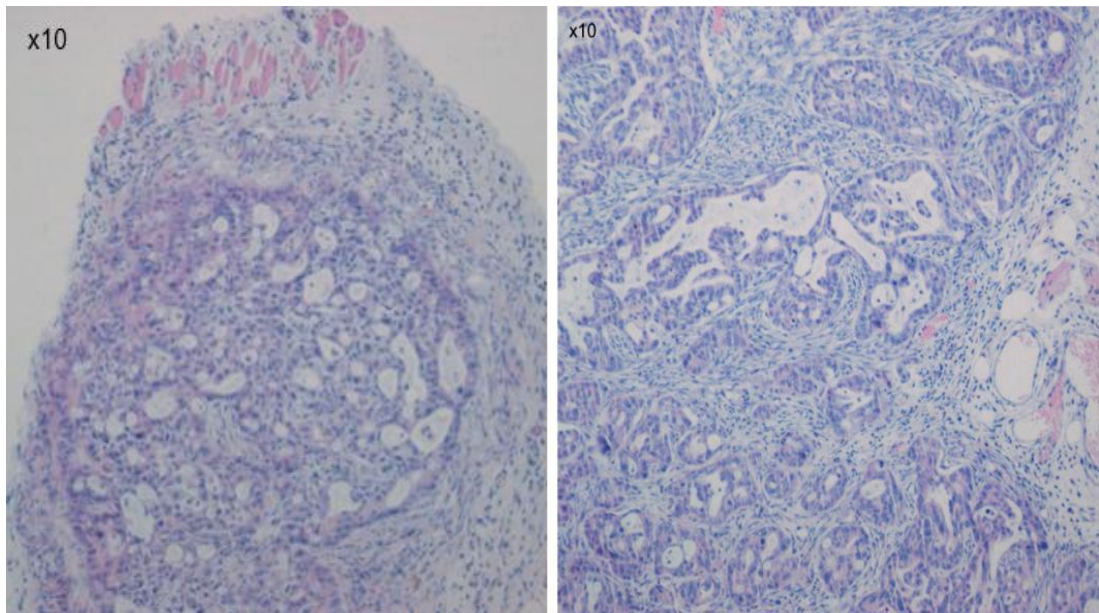
Figure 66: H&E staining of TFK-1 and EGI-1 xenografts.
TFK-1 on left an EGI-1 on right (both x10 magnification). Xenografts are seen as circumscribed tissue containing malignant cells.
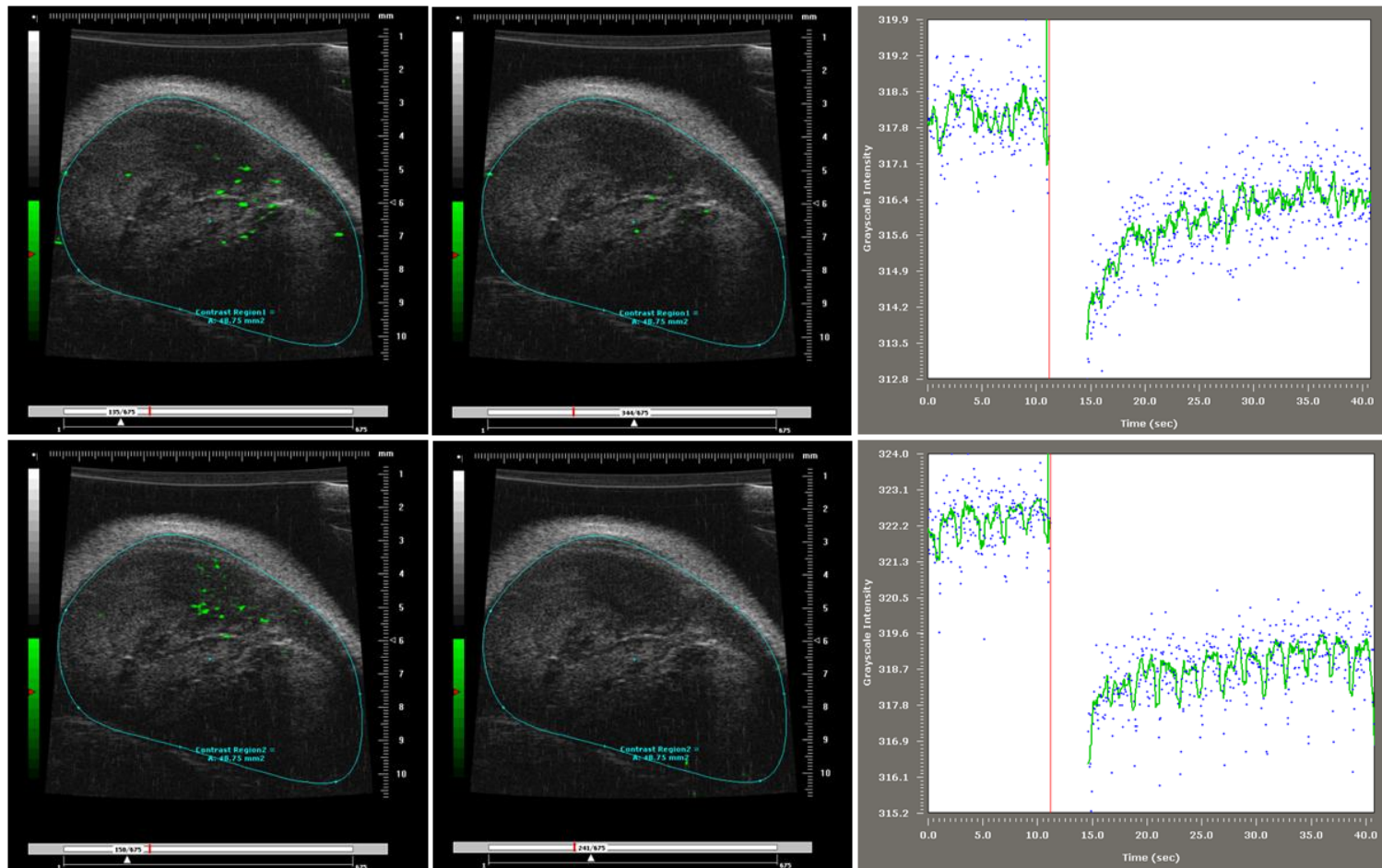
Figure 67: *In vivo* **US imaging of TFK-1 xenograft following intravenous administration of Micromarker MBs and destructive US pulse, with associated subtracted molecular signal data**

Top left image showing US appearance of tumour following administration of MBs bound to isotype-control antibodies (manifested as green coloured signal within tumour, reflective of both flowing and bound MBs); top middle image showing same section following application of destructive US pulse (green signal now indicative of only flowing MBs). Top right image demonstrating the difference in molecular signal intensity prior to (left of vertical red line) and after (right of vertical red line) application of destructive US pulse. Images in bottom panel showing corresponding findings following administration of CD105-bound MBs. A larger difference in signal intensity is apparent in this instance (note the difference in the y-axis scale magnitude between both graphs)
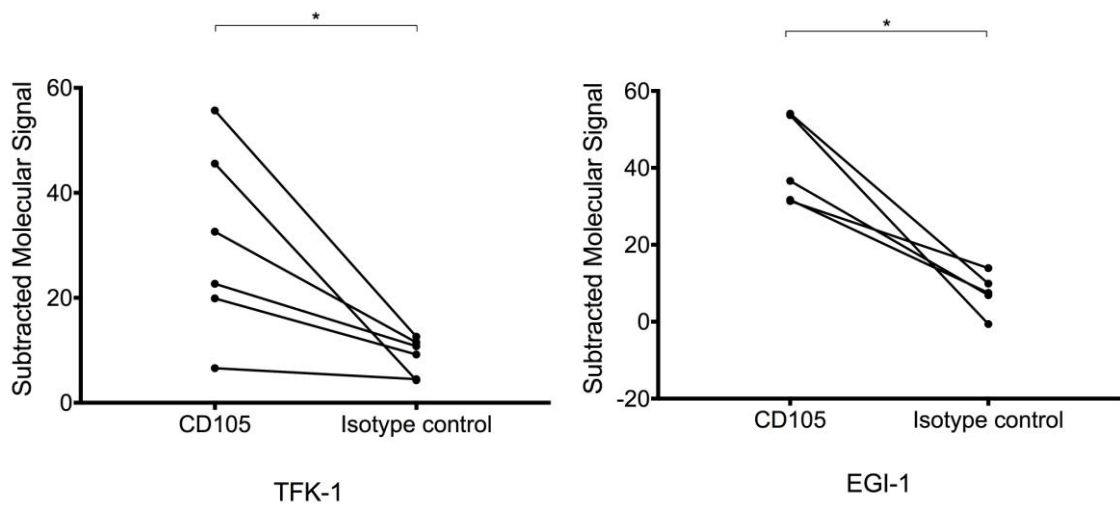
Figure 68: Depiction of binding of CD105 labelled Micromarker MBs versus isotype control MBs
A series of 6 measurements (for cell line TFK-1) and 4 measurements (for cell line EGI-1) used in the murine heterotopic xenograft model of CCA. A significant difference in subtracted molecular signal (indicative of the degree of MB binding to tumour endothelium) when subjected to a destructive US pulse is seen in both instances (TFK-1 p=0.028 and EGI-1 p=0.043) between CD105 and its isotype control. Wilcoxon sign rank tests used for matched data comparisons.
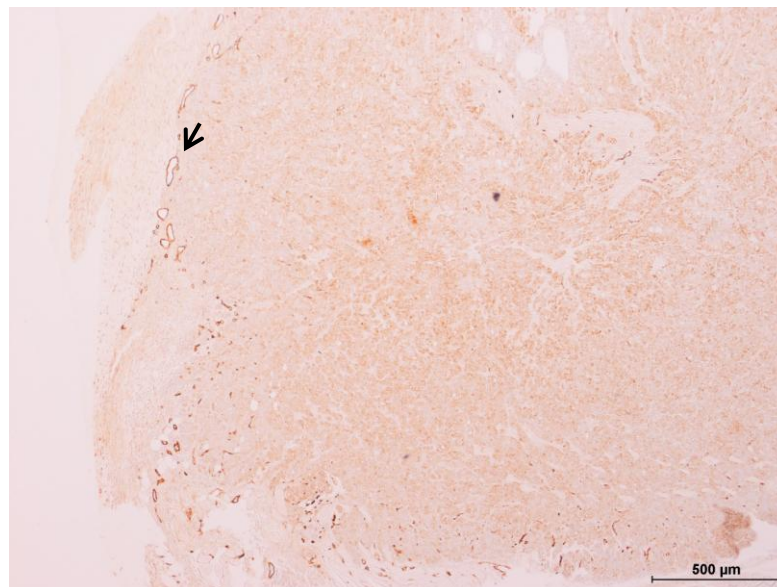
Figure 69: Image showing evidence of CD105 positive vessels at the periphery of EGI-1 xenograft tissue
CD105 positive murine vessels (arrow) are seen forming a rim around the subcutaneous xenograft. The latter was harvested following completion of *in vivo* CD105-MB binding experiments. Evidence of stromal CD105 expression is also noted within the substance of the xenograft tissue.

4.3 Discussion

The targeting of a biomarker that is overexpressed in cancer tissue for theragnostic use by systemic administration of an appropriate molecule or payload is an attractive concept. However, the notion is simplistic when compared to its realisation and the efficacy of such an approach in practice is suboptimal. The bio-distribution and pharmacodynamic characteristics of a given theragnostic molecule can prevent its effective localization to target tissue, with accumulation and/or metabolic degradation in normal tissues instead (Scott et al., 2012), leading to markedly diminished targeting efficacy. Even when considering the added physicochemical attributes of NPs that enable passive tumour targeting through EPR, NP localization to tumour is only to the order of approximately 5% when simply administered as intravenous injection (Bae and Park, 2011).

A method of improving delivery of systemic payloads to tumour tissue is to target tumour vascular endothelium as a preliminary step. Capillary vascular endothelium is the first physical barrier between the bloodstream and tumour interstitium, and this must be crossed in order for theragnostic particles to exert their actions. The concept of a delivery vehicle that can both carry theragnostic payloads and bind tumour endothelium is fulfilled by MB systems. MBs can be functionalized through the addition of ligands to its surface that allow endothelial binding of the former. Accordingly, this would enable a higher proportion of the payload to be optimally retained in tumour vasculature, prior to its release into tumour tissue. Such a system also serves to lessen exposure of payloads to processes that can result from continued circulation such as metabolism or immune-mediated neutralization, although other methods also exist to mitigate these effects such as payload PEG-ylation or inclusion in liposomal formulations.

Identifying the optimal endothelial marker for targeting in CCA was the first focus of my efforts in this chapter. An ideal endothelial target would be expressed exclusively or predominantly in tumour blood vessels, although no currently known marker fulfils this property. Nonetheless, as a body of literature pointed out that CD105 and VEGFR2 are expressed in proliferating endothelium (Dallas et al., 2008; Seon et al., 2011) as should be seen in cancer tissue, I investigated these markers in further detail.

CD31 was utilised primarily as a reference endothelial marker in my IHC work although interestingly, its impact in CCA prognosis has also been analysed previously. Thelen and associates examined the impact of CD31 MVD on disease prognosis in a series of 60 patients who underwent resection of PH-CCA. The mean MVD was found to be 28 (range 4 - 71), whereas cases were segregated into high and low MVD categories based on a value of 20. In this fashion, high MVD tumours were found to be significantly linked to higher risk of nodal involvement and local recurrence but not systemic metastasis, whilst on Cox regression analysis high MVD, along with nodal metastasis were independent predictors of adverse OS (Thelen et al., 2008). In contrast, I observed a median CD31 MVD of 45 (range 8-98) in this series, whilst a significantly lower CD31 MVD was associated with local recurrence. The expression of CD31 though significantly associated with OS on univariate analysis had no prognostic impact on this cohort in the Cox regression model. In a subsequent paper, Thelen and co-workers again analysed CD31 MVD in a group of 114 resected IH-CCA patients and noted a mean MVD of 13 (range 2-44). A significant association of high MVD (defined as a count above the mean of 13) was found with primary tumour stage, positive surgical margins, peri-neural infiltration and higher rates of recurrence. Multivariate analysis revealed a high MVD as a prognostic factor for poorer OS.(Thelen et al., 2010).

When considering CD105, there are currently no sizeable published series in the English language that delve into the tissue expression of this marker in CCA. One report investigating the influence of hypoxia inducible factor-1 in the response to photodynamic therapy in PH-CCA using an *in vitro* model also evaluated the tissue expression of CD105 in this cancer, in the marker's capacity as a hypoxia related protein. Of the two tissue samples analysed, dense staining of microvessels in tumour stroma was noted, and in contrast, no expression was seen in tumour parenchyma (Weijer et al., 2016). Whilst I also observed a high rate of stromal positivity in our cohort, tumour parenchyma was found to express CD105 as well in many of the cases. In addition, this series is the first of its kind to scrutinize the expression and prognostic impact of CD105 MVD in PH-CCA, and although this bore no significant statistical association with any patient factors, I was able to show that a MVD >31 was associated with significantly poorer OS.

The results of my VEGFR2 expression analysis were also noteworthy. I encountered very low MVD scores, with many samples showing no presence of the marker. Accordingly, I dichotomised its expression into positive and negative, with the former group comprising 52% of the total. The only factor significantly associated with VEGFR2 positivity was the occurrence of metastasis, although the marker carried no association with OS or DFS. Although various reports have examined the expression of various forms of VEGF and its impact on CCA, studies looking into VEGFR2 are scant, and assess tumoural expression as opposed to endothelial staining. Sang et al looked into the expression of VEGFR2 by IHC in 49 resected cases of PH-CCA and analysed positivity by means of computer-aided optical density measurements. They found mean VEGFR2 optical density to be significantly higher in those cases with nodal metastasis and somewhat paradoxically tumours with low to moderate differentiation, whilst these values were also higher in tumour tissue compared to benign biliary pathology. No data on the

effect of expression on survival was provided (Sang et al., 2013). Peng and associates during their study into the effects of Apatinib (a VEGFR2 inhibitor) on CCA cell lines also evaluated the expression of VEGFR2 in 104 cases of IH-CCA. Once again, tumoural expression was assessed as opposed to MVD, and positivity was noted in 60% of samples. Expression was found on cell membranes, cytosol and nuclei of tumour cells (Peng et al., 2016). Although specific inhibitors of VEGFR2 have not yet reached clinical translation, clinical trial data does exist on the use of the VEGF-A inhibitor Bevacizumab in advanced biliary tract cancers. Two phase-2 human trials have demonstrated modest activity of this drug against tumour with acceptable rate of adverse events, when used in combination with other chemotherapeutic or anti-EGFR agents (Lubner et al., 2010; Zhu et al., 2010). Nonetheless, my data in conjunction with that of others points to the heterogeneity of expression of molecular targets in CCA worldwide, and could explain the differing rates of tumour response to targeted therapies.

As is apparent in the literature on the use of MVD in various cancers, disparate results are often seen in the impact of MVD on disease prognosis, with both high and low MVD being shown as significantly associated with OS. Although differences in methodology and endothelial markers used can sometimes account for these observations, most of these findings are a true reflection of the varied influence of MVD on disease progression. MVD does not mirror the angiogenic activity of a tumour per se but rather indicates its metabolic burden. Thus even in the presence of much angiogenic activity or aggressive cancer biology, MVD can be low in those tumours with increased hypoxic tolerance, and as such should not be used to determine which patients might benefit from anti-angiogenic treatments (Hlatky et al., 2002; Nico et al., 2008). As my findings suggest, the use CD31-based hotspots for MVD measurements did not necessarily highlight the most active area of neo-

angiogenesis, as its expression is limited to established, mature endothelium. Both CD105 and VEGFR2 stained vessels that were not picked up by CD31.

In addition to the prognostic effect that was demonstrated with CD105 MVD in this series, an equally pertinent observation I made was the expression of CD105 in hepatic sinusoidal endothelium. Similar findings have been noted in related literature, with CD105 expression observed mostly in the outflow region of the sinusoids, adjacent to the terminal hepatic vein (Theuerkauf et al., 2001; Yu et al., 2007). Previous authors have also documented the expression of CD105 in both tumour and non-tumour bearing liver parenchyma (Ho et al., 2005; Minhajat et al., 2006; Nakamura, 2009) and put forth the view that in peri-tumoural areas its presence is perhaps indicative of a field change that predisposes to tumour progression (Nakamura, 2009). Nonetheless, my finding bears relevance in the development of a targeted particle directed against this molecule as off-target effects on hepatocytes would not be surprising under these circumstances. The use of focused high-frequency US to improve specificity of payload targeting by MBs can in theory ameliorate such lateral effects but in the case of tumours like PH-CCA that are intimately associated with the liver, the degree of specificity gained by US-aided MB sonoporation may be modest.

The first step towards exploring the feasibility of targeting tumour endothelium in an *in vivo* model was to verify CD105 expression in murine endothelial cells, as xenografts are supplied by native vessels. Accordingly, my IF experiments confirmed CD105 positivity on the surface of the murine SVR endothelial cell line. This finding gave us the background required to assess the binding of CD105 ligand coated MBs to SVR cells in an *in vitro* flow assay model aimed to simulate capillary blood flow. This demonstrated that CD105-MBs could bind SVR cells appreciably more than isotype control MBs under conditions of simulated capillary flow. Finally,

the results of my murine *in vivo* MB experiments revealed that these intravascular agents when functionalised with surface CD105 ligands were able to bind CCA xenograft endothelium at significantly higher levels than that seen with MBs with isotype control. The use of CD105-conjugated MBs has been reported in the literature previously. Korpanty and associates demonstrated using *in vitro* experiments that MBs could be functionalised with biotinylated CD105 by incorporating avidin into the MB shell. Using tagged fluorophores and in conditions of stasis (rather than flow), they were then able to demonstrate that these targeted MBs bound to endothelial cell cultures at significantly higher amounts than control MBs, but not so for fibroblast cultures (Korpanty et al., 2005). The same group in a subsequent paper showed that MBs conjugated with CD105 and VEGFR2 ligands were able to bind pancreatic cancer xenograft vasculature significantly better than control MBs, using contrast US imaging in a murine model. Mice treated with Gemcitabine when compared to control showed a significant reduction in vascularity as demonstrated with CD105-MB (Korpanty et al., 2007). In more recent work, Zhou and colleagues successfully transfected breast cancer xenografts in mice with the endostatin gene using CD105 conjugated MBs through the means of US directed MB destruction. Xenografts successfully transfected in this fashion showed evidence of significantly higher levels of endostatin expression when compared to control, along with significant reduction in tumour volumes (Zhou et al., 2015).

My results are therefore the first described use of CD105 functionalised commercial MBs in a model of CCA. Through the use of *in vitro* and *in vivo* models, I have shown that these MBs bind SVR cells significantly more than isotype control MBs under similar conditions. Willman and co-workers performed similar *in vivo* US experiments using micromarker MBs conjugated to VEGFR2 on heterotopic murine angiosarcoma and rat-glioma tumours. Their results showed significant rise in video signal from VEGFR2-conjugated MBs in comparison to control MBs, indicating that

VEGFR2 expression in vessels supplying these subcutaneous tumours could be non-invasively assessed (Willmann et al., 2008). Whilst I did not assess the efficacy of a targeted payload delivery to CCA tissue, the literature reveals that such MBs can be conjugated with a theragnostic particle to effect diagnosis and treatment. The degree of off-target effects to normal liver tissue is unknown at present, and is the potential Achilles heel in a targeted delivery system that relies on a homing biomarker that is expressed in both tumour and liver sinusoidal endothelium.

The success of a novel anti-cancer treatment paradigm in an animal model does not indicate its imminent success in human trials (van der Worp et al., 2010). However, even with the use of ectopic tumour sites, the use of mouse models of disease may reliably inform future human studies especially when variables such as the *in vivo* behaviour and kinetics of a candidate molecule are being investigated (Kerbel, 2003). In the case of CD105, phase-I human trials have already been conducted on the backdrop of promising anti-angiogenic effects seen in animal experiments. The IgG1 chimeric monoclonal antibody to CD105 (TRC105) when administered as an intravenous preparation was found to be well tolerated in a group of 50 patients with various refractory advanced solid cancers, with adverse events noted in 18% of the group, including hypo-proliferative anaemia. Stable disease at 2 months was noted in 47% of 45 evaluated patients, which dropped down to 14% of 44 patients at 4 months (Rosen et al., 2012). The agent has also been similarly evaluated in combination with Bevacizumab in another phase-I trial, with a good safety profile and evidence of anti-tumour activity seen in those patients refractory to VEGF inhibitor therapy (Gordon et al., 2014). At present, there are several on-going phase-II trials using TRC105 in combination with other agents in a variety of solid cancers (*Tracon Pharma*). A recent relevant phase-II study of TRC105 in advanced HCC patients who had progressed on Sorafenib also posted interesting observations despite its negative result. The trial accrued only 11 patients and the

overall rate of disease progression did not allow completion of all stages of the study. Nonetheless, durable anti-cancer activity was evident in only one patient and treatment tolerability overall was considered good. What can be inferred from these phase-I and II studies is primarily that anti-CD105 intravenous therapy has a good safety profile, and in particular no adverse events in relation to the liver were reported. One can postulate however that with a successful targeted approach using CD105 to CCA, both treatment efficacy and the rate of liver-related adverse events may be higher, although the incidence of systemic side effects may lessen.

5 Conclusions

This body of work set about to answer two pertinent questions in the context of the treatment of peri-hilar cholangiocarcinoma. The first objective was to establish whether NGAL and MMP9 had any prognostic impact in this malignancy and if these biomarkers possessed properties that enabled their targeting to diagnostic or therapeutic effect. I showed that whilst NGAL had a statistically significant association with lymph nodal metastasis, neither biomarker had a significant bearing on survival in this cohort. This could be reflective of an inadequate sample size that was not powerful enough to detect any such effects. Nonetheless, NGAL was also found to be expressed on the cell surface and tumour stroma, both of which are qualities that make it suitable for a targeting approach.

Secondly, I interrogated the vascular endothelial markers CD31, CD105 and VEGFR2 (the latter two of which are known to be intimately involved in tumour neo-angiogenesis) and found CD105 expression to be adversely associated with overall survival in this cancer. Using *in vitro* and *in vivo* models, I then showed CD105 conjugated MBs were able to specifically and significantly target tumour vasculature.

Based on these results, it can be surmised that a targeted delivery platform using CD105 conjugated MBs can be developed to home in to CCA tissue. In addition to therapeutic blockade of CD105, these MBs could be further functionalised to carry a relevant payload such as an anti-NGAL molecule, which when driven into tumour tissue under the influence of a destructive US pulse would exert theragnostic effects.

There are however further questions that require clarification before such a platform sees fruition. The degree of off-target binding with such a system and the nature of any off-target effects are currently unknown, and merit further investigation. Whilst employing biomarkers and ligands that are relatively specific for tumour tissue greatly aids targeting, no currently known molecule is unique to tumour tissue. In this respect, the quest for Ehrlich's "magic bullet" continues (Strebhardt and Ullrich, 2008).

6 References

Agrawal, S. and Belghiti, J. 2011. Oncologic resection for malignant tumors of the liver. *Annals of surgery.* **253**(4), pp.656-665.

Akamatsu, N., Sugawara, Y. and Hashimoto, D. 2011. Surgical strategy for bile duct cancer: Advances and current limitations. *World journal of clinical oncology.* **2**(2), pp.94-107.

Aljiffry, M., Walsh, M.J. and Molinari, M. 2009. Advances in diagnosis, treatment and palliation of cholangiocarcinoma: 1990-2009. *World journal of gastroenterology : WJG.* **15**(34), pp.4240-4262.

Alvaro, D. 2009. Serum and bile biomarkers for cholangiocarcinoma. *Current opinion in gastroenterology.* **25**(3), pp.279-284.

Alvaro, D., Macarri, G., Mancino, M.G., Marzioni, M., Bragazzi, M., Onori, P., Corradini, S.G., Invernizzi, P., Franchitto, A., Attili, A.F., Gaudio, E. and Benedetti, A. 2007. Serum and biliary insulin-like growth factor I and vascular endothelial growth factor in determining the cause of obstructive cholestasis. *Annals of internal medicine.* **147**(7), pp.451-459.

Arbiser, J.L., Moses, M.A., Fernandez, C.A., Ghiso, N., Cao, Y., Klauber, N., Frank, D., Brownlee, M., Flynn, E., Parangi, S., Byers, H.R. and Folkman, J. 1997. Oncogenic H-ras stimulates tumor angiogenesis by two distinct pathways. *Proc Natl Acad Sci U S A.* **94**(3), pp.861-866.

Bae, Y.H. and Park, K. 2011. Targeted drug delivery to tumors: myths, reality and possibility. *J Control Release.* **153**(3), pp.198-205.

Ben-Menachem, T. 2007. Risk factors for cholangiocarcinoma. *European journal of gastroenterology & hepatology.* **19**(8), pp.615-617.

Bismuth, H. and Corlette, M.B. 1975. Intrahepatic cholangioenteric anastomosis in carcinoma of the hilus of the liver. *Surg Gynecol Obstet.* **140**(2), pp.170-178.

Blechacz, B. and Gores, G.J. 2008a. Cholangiocarcinoma. *Clinics in liver disease.* **12**(1), pp.131-150, ix.

Blechacz, B. and Gores, G.J. 2008b. Cholangiocarcinoma: advances in pathogenesis, diagnosis, and treatment. *Hepatology.* **48**(1), pp.308-321.

Bolignano, D., Donato, V., Lacquaniti, A., Fazio, M.R., Bono, C., Coppolino, G. and Buemi, M. 2010. Neutrophil gelatinase-associated lipocalin (NGAL) in human neoplasias: a new protein enters the scene. *Cancer letters.* **288**(1), pp.10-16.

Bonet Beltran, M., Allal, A.S., Gich, I., Sole, J.M. and Carrio, I. 2011. Is adjuvant radiotherapy needed after curative resection of extrahepatic biliary tract cancers? A systematic review with a meta-analysis of observational studies. *Cancer Treat Rev.*

Borkham-Kamphorst, E., Drews, F. and Weiskirchen, R. 2011. Induction of lipocalin-2 expression in acute and chronic experimental liver injury moderated by pro-inflammatory cytokines interleukin-1beta through nuclear factor-kappaB activation. *Liver international : official journal of the International Association for the Study of the Liver.* **31**(5), pp.656-665.

Bragazzi, M., Cardinale, V., Carpino, G., Venere, R., Semeraro, R., Gentile, R., Gaudio, E. and Alvaro, D. 2012. Cholangiocarcinoma: Epidemiology and risk factors. *Transl Gastrointest Cancer* **1**, pp.21-32.

Bramhall, S.R., Schulz, J., Nemunaitis, J., Brown, P.D., Baillet, M. and Buckels, J.A. 2002. A double-blind placebo-controlled, randomised study comparing gemcitabine and marimastat with gemcitabine and placebo as first line therapy in patients with advanced pancreatic cancer. *Br J Cancer.* **87**(2), pp.161-167.

Bredow, S., Lewin, M., Hofmann, B., Marecos, E. and Weissleder, R. 2000. Imaging of tumour neovasculature by targeting the TGF-beta binding receptor endoglin. *Eur J Cancer.* **36**(5), pp.675-681.

Brinckerhoff, C.E. and Matrisian, L.M. 2002. Matrix metalloproteinases: a tail of a frog that became a prince. *Nat Rev Mol Cell Biol.* **3**(3), pp.207-214.

Budczies, J., Klauschen, F., Sinn, B.V., Gyorffy, B., Schmitt, W.D., Darb-Esfahani, S. and Denkert, C. 2012. Cutoff Finder: a comprehensive and straightforward Web application enabling rapid biomarker cutoff optimization. *PLoS One.* **7**(12), pe51862.

Budzynska, A., Nowakowska-Dulawa, E., Marek, T., Boldys, H., Nowak, A. and Hartleb, M. 2013. Differentiation of pancreatobiliary cancer from benign biliary strictures using neutrophil gelatinase-associated lipocalin. *J Physiol Pharmacol.* **64**(1), pp.109-114.

Candido, S., Abrams, S.L., Steelman, L.S., Lertpiriyapong, K., Fitzgerald, T.L., Martelli, A.M., Cocco, L., Montalto, G., Cervello, M., Polesel, J., Libra, M. and McCubrey, J.A. 2015. Roles of NGAL and MMP-9 in the tumor microenvironment and sensitivity to targeted therapy. *Biochim Biophys Acta.*

Cardinale, V., Semeraro, R., Torrice, A., Gatto, M., Napoli, C., Bragazzi, M.C., Gentile, R. and Alvaro, D. 2010. Intra-hepatic and extra-hepatic cholangiocarcinoma: New insight into epidemiology and risk factors. *World journal of gastrointestinal oncology.* **2**(11), pp.407-416.

Chakraborty, S., Kaur, S., Guha, S. and Batra, S.K. 2012. The multifaceted roles of neutrophil gelatinase associated lipocalin (NGAL) in inflammation and cancer. *Biochim Biophys Acta.* **1826**(1), pp.129-169.

Chan, E.S. and Yeh, M.M. 2010. The use of immunohistochemistry in liver tumors. *Clinics in liver disease.* **14**(4), pp.687-703.

Charbel, H. and Al-Kawas, F.H. 2011. Cholangiocarcinoma: epidemiology, risk factors, pathogenesis, and diagnosis. *Current gastroenterology reports.* **13**(2), pp.182-187.

Chen, W., Ayala-Orozco, C., Biswal, N.C., Perez-Torres, C., Bartels, M., Bardhan, R., Stinnet, G., Liu, X.D., Ji, B., Deorukhkar, A., Brown, L.V., Guha, S., Pautler, R.G., Krishnan, S., Halas, N.J. and Joshi, A. 2014. Targeting pancreatic cancer with magneto-fluorescent theranostic gold nanoshells. *Nanomedicine (Lond).* **9**(8), pp.1209-1222.

Chen, Y., Wang, X.L., Yan, Z.P., Cheng, J.M., Wang, J.H., Gong, G.Q., Qian, S., Luo, J.J. and Liu, Q.X. 2004. HDR-192Ir intraluminal brachytherapy in treatment of malignant obstructive jaundice. *World journal of gastroenterology : WJG.* **10**(23), pp.3506-3510.

Choi, B.I., Lee, J.M. and Han, J.K. 2004. Imaging of intrahepatic and hilar cholangiocarcinoma. *Abdominal imaging.* **29**(5), pp.548-557.

Choi, S.B., Kim, K.S., Choi, J.Y., Park, S.W., Choi, J.S., Lee, W.J. and Chung, J.B. 2009. The prognosis and survival outcome of intrahepatic cholangiocarcinoma following surgical resection: association of lymph node metastasis and lymph node dissection with survival. *Annals of surgical oncology.* **16**(11), pp.3048-3056.

Couinaud, C. 1957. *Le foie: études anatomiques et chirurgicales.* Masson & Cie.

Dallas, N.A., Samuel, S., Xia, L., Fan, F., Gray, M.J., Lim, S.J. and Ellis, L.M. 2008. Endoglin (CD105): a marker of tumor vasculature and potential target for therapy. *Clin Cancer Res.* **14**(7), pp.1931-1937.

Darwish Murad, S., Kim, W.R., Harnois, D.M., Douglas, D.D., Burton, J., Kulik, L.M., Botha, J.F., Mezrich, J.D., Chapman, W.C., Schwartz, J.J., Hong, J.C., Emond, J.C., Jeon, H., Rosen, C.B., Gores, G.J. and Heimbach, J.K. 2012. Efficacy of neoadjuvant chemoradiation, followed by liver transplantation, for perihilar cholangiocarcinoma at 12 US centers. *Gastroenterology.* **143**(1), pp.88-98 e83; quiz e14.

de Jong, M.C., Hong, S.M., Augustine, M.M., Goggins, M.G., Wolfgang, C.L., Hirose, K., Schulick, R.D., Choti, M.A., Anders, R.A. and Pawlik, T.M. 2011a. Hilar cholangiocarcinoma: tumor depth as a predictor of outcome. *Archives of surgery.* **146**(6), pp.697-703.

de Jong, M.C., Nathan, H., Sotiropoulos, G.C., Paul, A., Alexandrescu, S., Marques, H., Pulitano, C., Barroso, E., Clary, B.M., Aldrighetti, L., Ferrone, C.R., Zhu, A.X., Bauer, T.W., Walters, D.M., Gamblin, T.C., Nguyen, K.T., Turley, R., Popescu, I., Hubert, C., Meyer, S., Schulick, R.D., Choti, M.A., Gigot, J.F., Mentha, G. and Pawlik, T.M. 2011b. Intrahepatic Cholangiocarcinoma: An International Multi-Institutional Analysis of Prognostic Factors and Lymph Node Assessment. *Journal of clinical oncology : official journal of the American Society of Clinical Oncology.*

De Vreede, I., Steers, J.L., Burch, P.A., Rosen, C.B., Gunderson, L.L., Haddock, M.G., Burgart, L. and Gores, G.J. 2000. Prolonged disease-free survival after orthotopic liver transplantation plus adjuvant chemoirradiation for cholangiocarcinoma. *Liver Transpl.* **6**(3), pp.309-316.

DeOliveira, M.L., Cunningham, S.C., Cameron, J.L., Kamangar, F., Winter, J.M., Lillemoe, K.D., Choti, M.A., Yeo, C.J. and Schulick, R.D. 2007a. Cholangiocarcinoma: thirty-one-year experience with 564 patients at a single institution. *Annals of surgery.* **245**(5), pp.755-762.

DeOliveira, M.L., Cunningham, S.C., Cameron, J.L., Kamangar, F., Winter, J.M., Lillemoe, K.D., Choti, M.A., Yeo, C.J. and Schulick, R.D. 2007b. Cholangiocarcinoma: thirty-one-year experience with 564 patients at a single institution. *Ann Surg.* **245**(5), pp.755-762.

Deoliveira, M.L., Schulick, R.D., Nimura, Y., Rosen, C., Gores, G., Neuhaus, P. and Clavien, P.A. 2011. New staging system and a registry for perihilar cholangiocarcinoma. *Hepatology.* **53**(4), pp.1363-1371.

Deshpande, N., Needles, A. and Willmann, J.K. 2010. Molecular ultrasound imaging: current status and future directions. *Clin Radiol.* **65**(7), pp.567-581.

Devireddy, L.R., Gazin, C., Zhu, X. and Green, M.R. 2005. A cell-surface receptor for lipocalin 24p3 selectively mediates apoptosis and iron uptake. *Cell.* **123**(7), pp.1293-1305.

DeVita, V.T., Jr. and Chu, E. 2008. A history of cancer chemotherapy. *Cancer Res.* **68**(21), pp.8643-8653.

Diamandis, E.P. and Christopoulos, T.K. 1991. The biotin-(strept)avidin system: principles and applications in biotechnology. *Clin Chem.* **37**(5), pp.625-636.

Duff, S.E., Li, C., Garland, J.M. and Kumar, S. 2003. CD105 is important for angiogenesis: evidence and potential applications. *FASEB J.* **17**(9), pp.984-992.

Duskey, J.T. and Rice, K.G. 2014. Nanoparticle ligand presentation for targeting solid tumors. *AAPS PharmSciTech.* **15**(5), pp.1345-1354.

Ebata, T., Kamiya, J., Nishio, H., Nagasaka, T., Nimura, Y. and Nagino, M. 2009. The concept of perihilar cholangiocarcinoma is valid. *The British journal of surgery.* **96**(8), pp.926-934.

Eckel, F. and Schmid, R.M. 2007. Chemotherapy in advanced biliary tract carcinoma: a pooled analysis of clinical trials. *British journal of cancer.* **96**(6), pp.896-902.

Edge, S.B. and American Joint Committee on Cancer. 2010. *AJCC cancer staging manual.* 7th ed. New York: Springer.

Endo, I., House, M.G., Klimstra, D.S., Gonen, M., D'Angelica, M., Dematteo, R.P., Fong, Y., Blumgart, L.H. and Jarnagin, W.R. 2008. Clinical significance of intraoperative bile duct margin assessment for hilar cholangiocarcinoma. *Annals of surgical oncology.* **15**(8), pp.2104-2112.

Eroglu, Z., Stein, C.A. and Pal, S.K. 2013. Targeting angiopoietin-2 signaling in cancer therapy. *Expert Opin Investig Drugs.* **22**(7), pp.813-825.

Esposito, I. and Schirmacher, P. 2008. Pathological aspects of cholangiocarcinoma. *HPB : the official journal of the International Hepato Pancreato Biliary Association.* **10**(2), pp.83-86.

Farid, S. 2014. *A proteomics-based approach for the identification of biliary markers of cholangiocarcinoma*. thesis, University of Leeds (School of Medicine).

Farid, S.G., Craven, R.A., Peng, J., Bonney, G.K., Perkins, D.N., Selby, P.J., Rajendra Prasad, K. and Banks, R.E. 2011. Shotgun proteomics of human bile in hilar cholangiocarcinoma. *Proteomics.* **11**(10), pp.2134-2138.

Ferrara, N., Hillan, K.J., Gerber, H.P. and Novotny, W. 2004. Discovery and development of bevacizumab, an anti-VEGF antibody for treating cancer. *Nat Rev Drug Discov.* **3**(5), pp.391-400.

Fingleton, B. 2008. MMPs as therapeutic targets--still a viable option? *Semin Cell Dev Biol.* **19**(1), pp.61-68.

Fonsatti, E., Jekunen, A.P., Kairemo, K.J., Coral, S., Snellman, M., Nicotra, M.R., Natali, P.G., Altomonte, M. and Maio, M. 2000. Endoglin is a suitable target for efficient imaging of solid tumors: in vivo evidence in a canine mammary carcinoma model. *Clin Cancer Res.* **6**(5), pp.2037-2043.

Fonsatti, E. and Maio, M. 2004. Highlights on endoglin (CD105): from basic findings towards clinical applications in human cancer. *J Transl Med.* **2**(1), p18.

Fonsatti, E., Nicolay, H.J., Altomonte, M., Covre, A. and Maio, M. 2010. Targeting cancer vasculature via endoglin/CD105: a novel antibody-based diagnostic and therapeutic strategy in solid tumours. *Cardiovasc Res.* **86**(1), pp.12-19.

French, J.J., Midwinter, M.J., Bennett, M.K., Manas, D.M. and Charnley, R.M. 2005. A matrix metalloproteinase inhibitor to treat unresectable cholangiocarcinoma. *HPB (Oxford).* **7**(4), pp.289-291.

Friedl, A., Stoesz, S.P., Buckley, P. and Gould, M.N. 1999. Neutrophil gelatinase-associated lipocalin in normal and neoplastic human tissues. Cell type-specific pattern of expression. *Histochem J.* **31**(7), pp.433-441.

Galvin, P., Thompson, D., Ryan, K.B., McCarthy, A., Moore, A.C., Burke, C.S., Dyson, M., Maccraith, B.D., Gun'ko, Y.K., Byrne, M.T., Volkov, Y., Keely, C., Keehan, E., Howe, M., Duffy, C. and MacLoughlin, R. 2012. Nanoparticle-based drug delivery: case studies for cancer and cardiovascular applications. *Cell Mol Life Sci.* **69**(3), pp.389-404.

Gao, X., Cui, Y., Levenson, R.M., Chung, L.W. and Nie, S. 2004. In vivo cancer targeting and imaging with semiconductor quantum dots. *Nat Biotechnol.* **22**(8), pp.969-976.

Garrow, D., Miller, S., Sinha, D., Conway, J., Hoffman, B.J., Hawes, R.H. and Romagnuolo, J. 2007. Endoscopic ultrasound: a meta-analysis of test performance in suspected biliary obstruction. *Clinical gastroenterology and hepatology : the official clinical practice journal of the American Gastroenterological Association.* **5**(5), pp.616-623.

Gatto, M. and Alvaro, D. 2010. New insights on cholangiocarcinoma. *World journal of gastrointestinal oncology.* **2**(3), pp.136-145.

Gatto, M., Bragazzi, M.C., Semeraro, R., Napoli, C., Gentile, R., Torrice, A., Gaudio, E. and Alvaro, D. 2010. Cholangiocarcinoma: update and future perspectives. *Digestive and liver disease : official journal of the Italian Society of Gastroenterology and the Italian Association for the Study of the Liver.* **42**(4), pp.253-260.

Gordon, M.S., Robert, F., Matei, D., Mendelson, D.S., Goldman, J.W., Chiorean, E.G., Strother, R.M., Seon, B.K., Figg, W.D., Peer, C.J., Alvarez, D., Adams, B.J., Theuer, C.P. and Rosen, L.S. 2014. An open-label phase Ib dose-escalation study of TRC105 (anti-endoglin antibody) with bevacizumab in patients with advanced cancer. *Clin Cancer Res.* **20**(23), pp.5918-5926.

Grossman, E.J. and Millis, J.M. 2010. Liver transplantation for non-hepatocellular carcinoma malignancy: Indications, limitations, and analysis of the current literature. *Liver transplantation : official publication of the American Association for the Study of Liver Diseases and the International Liver Transplantation Society.* **16**(8), pp.930-942.

Grubman, S.A., Perrone, R.D., Lee, D.W., Murray, S.L., Rogers, L.C., Wolkoff, L.I., Mulberg, A.E., Cherington, V. and Jefferson, D.M. 1994. Regulation of intracellular pH by immortalized human intrahepatic biliary epithelial cell lines. *The American journal of physiology.* **266**(6 Pt 1), pp.G1060-1070.

Gruenberger, B., Schueller, J., Heubrandtner, U., Wrba, F., Tamandl, D., Kaczirek, K., Roka, R., Freimann-Pircher, S. and Gruenberger, T. 2010. Cetuximab, gemcitabine, and oxaliplatin in patients with unresectable advanced or metastatic biliary tract cancer: a phase 2 study. *Lancet Oncol.* **11**(12), pp.1142-1148.

Hernandez, J., Cowgill, S.M., Al-Saadi, S., Villadolid, D., Ross, S., Kraemer, E., Shapiro, M., Mullinax, J., Cooper, J., Goldin, S., Zervos, E. and Rosemurgy, A. 2008. An aggressive approach to extrahepatic cholangiocarcinomas is warranted: margin status does not impact survival after resection. *Annals of surgical oncology.* **15**(3), pp.807-814.

Hlatky, L., Hahnfeldt, P. and Folkman, J. 2002. Clinical application of antiangiogenic therapy: microvessel density, what it does and doesn't tell us. *J Natl Cancer Inst.* **94**(12), pp.883-893.

Ho, J.W., Poon, R.T., Sun, C.K., Xue, W.C. and Fan, S.T. 2005. Clinicopathological and prognostic implications of endoglin (CD105) expression in hepatocellular carcinoma and its adjacent non-tumorous liver. *World J Gastroenterol.* **11**(2), pp.176-181.

Hoffmann, R.T., Paprottka, P.M., Schon, A., Bamberg, F., Haug, A., Durr, E.M., Rauch, B., Trumm, C.T., Jakobs, T.F., Helmberger, T.K., Reiser, M.F. and Kolligs, F.T. 2011. Transarterial Hepatic Yttrium-90 Radioembolization in Patients with Unresectable Intrahepatic Cholangiocarcinoma: Factors Associated with Prolonged Survival. *Cardiovascular and interventional radiology.*

Homma, S., Nagamori, S., Fujise, K., Yamazaki, K., Hasumura, S., Sujino, H., Matsuura, T., Shimizu, K., Kameda, H. and Takaki, K. 1987. Human bile duct carcinoma cell line producing abundant mucin in vitro. *Gastroenterologia Japonica.* **22**(4), pp.474-479.

Hughes, M.A., Frassica, D.A., Yeo, C.J., Riall, T.S., Lillemoe, K.D., Cameron, J.L., Donehower, R.C., Laheru, D.A., Hruban, R.H. and Abrams, R.A. 2007. Adjuvant concurrent chemoradiation for adenocarcinoma of the distal common bile duct. *International journal of radiation oncology, biology, physics.* **68**(1), pp.178-182.

Ibrahim, S.M., Mulcahy, M.F., Lewandowski, R.J., Sato, K.T., Ryu, R.K., Masterson, E.J., Newman, S.B., Benson, A., 3rd, Omary, R.A. and Salem, R. 2008. Treatment of unresectable cholangiocarcinoma using yttrium-90 microspheres: results from a pilot study. *Cancer.* **113**(8), pp.2119-2128.

Ibsen, S., Schutt, C.E. and Esener, S. 2013. Microbubble-mediated ultrasound therapy: a review of its potential in cancer treatment. *Drug Des Devel Ther.* **7**, pp.375-388.

Jo Chae, K., Rha, S.Y., Oh, B.K., Koo, J.S., Kim, Y.J., Choi, J., Park, C. and Park, Y.N. 2004. Expression of matrix metalloproteinase-2 and -9 and tissue inhibitor of metalloproteinase-1 and -2 in intraductal and nonintraductal growth type of cholangiocarcinoma. *Am J Gastroenterol.* **99**(1), pp.68-75.

Johnson, L., Gunasekera, A. and Douek, M. 2010. Applications of nanotechnology in cancer. *Discov Med.* **9**(47), pp.374-379.

Jonat, W., Maass, H. and Stegner, H.E. 1986. Immunohistochemical measurement of estrogen receptors in breast cancer tissue samples. *Cancer Res.* **46**(8 Suppl), pp.4296s-4298s.

Kaltenthaler, E.C., Walters, S.J., Chilcott, J., Blakeborough, A., Vergel, Y.B. and Thomas, S. 2006. MRCP compared to diagnostic ERCP for diagnosis

when biliary obstruction is suspected: a systematic review. *BMC medical imaging.* **6**, p9.

Kawarada, Y., Isaji, S., Taoka, H., Tabata, M., Das, B.C. and Yokoi, H. 1999. S4a + S5 with caudate lobe (S1) resection using the Taj Mahal liver parenchymal resection for carcinoma of the biliary tract. *Journal of gastrointestinal surgery : official journal of the Society for Surgery of the Alimentary Tract.* **3**(4), pp.369-373.

Kerbel, R.S. 2003. Human tumor xenografts as predictive preclinical models for anticancer drug activity in humans: better than commonly perceived-but they can be improved. *Cancer Biol Ther.* **2**(4 Suppl 1), pp.S134-139.

Kessenbrock, K., Plaks, V. and Werb, Z. 2010. Matrix metalloproteinases: regulators of the tumor microenvironment. *Cell.* **141**(1), pp.52-67.

Khan, S.A., Davidson, B.R., Goldin, R., Pereira, S.P., Rosenberg, W.M., Taylor-Robinson, S.D., Thillainayagam, A.V., Thomas, H.C., Thursz, M.R. and Wasan, H. 2002. Guidelines for the diagnosis and treatment of cholangiocarcinoma: consensus document. *Gut.* **51 Suppl 6**, pp.VI1-9.

Khan, S.A., Toledano, M.B. and Taylor-Robinson, S.D. 2008. Epidemiology, risk factors, and pathogenesis of cholangiocarcinoma. *HPB : the official journal of the International Hepato Pancreato Biliary Association.* **10**(2), pp.77-82.

Kiessling, F., Fokong, S., Koczera, P., Lederle, W. and Lammers, T. 2012. Ultrasound microbubbles for molecular diagnosis, therapy, and theranostics. *J Nucl Med.* **53**(3), pp.345-348.

Kirimlioglu, H., Turkmen, I., Bassullu, N., Dirican, A., Karadag, N. and Kirimlioglu, V. 2009. The expression of matrix metalloproteinases in intrahepatic cholangiocarcinoma, hilar (Klatskin tumor), middle and distal extrahepatic cholangiocarcinoma, gallbladder cancer, and ampullary carcinoma: role of matrix metalloproteinases in tumor progression and prognosis. *The Turkish journal of gastroenterology : the official journal of Turkish Society of Gastroenterology.* **20**(1), pp.41-47.

Kitagawa, Y., Nagino, M., Kamiya, J., Uesaka, K., Sano, T., Yamamoto, H., Hayakawa, N. and Nimura, Y. 2001. Lymph node metastasis from hilar cholangiocarcinoma: audit of 110 patients who underwent regional and paraaortic node dissection. *Annals of surgery.* **233**(3), pp.385-392.

Kjeldsen, L., Johnsen, A.H., Sengelov, H. and Borregaard, N. 1993. Isolation and primary structure of NGAL, a novel protein associated with human neutrophil gelatinase. *The Journal of biological chemistry.* **268**(14), pp.10425-10432.

Klotz, L.V., Eichhorn, M.E., Schwarz, B., Seeliger, H., Angele, M.K., Jauch, K.W. and Bruns, C.J. 2012. Targeting the vasculature of visceral tumors:

novel insights and treatment perspectives. *Langenbecks Arch Surg.* **397**(4), pp.569-578.

Knuth, A., Gabbert, H., Dippold, W., Klein, O., Sachsse, W., Bitter-Suermann, D., Prellwitz, W. and Meyer zum Buschenfelde, K.H. 1985. Biliary adenocarcinoma. Characterisation of three new human tumor cell lines. *Journal of hepatology.* **1**(6), pp.579-596.

Korpanty, G., Carbon, J.G., Grayburn, P.A., Fleming, J.B. and Brekken, R.A. 2007. Monitoring response to anticancer therapy by targeting microbubbles to tumor vasculature. *Clin Cancer Res.* **13**(1), pp.323-330.

Korpanty, G., Grayburn, P.A., Shohet, R.V. and Brekken, R.A. 2005. Targeting vascular endothelium with avidin microbubbles. *Ultrasound Med Biol.* **31**(9), pp.1279-1283.

Krishna, M. 2013. Microscopic anatomy of the liver. *Clinical Liver Disease.* **2**(S1), pp.S4-S7.

Kusaka, Y., Tokiwa, T. and Sato, J. 1988. Establishment and characterization of a cell line from a human cholangiocellular carcinoma. *Research in experimental medicine. Zeitschrift fur die gesamte experimentelle Medizin einschliesslich experimenteller Chirurgie.* **188**(5), pp.367-375.

Lazarovits, J., Chen, Y.Y., Sykes, E.A. and Chan, W.C. 2015. Nanoparticle-blood interactions: the implications on solid tumour targeting. *Chem Commun (Camb).* **51**(14), pp.2756-2767.

Leelawat, K., Narong, S., Wannaprasert, J. and Leelawat, S. 2011. Serum NGAL to Clinically Distinguish Cholangiocarcinoma from Benign Biliary Tract Diseases. *Int J Hepatol.* **2011**, p873548.

Leelawat, K., Sakchinabut, S., Narong, S. and Wannaprasert, J. 2009. Detection of serum MMP-7 and MMP-9 in cholangiocarcinoma patients: evaluation of diagnostic accuracy. *BMC gastroenterology.* **9**, p30.

Li, Y., Zhang, Y. and Zheng, Q. 2005. Expression of RECK gene and MMP-9 in hilar cholangiocarcinoma and its clinical significance. *J Huazhong Univ Sci Technolog Med Sci.* **25**(5), pp.552-554.

Lubner, S.J., Mahoney, M.R., Kolesar, J.L., Loconte, N.K., Kim, G.P., Pitot, H.C., Philip, P.A., Picus, J., Yong, W.P., Horvath, L., Van Hazel, G., Erlichman, C.E. and Holen, K.D. 2010. Report of a multicenter phase II trial testing a combination of biweekly bevacizumab and daily erlotinib in patients with unresectable biliary cancer: a phase II Consortium study. *J Clin Oncol.* **28**(21), pp.3491-3497.

Matsuki, N., Ishikawa, T., Ichiba, S., Shiba, N., Ujike, Y. and Yamaguchi, T. 2014. Oxygen supersaturated fluid using fine micro/nanobubbles. *Int J Nanomedicine.* **9**, pp.4495-4505.

McLaughlan, J., Ingram, N., Smith, P.R., Harput, S., Coletta, P.L., Evans, S. and Freear, S. 2013. Increasing the sonoporation efficiency of targeted

polydisperse microbubble populations using chirp excitation. *IEEE Trans Ultrason Ferroelectr Freq Control.* **60**(12), pp.2511-2520.

Meza-Junco, J., Montano-Loza, A.J., Ma, M., Wong, W., Sawyer, M.B. and Bain, V.G. 2010. Cholangiocarcinoma: has there been any progress? *Canadian journal of gastroenterology = Journal canadien de gastroenterologie.* **24**(1), pp.52-57.

Minhajat, R., Mori, D., Yamasaki, F., Sugita, Y., Satoh, T. and Tokunaga, O. 2006. Organ-specific endoglin (CD105) expression in the angiogenesis of human cancers. *Pathol Int.* **56**(12), pp.717-723.

Miyagiwa, M., Ichida, T., Tokiwa, T., Sato, J. and Sasaki, H. 1989. A new human cholangiocellular carcinoma cell line (HuCC-T1) producing carbohydrate antigen 19/9 in serum-free medium. *In vitro cellular & developmental biology : journal of the Tissue Culture Association.* **25**(6), pp.503-510.

Mobius, C., Demuth, C., Aigner, T., Wiedmann, M., Wittekind, C., Mossner, J., Hauss, J. and Witzigmann, H. 2007. Evaluation of VEGF A expression and microvascular density as prognostic factors in extrahepatic cholangiocarcinoma. *European journal of surgical oncology : the journal of the European Society of Surgical Oncology and the British Association of Surgical Oncology.* **33**(8), pp.1025-1029.

Moniaux, N., Chakraborty, S., Yalniz, M., Gonzalez, J., Shostrom, V.K., Standop, J., Lele, S.M., Ouellette, M., Pour, P.M., Sasson, A.R., Brand, R.E., Hollingsworth, M.A., Jain, M. and Batra, S.K. 2008. Early diagnosis of pancreatic cancer: neutrophil gelatinase-associated lipocalin as a marker of pancreatic intraepithelial neoplasia. *Br J Cancer.* **98**(9), pp.1540-1547.

Moon, C.M., Bang, S. and Chung, J.B. 2011. The role of (18)F-fluorodeoxyglucose positron emission tomography in the diagnosis, staging, and follow-up of cholangiocarcinoma. *Surgical oncology.* **20**(1), pp.e10-17.

Morise, Z., Sugioka, A., Tokoro, T., Tanahashi, Y., Okabe, Y., Kagawa, T. and Takeura, C. 2010. Surgery and chemotherapy for intrahepatic cholangiocarcinoma. *World journal of hepatology.* **2**(2), pp.58-64.

Morrison, W.B. 2010. Cancer chemotherapy: an annotated history. *J Vet Intern Med.* **24**(6), pp.1249-1262.

Murakami, Y., Uemura, K., Sudo, T., Hayashidani, Y., Hashimoto, Y., Nakamura, H., Nakashima, A. and Sueda, T. 2009. Adjuvant gemcitabine plus S-1 chemotherapy improves survival after aggressive surgical resection for advanced biliary carcinoma. *Annals of surgery.* **250**(6), pp.950-956.

Nagino, M., Ebata, T., Yokoyama, Y., Igami, T., Sugawara, G., Takahashi, Y. and Nimura, Y. 2013. Evolution of surgical treatment for perihilar

cholangiocarcinoma: a single-center 34-year review of 574 consecutive resections. *Ann Surg.* **258**(1), pp.129-140.

Nakamura, T. 2009. Changes in expression of bile canalicular CD10 and sinusoidal CD105 (endoglin) in peritumoral hepatic tissue. *Tumori.* **95**(4), pp.495-500.

Nakanuma, Y., Sato, Y., Harada, K., Sasaki, M., Xu, J. and Ikeda, H. 2010. Pathological classification of intrahepatic cholangiocarcinoma based on a new concept. *World journal of hepatology.* **2**(12), pp.419-427.

Nakeeb, A., Pitt, H.A., Sohn, T.A., Coleman, J., Abrams, R.A., Piantadosi, S., Hruban, R.H., Lillemoe, K.D., Yeo, C.J. and Cameron, J.L. 1996. Cholangiocarcinoma. A spectrum of intrahepatic, perihilar, and distal tumors. *Annals of surgery.* **224**(4), pp.463-473; discussion 473-465.

Nathan, H. and Pawlik, T.M. 2010. Staging of intrahepatic cholangiocarcinoma. *Current opinion in gastroenterology.* **26**(3), pp.269-273.

Nico, B., Benagiano, V., Mangieri, D., Maruotti, N., Vacca, A. and Ribatti, D. 2008. Evaluation of microvascular density in tumors: pro and contra. *Histol Histopathol.* **23**(5), pp.601-607.

Nuntagowat, C., Leelawat, K. and Tohtong, R. 2010. NGAL knockdown by siRNA in human cholangiocarcinoma cells suppressed invasion by reducing NGAL/MMP-9 complex formation. *Clinical & experimental metastasis.* **27**(5), pp.295-305.

Paauwe, M., ten Dijke, P. and Hawinkels, L.J. 2013. Endoglin for tumor imaging and targeted cancer therapy. *Expert Opin Ther Targets.* **17**(4), pp.421-435.

Park, J., Kim, M.H., Kim, K.P., Park do, H., Moon, S.H., Song, T.J., Eum, J., Lee, S.S., Seo, D.W. and Lee, S.K. 2009. Natural History and Prognostic Factors of Advanced Cholangiocarcinoma without Surgery, Chemotherapy, or Radiotherapy: A Large-Scale Observational Study. *Gut and liver.* **3**(4), pp.298-305.

Paschoal, J.P., Bernardo, V., Canedo, N.H.S., Ribeiro, O.D., Caroli-Bottino, A. and Pannain, V.L. 2014. Microvascular density of regenerative nodule to small hepatocellular carcinoma by automated analysis using CD105 and CD34 immunoexpression. *Bmc Cancer.* **14**.

Patel, T. 2001. Increasing incidence and mortality of primary intrahepatic cholangiocarcinoma in the United States. *Hepatology.* **33**(6), pp.1353-1357.

Patel, T. 2002. Worldwide trends in mortality from biliary tract malignancies. *BMC cancer.* **2**, p10.

Peng, H., Zhang, Q., Li, J., Zhang, N., Hua, Y., Xu, L., Deng, Y., Lai, J., Peng, Z., Peng, B., Chen, M., Peng, S. and Kuang, M. 2016. Apatinib inhibits VEGF signaling and promotes apoptosis in intrahepatic cholangiocarcinoma. *Oncotarget.* **7**(13), pp.17220-17229.

Petrowsky, H. and Hong, J.C. 2009. Current surgical management of hilar and intrahepatic cholangiocarcinoma: the role of resection and orthotopic liver transplantation. *Transplantation proceedings.* **41**(10), pp.4023-4035.

Peyman, S.A., Abou-Saleh, R.H., McLaughlan, J.R., Ingram, N., Johnson, B.R., Critchley, K., Freear, S., Evans, J.A., Markham, A.F., Coletta, P.L. and Evans, S.D. 2012. Expanding 3D geometry for enhanced on-chip microbubble production and single step formation of liposome modified microbubbles. *Lab Chip.* **12**(21), pp.4544-4552.

Privratsky, J.R. and Newman, P.J. 2014. PECAM-1: regulator of endothelial junctional integrity. *Cell Tissue Res.* **355**(3), pp.607-619.

Pusztaszeri, M.P., Seelentag, W. and Bosman, F.T. 2006. Immunohistochemical expression of endothelial markers CD31, CD34, von Willebrand factor, and Fli-1 in normal human tissues. *J Histochem Cytochem.* **54**(4), pp.385-395.

Ramirez-Merino, N., Aix, S.P. and Cortes-Funes, H. 2013. Chemotherapy for cholangiocarcinoma: An update. *World J Gastrointest Oncol.* **5**(7), pp.171-176.

Ramos-Vara, J.A. 2005. Technical aspects of immunohistochemistry. *Vet Pathol.* **42**(4), pp.405-426.

Rosen, L.S., Hurwitz, H.I., Wong, M.K., Goldman, J., Mendelson, D.S., Figg, W.D., Spencer, S., Adams, B.J., Alvarez, D., Seon, B.K., Theuer, C.P., Leigh, B.R. and Gordon, M.S. 2012. A phase I first-in-human study of TRC105 (Anti-Endoglin Antibody) in patients with advanced cancer. *Clin Cancer Res.* **18**(17), pp.4820-4829.

Saijyo, S., Kudo, T., Suzuki, M., Katayose, Y., Shinoda, M., Muto, T., Fukuhara, K., Suzuki, T. and Matsuno, S. 1995. Establishment of a new extrahepatic bile duct carcinoma cell line, TFK-1. *The Tohoku journal of experimental medicine.* **177**(1), pp.61-71.

Sang, H., Li, T., Li, H. and Liu, J. 2013. Down-regulation of Gab1 inhibits cell proliferation and migration in hilar cholangiocarcinoma. *PLoS One.* **8**(11), pe81347.

Scott, A.M., Wolchok, J.D. and Old, L.J. 2012. Antibody therapy of cancer. *Nat Rev Cancer.* **12**(4), pp.278-287.

Segatelli, V., de Oliveira, E.C., Boin, I.F.S.F., Ataide, E.C. and Escanhoela, C.A.F. 2014. Evaluation and comparison of microvessel density using the markers CD34 and CD105 in regenerative nodules, dysplastic nodules and hepatocellular carcinoma. *Hepatology International.* **8**(2), pp.260-265.

Seon, B.K., Haba, A., Matsuno, F., Takahashi, N., Tsujie, M., She, X., Harada, N., Uneda, S., Tsujie, T., Toi, H., Tsai, H. and Haruta, Y. 2011. Endoglin-targeted cancer therapy. *Curr Drug Deliv.* **8**(1), pp.135-143.

Serafini, F.M., Sachs, D., Bloomston, M., Carey, L.C., Karl, R.C., Murr, M.M. and Rosemurgy, A.S. 2001. Location, not staging, of cholangiocarcinoma determines the role for adjuvant chemoradiation therapy. *The American surgeon.* **67**(9), pp.839-843; discussion 843-834.

Shaib, Y. and El-Serag, H.B. 2004. The epidemiology of cholangiocarcinoma. *Seminars in liver disease.* **24**(2), pp.115-125.

Shin, H.R., Oh, J.K., Masuyer, E., Curado, M.P., Bouvard, V., Fang, Y., Wiangnon, S., Sripa, B. and Hong, S.T. 2010a. Comparison of incidence of intrahepatic and extrahepatic cholangiocarcinoma--focus on East and South-Eastern Asia. *Asian Pacific journal of cancer prevention : APJCP.* **11**(5), pp.1159-1166.

Shin, H.R., Oh, J.K., Masuyer, E., Curado, M.P., Bouvard, V., Fang, Y.Y., Wiangnon, S., Sripa, B. and Hong, S.T. 2010b. Epidemiology of cholangiocarcinoma: an update focusing on risk factors. *Cancer science.* **101**(3), pp.579-585.

Shingu, Y., Ebata, T., Nishio, H., Igami, T., Shimoyama, Y. and Nagino, M. 2010. Clinical value of additional resection of a margin-positive proximal bile duct in hilar cholangiocarcinoma. *Surgery.* **147**(1), pp.49-56.

Shinohara, E.T., Guo, M., Mitra, N. and Metz, J.M. 2010. Brachytherapy in the treatment of cholangiocarcinoma. *International journal of radiation oncology, biology, physics.* **78**(3), pp.722-728.

Shinohara, E.T., Mitra, N., Guo, M. and Metz, J.M. 2008. Radiation therapy is associated with improved survival in the adjuvant and definitive treatment of intrahepatic cholangiocarcinoma. *International journal of radiation oncology, biology, physics.* **72**(5), pp.1495-1501.

Shinohara, E.T., Mitra, N., Guo, M. and Metz, J.M. 2009. Radiotherapy is associated with improved survival in adjuvant and palliative treatment of extrahepatic cholangiocarcinomas. *International journal of radiation oncology, biology, physics.* **74**(4), pp.1191-1198.

Shirabe, K., Shimada, M., Kajiyama, K., Hasegawa, H., Gion, T., Ikeda, Y., Takenaka, K. and Sugimachi, K. 1999. Expression of matrix metalloproteinase-9 in surgically resected intrahepatic cholangiocarcinoma. *Surgery.* **126**(5), pp.842-846.

Sirica, A.E., Dumur, C.I., Campbell, D.J., Almenara, J.A., Ogunwobi, O.O. and Dewitt, J.L. 2009. Intrahepatic cholangiocarcinoma progression: prognostic factors and basic mechanisms. *Clinical gastroenterology and hepatology : the official clinical practice journal of the American Gastroenterological Association.* **7**(11 Suppl), pp.S68-78.

Smith, A.H., Fujii, H., Kuliszewski, M.A. and Leong-Poi, H. 2011. Contrast ultrasound and targeted microbubbles: diagnostic and therapeutic

applications for angiogenesis. *J Cardiovasc Transl Res.* **4**(4), pp.404-415.

Smith, N.R., Baker, D., James, N.H., Ratcliffe, K., Jenkins, M., Ashton, S.E., Sproat, G., Swann, R., Gray, N., Ryan, A., Jurgensmeier, J.M. and Womack, C. 2010. Vascular endothelial growth factor receptors VEGFR-2 and VEGFR-3 are localized primarily to the vasculature in human primary solid cancers. *Clinical cancer research : an official journal of the American Association for Cancer Research.* **16**(14), pp.3548-3561.

Strebhardt, K. and Ullrich, A. 2008. Paul Ehrlich's magic bullet concept: 100 years of progress. *Nat Rev Cancer.* **8**(6), pp.473-480.

Sun, Q., Zhao, C., Xia, L., He, Z., Lu, Z., Liu, C., Jia, M., Wang, J. and Niu, J. 2014. High expression of matrix metalloproteinase-9 indicates poor prognosis in human hilar cholangiocarcinoma. *Int J Clin Exp Pathol.* **7**(9), pp.6157-6164.

Takada, T., Amano, H., Yasuda, H., Nimura, Y., Matsushiro, T., Kato, H., Nagakawa, T. and Nakayama, T. 2002. Is postoperative adjuvant chemotherapy useful for gallbladder carcinoma? A phase III multicenter prospective randomized controlled trial in patients with resected pancreaticobiliary carcinoma. *Cancer.* **95**(8), pp.1685-1695.

Tamada, K., Ushio, J. and Sugano, K. 2011. Endoscopic diagnosis of extrahepatic bile duct carcinoma: Advances and current limitations. *World journal of clinical oncology.* **2**(5), pp.203-216.

Tang, D., Nagano, H., Yamamoto, H., Wada, H., Nakamura, M., Kondo, M., Ota, H., Yoshioka, S., Kato, H., Damdinsuren, B., Marubashi, S., Miyamoto, A., Takeda, Y., Umeshita, K., Dono, K., Wakasa, K. and Monden, M. 2006. Angiogenesis in cholangiocellular carcinoma: expression of vascular endothelial growth factor, angiopoietin-1/2, thrombospondin-1 and clinicopathological significance. *Oncology reports.* **15**(3), pp.525-532.

Terada, T., Okada, Y. and Nakanuma, Y. 1996. Expression of immunoreactive matrix metalloproteinases and tissue inhibitors of matrix metalloproteinases in human normal livers and primary liver tumors. *Hepatology.* **23**(6), pp.1341-1344.

Thelen, A., Scholz, A., Benckert, C., Schroder, M., Weichert, W., Wiedenmann, B., Neuhaus, P. and Jonas, S. 2008. Microvessel density correlates with lymph node metastases and prognosis in hilar cholangiocarcinoma. *J Gastroenterol.* **43**(12), pp.959-966.

Thelen, A., Scholz, A., Weichert, W., Wiedenmann, B., Neuhaus, P., Gessner, R., Benckert, C. and Jonas, S. 2010. Tumor-associated angiogenesis and lymphangiogenesis correlate with progression of intrahepatic cholangiocarcinoma. *The American journal of gastroenterology.* **105**(5), pp.1123-1132.

Theuerkauf, I., Zhou, H. and Fischer, H.P. 2001. Immunohistochemical patterns of human liver sinusoids under different conditions of pathologic perfusion. *Virchows Arch.* **438**(5), pp.498-504.

Tomayko, M.M. and Reynolds, C.P. 1989. Determination of subcutaneous tumor size in athymic (nude) mice. *Cancer Chemother Pharmacol.* **24**(3), pp.148-154.

Tong, Z., Kunnumakkara, A.B., Wang, H., Matsuo, Y., Diagaradjane, P., Harikumar, K.B., Ramachandran, V., Sung, B., Chakraborty, A., Bresalier, R.S., Logsdon, C., Aggarwal, B.B., Krishnan, S. and Guha, S. 2008. Neutrophil gelatinase-associated lipocalin: a novel suppressor of invasion and angiogenesis in pancreatic cancer. *Cancer Res.* **68**(15), pp.6100-6108.

Tracon Pharma. [Online]. [Accessed 13/08/2016]. Available from: http://www.traconpharma.com/clinical_trials.php

Triebel, S., Blaser, J., Reinke, H. and Tschesche, H. 1992. A 25 kDa alpha 2-microglobulin-related protein is a component of the 125 kDa form of human gelatinase. *FEBS Lett.* **314**(3), pp.386-388.

Tyson, G.L. and El-Serag, H.B. 2011. Risk factors of cholangiocarcinoma. *Hepatology.*

Urata, K., Kawasaki, S., Matsunami, H., Hashikura, Y., Ikegami, T., Ishizone, S., Momose, Y., Komiyama, A. and Makuuchi, M. 1995. Calculation of child and adult standard liver volume for liver transplantation. *Hepatology.* **21**(5), pp.1317-1321.

Vacchelli, E., Aranda, F., Eggermont, A., Galon, J., Sautes-Fridman, C., Zitvogel, L., Kroemer, G. and Galluzzi, L. 2014. Trial Watch: Tumor-targeting monoclonal antibodies in cancer therapy. *Oncoimmunology.* **3**(1), pe27048.

Valle, J., Wasan, H., Palmer, D.H., Cunningham, D., Anthoney, A., Maraveyas, A., Madhusudan, S., Iveson, T., Hughes, S., Pereira, S.P., Roughton, M. and Bridgewater, J. 2010. Cisplatin plus gemcitabine versus gemcitabine for biliary tract cancer. *The New England journal of medicine.* **362**(14), pp.1273-1281.

van der Worp, H.B., Howells, D.W., Sena, E.S., Porritt, M.J., Rewell, S., O'Collins, V. and Macleod, M.R. 2010. Can animal models of disease reliably inform human studies? *PLoS medicine.* **7**(3), pe1000245.

van Oosten, M., Crane, L.M., Bart, J., van Leeuwen, F.W. and van Dam, G.M. 2011. Selecting Potential Targetable Biomarkers for Imaging Purposes in Colorectal Cancer Using TArget Selection Criteria (TASC): A Novel Target Identification Tool. *Transl Oncol.* **4**(2), pp.71-82.

Vazquez, I. and Bridgewater, J. 2011. Nonsurgical therapy of biliary tract cancer. *Current opinion in gastroenterology.* **27**(3), pp.258-261.

Vempati, P., Karagiannis, E.D. and Popel, A.S. 2007. A biochemical model of matrix metalloproteinase 9 activation and inhibition. *The Journal of biological chemistry.* **282**(52), pp.37585-37596.

Vilgrain, V. 2008. Staging cholangiocarcinoma by imaging studies. *HPB : the official journal of the International Hepato Pancreato Biliary Association.* **10**(2), pp.106-109.

Wang, A.Z., Langer, R. and Farokhzad, O.C. 2012. Nanoparticle delivery of cancer drugs. *Annu Rev Med.* **63**, pp.185-198.

Wang, W., Lin, J., Guha, S., Tong, Z., Cameron, A.G., Zhang, F., Qiu, X., Zou, C., Gao, X., Mawad, M.E. and Ke, S. 2011. Target-specific agents imaging ectopic and orthotopic human pancreatic cancer xenografts. *Pancreas.* **40**(5), pp.689-694.

Wang, Y.P., Yu, G.R., Lee, M.J., Lee, S.Y., Chu, I.S., Leem, S.H. and Kim, D.G. 2013. Lipocalin-2 negatively modulates the epithelial-to-mesenchymal transition in hepatocellular carcinoma through the epidermal growth factor (TGF-beta1)/Lcn2/Twist1 pathway. *Hepatology.* **58**(4), pp.1349-1361.

Weidner, N. 1995. Current pathologic methods for measuring intratumoral microvessel density within breast carcinoma and other solid tumors. *Breast Cancer Res Treat.* **36**(2), pp.169-180.

Weijer, R., Broekgaarden, M., Krekorian, M., Alles, L.K., van Wijk, A.C., Mackaaij, C., Verheij, J., van der Wal, A.C., van Gulik, T.M., Storm, G. and Heger, M. 2016. Inhibition of hypoxia inducible factor 1 and topoisomerase with acriflavine sensitizes perihilar cholangiocarcinomas to photodynamic therapy. *Oncotarget.* **7**(3), pp.3341-3356.

Weis, S.M. and Cheresh, D.A. 2011. Tumor angiogenesis: molecular pathways and therapeutic targets. *Nat Med.* **17**(11), pp.1359-1370.

Welzel, T.M., McGlynn, K.A., Hsing, A.W., O'Brien, T.R. and Pfeiffer, R.M. 2006. Impact of classification of hilar cholangiocarcinomas (Klatskin tumors) on the incidence of intra- and extrahepatic cholangiocarcinoma in the United States. *Journal of the National Cancer Institute.* **98**(12), pp.873-875.

West, J., Wood, H., Logan, R.F., Quinn, M. and Aithal, G.P. 2006. Trends in the incidence of primary liver and biliary tract cancers in England and Wales 1971-2001. *British journal of cancer.* **94**(11), pp.1751-1758.

Willmann, J.K. *A Pilot Trial Using BR55 Ultrasound Contrast Agent in the Assessment of Prostate Cancer.* [Online]. [Accessed 5th July]. Available from: https://clinicaltrials.gov/ct2/show/NCT02142608?term=NCT02142608&rank=1

Willmann, J.K., Paulmurugan, R., Chen, K., Gheysens, O., Rodriguez-Porcel, M., Lutz, A.M., Chen, I.Y., Chen, X. and Gambhir, S.S. 2008. US imaging

of tumor angiogenesis with microbubbles targeted to vascular endothelial growth factor receptor type 2 in mice. *Radiology.* **246**(2), pp.508-518.

Yamasaki, S. 2003. Intrahepatic cholangiocarcinoma: macroscopic type and stage classification. *Journal of hepato-biliary-pancreatic surgery.* **10**(4), pp.288-291.

Yang, L.Y., Lu, W.Q., Huang, G.W. and Wang, W. 2006. Correlation between CD105 expression and postoperative recurrence and metastasis of hepatocellular carcinoma. *BMC Cancer.* **6**, p110.

Yeh, J.S., Sennoga, C.A., McConnell, E., Eckersley, R., Tang, M.X., Nourshargh, S., Seddon, J.M., Haskard, D.O. and Nihoyannopoulos, P. 2015. A Targeting Microbubble for Ultrasound Molecular Imaging. *PLoS One.* **10**(7), pe0129681.

Yu, D., Zhuang, L., Sun, X., Chen, J., Yao, Y., Meng, K. and Ding, Y. 2007. Particular distribution and expression pattern of endoglin (CD105) in the liver of patients with hepatocellular carcinoma. *BMC Cancer.* **7**, p122.

Yu, Q. and Stamenkovic, I. 2000. Cell surface-localized matrix metalloproteinase-9 proteolytically activates TGF-beta and promotes tumor invasion and angiogenesis. *Genes Dev.* **14**(2), pp.163-176.

Zabron, A.A., Horneffer-van der Sluis, V.M., Wadsworth, C.A., Laird, F., Gierula, M., Thillainayagam, A.V., Vlavianos, P., Westaby, D., Taylor-Robinson, S.D., Edwards, R.J. and Khan, S.A. 2011. Elevated levels of neutrophil gelatinase-associated lipocalin in bile from patients with malignant pancreatobiliary disease. *Am J Gastroenterol.* **106**(9), pp.1711-1717.

Zach, S.B., E; Rückert, F. 2015. Primary Cholangiocellular Carcinoma Cell Lines. *J Stem Cell Res Transplant.* **2**(1), p7.

Zhang, Y., Fan, Y. and Mei, Z. 2012. NGAL and NGALR overexpression in human hepatocellular carcinoma toward a molecular prognostic classification. *Cancer Epidemiol.* **36**(5), pp.e294-299.

Zhou, Y., Gu, H., Xu, Y., Li, F., Kuang, S., Wang, Z., Zhou, X., Ma, H., Li, P., Zheng, Y., Ran, H., Jian, J., Zhao, Y., Song, W., Wang, Q. and Wang, D. 2015. Targeted antiangiogenesis gene therapy using targeted cationic microbubbles conjugated with CD105 antibody compared with untargeted cationic and neutral microbubbles. *Theranostics.* **5**(4), pp.399-417.

Zhu, A.X., Meyerhardt, J.A., Blaszkowsky, L.S., Kambadakone, A.R., Muzikansky, A., Zheng, H., Clark, J.W., Abrams, T.A., Chan, J.A., Enzinger, P.C., Bhargava, P., Kwak, E.L., Allen, J.N., Jain, S.R., Stuart, K., Horgan, K., Sheehan, S., Fuchs, C.S., Ryan, D.P. and Sahani, D.V. 2010. Efficacy and safety of gemcitabine, oxaliplatin, and bevacizumab in advanced biliary-tract cancers and correlation of changes in 18-

fluorodeoxyglucose PET with clinical outcome: a phase 2 study. *Lancet Oncol.* **11**(1), pp.48-54.

7   Appendices

7.1   Appendix A: Research Ethics Committee approval letter

NHS

National Research Ethics Service

NRES Committee Yorkshire & The Humber - Leeds East

Yorkshire and Humber REC Office
First Floor, Millside
Mill Pond Lane
Meanwood
Leeds
LS6 4RA

Tel: 0113 3050108
Fax:

18 July 2011

Mr K R Prasad
Department of HPB & Transplant Surgery
St James' University Hospital
Beckett Street
Leeds
LS9 7TF

RECEIVED
21 JUL 2011

Dear Mr Prasad

Study title:	Using bile proteomics in the development of diagnostic markers of biliary malignancy
REC reference:	06/Q1206/136
Amendment number:	3
Amendment date:	28 June 2011

The above amendment was reviewed on 14 July 2011 by the Sub-Committee in correspondence.

Ethical opinion

The members of the Committee taking part in the review gave a favourable ethical opinion of the amendment on the basis described in the notice of amendment form and supporting documentation with the condition that the researchers strictly maintain the linked-anonymised format.

Approved documents

The documents reviewed and approved at the meeting were:

Document	Version	Date
Notice of Substantial Amendment (non-CTIMPs)		28 June 2011
Covering Letter		29 June 2011

Membership of the Committee

The members of the Committee who took part in the review are listed on the attached sheet.

R&D approval

All investigators and research collaborators in the NHS should notify the R&D office for the relevant NHS care organisation of this amendment and check whether it affects R&D approval of the research.

Statement of compliance

The Committee is constituted in accordance with the Governance Arrangements for Research Ethics Committees (July 2001) and complies fully with the Standard Operating Procedures for Research Ethics Committees in the UK.

06/Q1206/136:	Please quote this number on all correspondence

Yours sincerely

Alan Ebbutt
Vice Chair

E-mail: jade.thorpe@nhs.net

Enclosures:	List of names and professions of members who took part in the review
Copy to:	Derek Norfolk, Leeds Teaching Hospitals NHS Trust
N/A. R&D contact not specified in database.

NRES Committee Yorkshire & The Humber - Leeds East

Attendance at Sub-Committee of the REC meeting on 14 July 2011

Name	Profession	Capacity
Prof Alan Ebbutt	Statistician	Expert
Ms Emily Griffiths	Deputy Risk Manager	Lay Plus

7.2 Appendix B: Ingredients for H69 (normal cholangiocyte cell line) culture medium

H69 Cell culture

Stock Reagents:

EGF	25 mg/mL solution in tissue culture medium *Sigma A2786 (5g powder)*
Adenine	24.3mg/200ul 1M HCl + 9.8ml H20 (100X stock) *Millipore 01-102 (100mg powder)*
Insulin	50mg/10ml 5mM HCl (1000X stock) *Sigma I2643 (50mg powder)*
Epinephrine	10mg/10ml 0.01M HCl (1000X stock) *Sigma E1653 (5g powder)*
T3-T	0.1ml tri-iodothyronine + 6ml transferrin (1000X stock)
• Tri-iodothyronine	6.8mg/25ul 20mM NaOH + 49.75ml H20 *Sigma T6397 (100mg powder)*
• Transferrin	50mg/6ml PBS *Sigma T2036 (100mg powder)*
Hydrocortisone	12.5mg/2.5ml ETOH

Equations

Hcl: 35% w/w	= 35g Hcl in 65g (65ml) H2O [Stock available in lab] = 53.84g Hcl in 100mls H2O (w/v) = 538.4g Hcl in 1L H20 = 14.76M Hcl (as 1M Hcl= 36.46g)
1M Hcl	= 0.677mls 35% w/w Hcl diluted to 10mls
5mM Hcl	= 0.05ml (50ul) of 1M Hcl diluted to 10mls
0.01M Hcl	= 0.1ml 1M Hcl diluted to 10mls)
20mM NaOH	= 10ul of 2M NaOH (available in lab) diluted to 1ml

Use 0.22u filter to sterilize all solutions after reconstitution, prior to adding to media

Cell Line:	H69
Derived from:	SV40 transformed human cholangiocyte cell line
Source:	Greg Gores Mayo Clinic Minnesota,

Culture media: 225ml DMEM w/ high glucose
225ml DMEM/F-12
50ml   Fetal bovine serum
5ml   Pen/Strep
5ml   Adenine (from 100x stock)
0.5ml Insulin (from 1000x stock)
0.5ml Epinephrine (from 1000x stock)
0.5ml T3-T (from 1000x stock)
10ng/ml EGF *(=5ug in 500mls media)*
62ul   Hydrocortisone

Freezing Media: 2.5 ml cell media
1.5 ml FBS
1.0 ml DMSO